CO_2 Capture by Aqueous Absorption
Summary of 3rd Quarterly Progress Reports 2008

Supported by the Luminant Carbon Management Program

and the

Industrial Associates Program for CO_2 Capture by Aqueous Absorption

by Gary T. Rochelle

Department of Chemical Engineering

The University of Texas at Austin

November 3, 2008

Introduction

This research program is focused on the technical obstacles to the deployment of CO_2 capture and sequestration from flue gas by alkanolamine absorption/stripping and on integrating the design of the capture process with the aquifer storage/enhanced oil recovery process. The objective is to develop and demonstrate evolutionary improvements to monoethanolamine (MEA) absorption/stripping for CO_2 capture from coal-fired flue gas. The Luminant Carbon Management Program and the Industrial Associates Program for CO_2 Capture by Aqueous Absorption support 15 graduate students. These students have prepared detailed quarterly progress reports for the period July 1, 2008 to September 30, 2008. This report includes manuscripts of 10 papers prepared for GHGT-9.

Conclusions

Hydroxyethyl-formamide (HEF), hydroxyethylimidazole (HEI) and formate are the major carbon containing oxidation products of MEA. HEF, HEI and ammonia are the major nitrogen containing oxidation products.

For MEA oxidative degradation, the apparent catalytic activity of dissolved metal catalysts is Cu > Cr/Ni > Fe > V.

Inhibitors A and B (reaction mechanism inhibitors) and EDTA (a chelating agent) were established as effective MEA oxidation inhibitors. Sodium sulfite and reaction intermediates formaldehyde and formate (all expected oxygen scavengers) were unsuccessful at inhibiting MEA oxidation.

When heated with CO_2 at 135^{o}C, the MEA dimer, hydroxyethylethylenediamine (HEEDA), is converted to the cyclic urea, 1-(2-hydroxyethyl)-2-imidazolidone

(HEIA). HEIA is a stable product of MEA thermal degradation and does not revert to HEEDA.

MEA urea formation from oxazolidone at stripper T was confirmed by mass spectroscopy.

The activation energy of MEA thermal degradation is 29 kcal/mol.

The apparent diffusion coefficient for CO_2 loading varies as viscosity$^{0.71}$.

Aqueous PZ absorbs CO_2 2-3 times faster than MEA solutions. Both piperazine and MEA liquid film mass transfer coefficients, k_g', can vary a factor of 10 over typical lean and rich CO_2 loading conditions. The CO_2 absorption rate does not depend on temperature or amine concentration, except in PZ at greater T and CO_2 loading.

The foaming tendency of CO_2 loaded 8 m PZ was increased a factor of 3.3 with 270 mM formaldehyde. Only 2 ppm of Dow Corning 2-3183A silicone antifoam eliminated this foam.

Three mass transfer tests with Sulzer Mellapak 250Y were performed: baseline, low surface tension ($\sigma \sim 30$ dynes/cm), and moderate viscosity ($\mu_L \sim 4$ cP, $\sigma \sim 55$ dynes/cm). There was no effect of viscosity and a weak effect of surface tension on the effective area. The current global (a_e/a_p) correlation for wetted area of structured packing is:

$$\frac{a_e}{a_p} = 1.198\left[(We_L)(Fr_L)^{-1/3}\right]^{0.121}$$

The liquid hold-up with Mellapak 250Y and 500Y packing increases with viscosity.

The new thermodynamic model developed by Hilliard was used in a RateSep^{TM} model to simulate stripper performance from a recent pilot plant run with 9 m MEA. The simulation results were able to match stripper performance, but only 25% of the packing was needed.

Stripping by a three-stage flash with 9 m MEA reduced the equivalent work by 0.5 kJ/mol CO_2 compared to a simple stripper with an equivalent maximum temperature. The three-stage flash required 1 kJ/mol CO_2 less than a simple stripper if solar heat was used for the three-stage flash.

In a preliminary analysis, 8 m PZ improves the energy performance of the stripper by 10% compared to 7 m MEA.

Accurate absorber modeling requires adequate segmentation for the liquid film. The use of accurate countercurrent segments resulted in higher temperatures than the reported pilot plant values reflecting possible heat losses.

The revised MEA model represents pilot plant data loadings and removal within 1%. Temperature profiles are 2 to 8°C off.

Intercooling was necessary to reach 90% removal in the absorber using the pre-determined stripper optimum values.

A process evaluation of crystallizing the equivalent of 100 ppm SO_2 as K_2SO_4 estimates \$0.033/ton CO_2 for energy and \$0.97/ton CO_2 for KOH.

Piperazine (probably PZ.6H_2O) precipitates from unloaded solution at 20°C/1.9 m PZ and 40°C/6 m PZ.

In 8 m PZ, PZ solids precipitate at 40°C/0.04 moles CO_2/equivalent PZ and at 20-25°C/0.25 moles CO_2/equivalent PZ. $^{+}HPZCOO^{-}$ solids may precipitate at CO_2 loading greater than 0.44.

Density in 8 m PZ is strongly correlated with dissolved CO_2 and will be used in the pilot plant as an on-line indicator of CO_2 loading.

At 40ºC, 0.9 to 12 m PZ gives CO_2 partial pressure of 500 and 5000 Pa at lean and rich loading of 0.3 and 0.4 mol CO_2/mole alkalinity. PZ volatility in lean 8 m PZ at 40ºC is 20e-6 atm.

At 40ºC, 7 m MDEA/2 m PZ, gives CO_2 partial pressure of 500 and 5000 Pa at lean and rich loading of 0.09 and 0.35 mol CO_2/mole alkalinity. The CO_2 capacity of the blended solvent is ~0.58 mol CO_2/kg $_{H2O+amine}$ compared to 0.35 for 7 m MEA. In lean 7 m MDEA/2 m PZ at 40°C, the estimated amine volatility is 11e-6 atm for PZ and 5 to 10e-6 atm for MDEA.

The dynamic response time of a simple stripper is related primarily to the liquid holdup in the sump and reboiler. If a constant ratio of heat rate and rich solvent is maintained during turndown of the stripper, there is very little change in the lean loading and other stripper performance variables.

Using ERCOT grid conditions in 2006, CO_2 capture plants with the choice of operating CO_2 capture at 20% or 100% load do not operate at 100% load until CO_2 price is at least \$15/tCO_2.

At 135°C, the loss of PZ in loaded 7 m MDEA/2 m PZ is 39 mmolal/day, about the same as MEA loss in 7 m MEA.

MDEA/PZ appears to be resistant to oxidative degradation. The oxidation of 7 m MDEA/2 m PZ produces formate at 0.01 mM/hr, compared to 0.6 mM/hr for 7 m MEA.

The rate of absorption of CO_2 in 7 m MDEA/2 m PZ is 6e-11 moles/s.cm^2.Pa at 40°C and an equilibrium CO_2 pressure of 3.5 kPa. This is 1.5 to 2 times faster than MEA.

1. Oxidative Degradation of Amimes *p. 111* *(GHGT paper)*

by Andrew Sexton

Aqueous amine solutions were batch loaded into 500 mL glass jacketed reactors and subjected to oxidative degradation at both low and high gas rates. Solutions at low gas were degraded with 100 mL/min of 98%O_2/2%CO_2 with mass transfer achieved by vortexing. Samples were drawn from the reactor during the course of the experiment and analyzed for degradation using ion chromatography and HPLC with evaporative light scattering detection. In a parallel apparatus 7.5 L/min of 15%O_2/2%CO_2 was sparged through 350 mL of solution; additional mass transfer was achieved by vortexing. A Fourier Transform Infrared Analyzer collected continuous gas-phase data on amine volatility and volatile degradation products.

Hydroxyethyl-formamide (HEF), hydroxyethylimidazole (HEI) and formate are the major carbon containing MEA oxidation products; HEF, HEI and ammonia are the major nitrogen containing degradation products. In terms of catalyst oxidation potential, Cu > Cr/Ni > Fe > V. The oxygen stoichiometry (ν) ranges from 1.5 mol MEA degraded/mol O_2 consumed for Cu and Fe catalyzed systems to 1.0 for vanadium catalyzed systems.

Inhibitors A and B (reaction mechanism inhibitors) and EDTA (a chelating agent) were established as effective MEA oxidation inhibitors. Sodium sulfite and reaction intermediates formaldehyde and formate (all expected oxygen scavengers) were unsuccessful at inhibiting MEA oxidation.

Cu catalyzes concentrated PZ oxidation, while Fe has no effect on PZ oxidation even at high catalyst concentration. MEA/PZ blends were more susceptible to oxidation than any other amine system investigated. It is believed that free radicals formed in the MEA oxidation process serve to accelerate the degradation of the PZ structure. All MEA analogs (ethylenediamine, glycine and ethylene glycol) and secondary/hindered amines (AMP, DEA and DGA) were resistant to oxidation in the presence of Fe or Cu, except for diethanolamine (DEA). This suggests that the alkanolamine structure is more susceptible to oxidative degradation.

For detailed information on the effect of catalysts and inhibitors on MEA degradation, refer to the Sexton paper submitted to GHGT-9.

2. Thermal Degradation *p. 118* *(GHGT paper)*

by Jason Davis

Thermal degradation of monethanolamine (MEA) is quantified as a function of initial amine concentration, CO_2 loading, and temperature over a range of expected stripper conditions in an amine absorber/stripper unit. The sum of the degradation products N,N'-di(2-hydroxyethyl)urea, 1-(2-hydroxyethyl)-2-imidazolidone, and N-(2-hydroxyethyl)ethylenediamine make up the majority of total MEA loss. The

temperature dependent rate constant has an activation energy similar to diethanolamine (DEA) of 29 kcal/mole which corresponds to a quadrupling of the degradation rate when the stripper temperature is increased 17°C. At 135°C the degradation rate varies from 2.5 to 6% per week. Using speciation data from an Aspen Plus® model of a stripper unit, losses in the packing are significant, but the majority of MEA loss occurs in the reboiler and reboiler sump. Thermal degradation is minor when the reboiler temperature is held below 110°C. The thermal degradation pathway for MEA deviates from the proposed mechanism of Polderman. The MEA dimer HEEDA is the precursor to the cyclic urea, HEIA, but Polderman had this reversed. HEEDA converted to HEIA stoichiometrically with CO_2 concentration when a solution of HEEDA and CO_2 was held at 135°C. HEIA was found to be a stable product of MEA degradation and does not revert to HEEDA in large quantities when held at elevated temperatures suggesting this pathway is irreversible.

MEA urea formation from oxazolidone was confirmed by mass spectroscopy. A solution of 50 wt % oxazolidone heated to 100°C for as little as 5 minutes converted to MEA urea in large quantities. The MEA urea is one of the first products formed in the MEA degradation experiments, but the concentration stays relatively low (<3 % of MEA concentration). Future work will include synthesis of the MEA urea and thermal degradation experiments to better define the degradation pathway.

The temperature dependent rate constant for MEA degradation was found to have an activation energy of 29 kcal/mol. Using data from Kennard and Meissen, it was determined that diethanolamine (DEA) also has an activation energy of 29 kcal/mol.

This work is also discussed in the attached GHGT-9 paper entitled "Thermal Degradation of Monoethanolamine at Stripper Conditions."

3. Rate Measurements for MEA and PZ ***p. 13*** *(report)* ***p. 125****(GHGT paper)*

by Ross E. Dugas

Effective diffusion coefficients were measured in the diffusion cell at 30˚C. The calculated diffusion coefficient showed a $(\text{viscosity})^{0.71}$ dependence for experiments on 9 m monoethanolamine (MEA) and 2, 5 and 8 m piperazine (PZ). This value compares reasonably to literature values.

New wetted wall column rate experiments were performed for MEA and PZ solutions at 80 and 100˚C. The liquid film mass transfer coefficient, k_g', does not seem to be affected by changes in temperature or amine concentrations in MEA solutions. Piperazine experiments in the wetted wall column show lower k_g' values at higher temperatures and higher CO_2 loadings. These conditions require

greater CO_2 fluxes and may increase the significance of the liquid film physical mass transfer coefficient, k_l^o. If k_l^o is not sufficiently large, diffusion of reactants and products near the interface can restrict CO_2 mass transfer giving reduced k_g' values.

A paper (attached) was prepared for GHGT-9 to present the results for MEA and PZ at 40 and 60°C.

4. Foaming of PZ solutions *p. 23 (report)*

by Xi Chen

The effect of amine concentration and various additives, including electrolytes, liquid hydrocarbon, and degradation products, on foaming tendency of aqueous piperazine with 0.3 mol CO_2/mol amine group(α) was measured. Some of the additives were also tested with 7 m monoethanolamine (MEA) with α= 0.4. Most of the tested chemicals increased the foaming tendency of amine solutions, but only formaldehyde up to 270 mM was able to increase the foaminess to the extent observed in our experiments on oxidative degradation.

5. Influence of Liquid Properties on Effective Mass Transfer Area of Structured Packing *p. 43 (report)* *p. 133 (GHGT paper)*

by Robert Tsai
(also supported by the Separations Research Program}

Three mass transfer tests with Sulzer Mellapak 250Y were performed: baseline, low surface tension ($\sigma \sim 30$ dynes/cm), and moderate viscosity ($\mu_L \sim 4$ cP, $\sigma \sim 55$ dynes/cm). The experimental database was updated to incorporate these data, which further bolstered our main conclusions: no effect of viscosity and a weak effect of surface tension on the effective area. The current global (a_e/a_p) correlation, able to represent the entire database within limits of ±15%, is as follows:

$$\frac{a_e}{a_p} = 1.198\left[(We_L)(Fr_L)^{-1/3}\right]^{0.121}$$

It should be noted that the model was changed from a basis of $(Ca_L)(Re_L)^{2/3}$ (presented in the previous quarterly report) to $(We_L)(Fr_L)^{-1/3}$, in consideration of the fact that the corrugation angle (α) has been held constant (45°) in the packings characterized thus far. $((Ca_L)(Re_L)^{2/3}$ and $(We_L)(Fr_L)^{-1/3}$ are identical when expanded to physical parameters, except that the former includes an additional α term.) A manuscript (attached) was prepared for GHGT-9 that summarizes essentially all of the mass transfer-related results that have been obtained in this body of research.

The hydraulic behavior (pressure drop and hold-up) of Mellapak 250Y under low surface tension conditions ($\sigma \sim 30$ dynes/cm) was investigated. Hold-ups appeared to be lower compared to the base case (water), similar to what was observed with Mellapak 500Y. Pressure drop trends, on the other hand, were difficult to definitively characterize.

6. Modeling Stripper Performance for CO_2 Removal

p. 51 *(report)*

p. 143 *(GHGT paper)*

by David Van Wagener

In this quarter comparative work for MEA was continued. A paper (attached) was prepared on much of this MEA work. Previously, there was a recent pilot plant run with 35% MEA carried out at the J. J. Pickle Research Campus, and the most recent MEA model developed by Marcus Hilliard was utilized to reconcile the data. All values could be matched using 25% of the actual packing height. The MEA model was also used to evaluate performance of a new configuration, a three-stage flash with a preheater. The three-stage flash performed best with solar heat as an energy source, and this configuration reduced the equivalent work requirement using 9 m MEA by 1 kJ/mol CO_2 compared to a 2.1 atm simple stripper. Lastly, a piperazine model also developed by Hilliard was used to compare the performance of MEA to PZ in a simple stripper. All simulations used equivalent rate streams, but a rich stream more concentrated in CO_2 was used for one piperazine case due to the faster rates expected in the absorber. The 8 m PZ case with a richer inlet proved to require 10% less energy than the 7 m MEA base case.

7. CO_2 Absorption Modeling Using Aqueous Amines

p. 56 *(report)*

p. 143 *(GHGT paper)*

by Jorge M. Plaza

A new model for the absorption of carbon dioxide from flue gas by aqueous MEA was presented in the 2nd quarterly report. It incorporates the thermodynamic model by Hilliard (2008) and simplified kinetics consisting of two equilibrium equations and four kinetic reactions. Carbamate formation rates were obtained by simulating the conditions of the laminar jet used by Aboudheir (2002) with an absorber model generated in Aspen Plus®. The bicarbonate forward rate was approximated using data presented by Rochelle *et al.* (2001). Density, viscosity, thermal conductivity and surface tension of the CO_2 – MEA – H_2O system along with carbon dioxide diffusivity in water were corrected based on work by Aspen Technology, Inc (Huiling & Chen, 2008). Reaction kinetics were revised considering the mentioned properties correction. Results are presented in this report

The final model incorporated the wetted area correlation developed by Tsai (Tsai *et al.*, 2008). Model validation work with the 9 m pilot plant data was revised. Liquid film segmentation was modified and 16 segments were determined to be optimal. Various packing segmentations were evaluated along with the countercurrent flow model. Temperature profiles using the later resulted higher than the experimental values. CO_2 loadings, MEA concentration and removal percentage were matched by the model. This report includes details on the modifications to the model and reconciliation results.

Work was conducted to specify an absorber for the optimized stripper conditions obtained by Van Wagener (Plaza *et al.*, 2008). Results showed that intercooling made it feasible to reach 90% removal with the specified conditions. The minimum packing height required was 5.2 m of Flexipac 1Y using optimized intercooling.

Work with the new MEA model is also included in the attached paper prepared for GHGT-9.

8. Reclaiming by Crystallization of Potassium Sulfate

p. 65 *(report)*

p. 150 *(GHGT paper)*

by Qing Xu

One side reaction in CO_2 capture when using MEA/PZ is the generation of sulfate from SO_2. This sulfate has to be removed so that the MEA/PZ solution can be reused for CO_2 capture. Potassium sulfate can be crystallized and separated from MEA/PZ solvent by the addition of potassium hydroxide. In previous work the solubility of K_2SO_4 in CO_2 loaded aqueous amine solution was measured and an empirical model was developed. Selected interaction parameters were regressed in CO_2-MEA-H_2O-K^+-SO_4^{-2} system using Aspen Plus® Electrolyte-NRTL model. Continuous crystallization experiments at 25 to 60ºC show that big crystals can form by mixing lean CO_2 loading amine solution and KOH solution with residence times from 3 min to 20 min, and the solid-liquid separation is easy to achieve. In this period, a process simulation of reclaiming using crystallization of potassium sulfate was done in Aspen Plus®. The interaction parameters from the Aspen Plus® regression were used. This simulation is based on a 500 MW power plant in the 2007 report by K. S. Fisher *et al*. Energy and chemical costs were estimated. The result shows that energy and chemical costs are \$0.038 and \$1.040 per ton of CO_2, respectively. So the total cost would be less than \$1/ton CO_2. Compared with \$55-67/ton CO_2 for a typical CO_2 capture using MEA, this reclaiming process cost is acceptable. A comprehensive paper (attached) describing this work has been prepared for GHGT-9.

9. Solvent Management of Concentrated Piperazine

p. 66 *(report)*

p. 158 *(GHGT paper)*

by Stephanie Freeman

The solubility envelope of concentrated PZ solutions has been investigated this quarter. The solid-liquid transition temperature of a variety of PZ solutions was measured and compared to literature data. For 8 m PZ, a CO_2 loading of 0.25 mol CO_2/mol alkalinity is required to maintain a liquid solution without precipitation at room temperature (20°C). Additionally, the solubility of PZ.6H_2O(s in unloaded solution at 20°C is 1.9 m PZ. The density of 7 m PZ ranges from 1.066 g/mL to 1.160 g/mL for 0.16 to 0.46 mol CO_2/equiv PZ at 20, 40, and 60°C. The density of 9 m PZ ranges from 1.084 g/mL to 1.181 g/mL with 0.15 to 0.44 mol CO_2/equiv PZ at 20, 40, and 60°C. The viscosity of 5, 7, 9, 10, 12, and 20 m PZ at 25, 40, and 60°C was measured.

A paper (attached) was prepared for GHGT-9 which presents all of the important performance data for concentrated PZ. Concentrated, aqueous piperazine (PZ) has been investigated as a novel amine solvent for carbon dioxide (CO_2) absorption. The CO_2 absorption rate with aqueous PZ is more than double that of 7 m MEA and volatility at 40°C ranges from 10 to 19 ppm. Thermal degradation is negligible in concentrated PZ solutions up to a temperature of 150°C, a significant advantage over MEA systems. Oxidative degradation of concentrated PZ solutions is appreciable in the presence of copper (4 mM), but negligible in the presence of chromium (0.6 mM), nickel (0.25 mM), iron (0.25 mM), and vanadium (0.1 mM). Initial system modeling suggests that 8 m PZ will use 5 to 10% less energy than 7 m MEA. The fast kinetics and low degradation rates suggest that concentrated PZ has the potential to be a preferred solvent for CO_2 capture.

10. Thermodynamics of Concentrated Piperazine and MDEA/PZ

p. 78*(report)*

p. 173 *(GHGT paper)*

by Bich-Thu Nguyen

The objective of this work is to explore the thermodynamic VLE behavior of piperazine (0.9-12 m PZ) and of methyldiethanolamine (MDEA)/PZ systems (2.7-8.7 m MDEA/0.4-2.6 m PZ). CO_2 solubility and amine volatility are studied as a function of temperature, loading, and amine concentration.

With PZ (0.9m-12.0m) at 40ºC, CO_2 partial pressure is measured to be 500 and 5000 Pa at lean and rich loading of 0.3 and 0.4 mol CO_2/equivalent of PZ, respectively. At stripper operating temperature of ~120ºC, CO_2 partial pressure is ~100,000 Pa at a loading of 0.3. The estimated CO_2 heat of absorption in PZ is -71 kJ/mol for 0.3 lean loading. The CO_2 solubility is represented by: $\ln P_{CO2} = 36.1$ -

(93.2 $kJmol^{-1}/R)(1/T)$ -13.9(Loading) + 8839(Loading/T) + 14.3($Loading^2$). PZ volatility is 4.8-33 ppm at 40ºC and 8-100 ppm at 60ºC.

With MDEA/PZ (2.7-8.7m MDEA/0.4-2.6m PZ) at 40ºC, CO_2 partial pressure is 500 and 5000 Pa at lean and rich loading of 0.09 and 0.35 mol CO_2/mol total alkalinity, respectively. The solubility of CO_2 in this amine blend is empirically modeled as: $\ln P_{CO2} = 36.7 - 8991.6(1/T) + 1.3[\ln(\text{Loading})] + 5061.5(T/\text{Loading}) - 21.4(\text{Loading}^2)$. The capacity of this blend is 0.58 mol CO_2/kg $_{H2O+amine}$ compared to 0.35 mol CO_2/kg $_{H2O+amine}$ for 7 m MEA. The CO_2 heat of absorption in MDEA/PZ is estimated to be ~62 kJ/mol at 0.3 mol CO_2/mol total alkalinity. PZ volatility in these systems ranges from 2-19 ppm at 40ºC. Similarly, MDEA volatility is between ~5-12 ppm at 40ºC for these blended systems.

11. Dynamic Operation of CO_2 Capture ***p. 93*** *(report)*

p. 166 *(GHGT paper)*

by Sepideh Ziaii

This quarter's work focuses on dynamic simulation of dynamic operation of CO_2 capture in response to the electricity load and demand variation. The contribution of this work is an attached full paper prepared for GHTG-9. The rate-based dynamic model, which was created in ACM® for the stripper with 30 wt % MEA, was used to simulate two dynamic scenarios, turn-off and turn-on, by making 80% changes in the stripper load. A simple ratio control strategy is implemented to control the rich solvent rate proportional to the reboiler heat rate change.

When ramping between 20% and 100% load over 15 minutes, the energy in KJ/mole CO_2 removed does not vary more than 2% during the transition. For the current simulation conditions, the liquid hold up time in the reboiler for 100% and 20% load operation is 5 and 25 minutes, respectively. Since the response time of the stripper is dominantly determined by the solvent residence time in the reboiler at the end of the ramp, turn-on scenario has a smaller time constant by a factor of 4.65 and reaches steady state about 30 minutes after ramping the heat and liquid rate, while the turn-off scenario reaches 2.5 hours after ramping the system.

12. System Level Implications of Flexible CO_2 Capture Operation ***p. 94*** *(report)*

p. 166 *(GHGT paper)*

by Stuart Cohen

A model of the Electric Reliability Council of Texas (ERCOT) electric grid uses a basic representation of plant dispatch and the ERCOT electricity market to investigate the implications of flexible carbon dioxide (CO_2) capture in response to

hourly electricity demand variations for a \$0–\$60/tCO_2 range of CO_2 price[1,2]. Using ERCOT grid conditions in 2006, CO_2 capture plants with the choice of operating CO_2 capture at 20% or 100% load do not operate at 100% load until CO_2 price is at least \$15/tCO_2. Below this CO_2 price, flexibility allows operating profits at eight CO_2 capture facilities to be several hundreds of millions of dollars greater than if CO_2 capture were operated continuously at 100% load; however, venting the CO_2 that is not captured at part-load could prevent the desired emissions reductions from being achieved. Significant CO_2 emissions reductions are achieved with flexible CO_2 capture above \$20/tCO_2, and the \$20-\$35/tCO_2 range offers the opportunity for tens to hundreds of millions of dollars in operating profit above that earned with continuous 100% load operation by allowing plant operators to pick the CO_2 capture operating point that results in the optimal combination of power output, electricity production costs, and electricity price. Coal-based facilities remain primarily as base load generation up to about \$40/tCO_2, so increases in average wholesale electricity price are equal to emissions costs at natural gas-fired facilities. CO_2 capture operation is secondary to CO_2 price in determining changes to wholesale electricity price; at a given CO_2 price, the average price increase from the case of no CO_2 capture to that with continuous 100% load operation is less than \$3/MWh[3].

13. Solvent Management of MDEA/Piperazine p. 108 (report) p. 173 (GHGT paper)

by Fred Closmann

(also supported by the Process Science & Technology Center)

A paper (attached) was prepared for GHGT-9. The solvent blend methyldiethanolamine/ piperazine (MDEA/PZ) has been investigated as an alternative for CO_2 capture from coal-fired power plants. MDEA/PZ offers advantages over monoethanolamine (MEA) and MDEA alone because of its resistance to thermal and oxidative degradation at typical absorption/stripping conditions. We measured thermal degradation rates of MDEA and PZ of -7 ± 20 mmolal/day and -9 ± 5 mmolal/day, respectively, in a loaded 7 m MDEA/2 m PZ solvent blend at 120°C. At 135°C, the PZ degradation rate in the loaded solvent blend is -39 ± 11 mmolal/day, which closely matches the appearance of unidentified diamine compounds. When sparged with 98% O_2 at 55°C, 7 m MDEA/2 m PZ with 1 mM Fe^{2+} produced 0.011 ± 0.001 mmoles formate/L-hr.

[1] All dollar values are displayed in 2006 US dollars.

[2] All quantities of CO_2 are displayed in metric tons.

At the same conditions, 7 m MDEA produced 0.024 ± 0.007 mmoles formate/L-hr. We determined that the resistance to oxidative degradation follows the order: MDEA/PZ>MDEA>PZ. The formation of amides in oxidatively degraded samples can be as much as twice the amount of formate produced. In the absence of PZ, MDEA forms amides at an order of magnitude greater rate. The volatility of MDEA in 7 m MDEA/2 m PZ at 40 and 60°C with low CO_2 loading is 6 to 11 ppm and 19 to 30 ppm, respectively. PZ activity decreases by nearly an order of magnitude in the solvent blend as loading of CO_2 is increased to a one-to-one ratio with PZ, giving a PZ volatility at 40^{o}C of 5 ppm. We calculated a CO_2 capacity of approximately 0.75 moles CO_2/kg amine+water, as compared to a capacity of 0.5 moles CO_2/kg amine+water for MEA under comparable conditions in an absorber/stripper configuration.

Diffusion, Rate and CO_2 Partial Pressure Measurements for Monoethanolamine and Piperazine Solutions

Progress Report for July 1 – September 30, 2008
by Ross Dugas
Supported by the Luminant Carbon Management Program
and the
Industrial Associates Program for CO_2 Capture by Aqueous Absorption
Department of Chemical Engineering
The University of Texas at Austin
October 18, 2008

Abstract

Effective diffusion coefficients were measured in the diffusion cell at 30˚C. The calculated diffusion coefficient showed a $(\text{viscosity})^{0.71}$ dependence for experiments on 9 m monoethanolamine (MEA) and 2, 5, and 8 m piperazine (PZ). This value compares reasonably to literature values.

New wetted wall column rate experiments were performed for MEA and PZ solutions at 80 and 100˚C. The liquid film mass transfer coefficient, k_g', does not seem to be affected by changes in temperature or amine concentrations in MEA solutions. Piperazine experiments in the wetted wall column show lower k_g' values at higher temperatures and higher CO_2 loadings. These conditions require greater CO_2 fluxes and may increase the significance of the liquid film physical mass transfer coefficient, k_l^o. If k_l^o is not sufficiently large, diffusion of reactants and products near the interface can restrict CO_2 mass transfer giving reduced k_g' values.

Introduction

This report contains information separated into 2 main parts: (1) diffusion characteristics of monoethanolamine and piperazine solutions, and (2) CO_2 partial pressure and rate measurements of MEA and PZ solutions at absorber and stripper conditions.

Diffusion experiments using a diaphragm cell were performed. Diffusion experiments on 9 m MEA and 2, 5, and 8 m PZ were tested.

CO_2 partial pressure and CO_2 absorption/desorption rate data has previously been obtained for 7, 9, 11, and 13 m MEA and 2, 5, 8, and 12 m piperazine PZ at absorber conditions (40 and 60˚C) using the wetted wall column. This report includes 80 and 100˚C data for many of those solutions. Data at 40 and 60^{o}C are reported and discussed in the attached paper prepared for GHGT-9.

As in previous work, solution CO_2 loadings are defined on an alkalinity basis. The alkalinity is essentially the number of nitrogen atoms on the amine: 1 for MEA but 2 for PZ. The CO_2 loading definition is shown in Equation 1.

$$CO_2 Loading = \frac{n_{CO2}}{n_{MEA} + 2n_{PZ}} \quad (1)$$

Results and Discussion

Diffusion Characteristics

Details about the diffusion cell apparatus, experimental design, and calculation methods for the diffusion experiments are detailed in a previous progress report (Rochelle *et al.,* 2008). The tabulated diffusion coefficient is an effective diffusion coefficient which is termed the membrane-cell integral diffusion coefficient, $\overline{D}$. It is a complex concentration and time averaged value which is not easily converted to the fundamental diffusion coefficient D (Smith, Flowers *et al.*, 2002). $\overline{D}$ is defined via Equation 2.

$$\overline{D} = \frac{C_{b,mean}\overline{D}^0(C_{b,mean}) - C_{t,mean}\overline{D}^0(C_{t,mean})}{C_{b,mean} - C_{t,mean}} \quad (2)$$

$\overline{D}^0(C)$ is the average diffusion coefficient with respect to concentration for the initial and the final concentration. $C_{b,mean}$ is the mean of the bottom chamber concentrations before and after the experiment. $C_{t,mean}$ is the mean of the top chamber concentrations before and after the experiment.

Table 1: Diaphragm Cell Results for Monoethanolamine and Piperazine Solutions

Solution	CO_2 Loading (mol/mol$_{alk}$)	Temp (C)	Time (h)	$\overline{D}$ (m^2/s)	Visc @ 25C (cP)
9m MEA	0.26↔0.36	30	93	3.7E-10	3.8
	0.44↔0.50	30	138	3.2E-10	4.5
2m PZ	0.24↔0.32	30	72	6.1E-10	1.7
	0.35↔0.41	30	146	5.8E-10	1.8
5m PZ	0.23↔0.32	30	166	2.5E-10	5.0
8m PZ	0.23↔0.30	30	237	1.2E-10	17

The viscosity-diffusion coefficient relationship is shown graphically in Figure 1. Figure 1 also includes a 1 m PZ, 0.50 loading data point from Sun (2005). It is not clear whether this is a measured or calculated value.

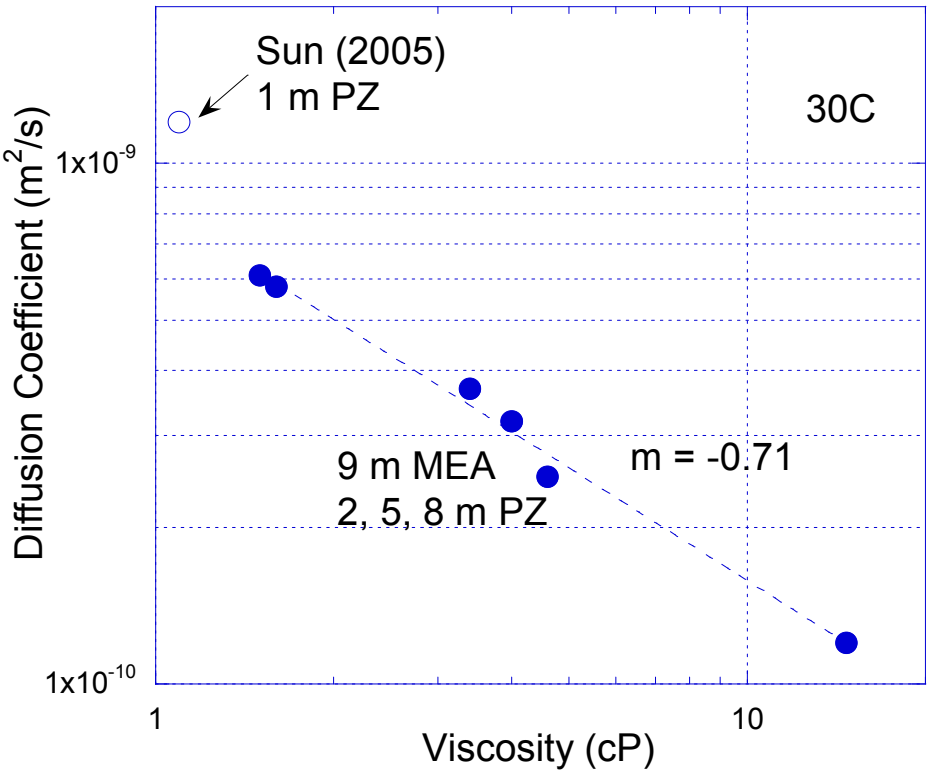

Figure 1: Diffusion Coefficient – Viscosity Relationship for Amine Solutions

The Sun data point is the for the diffusion coefficient of piperazine. The measured data points represent effective diffusion coefficients obtained from the diffusion cell. These effective diffusion coefficients are most likely indicative of the diffusion coefficient of the carbamate and protonated carbamate species. The Sun data point being raised slightly above the extrapolated curve may be related to the fact that piperazine is smaller than piperazine carbamate and therefore should diffuse somewhat faster.

The slope of the measured data points is 0.71 when plotted on a log-log plot. This relates to previous literature data organized by Versteeg (1996) in which the diffusivity of N_2O in amines most often depends on viscosity to the 0.80 power. However, this 0.8 dependence was not seen in aqueous solutions of AMP (Xu *et al.*, 1991). According to Snijder (1993), the diffusivity of the alkanolamine can be estimated by the modified Stokes-Einstein relation in which the diffusion coefficient has a 0.60 dependence on the viscosity. The measured viscosity dependence of 0.71 seems to be in line with the 0.60 and 0.80 dependences often seen for amine and N_2O diffusivity. The measured viscosity dependence may also vary from literature values because of the ionic nature of the solute.

CO_2 Partial Pressure and Rate Measurements

CO_2 partial pressure and rate measurements for MEA and PZ solutions have previously been reported at 40 and 60˚C (Rochelle *et al.*, 2008). The present report also includes some rate data at 80 and 100˚C. Due to equipment limitations, only lower loading solutions could be tested at 80 and 100˚C. Tables 2 and 3 include the updated rate and partial pressure data for MEA and PZ solutions. Figure 2 shows a CO_2 partial pressure plot for MEA while Figure 3 shows the same plot for PZ solutions.

Table 2: Rate and CO_2 Partial Pressure Data for 7, 9, 11, and 13 m MEA

MEA	Temp	CO_2 Ldg	P_{CO2}	k_g'
m	C	mol/mol_{alk}	Pa	$mol/s{\cdot}Pa{\cdot}m^2$
7	40	0.252	15.7	3.34E-06
7	40	0.351	77	1.40E-06
7	40	0.432	465	7.66E-07
7	40	0.496	4216	3.47E-07
7	60	0.252	109	2.92E-06
7	60	0.351	660	1.70E-06
7	60	0.432	3434	9.28E-07
7	60	0.496	16157	3.76E-07
7	80	0.271	1053	2.85E-06
7	80	0.366	4443	1.87E-06
7	80	0.444	18826	7.52E-07
7	100	0.271	5297	2.98E-06
7	100	0.366	19008	1.40E-06

MEA	Temp	CO_2 Ldg	P_{CO2}	k_g'
m	C	mol/mol_{alk}	Pa	$mol/s{\cdot}Pa{\cdot}m^2$
9	40	0.231	10.4	-
9	40	0.324	34	1.86E-06
9	40	0.382	107	1.40E-06
9	40	0.441	417	8.36E-07
9	60	0.496	5354	3.02E-07
9	60	0.231	61	3.80E-06
9	60	0.324	263	2.44E-06
9	60	0.382	892	1.47E-06
9	60	0.441	2862	9.57E-07
9	60	0.496	21249	3.24E-07
9	80	0.265	979	3.24E-06
9	100	0.265	4940	3.40E-06

MEA	Temp	CO_2 Ldg	P_{CO2}	k_g'
m	C	mol/mol_{alk}	Pa	$mol/s{\cdot}Pa{\cdot}m^2$
11	40	0.261	14.0	3.36E-06
11	40	0.353	67	1.76E-06
11	40	0.428	434	7.14E-07
11	40	0.461	1509	4.34E-07
11	60	0.261	96	3.35E-06
11	60	0.353	634	1.80E-06
11	60	0.428	3463	8.71E-07
11	60	0.461	8171	5.02E-07
13	40	0.252	12.3	3.08E-06
13	40	0.372	84	1.28E-06
13	40	0.435	491	6.96E-07
13	40	0.502	8792	1.62E-07
13	60	0.252	100	2.98E-06
13	60	0.372	694	1.54E-06
13	60	0.435	3859	7.56E-07
13	60	0.502	29427	1.93E-07

Table 3: Rate and CO_2 Partial Pressure Data for 2, 5, 8, and 12 m PZ

MEA	Temp	CO_2 Ldg	P_{CO2}	k_g'
m	C	mol/mol_{alk}	Pa	$mol/s{\cdot}Pa{\cdot}m^2$
2	40	0.240	96	3.32E-06
2	40	0.316	499	2.04E-06
2	40	0.352	1305	1.39E-06
2	40	0.411	7127	5.55E-07
2	60	0.240	559	3.33E-06
2	60	0.316	2541	2.06E-06
2	60	0.352	5593	1.38E-06
2	60	0.411	25378	3.84E-07
2	80	0.239	2492	3.34E-06
2	80	0.324	12260	1.32E-06
2	100	0.239	9569	2.40E-06
2	100	0.324	39286	9.12E-07

MEA	Temp	CO_2 Ldg	P_{CO2}	k_g'
m	C	mol/mol_{alk}	Pa	$mol/s{\cdot}Pa{\cdot}m^2$
5	40	0.226	65	4.39E-06
5	40	0.299	346	2.57E-06
5	40	0.354	1120	1.69E-06
5	40	0.402	4563	7.93E-07
5	60	0.226	385	4.75E-06
5	60	0.299	1814	2.62E-06
5	60	0.354	5021	1.80E-06
5	60	0.402	17233	6.59E-07
5	80	0.238	2192	4.67E-06
5	80	0.321	9699	1.91E-06
5	100	0.238	8888	3.52E-06
5	100	0.321	36960	1.02E-06

MEA	Temp	CO_2 Ldg	P_{CO2}	k_g'
m	C	mol/mol_{alk}	Pa	$mol/s{\cdot}Pa{\cdot}m^2$
8	40	0.231	68	4.27E-06
8	40	0.305	530	1.98E-06
8	40	0.360	1409	1.14E-06
8	40	0.404	8153	3.53E-07
8	60	0.231	430	4.41E-06
8	60	0.305	2407	2.02E-06
8	60	0.360	7454	9.57E-07
8	60	0.404	30783	3.20E-07
8	80	0.253	3255	3.61E-06
8	80	0.289	9406	1.97E-06
8	100	0.253	13605	2.18E-06
8	100	0.289	32033	1.20E-06
12	60	0.231	331	4.19E-06
12	60	0.289	1865	1.85E-06
12	60	0.354	6791	7.73E-07

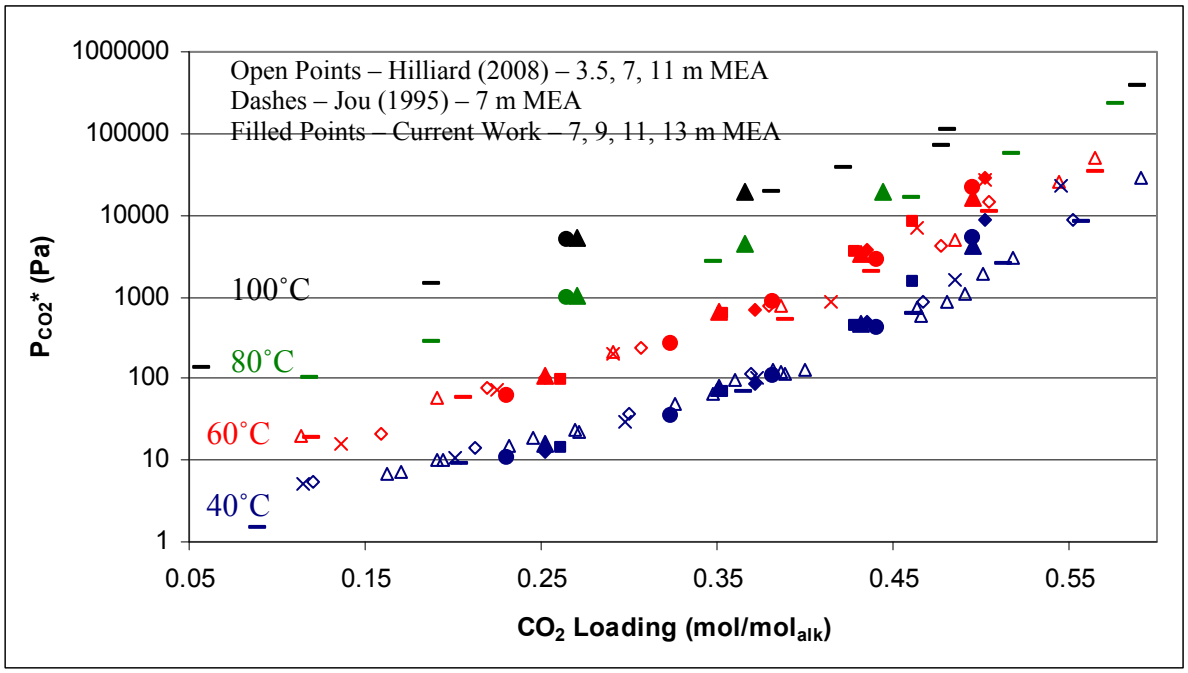

Figure 2: CO_2 Partial Pressure for Aqueous MEA

The current work matches the Hilliard (2008) data very well at 40 and 60˚C below 0.45 loading. Above 0.45 loading, the current work shows an increase in the CO_2 partial pressure which seems to be amine concentration dependent. The current work also matches the 40, 60, 80, and 100˚C data collected by Jou (1995).

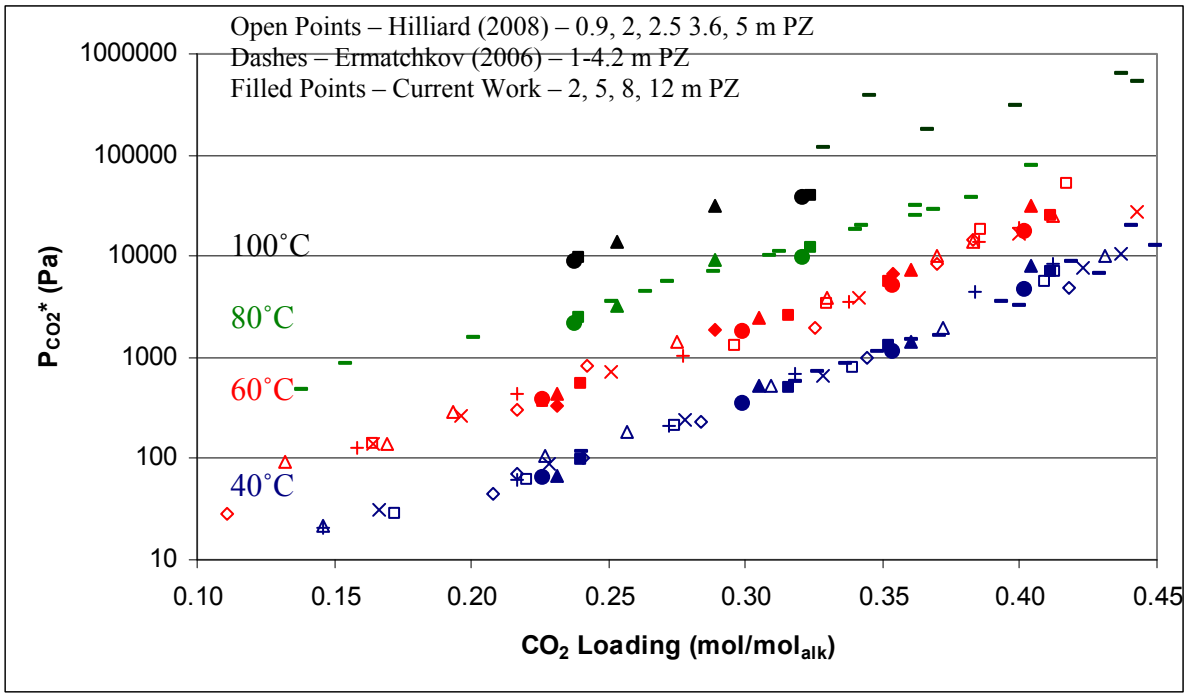

Figure 3: CO_2 Partial Pressure for Aqueous Piperazine

The current PZ CO_2 partial pressure measurements match 40 and 60˚C data obtained by Hilliard (2008). The current work also agrees with 40, 80, and 100˚C CO_2 partial pressure data collected by Ermatchkov (2006).

Wetted wall column obtained rates are shown in Figures 4 and 5 for MEA and PZ, respectively.

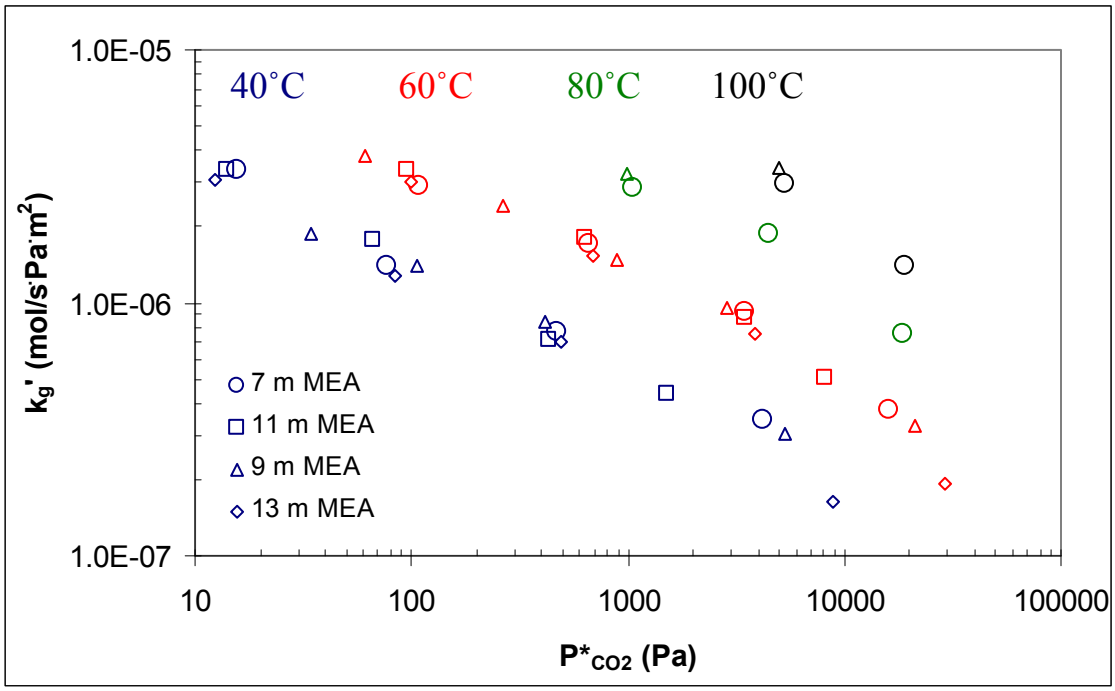

Figure 4: CO_2 Absorption/Desorption Rates for 7, 9, 11, and 13 m MEA at 40, 60, 80, and 100˚C.

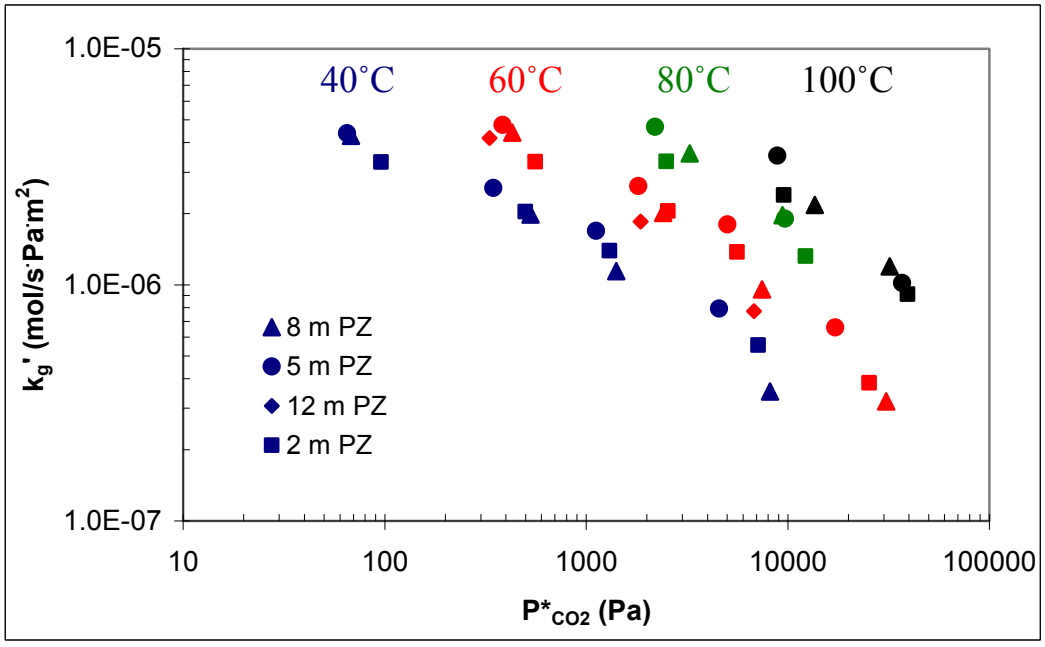

Figure 5: CO_2 Absorption/Desorption Rates for 2, 5, 8, and 12 m PZ at 40, 60, 80, and 100˚C.

Figures 4 and 5 both show clear trend lines for each temperature. The liquid film mass transfer coefficient, k_g', decreases by a factor of 10 from lean to rich conditions because the free amine decreases in rich solutions. The amine concentration does not seem to significantly affect the measured mass transfer coefficient, k_g', for either the MEA or PZ solutions. Generally, the temperature does not significantly affect k_g' either. Higher temperatures in Figures 4 and 5 cause an increase in the equilibrium partial pressure not the k_g' values.

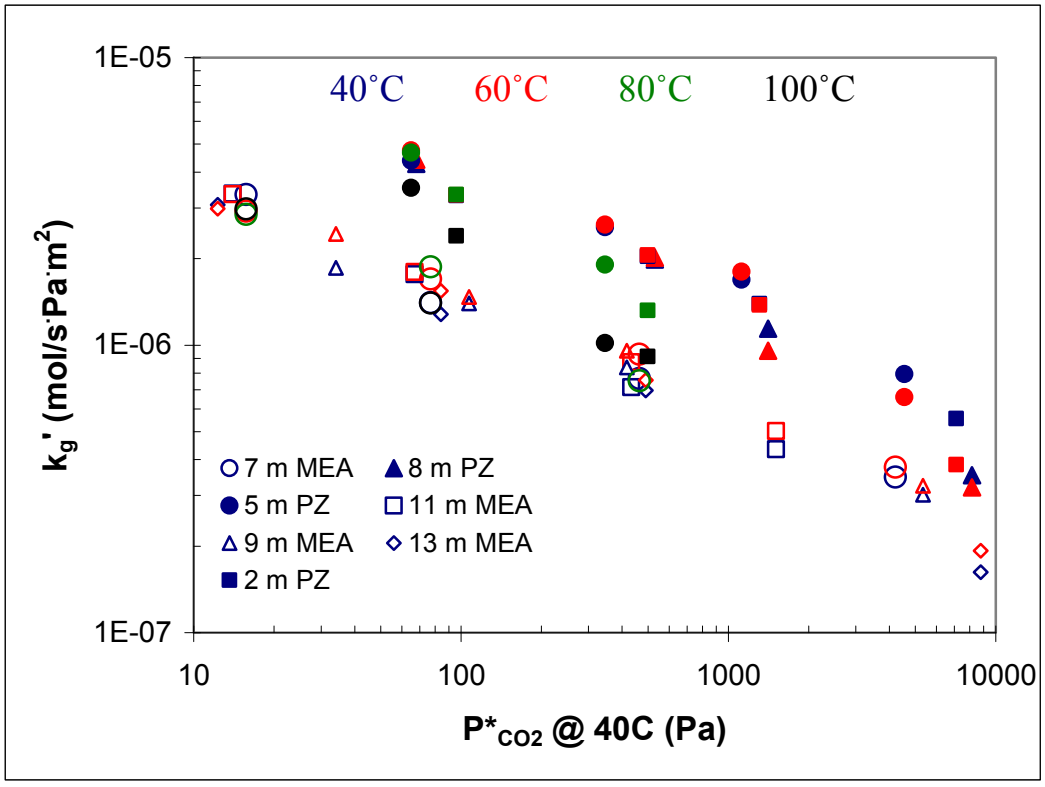

Figure 6: Absorption/Desorption Rates for CO_2 in MEA and PZ Solutions Plotted Versus the Equilibrium Partial Pressure at 40˚C

Figure 6 shows that the piperazine solutions absorb CO_2 2–3 times faster than MEA. None of the MEA points show significant deviations with changes in temperature. Richer solutions of piperazine start to show slightly smaller k_g' values at 60˚C than 40˚C. 80˚C PZ data show k_g' values below those of 60˚C at intermediate CO_2 loadings. The 100˚C PZ k_g' data falls below the 80˚C data even for the leanest loading. At intermediate loadings the 100˚C PZ rates are significantly lower than the cooler temperatures. This effect is likely due to diffusion of reactants and products to and from the interface. At higher temperature and loading, wetted wall column experiments require larger CO_2 fluxes and accumulation at the interface is more likely to be significant. This effect is likely more apparent in the PZ solutions because the PZ solutions are more viscous than MEA, resulting in lower diffusion coefficients. Only 2 and 5 m

PZ data is shown in Figure 6. It is possible that the 8 m PZ data may show a greater drop in k_g' because of the increased viscosity. Diffusion resistances on CO_2 mass transfer in the wetted wall column will be explored more fully in the near future.

Conclusions

The membrane-cell integral diffusion coefficient measured in the diffusion cell shows a $(\text{viscosity})^{0.71}$ dependence. These experiments likely represent the diffusion coefficient of carbamate species. This 0.71 power dependence compares to common literature values of 0.80 for the diffusion coefficient of N_2O (Versteeg *et al.*, 1996) and 0.6 for the diffusion coefficient of amines (Snijder *et al.*, 1993). Piperazine solutions absorb CO_2 2-3 times faster than MEA solutions. Both piperazine and MEA liquid film mass transfer coefficients, k_g', can vary by a factor of 10 over typical lean and rich CO_2 loading conditions.

MEA does not show temperature or amine concentration dependences on mass transfer rates. PZ experiments in the wetted wall column seem to become more prone to diffusion resistances at higher temperature and solution loadings.

References

Ermatchkov, V *et al*. "Solubility of Carbon Dioxide in Aqueous Solutions of Piperazine in the Low Gas Loading Region". *J Chem Eng Data*. 2006;51(5):1788–1796.

Hilliard, M. "A Predictive Thermodynamic Model for an Aqueous Blend of Potassium Carbonate, Piperazine, and Monoethanolamine for Carbon Dioxide Capture from Flue Gas". Ph.D Dissertation. University of Texas at Austin, 2008. 1025.

Jou, F-Y *et al*. "The Solubility of CO_2 in a 30 Mass Percent Monoethanolamine Solution". *Can J Chem Eng*. 1995;73(1):140–147.

Rochelle, GT *et al*. "CO_2 Capture by Aqueous Absorption: June 2008 Progress Report". http://www.che.utexas.edu/rochelle_group/Pubs/2nd_quarterly_report_2008.pdf.

Smith, MJ *et al*. "Method for the measurement of the diffusion coefficient of benzalkonium chloride". *Water Res*. 2002;36:1423–1428.

Snijder, ED *et al*. "Diffusion Coefficients of Several Aqueous Alkanolamine Solutions". *J Chem Eng Data.* 1993;38(3):475–480.

Sun, W-C *et al*. "Kinetics of the Absorption of CO_2 into Mixed Aqueous Solutions of 2-amino-2methyl-1-propanol and Piperazine". *Chem Engr Sci*. 2005;60(2):503–516.

Versteeg, GF *et al*. "On the Kinetics between CO_2 and Alkanolamines both in Aqueous & Non-aqueous Solutions. An Overview". *Chem Engr Comm*. 1996;144:113–158.

Xu, S *et al*. "Physical Properties of Aqueous AMP Solutions". *J Chem Eng Data*. 1991;36(1):71–75.

Foaming tendency of amine solutions with different additives

Progress Report for July – September, 2008

by Xi Chen

Supported by the Luminant Carbon Management Program

and the

Industrial Associates Program for CO_2 Capture by Aqueous Absorption

Department of Chemical Engineering

The University of Texas at Austin

November 4, 2008

Abstract

The effect of amine concentration and various additives, including electrolytes, liquid hydrocarbon, and degradation products, on foaming tendency of aqueous piperazine with 0.3 mol CO_2/mol amine group(α) was measured. Some of the additives were also tested with 7 m monoethanolamine (MEA) with α= 0.4. Most of the tested chemicals increased the foaming tendency of amine solutions, but only formaldehyde, with its possible range of content, was able to increase the foaminess to an extent as seen in oxidatively degraded PZ solution.

Introduction

Foaming is a problem that is widely encountered in gas treating plants and normally leads to serious consequences such as loss of absorption capacity of amine solution, reduced mass transfer area and efficiency, and carryover of amine solution to downstream plant. The causes of foaming have been widely discussed in the literature. It is generally believed that foaming is induced by various chemical contaminants including condensed liquid hydrocarbon, fine particulates like iron sulfide, additives containing surface active chemicals, and amine degradation products (Pauley, Hashemi *et al*., 1989; Pauley, 1991; Stewart and Lanning, 1994; Abdi and Meisen, 2000; von Phul, 2001; Spooner, Sheilan *et al*., 2006; Al-Dhafeeri, 2007).

Relatively few studies involving systematic and quantitative investigation of foaming in amine solutions have been published. Pauley and coworkers (1989) studied the effect of hydrocarbon contamination and organic acid of different lengths on the foaming tendency of MEA, MDEA, DEA, and formulated MDEA. All the contaminants investigated were found to increase the foaming tendency and

foam stability of amine solutions, but to different extents. McCarthy *et al.* (McCarthy and Trebble, 1996) studied the foaming tendency of DEA solutions in the presence of various contaminants including carboxylic acid. They found that, except for carboxylic acids with number of carbon >5, most of the contaminants added to the system did not produce a substantial difference in foamability compared to a clean DEA solution. Thitakamol and Veawab (2008) systematically investigated the effects of process parameters on foaming behavior of different alkanolamines such as MEA, MDEA, and AMP or their mixtures. Ranges of solutions, volume, and gas flow rates were identified and used to measure the foaminess coefficient. They found that most clean amine solutions did not foam, but the addition of degradation products and corrosion inhibitor increased the foaming tendency by up to 23%. The selection of parameters used in our study is partially based on their recommendation.

Piperazine, as a new diamine solvent, has received attention for its high adsorption capacity and fast kinetic reaction rate with CO_2 (Bishnoi and Rochelle, 2000). Most foaming studies have been focused on traditional amines and there has been no quantitative investigation of the foaming property of piperazine. In this study, efforts were focused on investigating and identifying the main causes for the PZ foaming problem observed in the pilot plant. The results obtained will be used for further study of the foaming effect on the CO_2 capture process, and developing efficient means for foaming control.

Experimental Methods

Experimental Setup. Foaming tests were performed using a method adapted from standard ASTM D892 for foaming tests of lubricating oils. As shown in Figure 1, the experimental setup included a 1000 ml graduated cylinder, a water bath equipped with an immersion digital circulator (Lauda E100, Ecoline), a gas diffusing stone (1 in. diam., porous fused crystalline alumina, avg pore size = 60 um, Fisher and a gas flow rate meter (EX-03217-12, Cole Parmer). Nitrogen was used instead of air to bubble the solution in order to prevent oxidative degradation and any alteration of the CO_2 loading of tested solutions during the experiment.

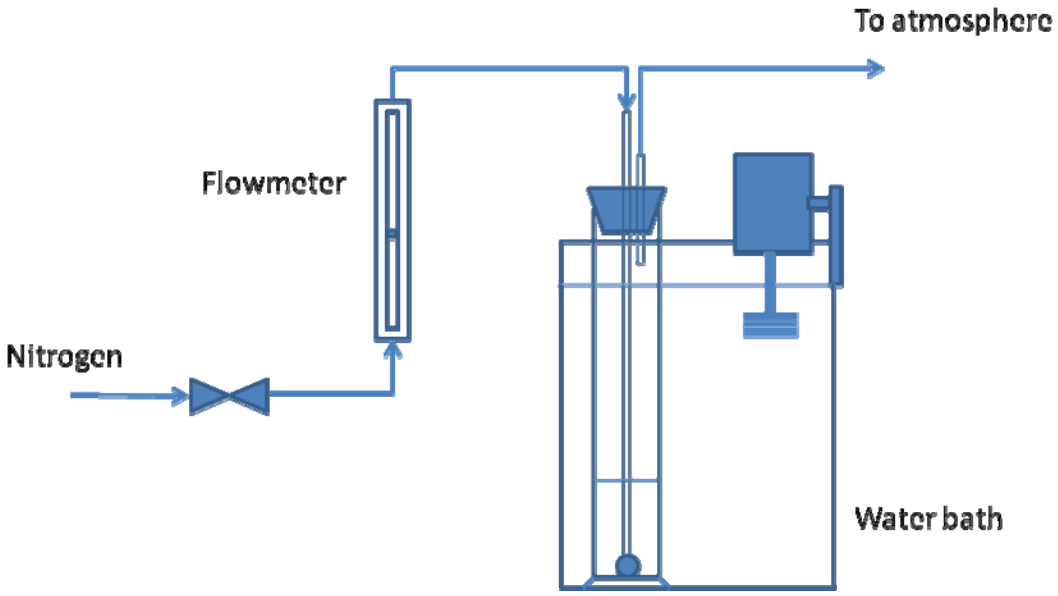

Figure 1: Schematic diagram for foaming experimental setup

Materials. Piperazine (PZ, 99%, Alfa Aesar) and MEA (99+%, Acros) were used as received. Amine solutions were prepared by dissolving amines in deionized water (Millipore, Direct-Q) followed by sparging the solutions with carbon dioxide (Coleman Instrument, 99.99%, Matheson) to achieve a specific loading. The typical concentration of solutions used in this study were 8 m PZ with α= 0.3 and 7 m MEA with α= 0.4.

Ferrous sulphate (99%, Reagent A.C.S, Spectrum), ferric chloride (Certified A.C.S, Fisher Chemical), Cupric sulphate (Analytical Reagent, Mallinckrodt), formaldehyde (37 wt % water solution, Certified A.C.S, Fisher Chemical), and formic acid (88 wt % water solution, Certified A.C.S, Fisher Chemical) were used as received. The antifoam used was Q2-3183A with silicone as the main component, obtained from Dow Corning.

Experimental Procedures. The cylinder cell containing 400 ml test solution was placed in the water bath which had been heated to 40^{o}C. The diffuser was inserted into the solution and the system was allowed approximately 20 minutes to reach equilibrium. The initial solution volume was recorded. Then the nitrogen was introduced to the graduated cylinder and the flow rate was set by adjusting the flow rate meter. In this work, a flow rate of 2×10^{-3} m/s (with respect to cross section area of graduated cylinder) was selected for all experiments. The blowing time counting was started simultaneously.

Since the interface between liquid and foam was hard to see for most test solutions, the total volume of contents in cylinder (liquid and foam, instead of the volume of foam only, was recorded each minute. Each foaming test experiment was run for

25 minutes and the data recorded from the last 15 minutes was averaged and reported as steady-state result.

Prior to the study of each specific additive, neat amine solution (without any additives) was run as a base line. Since those results for neat solutions were not exactly the same, a normalized foaminess coefficient was reported to compare different additives.

Data analysis. By subtracting the original liquid volume from the total volume in the cylinder, the total gas volume encapsulated by the liquid was obtained. The foaminess coefficient used in this study was defined as: $F = \frac{V_g}{G} = \frac{V_t - V_0}{G}$

Where V_g is the total steady volume (m^3) of gas trapped in the liquid, V_0 is the original liquid volume (m^3), V_t is the total steady volume (m^3) of content in the cylinder during foaming, and G is the gas flow rate (m/s). Normalized foaminess coefficient (F*), which was obtained by normalized F with respect to the foaminess coefficient of the neat amine solution (F_0), was defined as:

$$F^* = \frac{F}{F_0}$$

The break time of foam was measured as period for the foam to break completely after the gas flow was discontinued. It is used to estimate foam stability.

Results and Discussions

Amine concentration

The concentration of the PZ solution varied from 2 m to 8 m at 40°C and = 0.3 moles CO_2/equivalent PZ. Figure 2 shows that F* increases with PZ concentration within the studied range. This increase is attributed to increased viscosity of the amine solution. As the viscosity of the bulk solution is increased, the drainage of liquid in foam films and the subsequent coalescence is retarded. The enhanced foam stability is also reflected by the foam break time which was found to increase from 5 s to 29 s as shown in Table 1 in the Appendix.

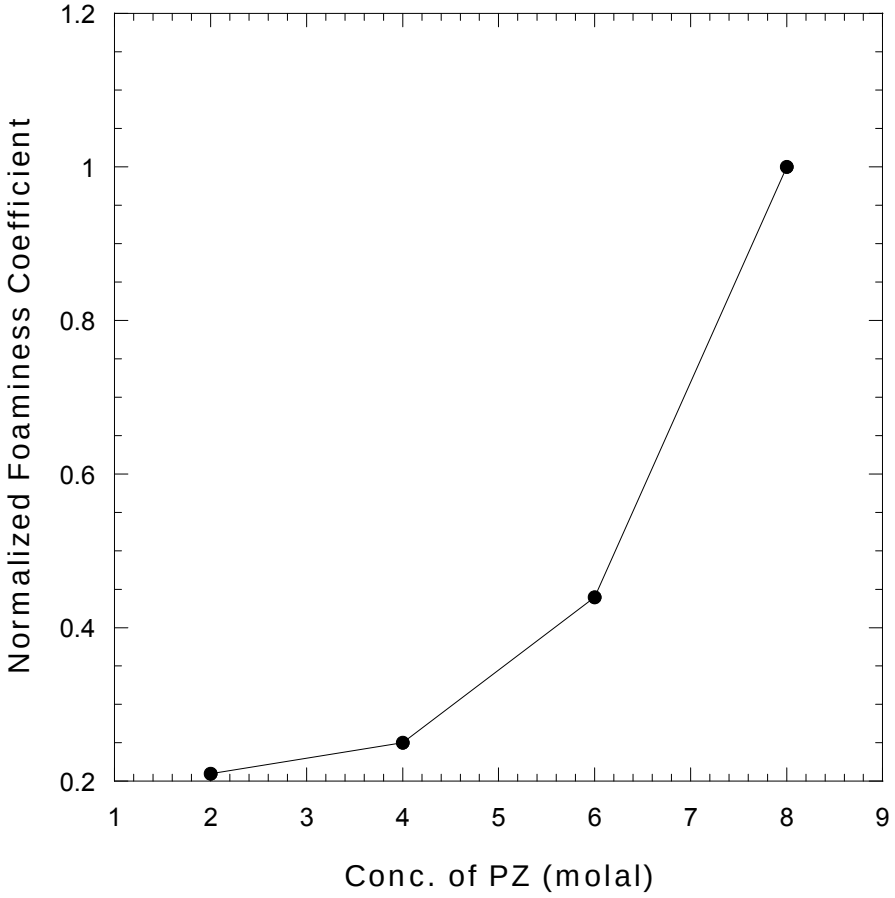

Figure 2: Effect of PZ concentration on normalized foaminess coefficient at 40ºC

Ferrous Ion

As steel materials are used for most gas treating facilities, it is necessary to study the effect of dissolved ferrous or ferric ions on foaming. 0.1 M $FeSO_4$ solution with 0.05 M H_2SO_4 was added to 8 m PZ solution under strong stirring at a rate of 1 drop/sec. The amount of Fe^{2+} in the amine solution was varied from 0 to 1.5 mM, to mimic the possible range of Fe^{2+} content in the real absorber. As shown in Figure 3, F* increased by about 40% as Fe^{2+} concentration was increased to 0.5

mM, then F* decreased slightly with a further increase of Fe^{2+}. It was found that the amine solution turned from light yellow to dark orange as Fe^{2+} was added. Moreover, a layer of orange precipitation was visible on the bottom of the reactor. It was inferred that the fine particles composed of ferrous oxides or ferrous hydroxide are responsible for the increase in the foaming tendency of amine solutions. As the Fe^{2+} exceeded 0.5 mM, foam break time was longer than 300 seconds and a stable foam layer of 3–4 mm in thickness remained on the top of the solutions after the gas flow was stopped.

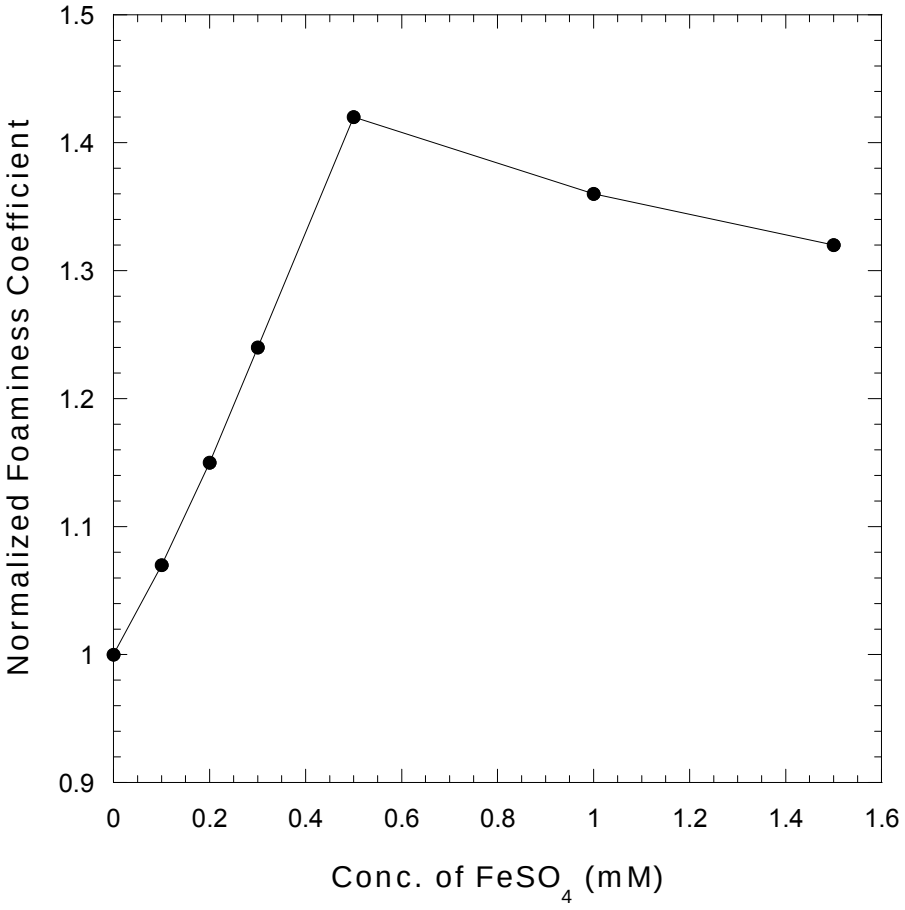

Figure 3: Normalized foaminess coefficient as a function of $FeSO_4$ concentration for 8 m PZ solution with = 0.3 at 40ºC.

The effect on Fe^{2+} for MEA solution was also studied. It should be noted that foaminess coefficient for neat MEA solutions, about 20×10^{-3} $m^2\cdot s$, is much lower than that for neat PZ solutions, which is around 85×10^{-3} $m^2\cdot s$. So MEA does not foam as much as PZ does. The effect of Fe^{2+} on MEA solutions is shown in Figure 4. A maximum in F* was observed as the [Fe^{2+}] was increased but in general the foaming tendency of MEA solutions was not sensitive to the presence of small amount of Fe^{2+}.

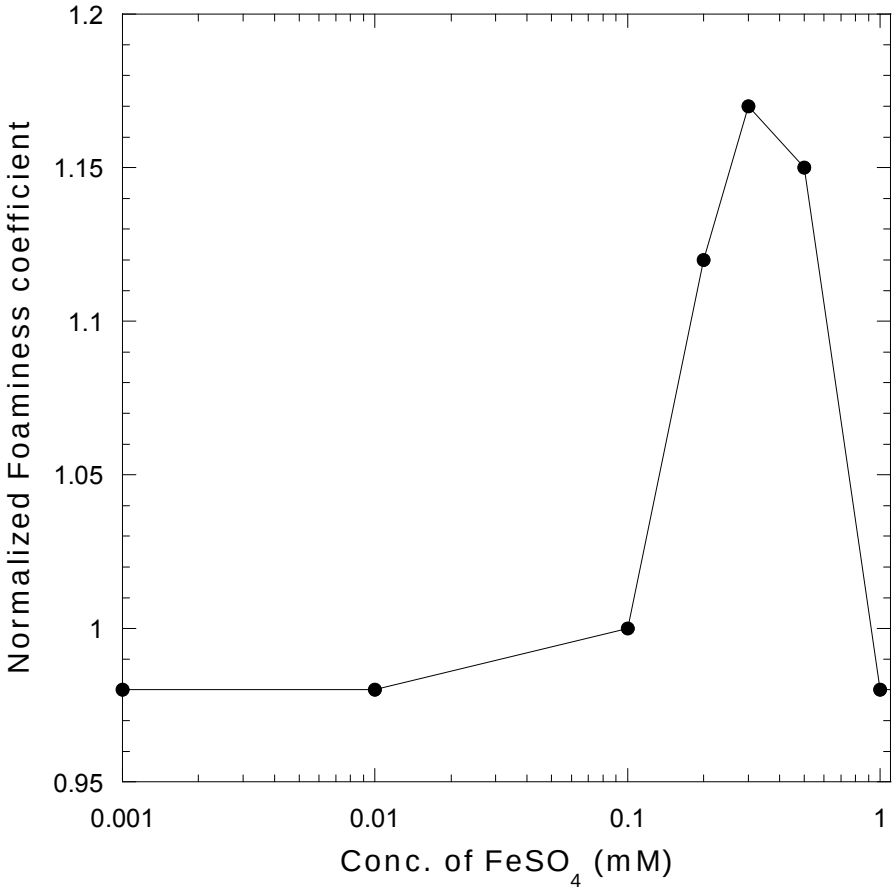

Figure 4: Normalized foaminess coefficient as a function of $FeSO_4$ concentration for 7 m MEA solution with α= 0.4 at 40ºC

Ferric Ion

Dissolved Fe^{2+} could be easily oxidized to ferric ion. 0.01-1 mM $FeCl_3$ was added to the amine solutions. Figure 5 shows that Fe^{3+} does not significantly affect the foaming tendency of PZ solutions. F* increased slightly with [Fe^{3+}], peaked at 0.2 mM, then dropped and leveled off. The ferric ion may not be able to form fine particles to stabilized foam as ferrous ion did.

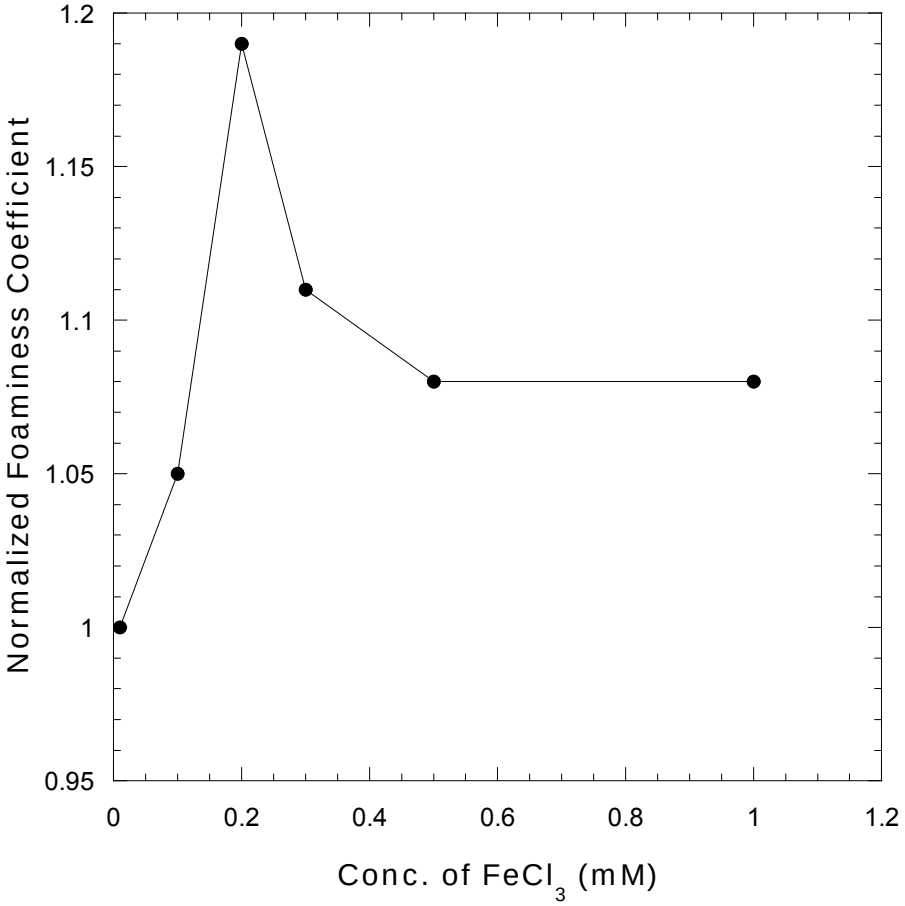

Figure 5: Normalized foaminess coefficient as a function of $FeCl_3$ concentration for 8 m PZ solution with α= 0.3 at 40ºC

Corrosion inhibitor and oxidation inhibitor

Cu^{2+} and V^{5+} are common chemicals added as corrosion inhibitors to amine solutions, so their possible effects on amine foaming property must be addressed. The same question needs to be answered for oxidation inhibitors, which are used to retard the oxidation of the amine. A proprietary product, "Inhibitor A", was used in our study. Figure 6 shows the effects of adding different combinations of additives on the foaming tendency of PZ solutions. F* was found to be less than 1 with additions of corrosion or oxidation inhibitor, which means these inhibitors do not contribute to foaming.

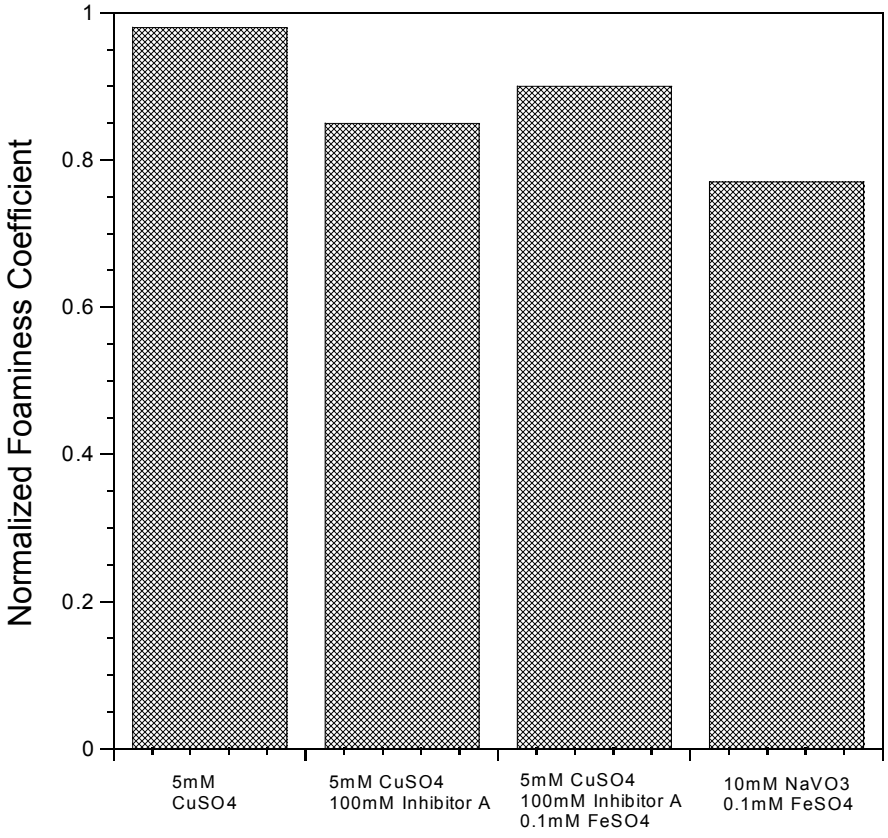

Figure 6: Effect of different chemical additives on normalized foaminess coefficient for 8 m PZ solution with α= 0.3 at 40ºC

Oxidation products

A previous progress report (Freeman and Rochelle, 2008) shows that formate is one of the primary oxidation products of PZ. Formaldehyde is also believed to be one of the intermediate products of oxidation. Thus different amounts of formic acid or formaldehyde were added to PZ solutions to study their effects on foamability. After adding 0.5 M formic acid to the PZ solutions, F increased only slightly from 81×10^{-3} $m^2 \cdot s$ to 85×10^{-3} $m^2 \cdot s$, which rules out the formic acid as a main foaming promoter.

Figure 7 shows that increasing the amount of formaldehyde dramatically affects the foamability of PZ solutions. As the concentration of formaldehyde was increased to 270 mM, the solution foamed to the point where its volume exceeded the limit of the graduated cylinder (1000 ml). Therefore F could only be estimated to be > 319×10^{-3} $m^2 \cdot s$, more than 3 times greater than the original neat solution.

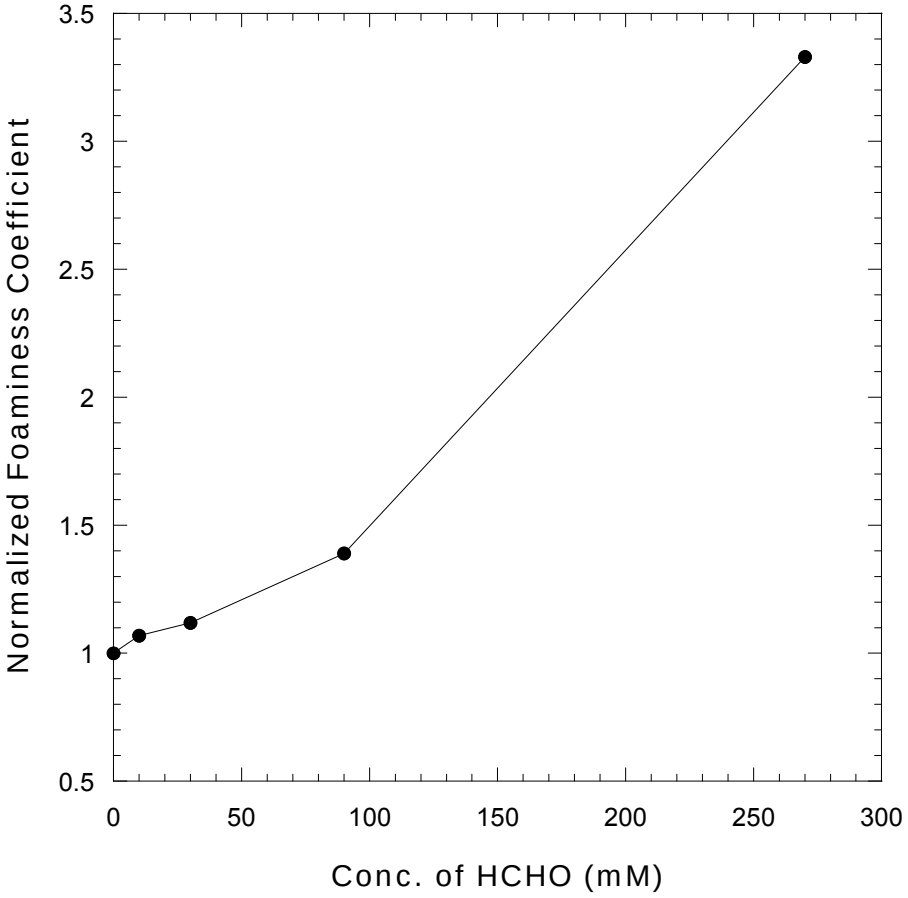

Figure 2: Normalized foaminess coefficient as a function of formaldehyde concentration for 8 m PZ solution with α= 0.3 at 40ºC. The number of F* reported at 270 mM HCHO is an estimation and it is less than the actual value.

Reaction occurred as HCHO was added to the PZ solution as a white substance appears suspended in the solutions. Therefore it was inferred that a condensation reaction may occur between formaldehyde and PZ. The products, which could be oligomer or polymer, might be very surface active and could enhance the foam

stability. An additional proof for this hypothesis is that the addition of 0.5 M formaldehyde to the MEA solution also caused a significant increase in foaming tendency. Since there is one primary amine group and one hydroxide group on MEA, it is possible that the condensation polymerization is likely to occur between formaldehyde and MEA.

Oxidatively degraded PZ solution at 55ºC (Sample OE4 in Freeman's progress report in 1st quarter of 2008) was also tested and the foaming coefficient was found to be comparable to the PZ solution with addition of 270 mM formaldehyde. Unfortunately, lab techniques have not been developed at this point to detect formaldehyde during the oxidative degradation process. The hypothesis that formaldehyde is the primary cause of the severe foaming problem of PZ needs to be proved in future work.

Liquid hydrocarbon

Previous studies have suggested that hydrocarbon may be an important cause of foaming observed in some plants. Heptane was used in this work to study the effect of hydrocarbon on foaming. The solubility of heptane in pure water at 40ºC is about 6×10^{-7} moles heptane/mole water, which is interpolated from Marche and coworker (Marche, Ferronato *et al.* 2003). It is difficult to add on amount of heptane below the solubility limit so the starting molar ratio of heptane to water was 8.7×10^{-6} and increased to 9×10^{-3}. The results are shown in Figure 8. Heptane did not significantly increase the foaming tendency of PZ solution. Moreover, as the amount of heptane was increased to $n_{hep}/n_{H2O}= 9\times10^{-3}$, it started to act as a defoamer. At this concentration heptane droplets dispersing in solution could be seen by the naked eye, which might contribute to the defoaming activity of heptane.

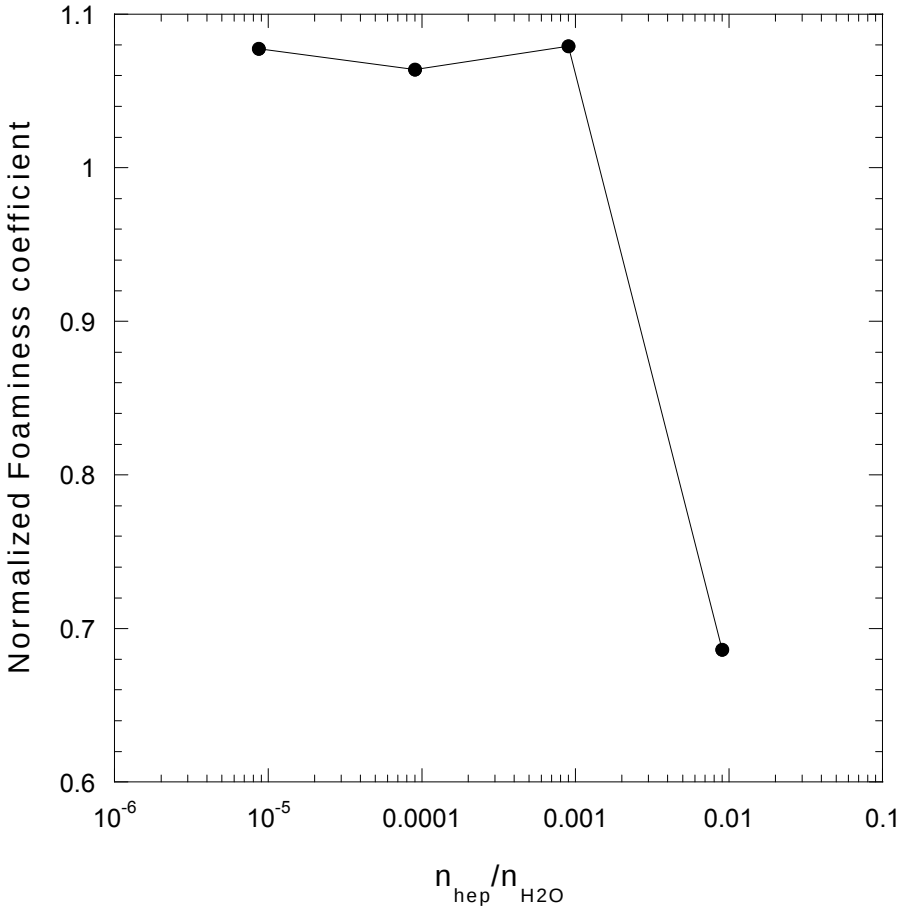

Figure 8: Normalized foaminess coefficient as a function of molar ratio of heptane to water for 8 m PZ solution with α= 0.3 at 40ºC

Antifoam

The effectiveness of antifoam in eliminating foaming of PZ solutions was tested. As illustrated in Figure 9, as low as 1 ppm antifoam is sufficient to reduce the foaminess coefficient by 15 to 20 times.

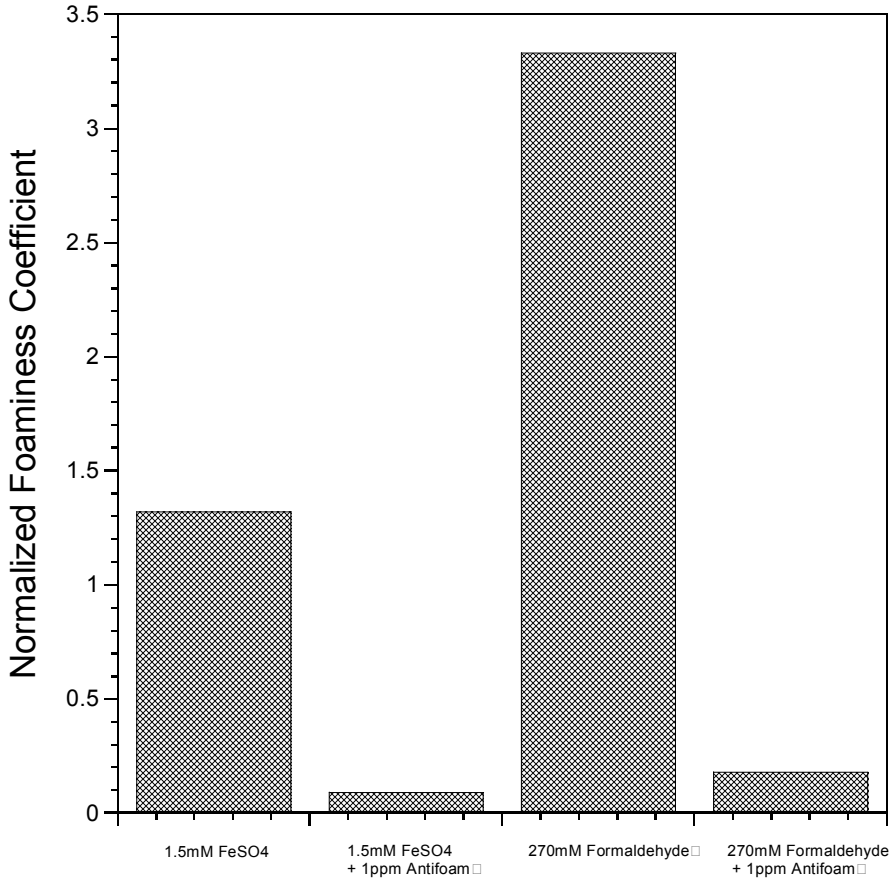

Figure 9: Effect of antifoam on normalized foaminess coefficient of solutions containing FeSO4 or formaldehyde at 40°C and α= 0.3

Sodium sulfite and formaldehyde

To verify the hypothesis that formaldehyde is the main promoter of foaming, another experiment was performed. It is well known that the sulfite can combine with formaldehyde to form hydroxymethanesulfonate which is soluble in water. Therefore sodium sulfite followed by 270 mM HCHO was added to the PZ solution. The foaming tendency of PZ with Na_2SO_3 or HCHO only was also tested for comparison. Note that Na_2SO_3 itself could increase foaming tendency. As shown inFigure 10, the presence of 270 mM Na_2SO_3 reduced F* of PZ with 270

mM HCHO from 3.3 to 1.4, but this was still higher than PZ solutions with 270 mM Na_2SO_3 only. It is likely that Na_2SO_3 competed with PZ in reacting with some of the HCHO and thus reduced the production of surface-active polymers. However, the addition of more Na_2SO_3 did not reduce the foaming of PZ contaminated with HCHO. Therefore Na_2SO_3 might not reverse the polymerization reaction between HCHO and PZ.

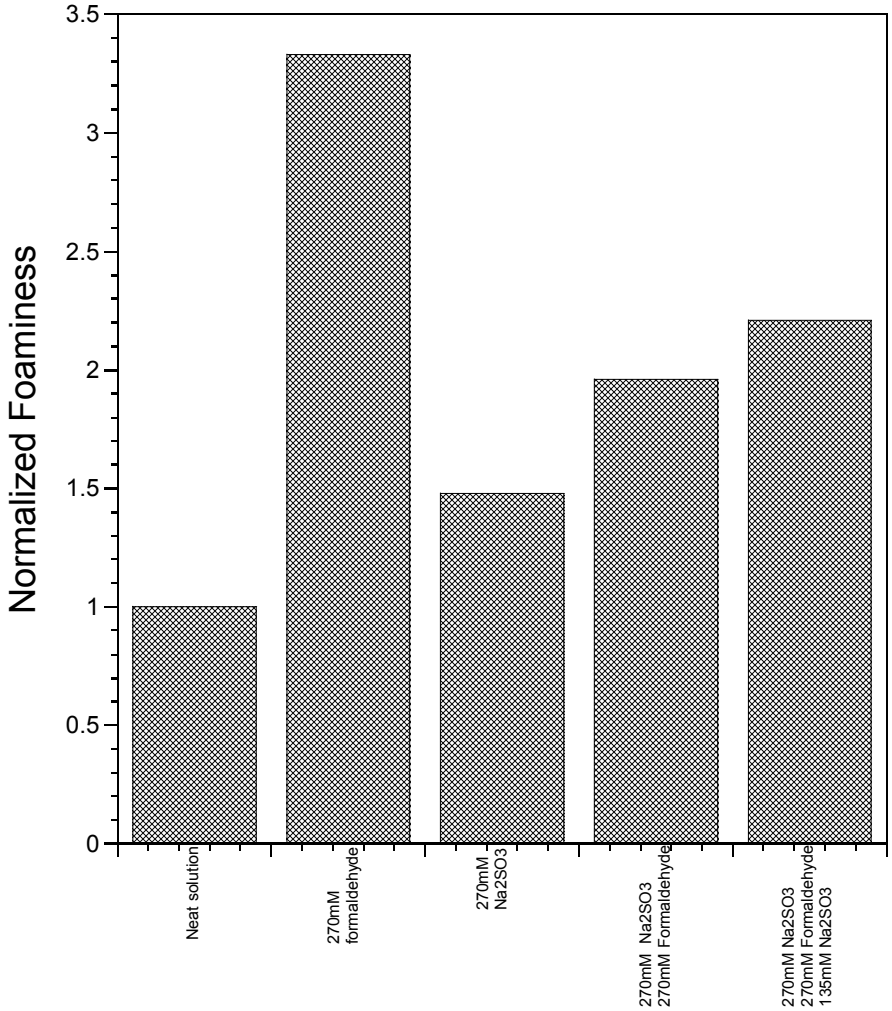

Figure 3: Effect of Na_2SO_3 on normalized foaminess coefficient of PZ solutions with or without HCHO at 40ºC and α= 0.3

Conclusions

Higher concentration of piperazine has a higher foaming tendency.

The presence of Fe^{2+} in solution could increase the foaming tendency of PZ solution by up to 40%, but it does not significantly affect the foaming of MEA solution.

Fe^{3+} up to 1 mM only slightly changes the foaming of PZ solution.

Addition of corrosion inhibitor Cu^{2+} or V^{5+} and oxidation inhibitor A does not increase foaming.

Formic acid does not change the foaming tendency of PZ solution; however, formaldehyde within its possible range greatly enhanced the foaming tendency.

Heptane has a negligible effect on the foaming tendency of PZ solutions as $n_{hep}/n_{H2O} < 9 \times 10^{-4}$, but it can destabilize foam as its concentration is increased to $n_{hep}/n_{H2O} = 9 \times 10^{-3}$.

A very small amount of silicone antifoam can greatly reduce foaming of contaminated PZ solutions.

It should be noted that although some additives tested in this study did not affect foaming tendency by themselves, the possibility that they could act as foaming promoters when other contaminants are present in the solutions is not excluded.

Appendix

Table 1: Summary of foaming test results in this work

Amine/Conc. (m)	α (mol/ mol)	N_2 flow rate (10^{-3}m/s)	Additives/Conc. (mM)	F ($10^{-3}m^2 \cdot s$)	Break time (s)	F*
PZ/2	0.3	2	X	16.7	5	0.21
PZ/4	0.3	2	X	19.5	7	0.25
PZ/6	0.3	2	X	34.9	12	0.44
PZ/8	0.3	2	X	78.8	29	1.00
PZ/8	0.3	2	FeCl3/0.01	73.1	27	1.00
PZ/8	0.3	2	FeCl3/0.1	76.5	28	1.05
PZ/8	0.3	2	FeCl3/0.2	87.0	31	1.19
PZ/8	0.3	2	FeCl3/0.3	81.1	35	1.11
PZ/8	0.3	2	FeCl3/0.5	79.1	35	1.08
PZ/8	0.3	2	FeCl3/1	78.7	40	1.08
PZ/8	0.3	2	X	85.8	30	1.00
PZ/8	0.3	2	FeSO4/0.1	92.2	35	1.07
PZ/8	0.3	2	FeSO4/0.2	98.8	39	1.15
PZ/8	0.3	2	FeSO4/0.3	106.3	48	1.24
PZ/8	0.3	2	FeSO4/0.5	122.1	>300	1.42
PZ/8	0.3	2	FeSO4/1.0	116.83	>300	1.36
PZ/8	0.3	2	FeSO4/1.5	113.33	>300	1.32
PZ/8	0.3	2	FeSO4/1.5 antifoam/1ppm	7.5	<2	0.09
PZ/8	0.3	2	X	64.9	30	1.00
PZ/8	0.3	2	FeSO4/0.1	67.7	37	1.04
PZ/8	0.3	2	FeSO4/0.3	182.0	75	2.80
PZ/8	0.3	2	FeSO4/1.0	181.7	>600	2.80

PZ/8	0.3	2	FeSO4/1 EDTA/100	238.5	>90	3.67
PZ/8	0.3	2	FeSO4/1 EDTA/100 antifoam/1ppm	12.5	<2	0.19
MEA/7	0.4	2	X	21.0	5	1.00
MEA/7	0.4	2	FeSO4/0.001	20.5	6	0.98
MEA/7	0.4	2	FeSO4/0.01	20.5	7	0.98
MEA/7	0.4	2	FeSO4/0.1	21.0	8	1.00
MEA/7	0.4	2	FeSO4/0.2	23.5	10	1.12
MEA/7	0.4	2	FeSO4/0.3	24.47	11	1.17
MEA/7	0.4	2	FeSO4/0.5	24.23	10	1.15
MEA/7	0.4	2	FeSO4/1.0	20.6	8	0.98
PZ/8	0.3	2.3	X	41.4	x	1.00
PZ/8	0.3	2.3	FeSO4 (solid)/0.11	44.6	x	1.08
PZ/8	0.3	2.3	FeSO4 (solid)/1.0	126.2	x	3.05
MEA/7	0.4	2.3	X	3.7	5	1.00
MEA/7	0.4	2.3	FeSO4 (solid)/0.11	29.0	6	7.84
MEA/7	0.4	2.3	FeSO4 (solid)/1.0	53.2	7	14.38
MEA/7	0.4	2.3	Formaldehyde/481	27.1	7	7.32
PZ/8 degraded oxidatively (OE4, 300ml)	0.3	2.3	CuSO4 inhibitor A	>303.5	N/A	N/A
PZ/8	0.3	2	X	88.3	31	1.00
PZ/8	0.3	2	CuSO4/5.0	86.3	30	0.98
PZ/8	0.3	2	CuSO4/5.0	75.0	33	0.85

			Inhibitor A/100			
PZ/8	0.3	2	CuSO4/5.0 Inhibitor A/100 FeSO4/0.1	79.8	35	0.90
PZ/8	0.3	2	NaVO3/10.0 FeSO4/0.1	67.6	28	0.77
PZ/8	0.27	2	X	80.5	28	1.00
PZ/8	0.27	2	Formic Acid/500	85.1	30	1.06
PZ/8	0.27	2	Formaldehyde/500	>338.3	>180	>4.20
PZ/8	0.3	2	X	95.8	34	1.00
PZ/8	0.3	2	Formaldehyde/10	102.8	34	1.07
PZ/8	0.3	2	Formaldehyde/30	107.4	35	1.12
PZ/8	0.3	2	Formaldehyde/90	133.6	50	1.39
PZ/8	0.3	2	Formaldehyde/270	>319	N/A	3.33
PZ/8	0.3	2	Formaldehyde/270 Antifoam/1ppm	17.4	20	0.18
PZ/8	0.3	2	Formaldehyde/270 Antifoam/2ppm	12.0	15	0.12
PZ/8	0.3	2	Na2SO3/270	141.4	55	1.48
PZ/8	0.3	2	Na2SO3/270 Formaldehyde/270	188.2	67	1.96
PZ/8	0.3	2	Na2SO3/270 Formaldehyde/270 Na2SO3/135	212.0	80	2.21
PZ/8	0.3	2	X	95.0	34	1.00
PZ/8	0.3	2	Heptane/41 ppm	102.4	34	1.08
PZ/8	0.3	2	Heptane/428 ppm	101.1	35	1.06
PZ/8	0.3	2	Heptane/4287 ppm	102.5	50	1.08

PZ/8	0.3	2	Heptane/40853 ppm	65.2	N/A	0.69

References

Abdi, MA & A Meisen. "Amine Degradation: Problems, Review of Research Achievements, Recovery Techniques". *Proc 2nd Int'l Oil, Gas and Petrochem Conf*. Tehran. 2000.

Al-Dhafeeri, MA. "Identifying sources key to detailed troubleshooting of amine foaming". *Oil & Gas J.* 2007;105(32):56.

Bishnoi, S & GT Rochelle."Absorption of carbon dioxide into aqueous piperazine: reaction kinetics, mass transfer and solubility". *Chem Eng Sci.* 2000;55(22):5531–5543.

Freeman, S & GT Rochelle. "Degradation of concentrated aqueous piperazine". *First Quarterly Progress Report*. 2008.

Marche, C *et al*. "Solubilities of n-Alkanes (C6 to C8) in Water from 30°C to 180°C". *J Chem & Eng Data*. 2003;48(4):967–971.

McCarthy, J & MA Trebble. "An experimental investigation into the foaming tendency of diethanolamine gas sweetening solutions". *Chem Eng Comm*. 1996;144:159–171.

Pauley, CR. "Face the facts about amine foaming". *Chem Eng Prog*. 1991;87(7):33–8.

Pauley, CR *et al*. "Analysis of foaming mechanisms in amine plants". *Proc Laurance Reid Gas Cond Conf.* 1989:219–47.

Pauley, CR *et al*. "Ways to control amine unit foaming offered". *Oil & Gas J*. 1989;87(50):67–75.

Spooner, B *et al*. "Iron Sulphides—Friend or Foe?" *Proc Laurance Reid Gas Cond Conf*. 2006:109.

Stewart, EJ & RA Lanning. "Reduce Amine Plant Solvent Losses". *Hydroc Proc*. 1994;73(5):67–81.

Thitakamol, B & A Veawab. "Foaming Behavior in CO_2 Absorption Process Using Aqueous Solutions of Single and Blended Alkanolamines". *Ind & Eng Chem Res*. 2008;47(1):216–225.

von Phul, SA. "Sweetening Process Foaming and Abatement". *Proc Laurance Reid Gas Cond Conf*. 2001: 251–280.

Influence of Viscosity and Surface Tension on the Effective Mass Transfer Area of Structured Packing

Quarterly Report for July 1 – September 30, 2008

by Robert Tsai

Supported by the Luminant Carbon Management Program

Department of Chemical Engineering

The University of Texas at Austin

October 9, 2008

Abstract

Three mass transfer tests with Sulzer Mellapak 250Y were performed: baseline, low surface tension ($\sigma \sim 30$ dynes/cm), and moderate viscosity ($\mu_L \sim 4$ cP, $\sigma \sim 55$ dynes/cm). The experimental database was updated to incorporate these data, which further bolstered our main conclusions: no effect of viscosity and a weak effect of surface tension on the effective area. The current global (a_e/a_p) correlation, able to represent the entire database within limits of ±15%, is as follows:

$$\frac{a_e}{a_p} = 1.198\left[(We_L)(Fr_L)^{-1/3}\right]^{0.121}$$

It should be noted that the model was changed from a basis of $(Ca_L)(Re_L)^{2/3}$ (presented in the previous quarterly report) to $(We_L)(Fr_L)^{-1/3}$, in consideration of the fact that the corrugation angle (α) has been held constant (45°) in the packings characterized thus far. $((Ca_L)(Re_L)^{2/3}$ and $(We_L)(Fr_L)^{-1/3}$ are identical when expanded to physical parameters, except that the former includes an additional α term.) A manuscript for the upcoming 9th International Conference on Greenhouse Gas Control Technologies (GHGT-9) was prepared that summarizes essentially all of the mass transfer-related results that have been obtained in this body of research.

The hydraulic behavior (pressure drop and hold-up) of Mellapak 250Y under low surface tension conditions ($\sigma \sim 30$ dynes/cm) was investigated. Hold-ups appeared to be lower compared to the base case (water), similar to what was observed with Mellapak 500Y. Pressure drop trends, on the other hand, were difficult to definitively characterize.

Introduction

Packing is commonly used in industrial processes as a means of promoting efficient gas-liquid contact. One important application for which packed columns are being considered is treating flue gas for CO_2 capture. The conventional method consists of an aqueous amine solvent such as monoethanolamine (MEA) contacting the gas, resulting in the absorption of CO_2 (Kohl & Nielsen, 1997). The enriched solvent is sent to a stripper for regeneration and is then recycled back to the absorber. Gas-liquid contact in both the absorber and stripper is enhanced through the use of packing.

Reliable mass transfer models are necessary for design and analysis purposes. A critical factor involved in modeling is the prediction of the effective interfacial area of packing (a_e), which can be considered as the total gas-liquid contact area that is actively available for mass transfer. The current research effort is focused on this parameter. Characterization of effective areas is vital to amine-based CO_2 capture at the industrial level, because absorption rates actually become independent of conventional mass transfer coefficients (k_G or k°_L) but remain directly proportional to the effective area. Thus, it is highly desirable to have an accurate area model.

Numerous packing area correlations have been presented in the literature, but none has been shown to be predictive over a wide range of conditions. The Rocha-Bravo-Fair (Rocha *et al*., 1996) and Billet-Schultes (Billet and Schultes, 1993) models, two of the more widely used correlations for structured packing, seem to be notably poor in their predictions involving aqueous systems. Wang *et al*. (2005) performed a comprehensive review of the available models. The various correlations predict different and sometimes even contradictory effects of liquid viscosity and surface tension, properties that would be expected to fundamentally influence the wetted area of packing. It is evident that their role is not well understood, and there is a definite need for work in this subject matter.

The Separations Research Program (SRP) at the University of Texas at Austin has the capability of measuring packing mass transfer areas. Measurements are performed by absorbing CO_2 from air with 0.1 M NaOH in a 427 mm (16.8 in) ID column. Unfortunately, physical parameters are limited to those of water, making it potentially inaccurate to extend these results to other fluids of interest, such as amine solvents, due to the differences in viscosity and surface tension.

Limited understanding of the fluid mechanics and mass transfer phenomena in packed columns has been noted, and the need for experiments over a broader range of conditions has been identified (Wang *et al*., 2005). The goal of this research is to address these shortcomings and ultimately develop an improved effective area model for structured packing. The general objectives are to:

- Develop a fundamental understanding of the fluid mechanics associated with structured packing operation;
- Determine suitable chemical reagents to modify the surface tension and viscosity of the aqueous caustic solutions employed to make packing area measurements, and characterize potential impacts of such additives on the CO_2-NaOH reaction kinetics;
- Expand the SRP database by measuring the mass transfer areas of several different structured packings over a range of liquid viscosities and surface tensions;
- Combine the data and theory into a semi-empirical model that captures the features of the tested systems and adequately represents effective area as a function of viscosity, surface tension, and liquid load.

Experimental

427 mm ID Packed Column

The packed column had an outside diameter of 460 mm (18 in), inside diameter of 427 mm (16.8 in), and a 3 m (10 ft) packed height. For details regarding the apparatus and procedure for mass transfer or hydraulic tests, earlier quarterly reports may be consulted.

Goniometer

The goniometer (ramé-hart Inc., Model #100-00) included an adjustable stage, a syringe support arm, a computer-linked camera for live image display, and a light source (see Q3 2006 report). This system was used in conjunction with FTA32 Video 2.0 software (developed by First Ten Angstroms, Inc.) to make surface tension measurements via the pendant drop method.

Rheometer

The Physica MCR 300 rheometer (Anton Paar, USA) employed for viscosity measurements was first described in the Q4 2006 report. The apparatus was equipped with a cone-plate spindle (CP 50-1). Temperature was regulated (±0.1°C) with a Peltier unit (TEK 150P-C) and a Julabo F25 water bath unit (for counter-cooling). Measurement profiles consisted of a logarithmically increased or decreased shear rate (100 to 500 s^{-1}), with 10-20 data points recorded at 15 second intervals. Viscosity was determined from a plot of shear stress (measured) vs. shear rate.

Materials

A nonionic surfactant, Tergitol^{TM} NP-7 (Dow), was used to reduce the surface tension of solutions. POLYOX WSR N750 (Dow) – essentially, poly(ethylene

oxide) with a molecular weight of 300,000 – was employed as a viscosity enhancer. Dow Corning® Q2-3183A antifoam was used for foam suppression.

Results and Discussion

Mass Transfer Area Database

The results obtained from the WWC and packed column are summarized and discussed in the GHGT-9 manuscript (attached).

Mellapak 250Y – Hydraulics

The hydraulic behavior of Sulzer Mellapak 250Y (M250Y) structured packing was investigated under low surface tension conditions ($\sigma \sim 30$ dynes/cm). Figures 1 and 2 present the data at liquid loads of 2.5 and 10 gpm/ft^2 together with baseline results (obtained with water), zoomed in on the pre-loading region. A correlation for the dry pressure drop (ΔP_{dry}) was developed from numerous measurements, since they were found to be quite consistent. The data are plotted as normalized pressure drops to exaggerate any surface tension-associated effects.

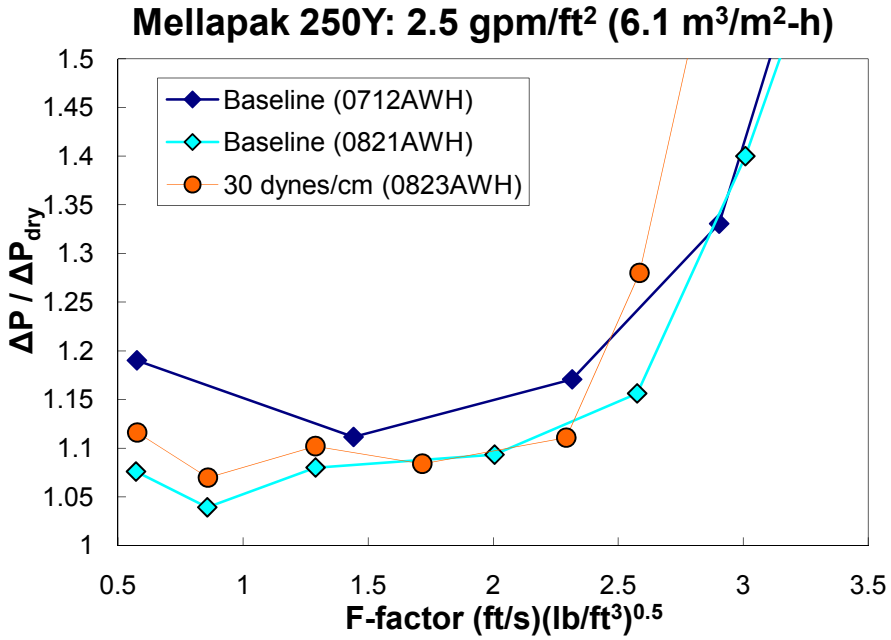

Figure 1: Mellapak 250Y pressure drop data at liquid load of 2.5 gpm/ft^2

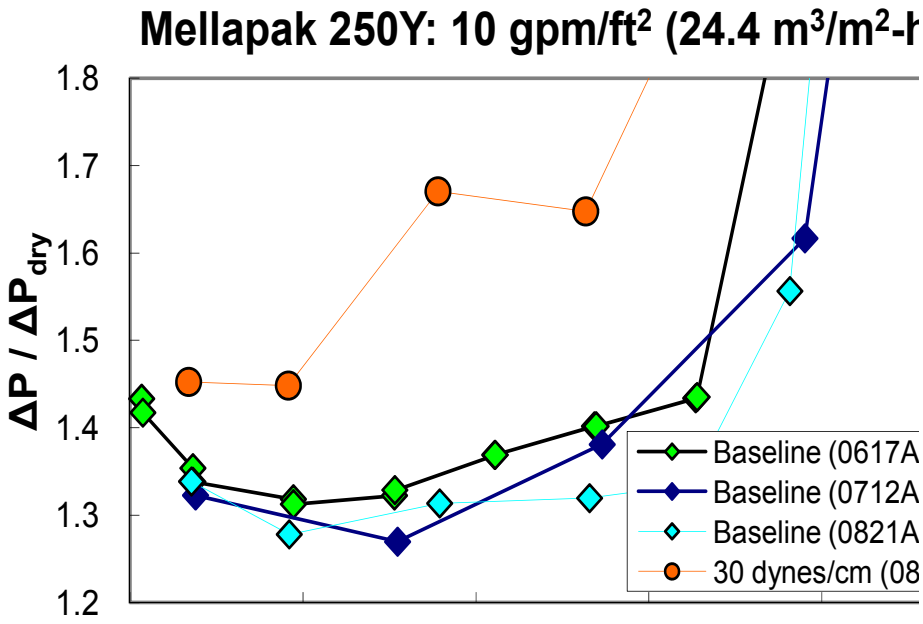

Figure 2: Mellapak 250Y pressure drop data at liquid load of 10 gpm/ft^2

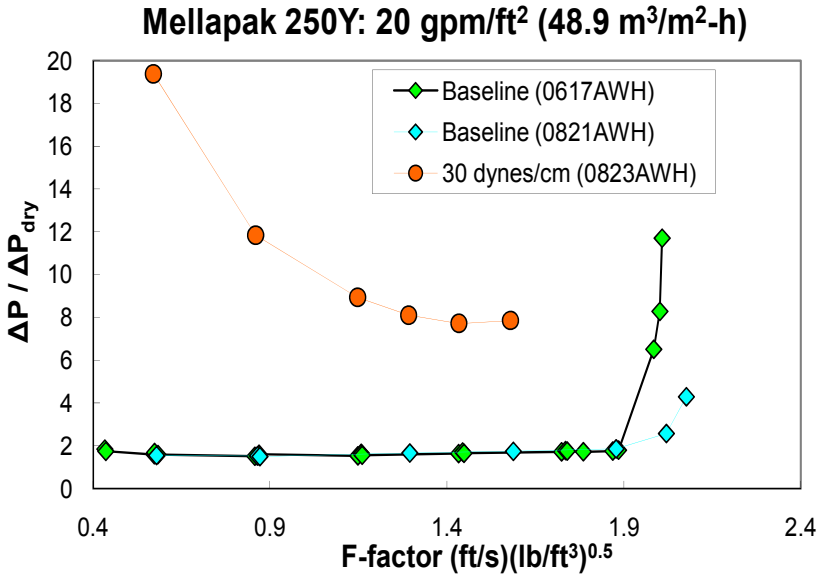

Figure 3: Mellapak 250Y pressure drop data at liquid load of 20 gpm/ft^2

Figures 1 and 2 illustrate the inconsistent behavior observed with the low surface tension system. Pressure drops were comparable to water at the lower liquid loads ($\leq$ 5 gpm/ft^2) but deviated (greater ΔP) at higher loads. This is in contrast with Mellapak 500Y, where a reduced surface tension resulted in consistently lower pressure drops relative to the base case (see Q2 2008 report). Capillary phenomena (i.e. liquid bridging and pooling) have often been proposed to explain the distinction between M250Y and M500Y (Tsai *et al*., 2008) and could serve as a possible reason again here. A reduction in pressure drop for M500Y would be understandable, due to elimination of "trapped" liquid within the narrow crevices of the packing. These would be much less of an issue with M250Y, so likewise, the effect of surface tension would be expected to be minimal. This was indeed the case at the lower, presumably foam-free liquid loads. At the higher loads (e.g. 10, 15 gpm/ft^2), mild foaming could have perhaps contributed to the pressure drop, even though the trend was not really indicative of a foaming problem – where (ΔP/ΔP$_{dry}$) traditionally has exhibited a decrease with F-factor (Figure 3).

Figure 4 compares the low surface tension hold-up data with the base case. The results are presented as a differential hold-up: (measured hold-up) – (average hold-up with water at the same liquid load).

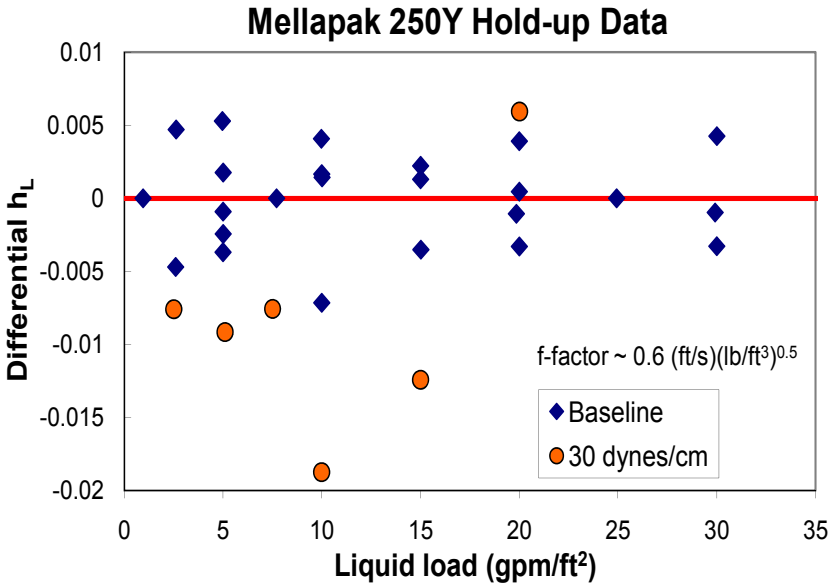

Figure 4: Mellapak 250Y hold-up data

The reduced surface tension resulted in marginally lower hold-up values. This was to be anticipated with M500Y (see Q2 2008 report) but not necessarily with

M250Y. The deviation at 20 gpm/ft^2 was likely due to foam; based on past experience with M500Y, foam tends to increase the measured hold-up (relative to identical conditions with seemingly less or no foam). This would suggest that the measurements at 10 and 15 gpm/ft^2 were not affected by foam, as was speculated earlier.

Conclusions

Hydraulic data for Mellapak 250Y and 500Y have been obtained over a range of viscosities (1–15 cP) and surface tensions (30–72 dynes/cm). For both packings, the liquid hold-up trends appear to be similar: an increase in hold-up with viscosity (data not shown in this report) and a slight decrease in hold-up under low surface tension conditions ($\sigma \sim 30$ dynes/cm). The latter result was expected to be more drastic for M500Y, but this was not the case. The pressure drop behavior of the packings was not as consistent – at least, with respect to surface tension. The surfactant system generally yielded lower pressure drops relative to water for M500Y (coinciding with reduced hold-ups). The pressure drops for M250Y, on the other hand, were either unchanged or higher. Pressure drop and hold-up should probably be linked closely together, but at the moment, the various data sets do not seem particularly relatable.

Future Work

Mass transfer experiments with a prototype 500-series packing are presently being conducted, to see if the surface tension effect observed with Mellapak 500Y can be reproduced. Hydraulic and mass transfer tests with Mellapak 250X (60˚ corrugations) at various viscosities and surface tensions are also planned. The current mass transfer model will be further refined by means of these additional data, as well as theoretical considerations.

Nomenclature

a_e = effective area of packing, m^2/m^3

a_p = specific (geometric) area of packing, m^2/m^3

h_L = (total) liquid hold-up, dimensionless

P = pressure, Pa

Greek Symbols

μ = dynamic viscosity, kg/(m-s)

σ = surface tension, N/m

Subscripts

G = gas phase

L = liquid phase

Dimensionless Groups

a_f = fractional area of packing, a_e/a_p

Ca = Capillary number, $\frac{\mu u}{\sigma}$

Fr = Froude number, $\frac{u^2}{g\delta}$

Re = Reynolds number, $\frac{\rho u \delta}{\mu}$

We = Weber number, $\frac{\rho u^2 \delta}{\sigma}$

References

Billet, R & M Schultes. "Predicting Mass Transfer in Packed Columns". *Chem Eng Technol.* 1993;16 (1):1–9.

Kohl, A & R Nielsen. *Gas Purification*; Gulf Publishing Co.: Houston, 1997.

Rocha, JA, JL Bravo, JR Fair. "Distillation Columns Containing Structured Packings: A Comprehensive Model for Their Performance. 2. Mass-Transfer Model". *Ind Eng Chem Res.* 1996;35 (5):1660–1667.

Tsai, RE, P Schultheiss, A Kettner, JC Lewis, AF Seibert, RB Eldridge,GT Rochelle. "Influence of Surface Tension on Effective Packing Area". *Ind Eng Chem Res.* 2008;47 (4):1253–1260.

Wang, GQ, XG Yuan, KT Yu. "Review of Mass-Transfer Correlations for Packed Columns". *Ind Eng Chem Res.* 2005;44(23):8715–8729.

Modeling Stripper Performance for CO_2 Removal

Quarterly Report for July 1 – September 30, 2008

by David Van Wagener

Supported by the Luminant Carbon Management Program

and the

Industrial Associates Program for CO_2 Capture by Aqueous Absorption

Department of Chemical Engineering

The University of Texas at Austin

October 20, 2008

Abstract

In this quarter comparative work for MEA was continued. A pilot plant run with 35% MEA was carried out recently at the J. J. Pickle Research Campus, and the last MEA model developed by Marcus Hilliard was utilized to reconcile the data. All values were able to be matched using 25% of the actual packing height. The MEA model was also used to evaluate performance of a new configuration, a three-stage flash with a preheater. The three-stage flash performed best with solar heat as an energy source, and this configuration reduced the equivalent work requirement using 9 m MEA by 1 kJ/mol CO_2 compared to a 2.1 atm simple stripper. Lastly, a piperazine model also developed by Hilliard was used to compare the performance of MEA to PZ in a simple stripper. All simulations used equivalent rate streams, but a rich stream more concentrated in CO_2 was used for one piperazine case due to the faster rates expected in the absorber. The 8 m PZ case with a richer inlet proved to require 10% less energy than the 7 m MEA base case.

Introduction

Piperazine is of interest as a solvent because it has no detectable thermal degradation at least up to 150°C. Many explored stripper configurations operate more efficiently at high temperatures, so it is expected that piperazine will perform better than the baseline, MEA. In addition to being able to operate at high temperatures, piperazine has two amine groups. Since each molecule has twice the alkalinity of MEA, it will achieve richer solutions in the absorber with faster rates, and it will require less sensible heat and the stripper with a higher capacity.

Methods and Results

In addition to the work detailed in the paper for GHGT-9 (attached), work was also done this quarter using the H_2O-PZ-CO_2 to simulate a simple stripper section. 8 m PZ has been projected to perform better than the baseline, MEA, due to its two amine groups per molecule, which increase its capacity and reaction rates. Modeling has not been done for this solvent because it was thought that concentrated piperazine solvents were not soluble. However, dissolving piperazine in water while loading the solution results in a higher solubility due to the formation of electrolyte species. The simple stripper was modeled using 8 m PZ as well as 7 m MEA and 9 m MEA. The simulations were performed in Aspen Plus® using thermodynamic packages developed by Hilliard (2008). The packages utilize the electrolyte-NRTL method and include many regressed parameters, including constants for the binary interaction parameters, τ.

All solvents were simulated using a rich feed loading corresponding to a 5 kPa P^*_{CO2} at 40°C. Additionally, 8 m PZ was simulated using a 7.5 kPa P^*_{CO2} at 40°C, justified by the fact that its reaction rate with CO_2 is roughly double compared to MEA. Other variables held constant in the simulations included a 5°C cold side temperature approach for the cross heat exchanger, a 10°C approach in the reboiler, 15 m of MTL's CMR NO-2P packing, an 80% approach to flood, and final compression to 5 MPa. The equivalent work was minimized by varying the specified lean loading. The response of the equivalent work to the specified lean loading is demonstrated in Figure 1.

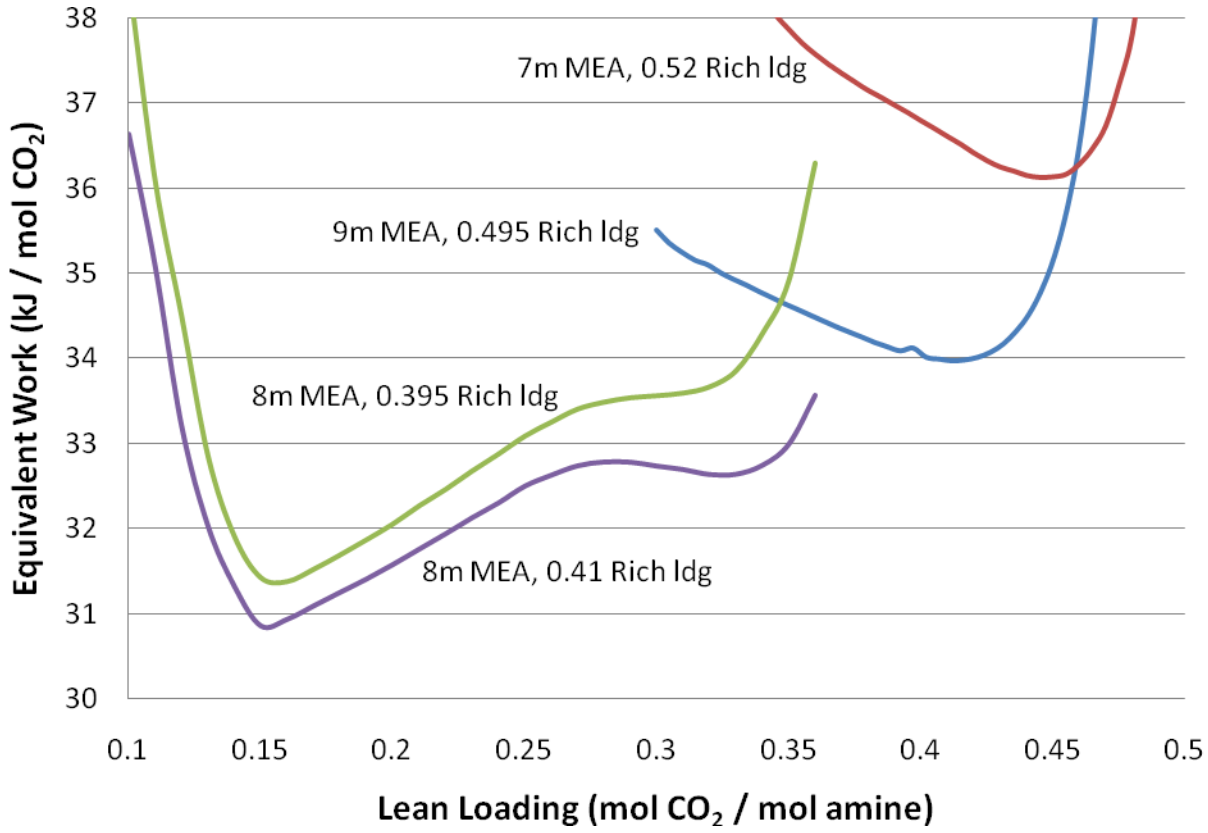

Figure 1: Equivalent Work Response to specified lean loading. All solvents modeled with 5 kPa P^*_{CO2} at 40°C except 8 m PZ which was also modeled with 7.5 kPa P^*_{CO2} at 40°C. Compression to 5 MPa, 5°C cross exchange approach, 15 m CMR packing, 80% approach to flood.

The piperazine solvent has a clear benefit over the baseline, 7 m MEA, as well as the improved baseline, 9 m MEA. The proposed optimum of the richer 8 m PZ is 32.6 kJ/mol CO_2 and it occurs with a lean loading of 0.32. This energy requirement is roughly a 10% improvement over the baseline, which required 36.1 kJ/mol CO_2 at its optimum. The simulation results suggest that the rich 8 m PZ has a global optimum of 30.9 kJ/mol CO_2 with a lean loading of 0.15, but the reduction in equivalent work at low lean loadings is probably due to inaccurate extrapolation by the model. As shown by figures 2 and 3, the heat capacity and heat of vaporization for CO_2 varies wildly past a temperature of 110°C. In the simulations the total work began decreasing as the reboiler temperature surpassed 110°C and therefore, are judged to be inaccurate for the time being.

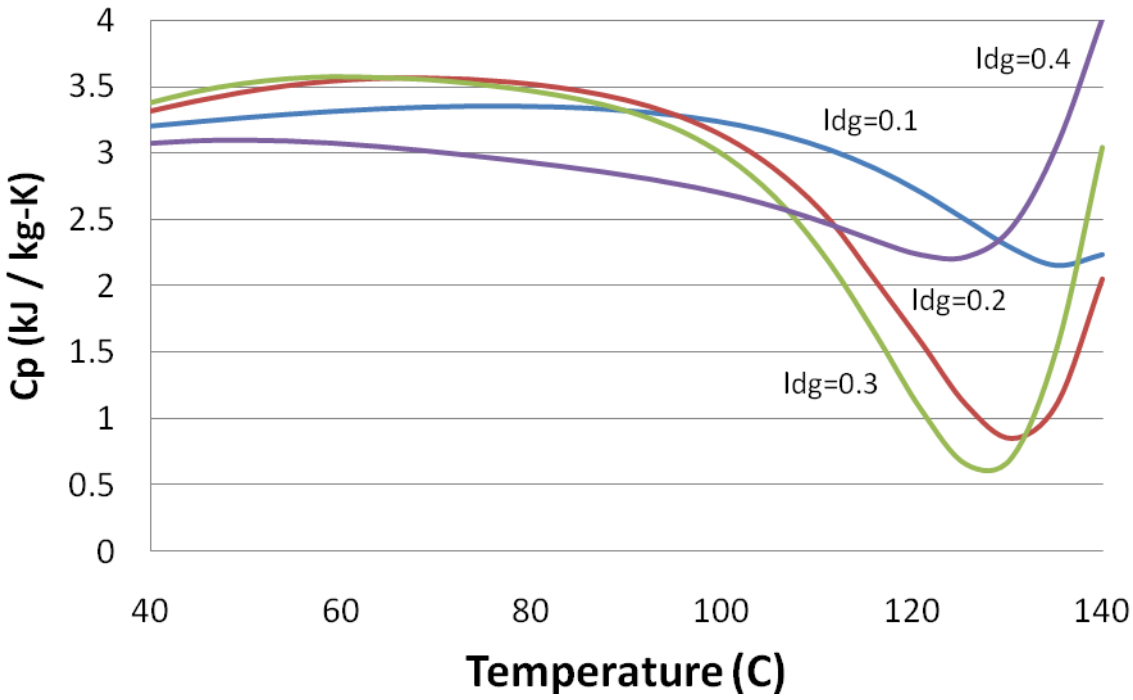

Figure 2: Heat Capacity Predicted by Hilliard Piperazine Model in Aspen Plus®

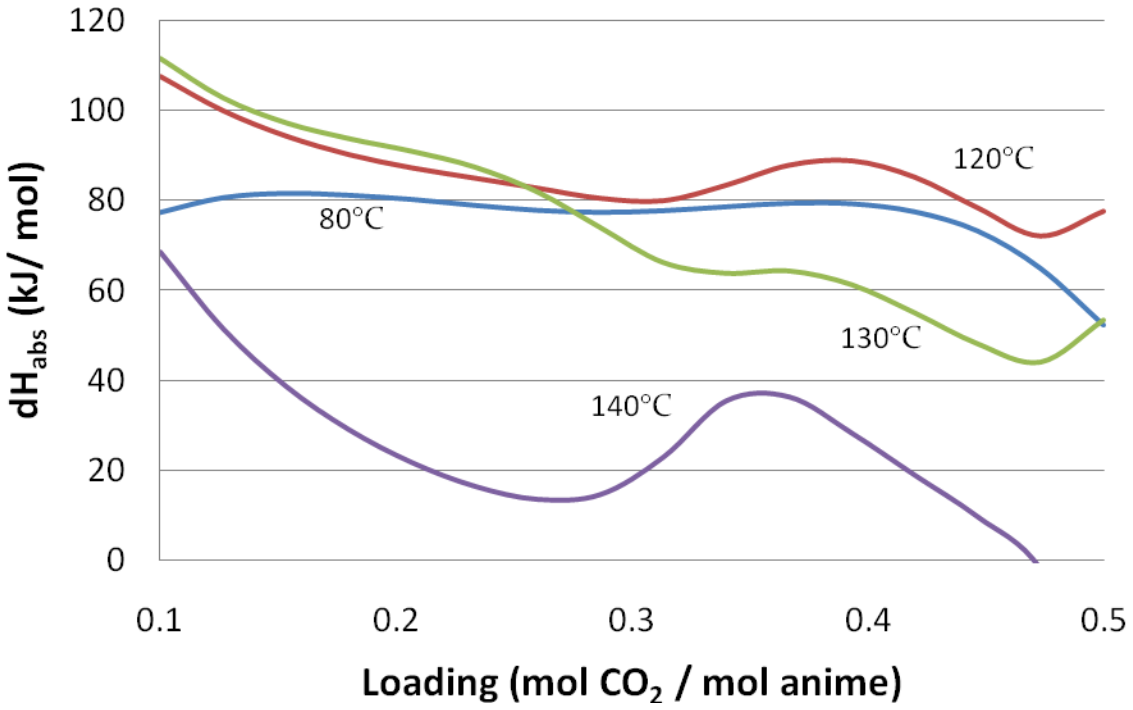

Figure 3: ΔHabs of CO_2 Predicted by Hilliard Piperazine Model in Aspen Plus®

Conclusions

- The new MEA model developed by Hilliard was applied to recent pilot plant results. The simulation results could be matched to the experimental results, but only 25% of the packing was needed.
- The three-stage flash configuration proved to be beneficial for 9 m MEA compared to a simple stripper. While still using steam heating, the three-stage flash required 0.5 kJ/mol CO_2 less than a simple stripper with an equivalent maximum temperature.
- The three-stage flash required 1 kJ/mol CO_2 less than a simple stripper with a maximum equivalent temperature if solar heat was used for the three-stage flash.
- Solar heat does not improve the performance of a simple stripper with a typical kettle or thermosyphon reboiler.
- In a preliminary analysis, 8 m PZ improves the performance of the stripper section by 10% compared to 7 m MEA.

Future Work

The piperazine model will be applied to the double matrix and three-stage flash configurations. If high temperatures are desirable for these configurations, the model must first be adjusted to perform better at high temperatures.

A variety of configurations with varying levels of complexity will be developed and analyzed to determine any correlation between complexity and performance.

References

Chen, E. "Carbon Dioxide Absorption into Piperazine Promoting Potassium Carbonate Using Structured Packing." Ph.D. Dissertation. University of Texas at Austin, 2007.

Hilliard, M. "A Predictive Thermodynamic Model for an Aqueous Blend of Potassium Carbonate, Piperazine, and Monoethanolamine for Carbon Dioxide Capture from Flue Gas". Ph.D. Dissertation. University of Texas at Austin, 2008.

Onda, K, Takeuchi, H, Okumoto,Y. "Mass transfer coefficients between gas and liquid phases in packed columns". *J Chem Eng Jpn.* 1968;1:56–62.

Oyenekan, B. "Modeling of Strippers for CO_2 Capture by Aqueous Amines". Ph.D. Dissertation. University of Texas at Austin, 2007.

Modeling CO_2 Absorption Using Aqueous Amines

Progress Report for July – September, 2008

by Jorge M. Plaza

Supported by the Luminant Carbon Management Program

and the

Industrial Associates Program for CO_2 Capture by Aqueous Absorption

Department of Chemical Engineering

The University of Texas at Austin

November 3, 2008

Abstract

A new model for the absorption of carbon dioxide from flue gas by aqueous MEA was presented in the 2nd quarter report (Plaza, 2008). It incorporates the thermodynamic model by Hilliard (2008) and simplified kinetics consisting of two equilibrium equations and four kinetic reactions. Carbamate formation rates were obtained by simulating the conditions of the laminar jet used by Aboudheir (2002) with an absorber model generated in Aspen Plus®. The bicarbonate forward rate was approximated using data presented by Rochelle *et al.* (2001). Density, viscosity, thermal conductivity and surface tension of the CO_2 – MEA – H_2O system along with carbon dioxide diffusivity in water were corrected based on work by Aspen Technology, Inc. (Huiling and Chen, 2008). Reaction kinetics were revised considering the mentioned properties correction. Results are presented in this report.

The final model incorporated the wetted area correlation developed by Tsai (Tsai *et al.*, 2008). Model validation work with the 9 m pilot plant data was revised. Liquid film segmentation was modified and 16 segments were determined to be optimal. Various packing segmentations were evaluated along with the countercurrent flow model. Temperature profiles using the latter resulted higher than the experimental values. CO_2 loadings, MEA concentration, and removal percentage were matched by the model. This report includes details on the modifications to the model and reconciliation results.

Work was conducted to specify an absorber for the optimized stripper conditions obtained by Van Wagener (Plaza *et al.*, 2008). Results showed that intercooling made it feasible to reach 90% removal with the specified conditions. The minimum packing height required was 5.2 m of Flexipac 1Y using optimized intercooling.

Description

MEA Model Development

As described in the 2nd quarter report (Plaza, 2008) Aboudheir (2002) generated rate data for CO_2 absorption in MEA using a laminar jet at various amine concentrations, CO_2 loadings, and temperatures. This data was used to evaluate the forward rate constants for the formation of carbamate using Aspen Plus® RateSep™. Kinetics were represented using the following set of reactions:

$$2\ MEA + CO_2 \rightarrow MEA^+ + MEACOO^- \quad (1)$$

$$MEA^+ + MEACOO^- \rightarrow 2\ MEA + CO_2 \quad (2)$$

$$MEA + CO_2 + H_2O \rightarrow HCO_3^- + MEA^+ \quad (3)$$

$$MEA^+ + HCO_3^- \rightarrow MEA + CO_2 + H_2O \quad (4)$$

Two similar equilibrium reactions were used to represent the chemistry:

$$2\ MEA + CO_2 \leftrightarrow MEA^+ + MEACOO^- \quad (5)$$

$$MEA + CO_2 + H_2O \leftrightarrow HCO_3^- + MEA^+ \quad (6)$$

Parameters for density, viscosity, thermal conductivity, and surface tension of the CO_2 – MEA – H_2O mixture and for the diffusivity of carbon dioxide in water were modified based on work by Aspen Technology, Inc. (Huiling and Chen, 2008) to better match experimental values.

The carbamate reaction kinetic constants were obtained following the same methodology used in the second quarter. There was no significant change in the values of the constants. The resulting expressions are as follows:

$$forward\ rate\left(\frac{kmol}{m^3-s}\right) = 5.31\times10^9\ exp\left(-\frac{14610}{8.314}\right)a_{MEA}^2\,a_{CO_2} \quad (7a)$$

$$Reverse\ rate\left(\frac{kmol}{m^3-s}\right) = 4.75\times10^8\ exp\left(-\frac{102740}{8.314}\right)a_{MEACOO^-}a_{MEAH^+} \quad (7b)$$

The bicarbonate reaction rate expressions were not changed from the second quarter:

$$forward\ rate\left(\frac{kmol}{m^3-s}\right) = 9026\ exp\left(-\frac{49000}{8.314}\right)a_{MEA}\,a_{CO_2} \quad (8a)$$

$$Reverse\ rate\left(\frac{kmol}{m^3-s}\right) = 2917\ exp\left(-\frac{114280}{8.314}\right)\frac{a_{HCO_3^-}a_{MEAH^+}}{a_{H_2O}} \quad (8b)$$

Pilot plant model validation

The proposed model was used to simulate the conditions of the October 2007 Pilot Plant MEA campaign at the University of Texas at Austin Pickle Research Center. The stream conditions recorded for the absorber are presented in Figure 1. This campaign used 35 wt % MEA and 2 packing beds of 3.05 m (equivalent to 6.10 m of packing as Figure 1 shows).

Modifications to the previous validation work included the incorporation of the physical properties parameters developed by Aspen and the inclusion of a Fortran subroutine to calculate interfacial area based on the work by Tsai (Tsai *et al.*, 2008).

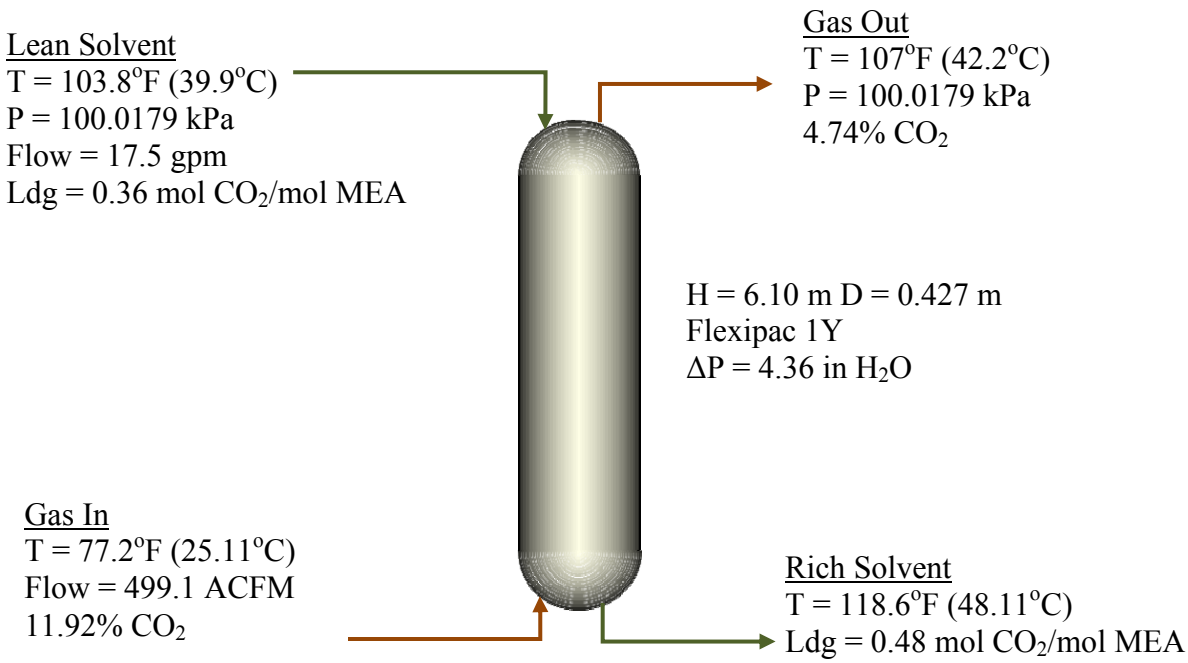

Figure 1: October 2007 MEA Campaign reported absorber stream conditions

The inlet conditions were entered into an absorber model in Aspen Plus®. As in previous work the absorber packing was divided into 12 equal stages and the liquid film was maintained segmented into 40 parts. In an effort to reduce the number of segments in the film, the interfacial CO_2 composition profile was plotted to determine the best way to represent behavior at the boundary layer with less segments. Figure 2 shows the resulting profiles for three segmentation schemes: 40 equally spaced segments, 10 segments (six segments within the 10% distance from the interface) and 16 optimized segments. The latter were defined by looking at the 40 segment plot including more points where large slope changes were observed. As the figure shows the 16 segments better represent the larger curvature change between 1μm and 0.1 μm that had been missed by the equally spaced segmentation. The effects of film segmentation are visible in the temperature profiles (Figure 3). The no segmentation profiles are well below the reported pilot plant values. The effect of segmentation in loadings and removal is shown in Table 1.

Table 1: Model performance results for the pilot plant absorber with various liquid film segments

Segments	None	40	16	10
Rich loading (mol CO_2/mol MEA)	0.4330	0.4202	0.4216	0.4202
Removal (%)	75.8%	66.5%	66.8%	66.5%

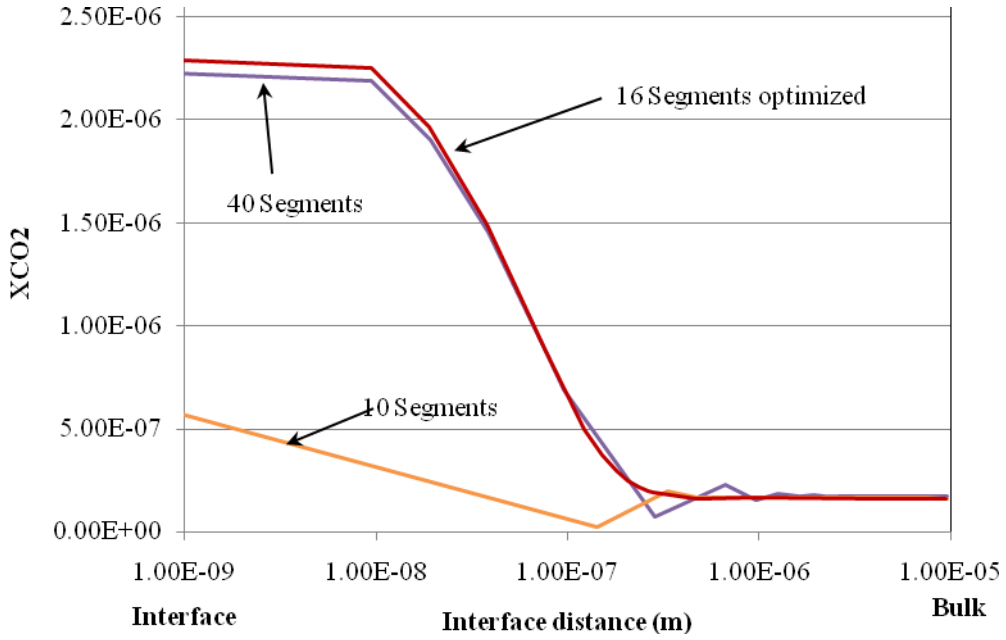

Figure 2: Liquid Interface CO_2 concentration profiles

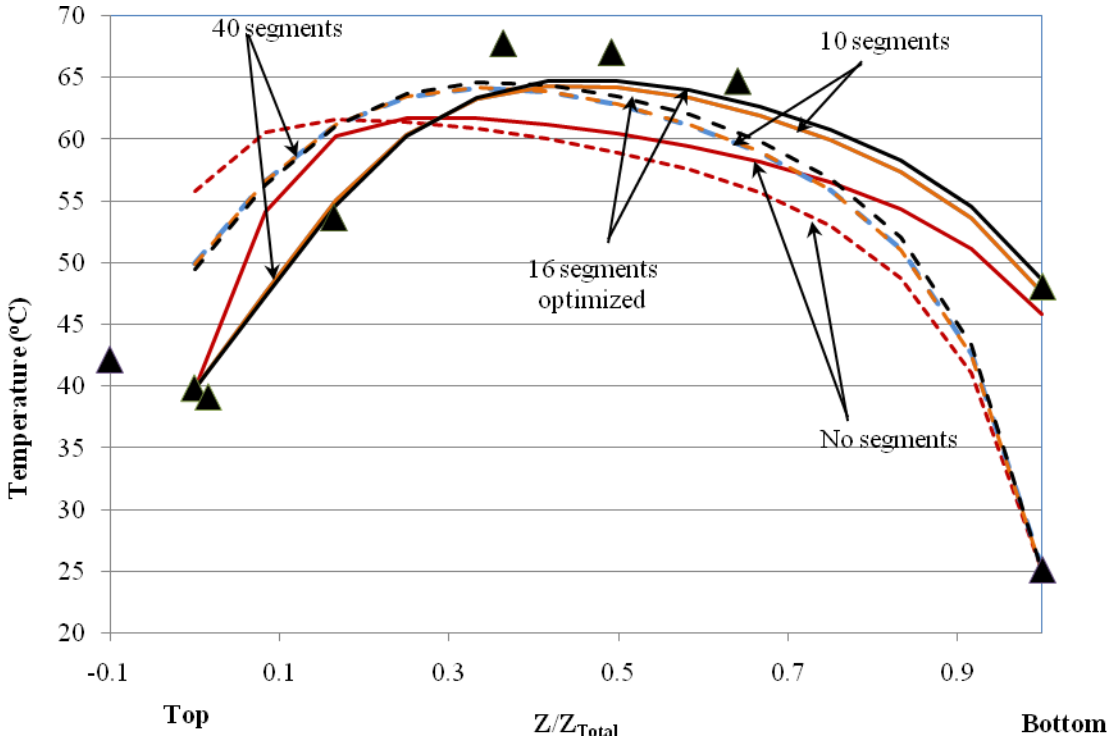

Figure 3: Absorber temperature profiles with various segmentation schemes. The point at a relative position of -0.1 represents a measurement downstream of the column. Pilot plant (▲), liquid profile (—), vapor profile (--).

The proposed model was adjusted to match experimental data from the MEA Pilot Plant run using the parameter estimation and reconciliation tool in Aspen Plus® 2006.5. This tool uses pilot plant measurements along with model parameters and inputs, and an assigned standard deviation based on equipment accuracy, data uncertainty, and/or engineering judgment and creates an objective function to minimize that includes the sum of the squared measurement errors:

$$f = \sum_{i=1}^{n} \frac{PP_i - m_i}{\sigma_i} \quad (9)$$

Where *PP* represents the experimental data, *m* is the model prediction of the experimental data, and σ is the assigned standard deviation. The latter serves as a boundary for the values that the model prediction can use. Table 2 shows the specified standard deviations and final results.

Reconciliation using 12 well-mixed segments did not adequately represent the absorber temperature profile. Results showed large (15°C) changes near liquid and gas inlets. Thus, the absorber packing segmentation and flow model were revised. The absorber was divided into 20 well-mixed segments with 8 segments in the 1.5m of packing near the extremes of the column and 4 segments for the remaining

center 3.1m. The resulting profiles closely matched the pilot plant temperatures (see Figure 4), lean loading (0.365), rich loading (0.475), and removal (59.5%). However, since no heat loss had been considered in this analysis, temperatures were expected to be higher than pilot plant values. The segment flow model was changed to countercurrent and 40 equally spaced segments were used.

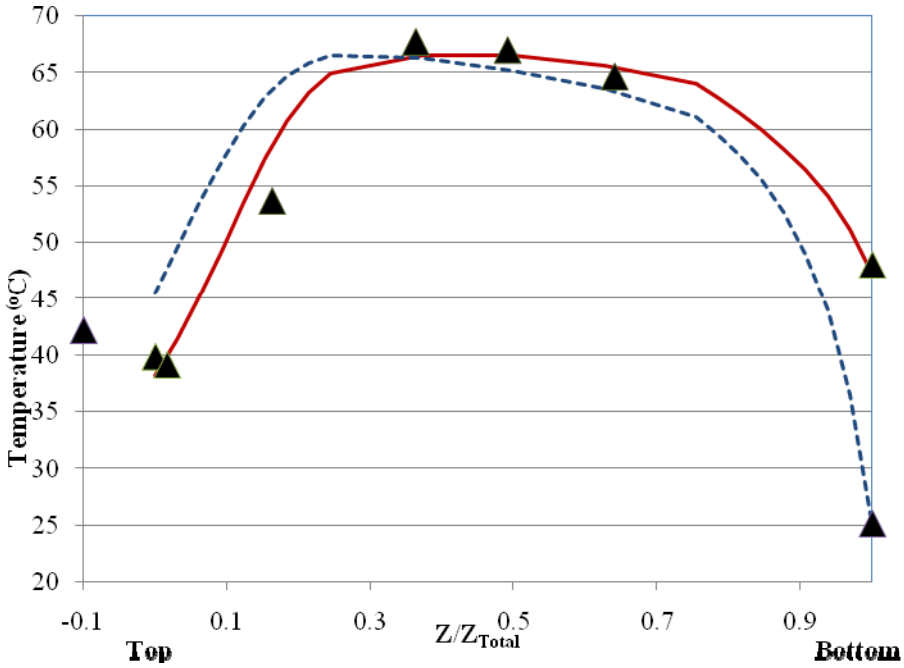

Figure 4: Temperature profiles for an absorber column segmented into two 1.5m sections with 8 segments and 4 segments in the center (3.1m). Pilot plant (▲), liquid profile (—), vapor profile (--).

Table 2: Pilot Plant Reconciliation, 9 m MEA, 6.10 m absorber packing, 0.43 m Diameter

Variable	Pilot Plant Value	Specified deviation	Reconciled Value	Actual Deviation (%)
Area Factor	1.0	----	0.816	----
Rich ldg (mol CO_2/mol MEA)	0.48	1%	0.469	2.3
Inlet Gas (mol/hr)	34572	5%	33346	3.5
Y_{CO2} – In	0.119	5%	0.1192	0.0
Y_{CO2} – Out	0.047	5%	0.0501	5.7
T_G – In (°C)	25.1	1	25.1	0
T_G – Out (°C)	42.2	20	46.1	3.9

The variables and parameters used for the reconciliation and their chosen standard deviations along with the resulting model predictions are presented in Table 2. The only manipulated model parameter was the interfacial area factor which corrected the calculated interfacial area. High standard deviations (20°C) were specified for the outlet gas and the top column temperatures because they were considered less reliable. The water (water – Lean) and CO_2 content (CO_2 – Lean) of the lean feed were treated as reconcilable experimental values. The resulting values give a lean loading of 0.365 which is 1% greater than the measured value (0.36). Figure 1 compares the resulting model temperature profiles with the experimental results.

T_L – In (°C)	39.9	4	38.2	1.7
T_L – Out (°C)	44.9	4	46.7	1.8
Column T (°C)				
Top	39.2	20	34.8	4.4
T1	53.7	2	53.8	0.1
T2	67.8	2	70.8	3.0
T3	67.1	2	69.4	2.3
T4	64.7	2	67.0	2.3
Bottom	48.1	3	46.7	1.4
Water – Lean (mol/hr)	143600	0.5%	143700	0.1
CO_2 – Lean (mol/hr)	8202	2%	8307	1.3
CO_2 Removal (%)l	60.0	1%	59.9	0.2

The reconciled flow rates, compositions, and the CO_2 removal are within 1 to 6% reported values, reflecting moderate adjustments to close the mass balance. CO_2 removal and other pilot plant measurements were matched by adjusting the wetted area prediction of the Tsai model by a factor of 0.82.

GHGT-9 Article

Van Wagener (Plaza *et al*. 2008) determined optimum rich and lean loadings, and solvent rates to obtain minimum stripper work requirements. These values were used to specify an absorber capable of reaching 90% removal. Results and analysis were included in a paper prepared for GHGT-9.

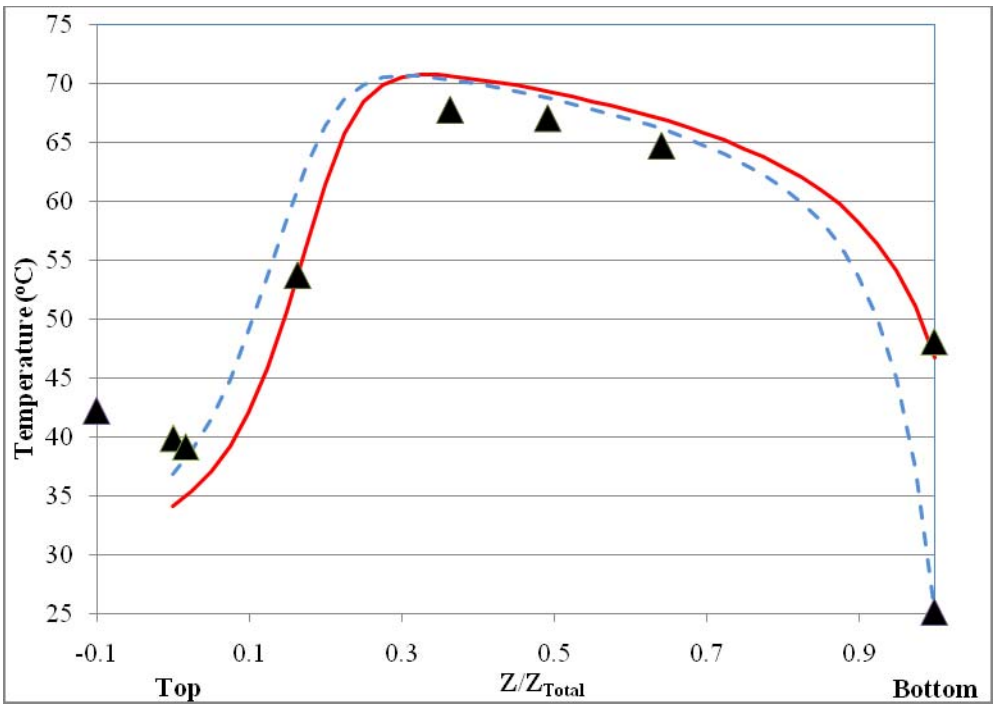

Figure 4: Reconciled temperature profiles for the pilot plant absorber. Pilot plant (▲), liquid profile (—), vapor profile (--).

Conclusions

The new MEA model kinetic constants did not change after the physical properties parameters were adjusted based on the work by AspenTech®.

Adequate segmentation for the liquid film allows reducing the number of segments and maintaining correct absorber representation. It also reduces computing time and gives more robustness to the model.

The use of countercurrent segments resulted in higher temperatures than the reported pilot plant values reflecting possible heat losses. However, this model does not account for possible backmixing. No pilot plant data are available to account for heat losses or possible backmixing so validation of the flow model selection is limited.

Reconciled pilot plant data show the proposed absorber model is capable of simulating operation of the absorber. Loadings and removal were around 1% off the measured value. Temperature profiles are 2 to 8^{o}C off the reported values. This may correspond to the unaccounted heat losses.

Intercooling was necessary to reach 90% removal in the absorber using the pre-determined stripper optimum values. Furthermore, optimum placement of the intercooled stage reduced packing height by 13% (Plaza *et al*., 2008).

Future Work

Work will be focused on developing a CO_2 absorber model for the piperazine solvent using the Hilliard (2008) thermodynamic representation.

The developed piperazine model will be validated using pilot plant data from the campaign scheduled for November 2008.

References

Aboudheir, A. "Kinetics, Modeling and Simulation of CO_2 Absorption into Highly Concentrated and Loaded MEA Solutions." Ph.D. Dissertation. University of Regina. 2002.

Hilliard, MD. "A Predictive Thermodynamic Model for an Aqueous Blend of Potassium Carbonate, Piperazine, and Monoethanolamine for Carbon Dioxide Capture from Flue Gas". Ph.D. Dissertation. University of Texas at Austin. 2008.

Huiling, Q & CC Chen. "Modeling Transport Properties of CO_2 Capture Systems with Aqueous Monoethanolamine Solution". Internal Report. Aspen Technology, Inc. 2008.

Rochelle *et al.* "Modeling CO_2 Absorption Using Aqueous Amines". Progress Report for 3rd Quarter 2008. University of Texas at Austin.

Plaza, JM *et al.* "Modeling CO_2 Capture with Aqueous Monoethanolamine". *9th Int'l Conf Greenhouse Gas Control Technologies*. Washington DC, Elsevier. 2008.

Rochelle, GT *et al*. "Research Needs for CO_2 Capture from Flue Gas by Aqueous Absorption/ Stripping." US Department of Energy - Federal Energy Technology Center. 2001.

Tsai, RE *et al.* "Influence of Viscosity and Surface Tension on the Effective Mass Transfer Area of Structured Packing." *9th Int'l Conf Greenhouse Gas Control Technologies*. Washington DC, Elsevier. 2008.

Reclaiming by Crystallization of Potassium Sulfate

Progress Report for July 1– Sep. 30, 2008

by Qing Xu

Supported by the Luminant Carbon Management Program

and the

Industrial Associates Program for CO_2 Capture by Aqueous Absorption

Department of Chemical Engineering

The University of Texas at Austin

October 8, 2008

Summary

One side reaction in CO_2 capture when using MEA/PZ is the generation of sulfate from SO_2. This sulfate has to be removed so that the MEA/PZ solution can be reused for CO_2 capture. Potassium sulfate can be crystallized and separated from MEA/PZ solvent by the addition of potassium hydroxide. In previous work the solubility of K_2SO_4 in CO_2 loaded aqueous amine solution was measured and an empirical model was developed. Selected interaction parameters were regressed in CO_2-MEA-H_2O-K^+-SO_4^{-2} system using Aspen Plus® Electrolyte-NRTL model. Continuous crystallization experiments at 25 to 60ºC show that big crystals can form by mixing lean CO_2 loading amine solution and KOH solution with residence time from 3 min to 20 min, and the solid-liquid separation is easy to achieve. In this period, a process simulation of reclaiming using crystallization of potassium sulfate was done in Aspen Plus®. The interaction parameters from Aspen regression were used. This simulation is based on a 500 MW power plant in the 2007 report (K. S. Fisher *et al*.). Energy and chemical costs were estimated. The result shows that energy and chemical costs are \$0.038 and \$1.040 per ton of CO_2, respectively. So the total cost would be less than \$1.1/ton CO_2. Compared with \$55-67/ton CO_2 for typical CO_2 capture using MEA, this reclaiming process cost is acceptable. A comprehensive paper (attached) describing this work has been prepared for GHGT-9.

Reference

Fisher, KS, GT Rochelle, C Schubert, "Advanced amine solvent formulations and process integration for near-term CO_2 capture success". Final report to DOE, 2007.

Physical Properties of Concentrated Aqueous Piperazine

Quarterly Report for July 1 – September 30, 2008

by Stephanie Freeman

Supported by the Luminant Carbon Management Program

and the

Industrial Associates Program for CO_2 Capture by Aqueous Absorption

Department of Chemical Engineering

The University of Texas at Austin

November 4, 2008

Abstract

The solubility envelope of concentrated PZ solutions has been investigated this quarter. The solid-liquid transition temperature of a variety of PZ solutions was measured and compared to literature data. For 8 m PZ, a CO_2 loading of 0.25 mol CO_2/mol alkalinity is required to maintain a liquid solution without precipitation at room temperature (20°C). Additionally, the solubility of $PZ.6H_2O$(s) in unloaded solution at 20°C is 1.9 m PZ. The density of 7 m PZ ranges from 1.066 g/mL to 1.160 g/mL for 0.16 to 0.46 mol CO_2/equiv PZ at 20, 40, and 60°C. The density of 9 m PZ ranges from 1.084 g/mL to 1.181 g/mL with 0.15 to 0.44 mol CO_2/equiv PZ at 20, 40, and 60°C. The viscosity of 5, 7, 9, 10, 12, and 20 m PZ at 25, 40, and 60°C was measured.

A paper (attached) was prepared for GHGT-9 which presents all of the important performance data for concentrated PZ.

Introduction

Concentrated aqueous piperazine (PZ) is being investigated as a possible alternative to 30 wt % (or 7 m) MEA in absorber/stripper systems to remove CO_2 from coal-fired power plant flue gas. Aqueous PZ has been given a proprietary name of ROC20 for 10 m PZ and ROC16 for 8 m PZ. Previous reports include the proprietary name, while the concentration of PZ will be explicitly used in this document.

Preliminary investigations of PZ have shown numerous advantages over 7 m MEA systems. Aqueous concentrated PZ produces less degradation both thermally and oxidatively as previously shown at concentrations of 5 and 8 m. The kinetics of CO_2 absorption are faster in concentrated PZ, as shown by Cullinane, and are

currently being measured by Dugas. The capacity of concentrated PZ is greater than that of MEA while the heat of absorption and volatilities are comparable.
As reported last quarter, the heat of absorption of concentrated PZ solutions is comparable to MEA over a range of temperatures. Above a loading of approximately 0.1 mol CO_2/equiv PZ, there was little difference in the values for the heat of absorption between 80, 100, and 120°C. At all temperatures, the heat of absorption decreased as loading increased and fell off as loading reached 0.4 mol CO_2/equiv PZ, producing a trend different from other amines whose heat of absorption remains constant from loadings of 0 to 0.5 mol CO_2/mol amine before dropping off. The heat of absorption data is still being analyzed for any pertinent trends.
This quarter was focused on gathering physical data on concentrated PZ solutions and preparing for the GHGT-9 conference in November. Additional density, viscosity, and solubility data have been collected and analyzed. The solid-liquid transition temperature of a variety of PZ solutions has been measured and compared to literature sources. A manuscript for submission to the GHGT-9 conference has been prepared and is attached as an appendix to this report.

Experimental Methods

Analytical Methods

Total Inorganic Carbon Analysis (TIC): Quantification of CO_2 loading was performed using a total inorganic carbon analyzer. In this method, a sample is acidified with 30 wt % H_3PO_4 to release the CO_2 present in solution. The CO_2 is carried in the nitrogen carrier gas stream to the detector. PicoLog software is used to record the peaks that are produced from each sample. A calibration curve is prepared at the end of each analysis using a TIC standard mixture of K_2CO_3 and $KHCO_3$. The TIC method quantifies the CO_2, CO_3^{-2}, and HCO_3^- present in solution. These species are in equilibrium in the series of reactions shown below.

$$CO_3^{2-} + 2H^+ \leftrightarrow HCO_3^- + H^+ \leftrightarrow H_2CO_3 \leftrightarrow CO_2 + H_2O$$

Acidification of the sample shifts the equilibrium toward CO_2 which bubbles out of solution and is detected in the analyzer.

Acid pH Titration: Titration with 0.2 N H_2SO_4 is used to determine the concentration of amines in experimental samples. The automated Titrando apparatus (Metrohm AG, Herisau, Switzerland) is used for this method. A known mass of sample is diluted with water and the autotitration method is then used. The Titrando titrates the sample with acid while monitoring the pH. The equivalence points are recorded. The equivalence point around a pH of 3.9 corresponds to basic amine species in solution. The test is not sensitive to the type of amine, so if PZ has degraded to EDA, the titration test will detect the sum of contributions from the species.

Densitometer: A Mettler-Toledo DE40 densitometer was acquired by the Rochelle laboratory in the first quarter of 2007 (Mettler-Toledo, Inc, Columbus, Ohio, USA). This densitometer measures density by vibrating the glass u-tube inside the meter at a certain frequency. When a liquid of a particular density is present, the frequency of vibration is changed. Samples with higher densities produce lower frequencies. Calibration is performed with air and degassed-deionized (DDI) water at each temperature that measurements are taken. The accuracy is reported to be 0.0001 g/cm^3 with a temperature range of 4 to 90°C (Mettler-Toledo, 2008). The goal of density measurements is to develop a correlation between the density of amine solutions and the CO_2 loading. Liquid samples are pumped into the measurement u-tube and pumped out after the measurement is completed. The u-tube is cleaned with DI water and acetone after each sample. The densitometer is connected to a computer to record the values after each measurement.

Viscosity Measurements: Viscosity of solutions was measured using a Physica MCR 300 cone and plate rheometer (Anton Paar, Graz, Austria). The apparatus allows precise temperature control for measuring viscosity at temperatures ranging from 25 to 70°C. To take a measurement, 700 mL of solution is loaded onto the measurement disk. The instrument accelerates the top disk at a predetermined angular speed and measures the shear stress over time. The program that is used increases the angular speed from 100 to 1000 over a period of 100 seconds, measuring shear stress every 10 seconds. Viscosity is calculated for each sampling instance and an average and standard deviation are calculated from the 10 individual measurements.

Results

The focus of this quarter has been on density, viscosity, solubility, and heat of absorption measurements of concentrated PZ solutions.

Results of Density Measurements

The acquisition of the new Mettler-Toledo densitometer has made density measurements an easy and fast test. Density data on a variety of PZ solutions have been gathered to form a database of concentrated PZ density data. Additions to the database this quarter are density measurements for 7 and 9 m PZ at 20, 40, and 60°C over a range of loadings. The data are displayed in **Error! Reference source not found.**. In this figure, the relationship between density and the weight fraction of CO_2, a surrogate for CO_2 loading, is shown.

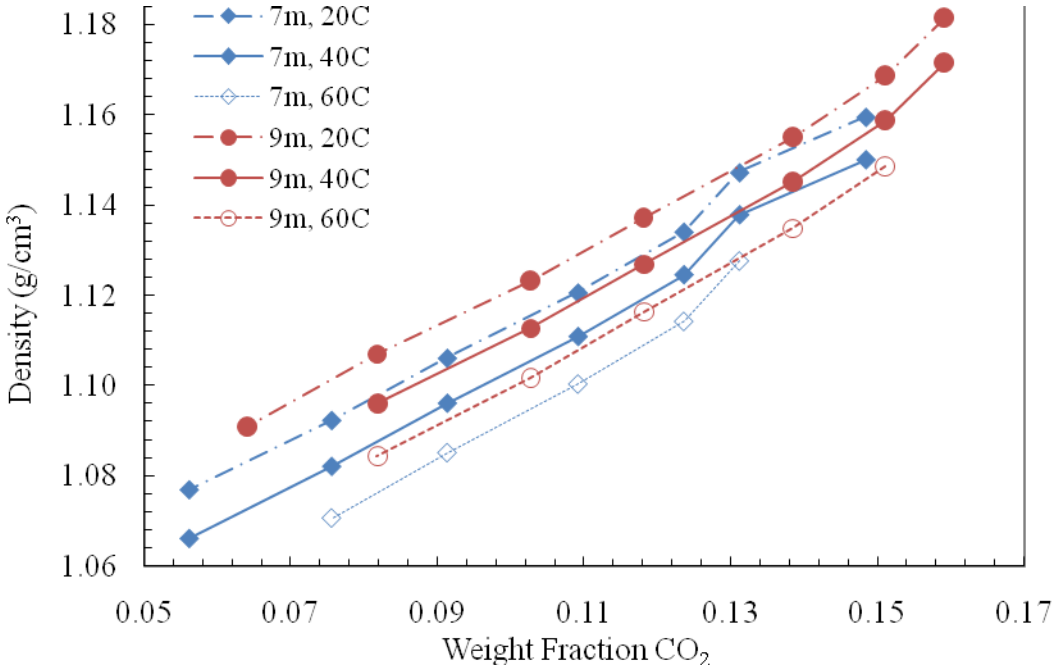

Figure 1: Density of 7 and 9 m PZ Solutions

Density Regression for 8 m PZ Solutions

In preparation for the pilot plant run planned for November and December 2008, a density correlation for 8 m PZ was created. Only 8 m PZ data was correlated because this is the pilot plant concentration. This allowed for a simplified regression that is only dependent on the mass fraction of CO_2 and temperature. The final regression contains four terms with an intercept and is shown below in Eqn. 1.

$$\rho_{pred} = 1.076 + 0.494(wt) + 1.580(wt)^2 - 0.00034T + 0.000166T(wt) \quad \text{Eqn. 1}$$

In Eqn. 1, the density is predicted as g/mL with T in °F and wt as the weight fraction of CO_2. This regression provides an accurate prediction of 8 m PZ solution densities as shown in Figure 2. The overall r^2 value of the regression is 0.9995 with a standard error of 0.000664 g/mL.

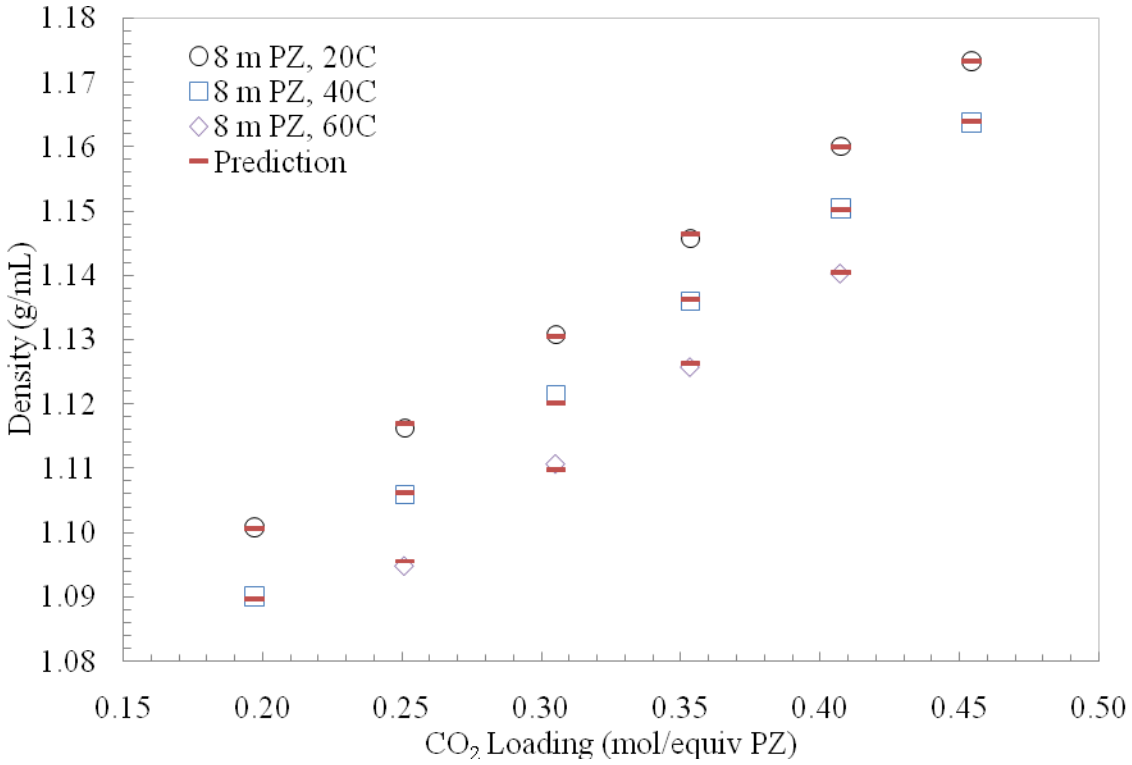

Figure 2: Prediction of Density for 8 m PZ Solutions

Results of Viscosity Measurements

Viscosity measurements are included in the database of physical properties of PZ. This quarter, viscosity measurements for 5, 7, 8, 10, 12, and 20 m PZ were performed. The viscosity data are presented below. Along with the 8 m PZ viscosity data reported in the previous quarterly report, the viscosity database is fairly complete for concentrated PZ.

Table 1: Viscosity Data for 5 to 20 m PZ at 25, 40, and 60°C

Conc. (m)	CO_2 Loading (mol/equiv PZ)	Viscosity (cP) T = 25°C	T = 40°C	T = 60°C
5	0.459	6.01 ± 0.018	3.75 ± 0.010	2.50 ± 1.833
5	0.446	5.94 ± 0.014	3.75 ± 0.014	2.37 ± 0.033
5	0.421	5.93 ± 0.015	3.69 ± 0.014	2.31 ± 0.019
5	0.375	5.87 ± 0.018	3.61 ± 0.011	2.23 ± 0.023
5	0.318	5.46 ± 0.022	3.46 ± 0.007	2.14 ± 0.021
5	0.263	5.34 ± 0.039	3.35 ± 0.015	2.03 ± 0.019
5	0.208	5.34 ± 0.039	3.23 ± 0.012	1.95 ± 0.018
7	0.457	12.82 ± 0.063	7.85 ± 0.094	5.27 ± 0.243
7	0.399	12.60 ± 0.047	7.62 ± 0.082	4.85 ± 0.104
7	0.368	12.34 ± 0.052	7.22 ± 0.076	4.81 ± 0.216

7	0.321	11.60	±	0.000	6.93	±	0.070	4.22	±	0.057
7	0.264	11.34	±	0.052	6.48	±	0.053	3.72	±	0.058
7	0.204	10.85	±	0.053	6.35	±	0.039	3.54	±	0.050
9	0.456	26.72	±	0.079	15.21	±	0.110	10.24	±	0.466
9	0.406	25.34	±	0.052	14.62	±	0.132	9.16	±	0.214
9	0.362	23.99	±	0.032	13.90	±	0.115	8.44	±	0.186
9	0.303	23.10	±	0.047	12.60	±	0.105	7.56	±	0.143
9	0.250	22.03	±	0.048	12.09	±	0.120	6.32	±	0.060
9	0.214	20.82	±	0.042	11.09	±	0.088	5.66	±	0.036
10	0.421	37.48	±	0.352	21.18	±	0.239	11.88	±	0.352
10	0.384	35.45	±	0.227	19.89	±	0.407	11.06	±	0.237
10	0.311	33.42	±	0.220	18.08	±	0.210	9.78	±	0.342
10	0.261	31.37	±	0.189	16.92	±	0.253	9.08	±	0.069
12	0.412	18.32	±	0.290	33.43	±	0.316	63.22	±	0.361
12	0.361	60.17	±	0.236	31.42	±	0.413	15.11	±	0.213
12	0.312	57.22	±	0.297	27.18	±	0.215	13.34	±	0.255
12	0.256	52.68	±	0.181	26.01	±	0.213	11.78	±	0.294
12	0.203	49.35	±	0.127	23.62	±	0.286	10.22	±	0.162
20	0.258	534.30	±	2.058	138.90	±	0.994	57.14	±	0.420
20	0.211	373.10	±	0.994	120.30	±	0.483	40.88	±	0.286
20	0.160	304.10	±	0.994	95.61	±	0.357	30.00	±	0.176

Results of Solid Solubility Measurements

A large variety of solubility measurements have been taken this quarter. All PZ solutions analyzed for concentration and CO_2 loading were included in a database of solubility data.

Solutions were qualitatively classified as either soluble or insoluble solutions. Insoluble solutions either precipitated immediately upon creation or crashed out of solution after days or weeks. Figures created to show the solubility envelope of PZ solutions at 21°C and 40°C have been updated since last quarter. Any additional solubility testing conducted has been added to the figures. The updated solubility graphs are shown in Figures 3 & 4. The solid lines in each figure are solid-liquid equilibrium predictions from Hilliard's e-NRTL model (Hilliard, 2008).

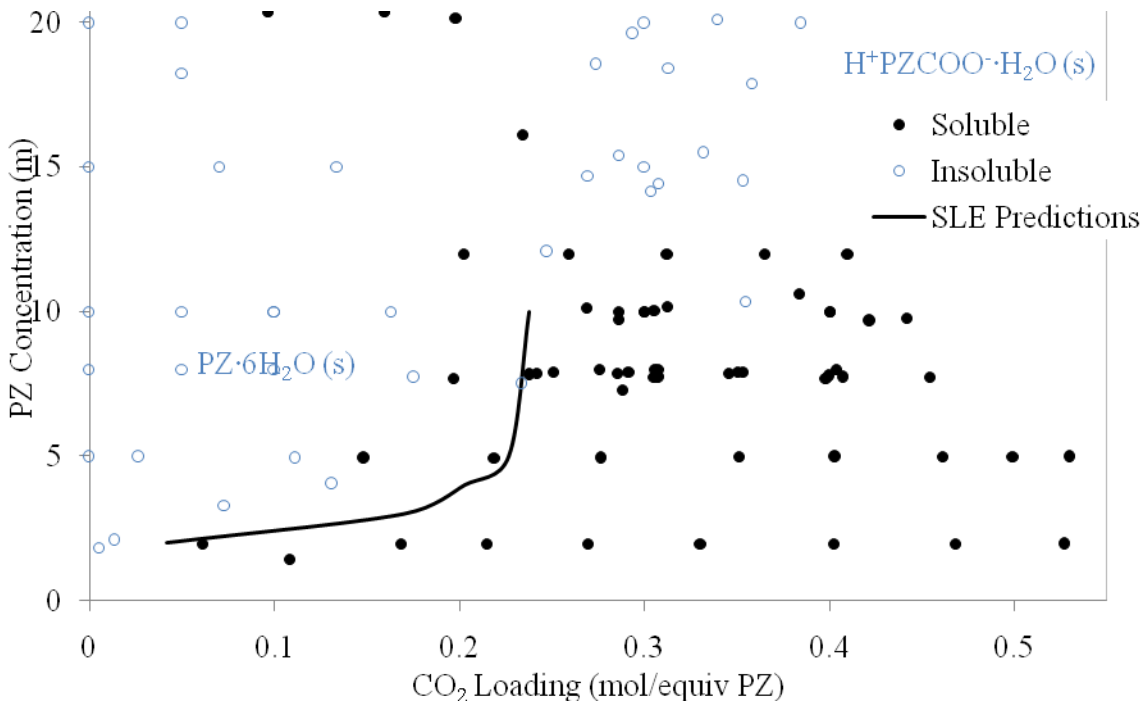

Figure 3: Solubility of 1 to 20 m PZ Solutions at 21°C

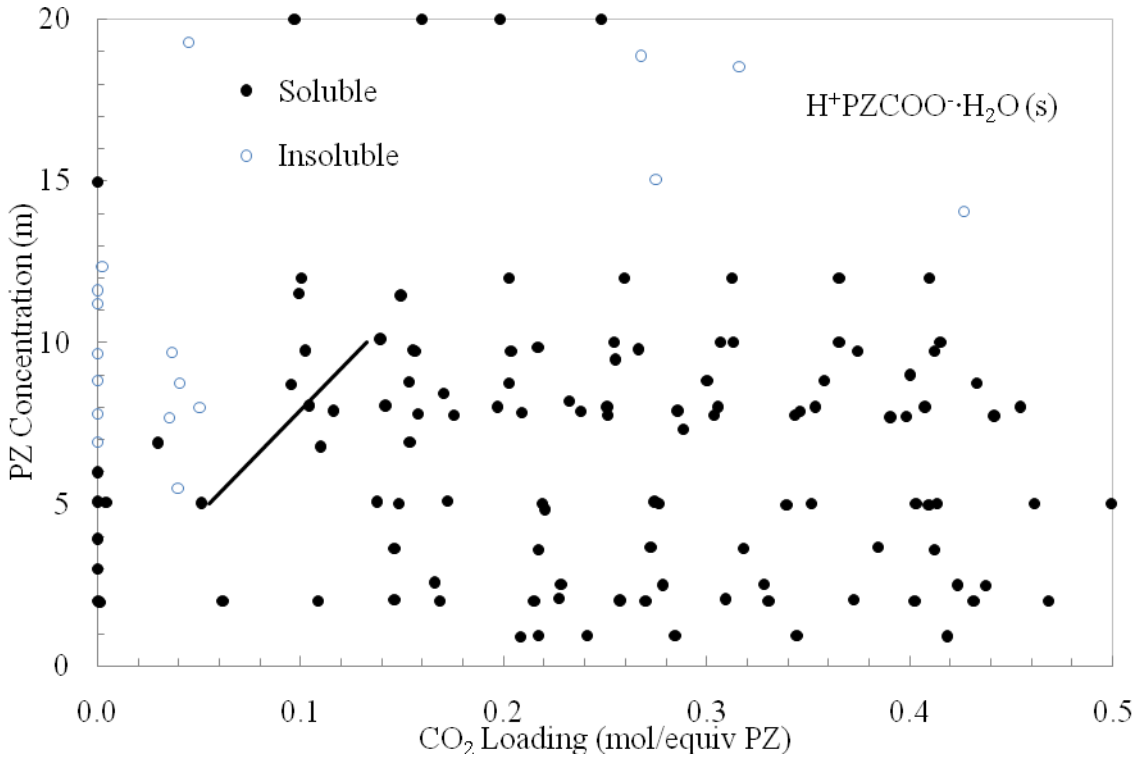

Figure 4: Solubility of 1 to 20 m PZ Solutions at 40°C

In addition to traditional solubility observations, the transition temperature for a variety of PZ solutions has been measured. The transition temperature in this sense is the temperature at which, while cooling slowly, the first crystals begin to form in the PZ solution. This measurement was performed by heating each solution beyond its transition point and then slowly cooling at a rate of approximately 1°C per 5 minutes until the first point of crystallization is observed. The transition temperature for 8 m PZ is shown in Figure 5. To demonstrate possible hysteresis in the transition of PZ solutions from liquid to solid, the melt temperature is also shown on the graph. This is the temperature to which the crystallized solution must be heated for all the crystals to redissolve.

The transition temperature for unloaded PZ solutions at a variety of amine concentrations is shown in Figure 6. In unloaded solutions, there is a eutectic point demonstrated in the figure around 62 wt %. The data collected this quarter only partially match the previous data published by Dow Chemical Corporation that indicated this eutectic point. Work in the next quarter will add to this data set to verify this eutectic point.

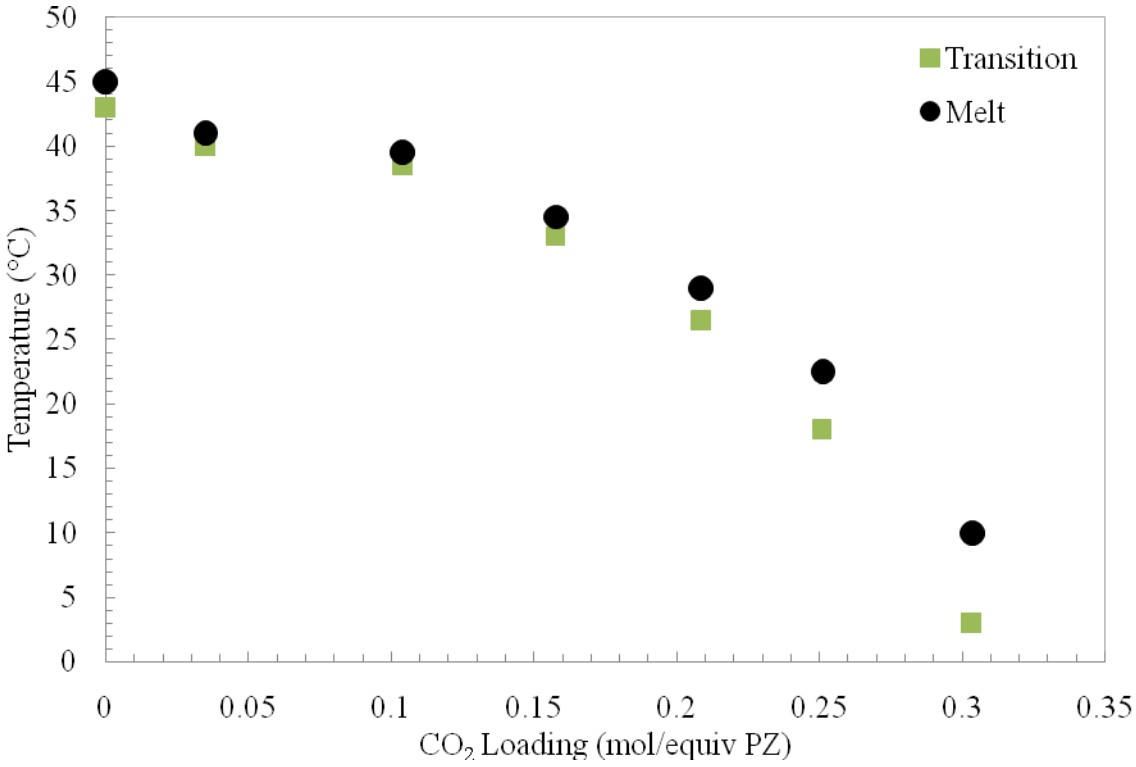

Figure 5: Transition Temperature for 8 m PZ

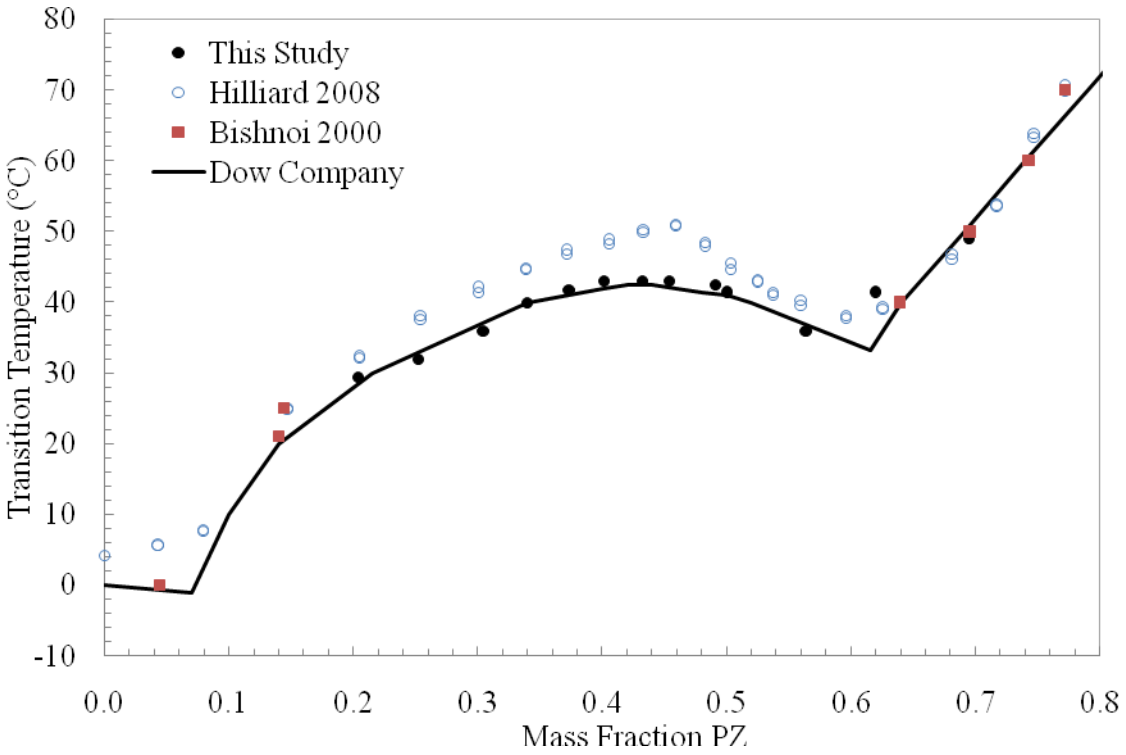

Figure 6: Solid-Liquid Transition Temperatures for Unloaded PZ (Bishnoi, 2000; Huntsman, 2005; Hilliard, 2008)

Discussion

Density and Viscosity Measurements

Collection of density and viscosity measurements has added to the knowledge base of concentrated, aqueous PZ solutions this quarter. The regression developed for 8 m PZ density will be used in the upcoming pilot plant run to determine CO_2 loading online through the weight fraction of CO_2 present in solution.

Solubility Measurements

The measurements related to PZ solubility completed this quarter are a valuable asset to fully understanding the precipitation behavior of PZ. Understanding the solubility envelope of PZ is crucial for any large-scale application of this solvent. The solubility measurements have shed further light on the speciation of the solution. NMR-based speciation of an 8 m solution has not been completed to date, but using the 5 m speciation and the solubility results can shed some light on the 8 m speciation. The speciation for a 5 m PZ solution is shown in Figure 7 below (Hilliard, 2008).

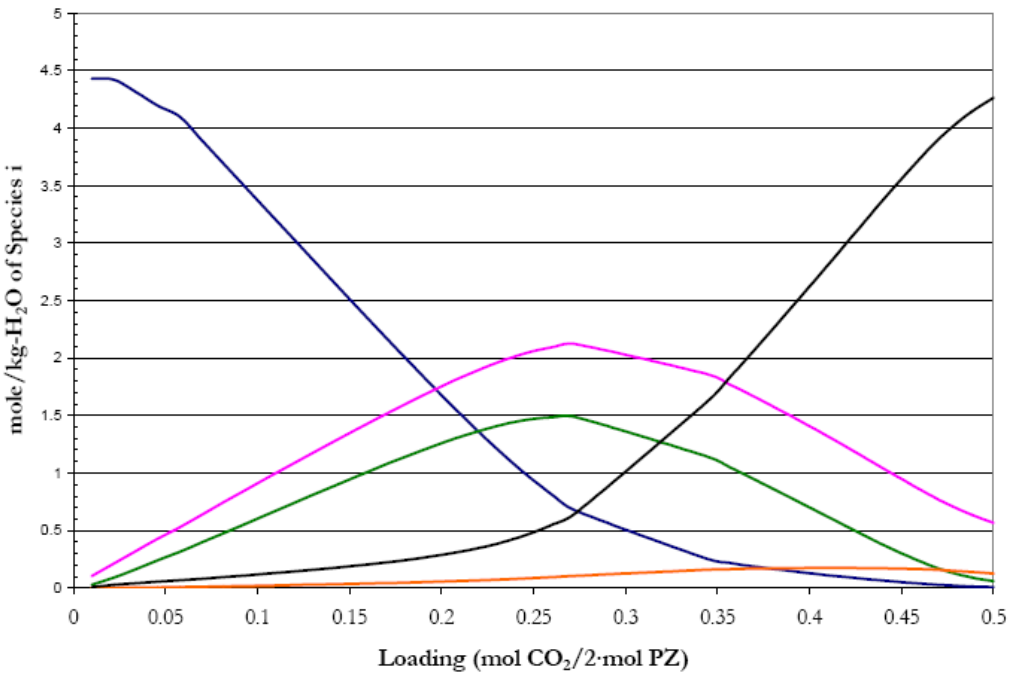

Figure 7: Predictions for the Liquid Phase Speciation in 5 m PZ at 40°C (Hilliard, 2008). Lines: —, PZ; —, PZH^+; —, $PZCOO^-$; —, $PZ(COO^-)_2$; —, H^+PZCOO^-

As CO_2 is added to an 8 m PZ solution and the loading is increased, the speciation likely follows the example of 5 m PZ where the free PZ decreases and the PZH^+ and the $PZCOO^-$ increases. Based on Figure 7 above, the solubility of PZ solutions at 40°C, an 8 m PZ solution is soluble above a loading of approximately 0.1 mol CO_2/equiv PZ. Both PZH^+ and $PZCOO^-$ are more soluble than the free PZ and are in high enough concentration around a loading of 0.1 to make the entire solution soluble. From that point on, the PZ is in forms that are soluble at these conditions and the solution remains a liquid. As a rich loading is reached, the concentration of soluble PZH^+ and $PZCOO^-$ begin to decrease while the concentration of H^+PZCOO^- begins to dominate. Since 8 m PZ solutions are not soluble above a loading of approximately 0.45 – 0.48 mol CO_2/equiv PZ, it can be inferred that the solubility of H^+PZCOO^- is less than other PZ species and begins to precipitate. XRD studies conducted by Qing Xu indicate that at least some of the precipitation occurring at rich loadings is in the form of $H^+PZCOO^-\cdot H_2O$ (Xu, 2008). This would imply that the solubility of H^+PZCOO^- is low and it precipitates as a hydrated salt at rich loadings.

More work is needed to fully understand the solubility envelope for 8 m PZ and other high PZ concentrations. Two major areas lacking understanding at this point are the solubility limits on the rich end and the speciation of 8 m PZ at various

loadings. The first area will be addressed in the next quarter while the speciation will be done at a later time.

Conclusions

This quarter has focused on continuing physical property measurements of concentrated, aqueous PZ solutions. The solubility of unloaded PZ at 20°C is approximately 14 wt % PZ, or 1.9 m PZ. The solubility of unloaded PZ at 40°C is approximately 34 wt %, or 6.0 m PZ. For 8 m PZ, a CO_2 loading of approximately 0.25 mol CO_2/mol alkalinity is required to maintain a liquid solution without precipitation at room temperature (20°C). Precipitation will occur if the loading falls below this value. At 40°C, a CO_2 loading of approximately 0.04 mol CO_2/mol alkalinity is required to maintain an aqueous solution for 8 m PZ. Precipitation from solutions in the low loading regions is most likely $PZ \cdot 6H_2O$. For both temperatures, precipitation will occur at loadings above 0.45–0.49 mol CO_2/mol alkalinity. Precipitation from solutions in the high loading region is at mostly $H^+PZCOO^- \cdot H_2O$.

The density of PZ solutions has been found to be highly correlated with the weight fraction of dissolved CO_2 in solution. This relationship will be used as an indicator of CO_2 loading from online density measurements in the upcoming pilot plant runs.

Future Work

The measurement of physical properties of PZ solutions will continue while focusing rich end solubility. In addition, oxidative degradation work will continue on concentrated PZ solutions.

References

Bishnoi, S. "Carbon Dioxide Absorption and Solution Equilibrium in Piperazine Activated Methyldiethanolamine". University of Texas at Austin. Ph.D. Dissertation; 2002. 292.

Hilliard, MD. "A Predictive Thermodynamic Model for an Aqueous Blend of Potassium Carbonate, Piperazine, and Monoethanolamine for Carbon Dioxide Capture from Flue Gas". University of Texas at Austin. Ph.D. Dissertation; 2008. 1083.

Huntsman. Diglycolamine® Agent - Product Information. 2005. 60.

Mettler-Toledo. "Comparison of different measuring techniques for density and refractometry". Retrieved 08 June, 2008, from http://us.mt.com/mt/ed/faq/Comparision_measuring_methods_for_DERE_Editorial-Faq_1092390712029.jsp.

Xu, Q. 4th Quarterly Progress Report of 2008 for the Rochelle Research Group.

Thermodynamics of Concentrated Piperazine and MDEA/PZ

Progress Report for July 1 – September 30, 2008

by Thu Nguyen

Supported by the Luminant Carbon Management Program

and the

Industrial Associates Program for CO_2 Capture by Aqueous Absorption

Department of Chemical Engineering

The University of Texas at Austin

October 27, 2008

Abstract

The objective of this work is to explore the thermodynamic VLE behavior of piperazine (0.9–12 m PZ) and of blended MDEA/PZ systems (2.7–8.7 m MDEA/0.4–2.6 m PZ). In particular, CO_2 solubility and amine volatility are studied as a function of temperature, loading, and amine concentration in these systems.

With PZ (0.9 m–12.0 m) at 40ºC, the CO_2 partial pressure is 500 and 5000 Pa at lean and rich loading of 0.3 and 0.4 mol CO_2/equivalent of PZ, respectively. At stripper operating temperature of ~120ºC, CO_2 partial pressure is ~100,000 Pa at a loading of 0.3. The estimated CO_2 heat of absorption in PZ is -71 kJ/mol for 0.3 lean loading. The CO_2 solubility is represented by: $\ln P_{CO2} = 36.1 - (93.2\ kJmol^{-1}/R)(1/T) - 13.9(Loading) + 8839(Loading/T) + 14.3(Loading^2)$. PZ volatility is 4.8–33 ppm at 40ºC and 8–100 ppm at 60ºC.

With MDEA-PZ (2.7–8.7 m MDEA/0.4–2.6 m PZ) at 40ºC, CO_2 partial pressure is 500 and 5000 Pa at lean and rich loading of 0.09 and 0.35 mol CO_2/mol total alkalinity, respectively. The solubility of CO_2 in this amine blend is empirically modeled as: $\ln P_{CO2} = 36.9 - 9064.8(1/T) + 1.3(\text{Ln Loading}) + 5064(Loading/T) - 21.2(Loading^2)$. The capacity of this blend is 0.58 mol CO_2/kg $_{H2O+amine}$ compared to 0.35 mol CO_2/kg $_{H2O+amine}$ for 7 m MEA. The CO_2 heat of absorption in MDEA-PZ is estimated to be ~62 kJ/mol at 0.3 mol CO_2/mol total alkalinity. PZ volatility

in these systems ranges from 2–19 ppm at 40ºC. Similarly, MDEA volatility is between ~5–12 ppm at 40ºC for these blended systems.

Introduction

This work discusses the Vapor Liquid Equilibria of both piperazine (0.9–12 m PZ) and methyldiethanolamine/piperazine (2.7–8.7 m MDEA/0.4–2.6 m PZ). CO_2 solubility and amine volatility for these solutions are studied as a function of loading, temperature, and amine concentration.

Experimental Methods

The vapor composition of CO_2 and the amines, required for determining their partial pressures, is measured using a Stirred Reactor coupled with an FTIR analyzer (Fourier Transform Infrared Spectroscopy) manufactured by Gasmet Inc. Figure 1 shows the VLE experimental setup.

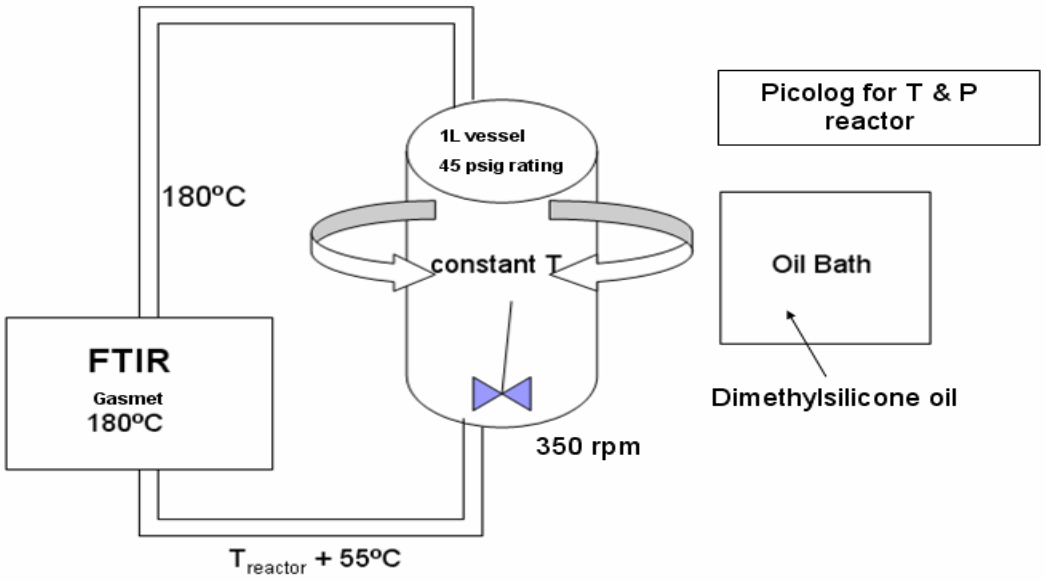

Figure 1: Schematic of VLE Experimental Setup (Stirred Reactor Coupled with FTIR)

The 1L glass reactor is well-stirred and kept isothermal by use of dimethylsilicone oil circulating from the oil bath. The reactor is insulated from the surrounding by wrapping foil. As the experiment proceeds, vapor from the headspace of the reactor is continually being drawn off into a heated line kept at an elevated temperature of 180ºC which is also the FTIR operating temperature. It is critical to have both the line and analyzer kept at a very high temperature to prevent possible condensation or adsorption of vapor amine to any of the inner surfaces. The FTIR is capable of multi-component analysis as it is able to measure both CO_2 solubility and volatility of the rest of the gaseous species present, including the amines of

interest. After the gas passes through the FTIR, it is taken back to the reactor via a line kept at approximately 55ºC higher than the equilibrium reactor temperature. It was determined that the 55ºC difference is sufficient to ensure that the return gas does not upset the solution that is in equilibrium with the gas inside the reactor.

Loading is initially determined gravimetrically by weighing the amount of CO_2 that is sparged into the amine solution. At the end of the VLE experiment, the loading is again verified by means of the Total Inorganic Carbon method which measures the amount of CO_2 evolution into 30 weight % H_3PO_4.

Data

Table 1: CO_2 Solubility for PZ System (0.9 m–12.0 m) from 40ºC–120ºC

PZ Conc (m)	Temperature (C)	Loading (mol CO_2/equiv PZ)	P_{CO2} (Pa)
0.90	40	0.21	44
0.90	40	0.22	71
0.90	40	0.24	103
0.90	40	0.28	234
0.90	40	0.34	987
0.90	40	0.42	4850
0.90	60	0.11	29
0.90	60	0.22	299
0.90	60	0.24	841
0.90	60	0.33	1930
0.90	60	0.37	8290
0.90	60	0.38	14700
2.00	60	0.13	92
2.00	60	0.19	296
2.00	60	0.28	1400
2.00	60	0.33	3950
2.00	60	0.37	9910
2.00	60	0.41	24700
2.00	60	0.17	142
2.00	60	0.38	13700
2.00	40	0.15	22
2.00	40	0.23	106
2.00	40	0.26	184
2.00	40	0.31	526
2.00	40	0.37	1950
2.00	40	0.43	10100
2.50	40	0.17	32
2.50	40	0.23	88
2.50	40	0.28	247
2.50	40	0.33	662
2.50	40	0.42	7510

2.50	40	0.44	10600
2.50	60	0.16	141
2.50	60	0.20	263
2.50	60	0.25	725
2.50	60	0.34	3960
2.50	60	0.40	16900
2.50	60	0.44	27400
3.60	60	0.16	129
3.60	60	0.22	431
3.60	60	0.28	1050
3.60	60	0.34	3490
3.60	60	0.39	13600
3.60	60	0.40	19300
3.60	40	0.15	21
3.60	40	0.22	63
3.60	40	0.27	211
3.60	40	0.32	687
3.60	40	0.38	4370
3.60	40	0.41	8420
5.00	40	0.17	29
5.00	40	0.22	61
5.00	40	0.27	211
5.00	40	0.34	798
5.00	40	0.41	5710
5.00	40	0.41	6990
5.00	60	0.16	137
5.00	60	0.23	365
5.00	60	0.30	1290
5.00	60	0.33	3310
5.00	60	0.39	18300
5.00	60	0.42	51400
2.00	40	0.24	96
2.00	40	0.32	499
2.00	40	0.35	1305
2.00	40	0.41	7127
2.00	60	0.24	559
2.00	60	0.32	2541
2.00	60	0.35	5593
2.00	60	0.41	25378
2.00	80	0.24	2492
2.00	80	0.32	12260
2.00	100	0.24	9569
5.00	40	0.23	65
5.00	40	0.30	346
5.00	40	0.35	1120

5.00	40	0.40	4563
5.00	60	0.23	385
5.00	60	0.30	1814
5.00	60	0.35	5021
5.00	60	0.40	17233
5.00	80	0.32	9699
5.00	100	0.32	36960
8.00	40	0.23	68
8.00	40	0.31	530
8.00	40	0.36	1409
8.00	40	0.40	8153
8.00	60	0.23	430
8.00	60	0.31	2407
8.00	60	0.36	7454
8.00	60	0.40	30783
8.00	80	0.25	3255
8.00	80	0.29	9406
8.00	100	0.25	13605
8.00	100	0.29	32033
12.00	60	0.23	331
12.00	60	0.29	1865
12.00	60	0.35	6791
2.01	120	0.10	4810
2.01	120	0.14	8930
2.05	120	0.16	13940
2.05	120	0.22	29140
2.01	120	0.24	41230
3.97	120	0.11	5990
3.84	120	0.15	10940
4.44	120	0.20	25320
3.84	120	0.24	42930
4.44	120	0.24	46930
3.97	120	0.29	95300
8.00	40	0.30	304
8.00	40	0.40	3641
8.00	60	0.30	1781

Table 2: PZ Volatility in PZ System (0.9 m–12.0 m) at 40ºC and 60ºC

Temperature (C)	PZ Conc (m)	Loading (mol CO2/equiv PZ)	P_{PZ} (kPa)
40	0.89	0.208	0.0008
40	0.91	0.217	0.0009
40	0.93	0.241	0.0009
40	0.91	0.284	0.0007
40	0.91	0.344	0.0007

40	0.90	0.418	0.0005
40	2.03	0.146	0.0021
40	2.08	0.227	0.0018
40	2.02	0.257	0.0017
40	2.05	0.309	0.0015
40	2.03	0.372	0.0014
40	1.99	0.431	0.0011
40	2.57	0.166	0.0023
40	2.50	0.228	0.0021
40	2.49	0.278	0.0018
40	2.50	0.328	0.0015
40	2.49	0.423	0.0013
40	2.48	0.437	0.0012
40	3.63	0.146	0.0033
40	3.59	0.217	0.0025
40	3.65	0.272	0.0021
40	3.61	0.318	0.0018
40	3.65	0.384	0.0014
40	3.58	0.412	0.0014
40	5.09	0.172	0.0031
40	4.83	0.220	0.0029
40	5.07	0.274	0.0022
40	4.97	0.339	0.0010
40	4.96	0.409	0.0008
40	5.02	0.413	0.0009
40	8.00	0.300	0.0019
40	8.00	0.400	0.0010
40	8.00	0.250	0.0031
60	0.91	0.111	0.0033
60	0.91	0.217	0.0020
60	0.91	0.242	0.0016
60	0.89	0.325	0.0011
60	0.89	0.370	0.0009
60	0.91	0.383	0.0008
60	2.03	0.132	0.0056
60	2.02	0.193	0.0048
60	2.03	0.275	0.0029
60	2.02	0.330	0.0022
60	2.02	0.370	0.0018
60	2.00	0.412	0.0013
60	1.90	0.169	0.0051
60	2.07	0.383	0.0019
60	2.51	0.164	0.0062
60	2.50	0.196	0.0053
60	2.53	0.251	0.0046

60	2.52	0.341	0.0031
60	2.53	0.400	0.0025
60	2.45	0.443	0.0022
60	3.63	0.158	0.0075
60	3.58	0.217	0.0064
60	3.58	0.277	0.0049
60	3.60	0.338	0.0038
60	3.67	0.385	0.0031
60	3.66	0.400	0.0028
60	5.18	0.164	0.0102
60	5.05	0.226	0.0075
60	5.08	0.296	0.0056
60	5.05	0.330	0.0049
60	5.02	0.386	0.0029
60	4.96	0.417	0.0022
60	8.00	0.300	0.0082
60	8.00	0.400	0.0067

Table 3: CO_2 Solubility in MDEA-PZ System at 40ºC–70ºC

Concentration (m)	T(C)	Loading (mol CO2/mol tot alk)	P_{CO2} (Pa)
7.7m MDEA / 1.1 m PZ	40	0.024	33
7.7m MDEA / 1.1 m PZ	40	0.054	115
7.7m MDEA / 1.1 m PZ	40	0.065	236
7.7m MDEA / 1.1 m PZ	40	0.079	367
7.7m MDEA / 1.1 m PZ	40	0.124	1140
7.7m MDEA / 1.1 m PZ	40	0.124	1335
7.7m MDEA / 1.1 m PZ	40	0.166	2550
7.7m MDEA / 1.1 m PZ	40	0.252	7480
7.7m MDEA / 1.1 m PZ	70	0.005	34
7.7m MDEA / 1.1 m PZ	70	0.012	241
7.7m MDEA / 1.1 m PZ	70	0.018	491
7.7m MDEA / 1.1 m PZ	70	0.041	780
7.7m MDEA / 1.1 m PZ	70	0.082	3600
7.7m MDEA / 1.1 m PZ	40	0.058	217
7.7m MDEA / 1.1 m PZ	40	0.115	943
7.0 m MDEA / 2.0m PZ	40	0.190	3550
7.0 m MDEA / 2.0m PZ	60	0.190	15600

Table 4: Amine Volatility in MDEA-PZ System at 40ºC and 60ºC

Solution Concentration	Temperature (C)	Loading (mol CO2/mol PZ)	MDEA (ppm)	
4M MDEA/0.6M PZ	40	0.0	6.4	
4M MDEA/0.6M PZ	40	0.5	5.2	

4M MDEA/0.6M PZ	40	1.0	5.9	
4M MDEA/1.2M PZ	40	0.0	5.7	
4M MDEA/1.2M PZ	40	0.5	6.6	
4M MDEA/1.2M PZ	40	1.0	6.9	
2M MDEA/0.3M PZ	40	0.0	11.1	
2M MDEA/0.3M PZ	40	0.5	12.0	
2M MDEA/0.3M PZ	40	1.0	11.0	
2M MDEA/0.6M PZ	40	0.0	9.0	
2M MDEA/0.6M PZ	40	0.5	9.5	
2M MDEA/0.6M PZ	40	1.0	9.2	
4M MDEA/0.6M PZ	60	0.0	26.0	
4M MDEA/0.6M PZ	60	0.5	24.8	
4M MDEA/0.6M PZ	60	1.0	27.1	
4M MDEA/1.2M PZ	60	0.0	25.0	
4M MDEA/1.2M PZ	60	0.5	27.8	
4M MDEA/1.2M PZ	60	1.0	28.6	
2M MDEA/0.3M PZ	60	0.0	30.8	
2M MDEA/0.3M PZ	60	0.5	25.3	
2M MDEA/0.3M PZ	60	1.0	24.6	
2M MDEA/0.6M PZ	60	0.0	19.3	
2M MDEA/0.6M PZ	60	0.5	22.2	
2M MDEA/0.6M PZ	60	1.0	22.5	

Results

CO_2 solubility, measured in terms of CO_2 partial pressure in Pa, is determined for PZ-CO_2-H_2O system ranging from 0.9 m–12.0 m. Figure 2 displays CO_2 partial pressure for loaded PZ from 40ºC–120ºC at 0.0–0.5 mol CO_2/2*mol PZ (as there are two amine equivalents per mole of PZ).

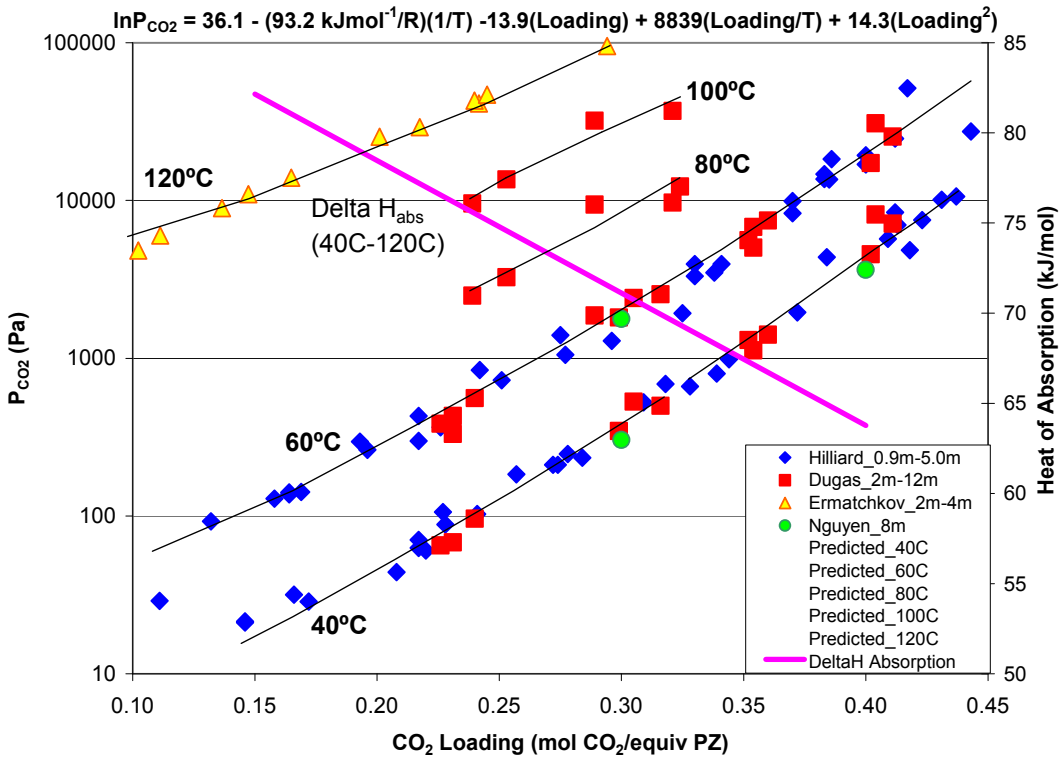

Figure 2: CO_2 Solubility for PZ-CO_2-H_2O System (0.9 m–12.0 m) from 40ºC–120ºC

At any given PZ concentration, the CO_2 partial pressure increases with loading as more CO_2 is introduced into the system. Furthermore, this partial pressure is greater at higher temperature. The experimental data is suitably modeled by the empirical expression shown below:

$$\ln (P_{CO2}) = 36.1 - (93.2\ kJmol^{-1}/R)(1/T) - 13.9(Loading) + 8839(Loading/T) + 14.3(Loading^2)$$

By taking the derivative of the empirical model with respect to (1/T) per the Clausius-Clapeyron relationship, it is possible to obtain an expression for ΔH of absorption as a function of loading.

$$\Delta H_{abs} = (93.2\ kJ/mol) - 8839(Loading / R)$$

ΔH_{abs} for CO_2 in these solutions ranges from ~65-83 kJ/mol which is comparable to other amines.

PZ volatility is determined for PZ-CO_2-H_2O (0.9–4.0 m) at 40ºC and 60ºC with 0–0.5 mol CO_2/2*mol PZ. Figure 3 shows PZ volatility values calculated as a function of loading and temperature.

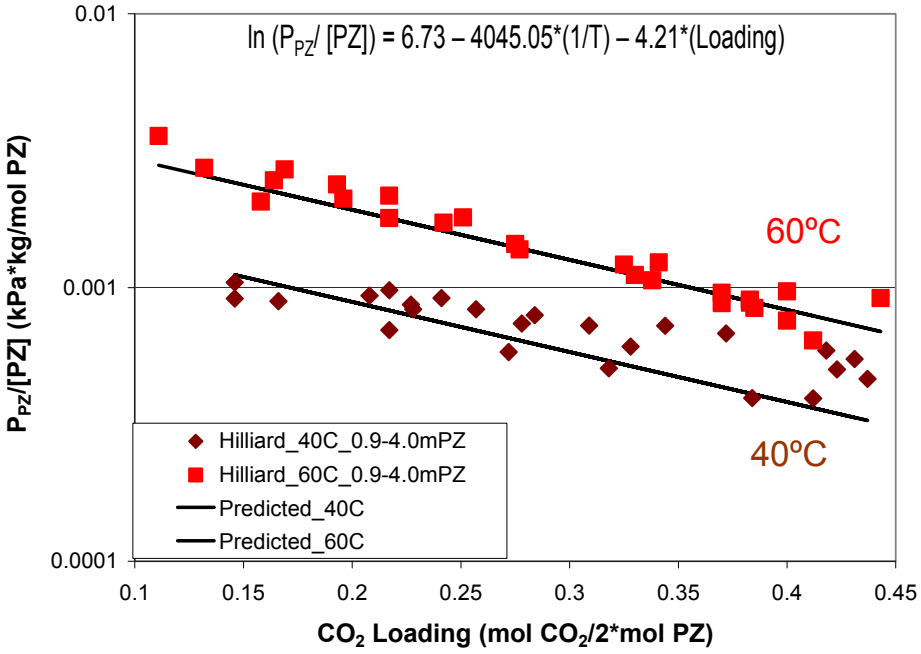

Figure 3: PZ Volatility for PZ System (0.9 m–4.0 m) at 40ºC and 60ºC

The volatility of PZ decreases with loading as more PZ is consumed in the presence of greater CO_2. The volatility also increases with temperature. The empirical fit presented on the plot seems to capture the experimental data adequately. PZ volatility at 5 m and 8 m is plotted separately in Figure 4 to allow for greater visibility of existing trends.

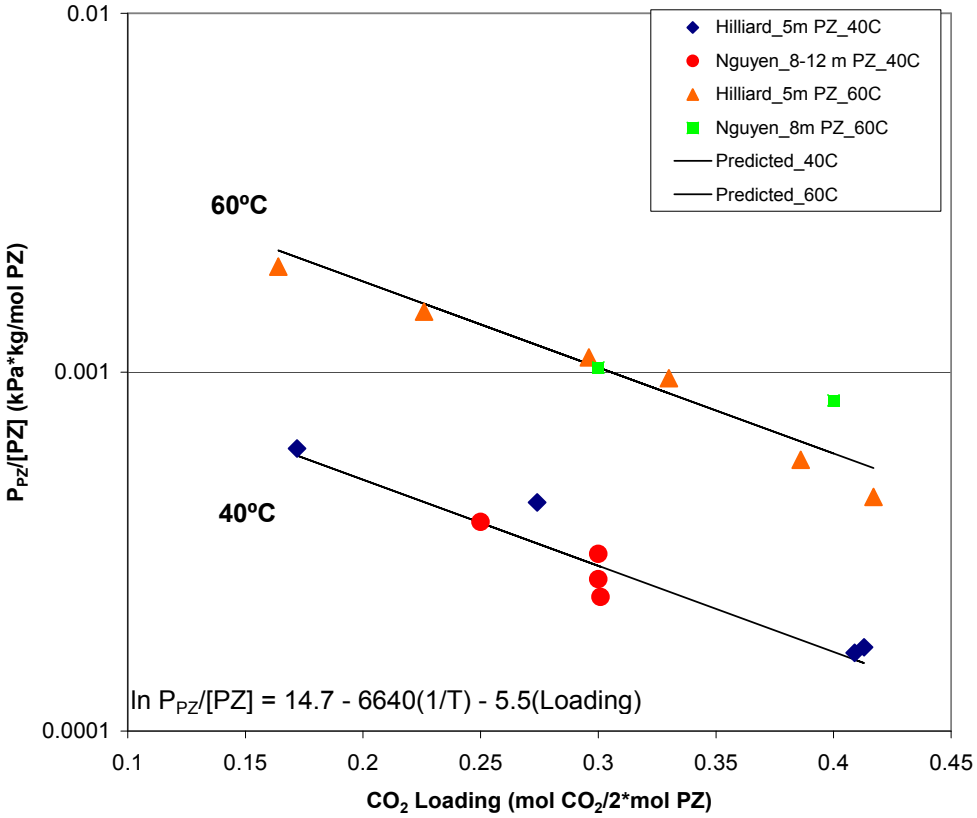

Figure 4: PZ Volatility for PZ System (5 m and 8 m) at 40ºC and 60º

For the MDEA/PZ system, CO_2 solubility is studied over the range of 2.7–8.7 m MDEA/0.4–2.6 m PZ at 40ºC–70ºC. Figure 5 displays CO_2 partial pressure for MDEA/PZ.

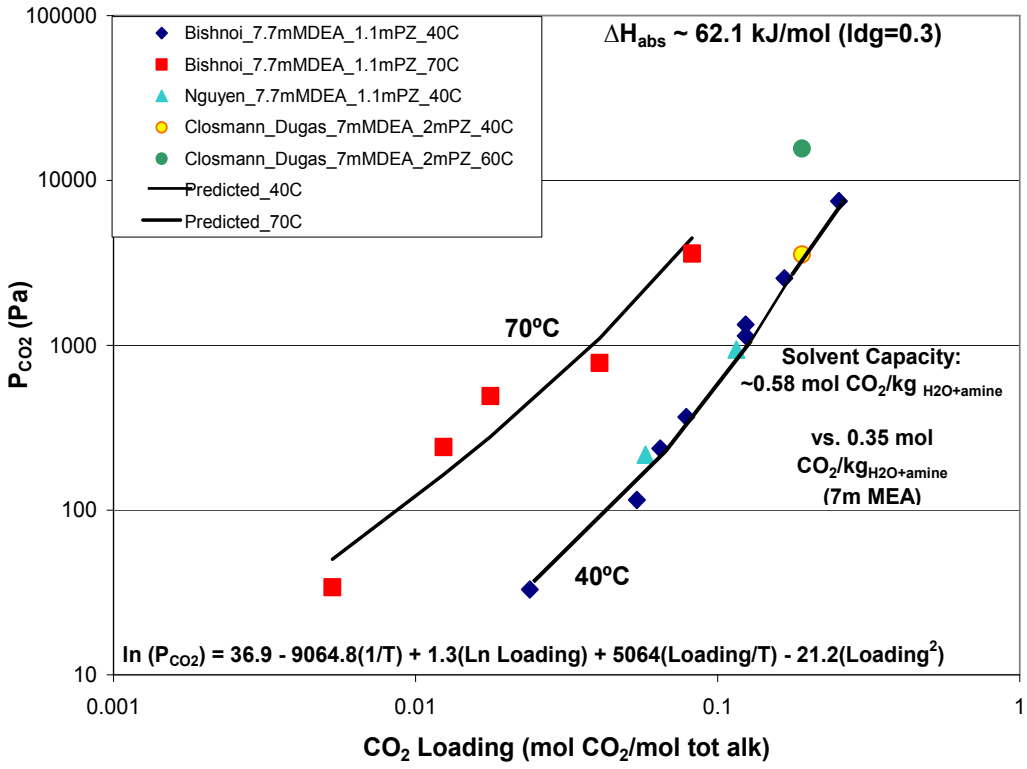

Figure 5: CO_2 Solubility for MDEA/PZ (2.7 m–8.7 m MDEA/0.4 m–2.6 m PZ) at 40º–70ºC

CO_2 partial pressure increases with loading as more CO_2 is introduced into the system. Likewise, it increases with temperature. When the temperature of a blended solution is raised, the solubility of CO_2 into the solution decreases and thus results in more CO_2 remaining in the vapor. The blended solvent's capacity is computed to be ~0.58 mol CO_2/kg $_{H2O+amine}$ under the assumption of 500 Pa and 5000 Pa for lean and rich CO_2 partial pressures, respectively. The blended solvent's capacity is higher than that of 7 m MEA which is only ~0.35 mol CO_2/kg $_{H2O+amine}$. Finally, the experimental data is fitted by the following empirical model:

$$\ln P_{CO2} = 36.9 - 9064.8(1/T) + 1.3(\text{Ln Loading}) + 5064(\text{Loading}/T) - 21.2(\text{Loading}^2)$$

In taking the derivative of the above empirical expression with respect to 1/T, the ΔH_{abs} estimated at a loading of 0.3 mol CO_2/mol total alkalinity is found to be ~62.1 kJ/mol which is comparable to that of PZ under similar conditions.

Figure 6 presents the volatility of PZ in the mentioned MDEA/PZ blends.

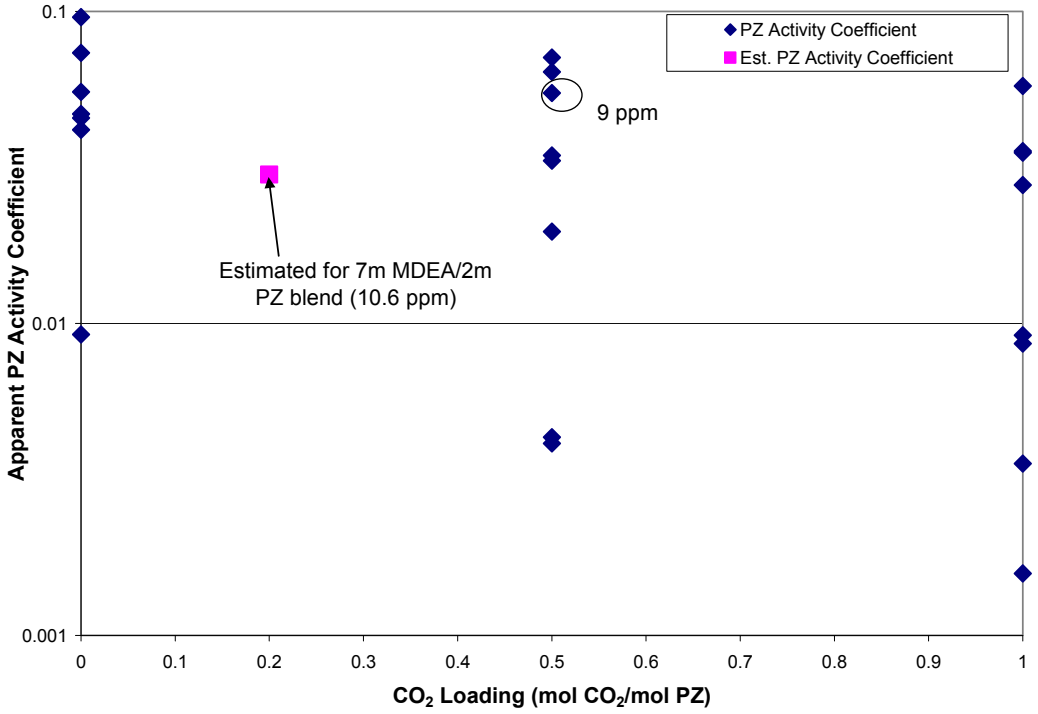

Figure 6: PZ Volatility in MDEA–PZ Blends (2.7 m–8.7 m MDEA/0.4 m–2.6 m PZ)

The apparent PZ activity coefficient for these various blended concentrations is much less than unity – a phenomenon which indicates that PZ and associated carbamate products are fairly non-volatile and prefer to stay in solution. There is an effect of loading on PZ volatility and most likely of temperature and total amine concentration as well.

The volatility of MDEA in these systems is measured and is presented in terms of ppm at 1 atm in Figure 7.

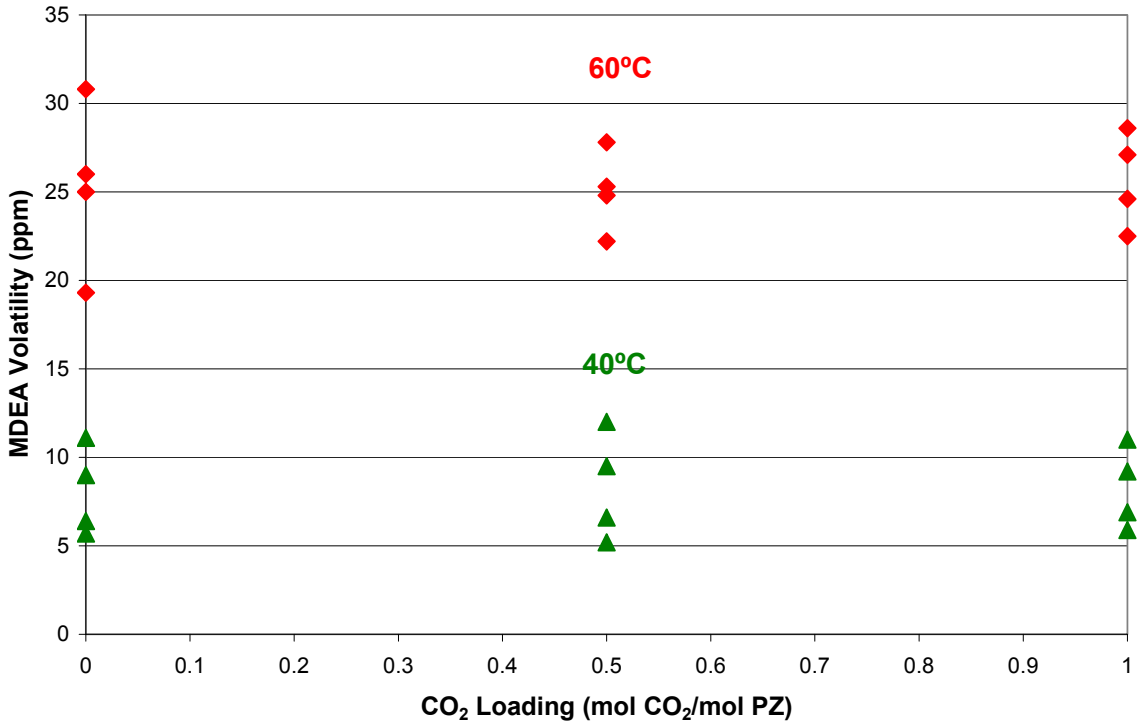

Figure 7: MDEA Volatility in MDEA/PZ Blends (2.7 m–8.7 m MDEA/0.4 m–2.6 m PZ)

MDEA volatility is greater at higher temperatures as the data at 60ºC is higher than that at 40ºC. This is because the amine has higher vapor pressure at higher temperature. Note that there is no apparent correlation of MDEA volatility to loading or amine concentration as CO_2 reacts preferentially with PZ more so than it does with MDEA.

Conclusion

For PZ systems (0.9 m–12.0 m) at typical absorber operating temperature of 40ºC, CO_2 partial pressure is ~500 Pa and ~5000 Pa at lean and rich loadings of 0.3 and 0.4 mol CO_2/equivalent of PZ, respectively. At stripper operating temperature of ~120ºC, CO_2 partial pressure is ~100,000 Pa for a loading of 0.3. The estimate CO_2 heat of absorption is -71.1 kJ/mol for 0.3 loading in PZ system. PZ volatility at 40ºC is ~ 4.8-33 ppm and is 8–100 ppm at 60ºC.

For MDEA-PZ system (2.7 m–8.7 m MDEA/0.4 m–2.6 m PZ) at 40ºC, CO_2 partial pressure is ~500 Pa and ~5000 Pa at lean and rich loadings of 0.09 and 0.35 mol CO_2/mol total alkalinity, respectively. In addition, the estimated capacity of the blended solvent is ~0.58 mol CO_2/kg $_{H2O+amine}$ – one that is certainly greater than

that of the baseline 7 m MEA solvent. The CO_2 heat of absorption is estimated to be ~ 62.1 kJ/mol at a loading of ~0.3 mol CO_2/mol total alkalinity. MDEA volatility is ~5–12 ppm at 40ºC for these blended systems. PZ volatility in these systems ranges from 2–19 ppm at 40ºC.

Future Work

We plan to further investigate VLE of higher concentration PZ systems (8, 10, 12 m) and of MDEA-PZ system (7 m MDEA/2 m PZ). Ultimately, there is plan to build a thermodynamic model for MDEA-PZ in Aspen which will reconcile with a pre-existing Fortran model for the blend. In addition, heat capacity will be measured for PZ system (8 m) for loadings of 0.15–0.45 mol CO_2/equivalent of PZ. Finally, an effort will be made to construct a high temperature VLE apparatus (100ºC–120ºC) for future solubility and volatility measurements.

Dynamic Operation of Amine Scrubbing in Response to Electricity Demand and Pricing

Quarterly Report for July 1 – September 30, 2008

By Sepideh Ziaii

Supported by the Luminant Carbon Management Program

And the

Industrial Associates Program for CO_2 Capture by Aqueous Absorption

Department of Chemical Engineering

The University of Texas at Austin

October 8, 2008

Abstract

This quarter's work focuses on dynamic simulation of dynamic operation of CO_2 capture in response to the electricity load and demand variation. This work is outlined in the attached paper prepared for GHTG-9. The rate-based dynamic model, which was created in ACM® for the stripper with 30 wt % MEA, was used to simulate two dynamic scenarios, turn-off and turn-on, by making 80% changes in the stripper load. A simple ratio control strategy is implemented to control the rich solvent rate proportional to the reboiler heat rate change.

When ramping between 20% and 100% load over 15 minutes, the energy in KJ/mole CO_2 removed does not vary more than 2% during the transition. For the current simulation conditions, the liquid hold up time in the reboiler for 100% and 20% load operation is 5 and 25 minutes, respectively. Since the response time of the stripper is dominantly determined by the solvent residence time in the reboiler at the end of the ramp, turn-on scenario has a smaller time constant by a factor of 4.65 and reaches steady state about 30 minutes after ramping the heat and liquid rate, while the turn-off scenario reaches steady state 2.5 hours after ramping the system.

Electric Grid Level Implications of Flexible CO_2 Capture Operation

Progress Report for July 1 – September 30, 2008

by Stuart Cohen

Supported by the Luminant Carbon Management Program

and the

Industrial Associates Program for CO_2 Capture by Aqueous Absorption

Department of Chemical Engineering

The University of Texas at Austin

October 27, 2008

Abstract

A model of the Electric Reliability Council of Texas (ERCOT) electric grid uses a basic representation of plant dispatch and the ERCOT electricity market to investigate the implications of flexible carbon dioxide (CO_2) capture in response to hourly electricity demand variations for a \$0-\$60/tCO_2 range of CO_2 price[4,5]. Using ERCOT grid conditions in 2006, CO_2 capture plants with the choice of operating CO_2 capture at 20% or 100% load do not operate at 100% load until CO_2 price is at least \$15/tCO_2. Below this CO_2 price, flexibility allows operating profits at eight CO_2 capture facilities to be several hundreds of millions of dollars greater than if CO_2 capture were operated continuously at 100% load; however, venting the CO_2 that is not captured at part-load could prevent the desired emissions reductions from being achieved. Significant CO_2 emissions reductions are achieved with flexible CO_2 capture above \$20/tCO_2, and the \$20-\$35/tCO_2 range offers the opportunity for tens to hundreds of millions of dollars in operating profit above that earned with continuous 100% load operation by allowing plant operators to pick the CO_2 capture operating point that results in the optimal combination of power output, electricity production costs, and electricity price. Coal-based facilities remain primarily as base load generation up to about \$40/tCO_2, so increases in average wholesale electricity price are equal to emissions costs at natural gas-fired facilities. CO_2 capture operation is secondary to CO_2 price in determining changes to wholesale electricity price; at a given CO_2 price,

[4] All dollar values are displayed in 2006 US dollars.

[5] All quantities of CO_2 are displayed in metric tons.

the average price increase from the case of no CO_2 capture to that with continuous 100% load operation is less than \$3/MWh[6].

Motivation for Investigating Flexible CO_2 Capture

Flexible operation of a post-combustion amine absorption/stripping system could allow plant operators to recover some or all of the energy required for CO_2 capture and use it for power generation when electric grid conditions deem this practice desirable. Flexible operation would consist of redirecting some or all of the steam being used for solvent regeneration and to drive CO_2 compressors back to the power generation turbine system, resulting in part or zero-load CO_2 capture but increased electricity output. A plant operator could choose from two or more CO_2 capture operating points depending on electricity demand and other market conditions.

Previous work has shown that operating CO_2 capture at zero-load during annual peak electricity demand can eliminate the need to spend billions of dollars to replace generation capacity lost when CO_2 capture operates at 100% load. In this application, flexible operation could relieve grid capacity constraints that may otherwise by imposed by CO_2 capture retrofits. A modeling study of the ERCOT grid determined that such capital savings could be achieved with fewer than 100 hours of zero-load CO_2 capture operation, allowing CO_2 emissions reductions to approach those achieved with continuous 100% load operation (Cohen *et al.,* 2008).

Instead of investigating flexibility to relieve grid capacity constraints, this work explores the implications of flexible operation in response to hourly variations in the electricity market conditions that result from changes in CO_2 price and electricity demand. By adding additional control over power plant output, flexible CO_2 capture could allow plant operators to utilize CO_2 capture in the most economical way possible.

Modeling Flexible CO_2 Capture in Response to Varying Electricity Demand in a CO_2 Regulated Electric Grid

Model Purpose

The major focus of this quarter has been refinement and development of the modeling methodology described in the second quarter report for 2008. Some of the methodology, results, and conclusions in this report are repeated in the paper submitted to the GHGT-9 conference entitled "Dynamic Operation of Amine Scrubbing in Response to Electricity Demand and Pricing." The content below expounds on this work's contribution to that paper and includes additional results.

---

[6] Electricity production is displayed in Megawatt-hours.

The model uses a basic representation of plant dispatch and the Electric Reliability Council of Texas (ERCOT) electricity market to investigate the implications of flexible CO_2 capture operation in response to hourly variations in electricity demand over the course of a year. The model describes the performance, economics, and CO_2 emissions amongst power plants in a CO_2 constrained electric grid under several scenarios of CO_2 capture operation.

A Review of Previous Modeling Methodology

The model incorporates a cost of CO_2 emissions either by assuming a constant CO_2 price that could represent a CO_2 tax, or by allowing CO_2 price to fluctuate around an average value to characterize possible CO_2 price variations in a cap and trade system. Electricity production costs for each plant are calculated as the sum of fuel costs, other operation and maintenance (O&M) costs, and any applicable CO_2 emissions cost. For plants utilizing CO_2 capture, the percent of CO_2 removed from flue gas and the energy required per unit of CO_2 removed is used to adjust the plant's heat rate and CO_2 emissions rate before calculating production costs. Production costs are then used to create a dispatch order from which the model chooses to utilize the least to most expensive plants until electricity demand in a particular hour is met. As a basic representation of the ERCOT competitive market for electricity, the last and most expensive plant dispatched in each hour is taken as the marginal generating facility that sets the wholesale electricity price in that hour. From hourly electricity prices, plant output, and production costs, profits can be calculated. Capital charges are not included in production costs because these sunk costs are not factored directly into dispatch decisions. CO_2 emissions can also be found from calculated plant generation.

The model does not consider transmission constraints or any other technical or geographical influences on plant generation. It also does not incorporate any restrictions on plant ramp rate or where a plant may be dispatched in the dispatch order. While these limitations prevent the model from determining highly accurate results, the model remains an effective tool for assessing the electric grid level implications of flexible CO_2 capture.

Additional detail on modeling methodology and a section describing model validation can be found in the second quarter report for 2008.

New Model Additions

The primary addition to the model is an operational strategy for flexible CO_2 capture that seeks to maximize hourly profits given the choice of two operating conditions. That scenario, identified as *FLEX Profit,* is described fully in the "Scenarios Considered" section below.

For power plants designated to use CO_2 capture, the model now incorporates a finite CO_2 removal and CO_2 capture energy requirement when the CO_2 capture

system is operated at a reduced load. This methodology allows for a more accurate representation of a CO_2 capture "off" operating point that is likely to involve a residual energy penalty and possibly even some CO_2 removal if turning CO_2 capture "off" does not involve bringing the entire absorption/stripping system to a complete halt.

In order to more accurately determine electricity production costs with CO_2 capture, several additional O&M costs specifically associated with CO_2 capture are now included in the model. Fixed operation and maintenance (FOM) costs include labor, maintenance, and administration; variable operation and maintenance (VOM) costs include solvent makeup, caustic used for solvent reclaiming, reclaimer waste disposal, water used in the CO_2 capture and compression system, and CO_2 transport and storage. Parameters used to calculate these O&M costs are summarized in Table 1 below. All FOM costs are calculated using the methodology in Rao, Rubin & Berkenpas (2004), modified to find costs per unit MWh produced. Maintenance costs assume that the total plant cost of the CO_2 capture system is \$908/kW[7] (Rubin, 2007). VOM costs are calculated based on the amount of CO_2 removed in a given hour, which can vary depending on the operating point of the CO_2 capture system (zero-load, part-load, or full-load).

Table 1: Parameters used to calculate the fixed and variable operation and maintenance costs associated with CO_2 capture (Rao and Rubin, 2002; NETL, 2005; Rubin, 2007; USNETL, 2007)

Fixed Operation & Maintenance Cost Parameters		**Variable Operation & Maintenance Cost Parameters**	
Parameter	*Value*	*Parameter*	*Value*
Operating Labor (jobs/shift)	2	MEA Consumption (kgMEA/tCO_2)	1.5
Hourly Wage (\$/hr)	33	Caustic Consumption (kgNaOH/tCO_2)	0.075
Maintenance Cost (% of total plant cost for CO_2 capture system)	2.2	MEA Cost (\$/kgMEA)	2.36
Maintenance Cost Allocated to Labor (% of total maintenance cost)	12%	Caustic Cost (\$/kgNaOH)	0.46
Administration & Support Labor Cost (% of total labor cost)	30%	Waste Disposal Costs (\$/kg)	0.20
		Water Cost (\$/m^3)	0.27
		CO_2 Transport/Storage Cost (\$/tCO_2)	9.08

[7] Capacity costs are displayed in dollars per kilowatt of rated capacity.

CO_2 Capture Operation in the ERCOT Grid over a Range of CO_2 Prices

Model Input Settings

As in previous work, the model uses ERCOT hourly load data and plant performance parameters from 2006. Average fuel costs for Texas in 2006 were \$1.48/MMBTU[8] for coal and \$6.60/MMBTU for natural gas (USEIA, 2007; USEIA, 2008). Future work will explore the sensitivity of model results to changes in average fuel price and may also incorporate variability in natural gas price.

Eight of ERCOT's 15 coal-based plants are chosen to use post-combustion CO_2 capture so that operating CO_2 capture continuously at 100% load will reduce the average coal fleet emissions rate by roughly 50%. This decrease in CO_2 emissions would allow the average coal fleet emissions rate to approach that of typical natural gas-fired facilities. The eight plants chosen have the lowest sum of electricity production costs with CO_2 capture at 100% load plus the capital costs of any required CO_2 and sulfur dioxide (SO_2) removal equipment. High SO_2 removal is required to mitigate solvent degradation in the amine absorption/stripping unit, so it is assumed that SO_2 removal equipment must be installed along with a CO_2 removal system on any boiler units that do not currently have SO_2 removal in the flue gas stream. Capital costs assume \$221/kW for SO_2 removal equipment, \$908/kW for CO_2 removal equipment, and a high risk capital charge factor of 0.175 as recommended in a National Energy Technology Laboratory (NETL) report (Rubin, 2007; USNETL, 2007). It will be critical for any facility operating CO_2 capture to have a storage site in relative proximity to the power plant. In ERCOT, all coal-fired facilities are in the general vicinity of candidate enhanced oil recovery (EOR) wells or brine reservoirs along the Gulf Coast, so this characteristic is not used to eliminate any plants from candidacy for CO_2 capture retrofit (Ambrose *et al*., 2006). Available land for CO_2 capture equipment will also be a major factor in decisions regarding CO_2 capture retrofits, but no data on available land at each facility have been collected at this time.

In scenarios that allow flexibility, CO_2 capture may operate at 100% or 20% load, with performance defined using results from Ziaii's dynamic process model. CO_2 removal and total equivalent work, including pumping and compression work, are shown in Table 2 below. At 20% load, CO_2 that is not captured is assumed to be vented to the atmosphere. System response time is not included explicitly, but it is assumed that the results from one hour calculation intervals will approximate those found when considering the 1–2 hour response times described in Ziaii's modeling results.

[8] Units of heat input for each fuel type are displayed in million British thermal units (MMBTU).

Table 2: CO_2 capture system performance parameters at 100% and 20% load

CO_2 Capture Load	*CO_2 Removal*	*Total Equivalent Work (kJ/mol CO_2)*
100%	90.0%	42.72
20%	18.1%	42.54

Scenarios Considered

BAU: The business as usual scenario considers the actual ERCOT grid in 2006 without any CO_2 capture.

CCS Base: CO_2 capture is operated at 100% load continuously throughout the year.

FLEX Op Costs: Plants with CO_2 capture choose whichever of the 20% and 100% load operating conditions has the lowest production costs for that plant. At no cost of emitting CO_2, it will always be least expensive to operate at 20% load, and increasing the CO_2 price will eventually allow lower production costs at 100% load.

FLEX Profit: This scenario represents an important addition to the model by allowing an investigation of flexible CO_2 capture where plant operators seek the best mode of operation to increase profitability. *FLEX Profit* operates under the assumption of perfect knowledge of electricity demand and dispatch ordering prior to deciding whether to operate CO_2 capture at 20% or 100% load. In every hour, each plant with CO_2 capture calculates its hourly operating profits for two scenarios: if all plants with CO_2 capture operate at (A) 100% load or (B) 20% load. If profits are greater at a particular plant for Option A, that plant will operate CO_2 capture at 100% load; otherwise, it will operate at 20% load. Because the output capacity of plants with CO_2 capture is lower at 100% load, Option A is likely to have a higher electricity price.

The *FLEX Profit* scenario does not represent a profit maximization algorithm. Indeed, a particular plant may earn greater profits than in both Option A and Option B by operating at 20% load while all other plants choose to operate at 100% load. The plants that are operating at 100% load will have lower power output, which could drive up electricity prices. A single plant operating CO_2 capture at 20% load at this time could then improve profits by selling additional electricity as long as its additional output does not significantly reduce the electricity price. Such strategic behavior, however, is not considered in the analysis below.

For each of these four scenarios, the model is used to calculate grid behavior for CO_2 prices from \$0-\$60/tCO_2.

Power Plant and Electric Grid Operation

The solid lines on Figure 1 plot the total annual electricity generation in each scenario for all coal-fired plants in ERCOT over the range of CO_2 prices. For the three scenarios that utilize CO_2 capture, the dashed lines represent the portion of total coal-based generation that comes from coal-based facilities with CO_2 capture systems when operating CO_2 capture at 100% load. For *BAU* and *CCS Base*, total coal-based generation stays relatively constant up to about \$40/tCO_2, after which generation begins to fall noticeably with increasing CO_2 price. Continuous CO_2 capture 100% load in the *CCS Base* scenario is evident by its dotted line being horizontal at a level of about 48 million MWh. *FLEX Op Costs* and *FLEX Profit* almost always choose to keep CO_2 capture at 20% load below \$15/tCO_2, where total coal-based generation is slightly less than that of *BAU* due to the energy use of CO_2 capture at 20% load. Total coal-based generation in *FLEX Op Costs* drops slightly at \$20/tCO_2 when the two most efficient CO_2 capture facilities have lower production costs at 100% load; at \$25/tCO_2 and above, *FLEX Op Costs* follows the *CCS Base* curve exactly. While typical plant economic studies find that CO_2 prices of around \$40/tCO_2 are required to justify installation of a CO_2 capture system, these data indicate that once a system is installed, the CO_2 price to justify 100% load operation may be much lower (Rubin 2007). *FLEX Profit* requires a CO_2 price of about \$40/tCO_2 for CO_2 capture to remain at 100% load throughout the year, indicating that the \$20–\$35/tCO_2 range provides an opportunity for flexible CO_2 capture to improve operating profits above those earned with continuous 100% load operation. Dashed lines reveal how CO_2 price affects the frequency of operating CO_2 capture at 100% load in the *FLEX Op Costs* and *FLEX Profit* scenarios; calculated values for the percent of time throughout the year when CO_2 capture is operated at 100% load are shown in Table 3.

In general, Figure 1 demonstrates that below \$40/tCO_2, changes in total coal-based generation are due primarily to CO_2 capture operating practices. Because coal-fired plants make up just 20% of ERCOT installed capacity, plant dispatch order changes little below \$40/tCO_2 even in the absence of CO_2 capture (ERCOT 2006). Above this price point, reductions in total coal-based generation are due to substantial changes in dispatch order where natural gas-fired plants begin to replace coal-fired facilities for base load generation. For example, at \$50/tCO_2, coal-based plants operate as the marginal generator 21% of the time in *BAU* and 11% of the time for all other scenarios. Fuel switching only affects coal-fired plants without CO_2 capture, as is evident from the horizontal dashed lines above \$40/tCO_2 for all CO_2 capture scenarios. In an electric grid with a greater contribution of coal to the generation mix, fuel switching behavior is likely to occur at a lower CO_2 price.

Electricity demand remains constant across all scenarios and CO_2 prices, so any reduction in coal-based generation is offset by an equivalent increase in natural

gas-fired generation. Thus, plotting natural gas-fired generation vs. CO_2 price shows the opposite trends of those seen in total coal-based electricity output.

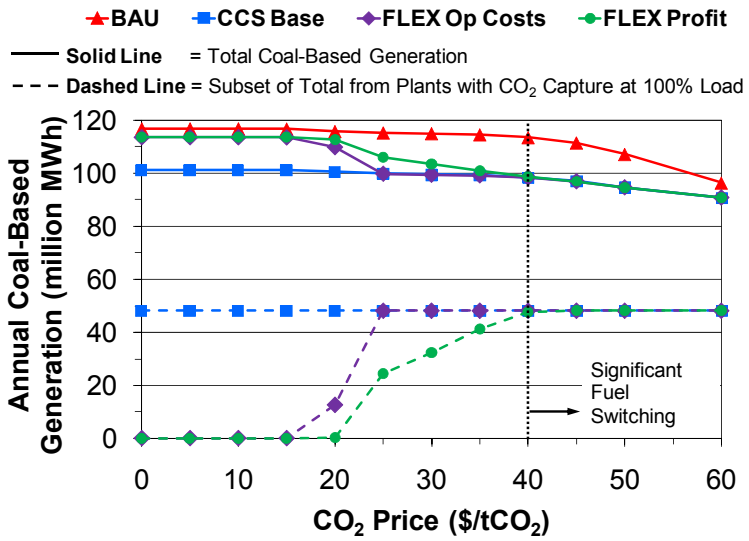

Figure 1: Solid lines show annual total coal-based electricity generation for each scenario vs. CO_2 price. For each scenario that uses CO_2 capture, dashed lines represent the subset of total coal-based generation from coal-fired plants when CO_2 capture is operated at 100% load.

Table 3: Percent of time throughout the year that CO_2 capture is operated at 100% load

CO_2 Price ($/tCO$_2$)	*0*	*10*	*20*	*30*	*40*	*50*	*60*
FLEX Op Costs	0.0%	0.0%	25%	100%	100%	100%	100%
FLEX Profit	0.0%	0.1%	0.6%	67%	99%	100%	100%

CO_2 Emissions Reductions

Figure 2 displays the reduction in annual coal fleet CO_2 emissions in each scenario for the range of CO_2 prices, with the percent reduction calculated relative to emissions levels in the *BAU* case with no CO_2 price. Aforementioned trends in coal fleet generation are evident in this figure. *BAU* emissions fall negligibly below \$15/tCO$_2$ and less than 5% below \$40/tCO$_2$, above which fuel switching allows significant emissions reductions.

CCS Base nearly achieves the desired 50% reduction in coal fleet CO_2 emissions at low CO_2 prices, and higher CO_2 prices allow further reductions as fuel switching begins to limit the output of coal-fired plants that do not use CO_2 capture. *FLEX Op Costs* begins with emissions reductions of about 10% at low CO_2 prices (when all CO_2 capture systems operate at 20% load), jumps to 20% at \$20/tCO_2, and then follows the *CCS Base* curve (when all CO_2 capture operates at 100% load) above \$25/tCO_2. *FLEX Profit* requires a CO_2 price of about \$25/tCO_2 before emissions reductions are much greater than those achieved with continuous 20% load operation. If CO_2 is vented when CO_2 capture is at part-load, flexibility may prevent the emissions reductions that could be achieved with continuous full-load operation, but reductions are still significant as long as the CO_2 price is high enough for production costs to be lower at 100% load.

Increased natural gas-based generation to make up for decreased output at coal-fired facilities partially offsets coal fleet emissions reductions. However, because natural gas-fired plant emissions rates are roughly half that of coal-fired plants without CO_2 capture, net electric grid emissions reductions are still very significant, as is shown in Table 4 below.

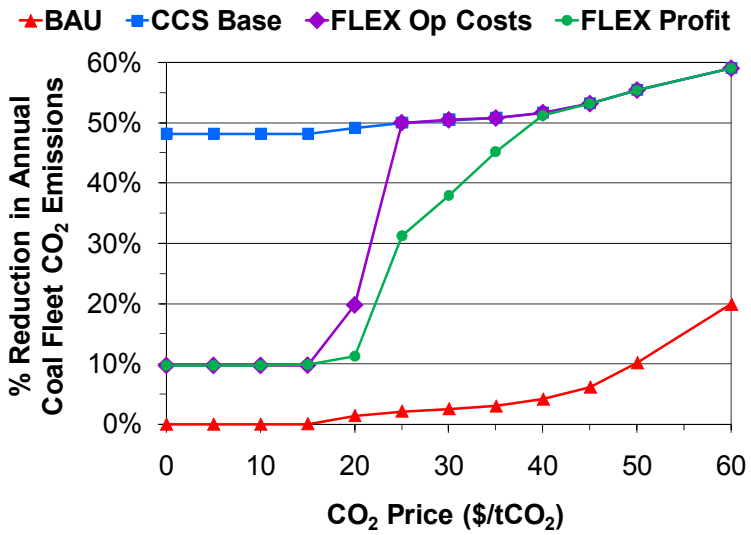

Figure 2: Reductions in annual CO_2 emissions in the ERCOT coal fleet in each scenario vs. CO_2 price

Table 4: Annual Total ERCOT CO_2 Emissions (million tCO_2) in each scenario for select CO_2 prices. The percent reduction relative the *BAU* scenario with no CO_2 price is shown in brackets.

CO_2 Price ($/t$CO_2$)	*0*	*10*	*20*	*30*	*40*	*50*	*60*
BAU	183 [0.0%]	183 [0.0%]	182 [0.7%]	181 [1.3%]	179 [2.0%]	175 [4.5%]	167 [12%]

CCS Base	132 [28%]	132 [28%]	132 [28%]	130 [29%]	129 [29%]	126 [31%]	124 [32%]
FLEX Op Costs	173 [5.6%]	173 [5.6%]	162 [11%]	130 [29%]	129 [29%]	126 [31%]	124 [32%]
FLEX Profit	173 [5.6%]	173 [5.6%]	171 [6.3%]	143 [22%]	130 [29%]	126 [31%]	124 [32%]

Economic Impacts of CO_2 Price and CO_2 Capture Flexibility

Figure 3 displays cumulative annual operating profits at the eight coal-fired facilities using CO_2 capture. When no CO_2 capture is available (*BAU*), operating profits fall dramatically as CO_2 price increases, though it takes a CO_2 price of about \$30/tCO_2 before it is more profitable to operate with CO_2 capture installed. Because lower emitting natural gas-fired plants continue to set electricity prices most of the time, production costs at coal-fired plants without CO_2 capture increase faster than electricity prices for a given CO_2 price increase, resulting in rapid profit decline. Operating profits are especially low for CO_2 prices above \$40/tCO_2 because coal-fired generators are often at or near the position of marginal generator. Though *CCS Base* has lower profits than *BAU* below \$30/tCO_2, it exhibits the opposite trend because emissions rates at coal-based plants with CO_2 capture are less than those of natural gas-fired facilities. *FLEX Op Costs* demonstrates that choosing between 100% and 20% CO_2 capture load allows much greater operating profitability than continuous 100% operation when CO_2 prices are too low to justify the operating expense. In the \$20-\$35/tCO_2 range, *FLEX Profit* improves profitability from *FLEX Op Costs* by allowing generators to consider the balance between production costs, power output, and electricity price at a given electricity demand and choose to operate in the most profitable manner. At \$25/tCO_2, such behavior improves operating profits by \$130 million over those earned with continuous 100% load operation. Flexibility has no impact on operating profits above \$35/tCO_2 in this static CO_2 price analysis; however, the value of flexibility is expected to be greater in a cap and trade regime where CO_2 prices could fluctuate between values that justify CO_2 capture operation and those that do not.

Calculated wholesale electricity prices, averaged over the year, increase predictably with CO_2 price at a rate of about \$0.50/MWh for each \$1/tCO_2 increase, which corresponds to a typical natural gas emissions rate of 0.5tCO_2/MWh (Figure 4). A slight increase in slope can be perceived for *BAU* above \$50/tCO_2 because of the increased use of coal-based plants as the marginal generator. Using CO_2 capture decreases total output at coal-fired facilities, requiring a more expensive marginal generator, but the average difference between electricity price in the *BAU* and *CCS Base* scenarios is only \$2.83/MWh for a given CO_2 price. Using CO_2 capture has a relatively small effect on average electricity prices relative to the dominating effect of CO_2 price.

In all scenarios, operating profits of natural gas-based generators increase monotonically with CO_2 price due to increased electricity prices and the greater use of natural gas during CO_2 capture operation and when CO_2 prices are high enough to justify fuel switching. Profits at nuclear and other non-CO_2-emitting generation sources increase significantly with CO_2 price because their production costs remain constant as CO_2 costs drive up electricity prices.

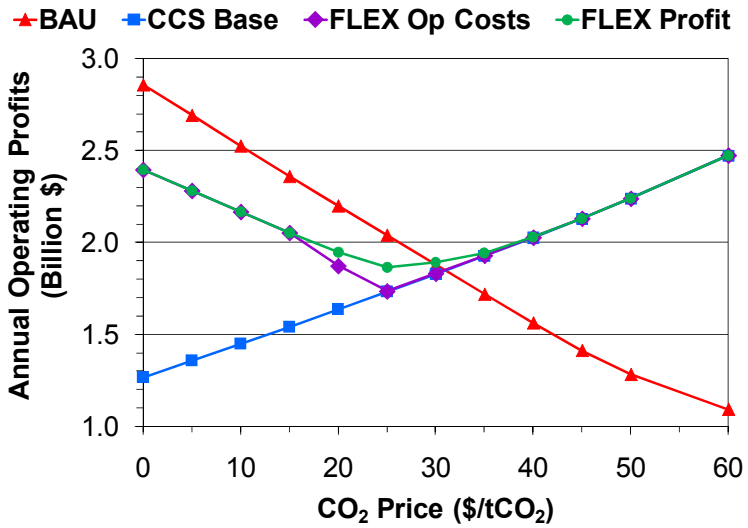

Figure 3: Cumulative annual operating profits in each scenario vs. CO_2 price for the eight coal-fired plants that use CO_2 capture (except in the *BAU* scenario)

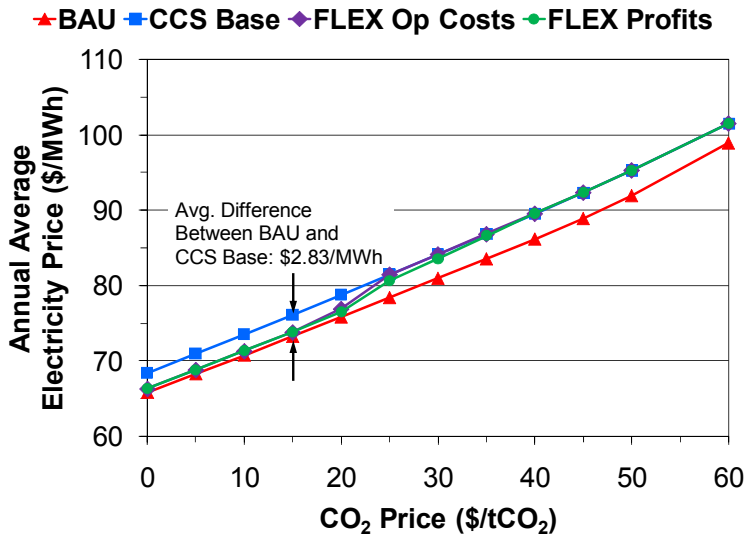

Figure 4: Average wholesale electricity price over the year for each scenario vs. CO_2 price

Discussion of Flexible Behavior in the *FLEX Profit* Scenario

Unlike *FLEX Op Costs*, where the choice between 20% and 100% CO_2 capture load is determined solely by electricity production costs, the chosen operating point in *FLEX Profit* depends on the relative changes in production cost, power output, and electricity price at each operating point. A CO_2 capture system will be operated at 20% load if the following inequality is true in a particular hour.

$$MW_{\substack{Power\\Output\\20\%}} * 1hr * \left(\frac{\$}{MWh}\bigg|_{\substack{Elec.\\Price\\20\%}} - \frac{\$}{MWh}\bigg|_{\substack{Prod.\\Cost\\20\%}} \right) > MW_{\substack{Power\\Output\\100\%}} * 1hr * \left(\frac{\$}{MWh}\bigg|_{\substack{Elec.\\Price\\100\%}} - \frac{\$}{MWh}\bigg|_{\substack{Prod\\Cost\\100\%}} \right)$$

Assuming that CO_2 price is high enough for production costs to be lower with 100% load CO_2 capture, the following inequalities must always be true. Electricity price is typically greater at 100% load because lower plant output at CO_2 capture facilities requires a more expensive plant to be dispatched as the marginal generator.

$$MW_{\substack{Power\\Output\\20\%}} > MW_{\substack{Power\\Output\\100\%}}$$

$$\frac{\$}{MWh}\bigg|_{\substack{Prod\\Cost\\20\%}} > \frac{\$}{MWh}\bigg|_{\substack{Prod\\Cost\\100\%}}$$

$$\frac{\$}{MWh}\bigg|_{\substack{Elec.\\Price\\20\%}} \leq \frac{\$}{MWh}\bigg|_{\substack{Elec.\\Price\\100\%}}$$

Thus, in order to justify operating at 20% load, the decrease in electricity price must not offset the gains from increased electricity sales. As CO_2 price increases, there is a greater difference between production costs at 100% and 20% load, so it becomes less likely that 20% load operation will allow greater operating profits. For a given CO_2 price, precisely when plants choose to be at 20% or 100% CO_2 capture load is dependent on the *difference* in electricity price (or equivalently, the difference in production costs of the marginal generator) at each operating point rather than the general *magnitude* of electricity price at a given electricity demand.

For example, at the highest annual peak electricity demand, there is a large difference in electricity price between the cases when all CO_2 capture plants are at 20% versus 100% load. As a result, *FLEX Profit* will choose to operate CO_2 capture at 100% load during these annual peaks. Contrary to prior intuition, it may be most economical for a coal-fired facility with CO_2 capture to operate at full-load during annual peak electricity demand, because doing so drives up electricity prices enough to offset the reduced plant output. Of course, this behavior is in conflict with using flexible CO_2 capture to relieve grid capacity constraints, so

economic or regulatory policy may be required to assure that flexible CO_2 capture is not used at a disadvantage to electric grid reliability.

Conclusions

The ERCOT grid model using plant level dispatch has been refined and extended in order to study flexible CO_2 capture operation in response to hourly electricity demand variations under a range of CO_2 prices. If production costs are not lower when CO_2 capture operates at 100% load, flexibility may improve annual operating profits by several hundred millions of dollars over those earned with continuous 100% load operation, though venting CO_2 at part-load operation may not achieve desired environmental benefits. Significant CO_2 emissions reductions can be achieved with flexible CO_2 capture as long as production costs are lower at 100% load. Above this CO_2 price, there is an additional range of CO_2 prices where flexibility can improve operating profits by tens to hundreds of millions of dollars by allowing plant operators to choose the CO_2 capture load that results in the most profitable operation in a given hour. The most profitable operating point does not generally depend on a particular magnitude of electricity demand or price; rather, it is a function of the relative changes in production costs, power output, and electricity price between operating points.

While \$40–\$50/tCO_2 may be the CO_2 price required to justify building a CO_2 capture facility, the CO_2 price to justify 100% load CO_2 capture may be closer to \$25/tCO_2. The CO_2 price required for operating profit to be greater with CO_2 capture installed is slightly higher. Because coal-based generation makes up just 20% of ERCOT's installed capacity, the CO_2 price required to cause significant fuel switching from coal to natural gas could be quite high, so natural gas-fired plants will continue to be the primary determinants of electricity price as long as natural gas fuel cost remains much higher than that of coal. Thus, until CO_2 price is high enough for coal-fired facilities to become frequent as the marginal generator, electricity prices will increase at about \$0.50/MWh for each \$1/tCO_2 increase. The use of CO_2 capture adds less than \$3/MWh to average electricity price.

Future Work

Further study of the *FLEX Profit* scenario will better quantify the electricity market conditions at which different operating points are most profitable. Having fully investigated this scenario, the next steps are to examine the sensitivity of model results to various input parameters such as fuel price, CO_2 capture performance, and CO_2 regulatory scheme (tax vs. cap and trade).

To improve the realism of model behavior, it will be important to incorporate a finite system response time into each transition between operating points as well as a representation of performance in this transition period.

To generate a more complete economic assessment of flexible CO_2 capture, future work will investigate some of the cost differences between a flexible and non-flexible CO_2 capture system. In addition, the model will be used with projected or estimated changes in various inputs over a period of years or decades in order to conduct a discounted cash flow analysis that will gauge the long term benefits of flexible CO_2 capture in terms of net present value or breakeven point.

References

Ambrose, WA *et al.* "Source-Sink Matching and Potential for Carbon Capture and Storage in the Gulf Coast". Austin, Gulf Coast Carbon Center, University of Texas at Austin. 2006.

Cohen, SM *et al.* "Turning CO_2 Capture On & Off in Response to Electric Grid Demand: a Baseline Analysis of Emissions and Economics". *ASME 2nd International Conference on Energy Sustainability*. Jacksonville. 2008.

ERCOT. 2006 Annual Report.

NETL. Carbon Capture and Sequestration Systems Analysis Guidelines. USDOE. 2005.

Rao, AB & ES Rubin. "A Technical, Economic, and Environmental Assessment of Amine-Based CO_2 Capture Technology for Power Plant Greenhouse Gas Control". Env Sci Tech. 2002;36(20):4467–4475.

Rao, AB *et al*. "An Integrated Modeling Framework for Carbon Management Technologies". Final report to DOE/NETL (Contract no. DE-FC26-00NT40935). Pittsburgh, PA, Center for Energy and Environmental Studies, Carnegie Mellon University. 2004.

Rubin, ES, C Chen & AB Rao. "Cost and performance of fossil fuel power plants with CO_2 capture and storage". *Energy Policy*. 2007;35:4444–4454.

USEIA. "Average Cost of Coal Delivered for Electricity Generation by State, Year-to-Date through October 2007 and 2006". epmxlfile4_10_b.xls, USDOE. 2007.

USEIA. Texas Natural Gas Wellhead Price, USDOE. 2008.

USNETL. Cost and Performance Baseline for Fossil Energy Plants. *Bituminous Coal and Natural Gas to Electricity*. JM Klara. 1. 2007.

Oxidative Degradation and Thermal Degradation Experiments

Quarterly Report for July 1– September 30, 2008

by Fred Closmann

Supported by the Luminant Carbon Management Program

and the

Industrial Associates Program for CO_2 Capture by Aqueous Absorption

Department of Chemical Engineering

The University of Texas at Austin

November 4, 2008

Abstract

In this quarter we concluded a series of oxidative degradation experiments on the 7 m MDEA/2 m PZ and the 7 m MDEA. Experiments were performed in a low gas flow apparatus under well stirred conditions and in the presence of various dissolved metals. A key indicator of the degradation of amine solvents is the production of formate in the solvent over time. When sparged with 98% O_2 at 55°C, 7 m MDEA/2 m PZ with 1 mM Fe^{2+} produced 0.011 ± 0.001 mM formate/hr. At the same conditions, 7 m MDEA produced 0.013 ± 0.001 mM formate/hr. When we take into account the amount of amide formed, measured as formate, 7 m MDEA/2 m PZ with 1 mM Fe^{2+} produced 0.021 ± 0.001 mmoles formate/L-hr. The formation of amides in oxidatively degraded samples can be as much as twice the amount of formate produced. Very little glycolate was measured in the oxidative degradation experiments of the solvent blend. Sexton (2008) measured the rate of production of formate at 0.39 mmoles/L-hr, which is an order of magnitude greater than the amount measured in the solvent blend. We determined that the resistance to oxidative degradation follows the order: MDEA/PZ=MDEA>PZ.

We completed a series of thermal degradation experiments on the blended solvent at loadings in the range of 0.1 to 0.4 moles CO_2/mole alkalinity. Most of those results are presented in the attached GHGT-9 paper, but the 135°C study was recently completed, and the estimated degradation rates have been revised based on the complete 42-day study. The revised data is included in Table 1. We measured thermal degradation rates of MDEA and PZ of -11 ± 11 mmolal/day and -7 ± 20 mmolal/day, respectively, in a loaded 7 m MDEA/2 m PZ solvent blend at

120°C. At 135°C, the PZ degradation rate in the solvent blend loaded at 0.2 moles CO_2/mole alk is -44 ± 2 mmolal/day, which is approximately three times the magnitude (16 ± 6 mmolal/day) of the appearance of unidentified diamine compounds in the same experiment. We utilized the rate of appearance of unidentified diamine compounds in the 7 m MDEA/2 m PZ thermal degradation studies to determine the energy of activation for the process resulting in the formation of unidentified diamines, assuming an Arrhenius relationship, and estimated the E_o to be 20.2 kJ/mol. This value was compared to the activation energy for the thermal degradation of MEA, which was 29 kJ/mol.

Table 1: Thermal Degradation Rates: Average MDEA/PZ Loss/Diamine Appearance Rates – Revised

Solvent	Temp (°C)	Duration (Days)	MDEA Deg Rate (mmolality/day)		PZ Deg Rate (mmolality/day)		Diamine Appearance Rate (mmolality/day)	
			? = 0.1	? = 0.2	? = 0.1	? = 0.2	? = 0.1	? = 0.2
7 m MDEA	100	63	-6 ± 6	-18 ± 52	NA	NA	NA	NA
	120	63	-0.3 ± 11	-31 ± 16	NA	NA	NA	NA
7 m MDEA/2 m PZ	100	54	-3 ± 13	-19 ± 4	-2 ± 4	-6 ± 1	1 ± 2	2 ± 2
	120	54	-11 ± 11	-7 ± 20	-7 ± 3	-9 ± 5	2 ± 2	5 ± 2
7 m MDEA/2 m PZ w/ 1 mM Fe^{2+}	100	42	NA	3 ± 13	NA	2 ± 5	NA	2 ± 3
	120	49	NA	-18 ± 28	NA	-11 ± 10	NA	12 ± 3
7 m MDEA/2 m PZ	135	28	-9 ± 8	-30 ± 15	-31 ± 3	-44 ± 2	20 ± 4	16 ± 6

? = All loadings in mols CO_2/mol total alkalinity.

The complete degradation work related to the 7 m MDEA/2 m PZ solvent blend is being presented as a poster and paper at the GHGT-9 conference in November 2008, and is attached to this quarterly report.

Finally, we collected CO_2 absorption rate data on the 7 m MDEA/2 m PZ with 0.19 moles CO_2/mole alkalinity using the wetted wall column. We measured k_g' values of 6.2E-11 moles/s*cm^2*Pa at 40°C, and 6.1E-11 moles/s*cm^2*Pa at 60°C at equilibrium partial pressures of 3.5 kPa and 15.6 kPa, respectively. These values are approximately 50% higher than similar data collected on a 7.7 m MDEA/1.2 m PZ blend (Bishnoi, 2000), and more than double the rates (k_g') measured for 7 m MEA (Dugas, 2008).

Future Work

Oxidative degradation experimental samples for the 7 m/2 m MDEA/PZ solvent blend will be analyzed to determine whether heat stable salts other than formate are being formed; to date, we have measured very little glycolate in our experiments on the 7 m MDEA/2 m PZ blend. Because we measured formate production rates at twice the magnitude when we performed sample hydrolysis

with 5N NaOH to reverse the formation of amides, we will investigate amide formation using IC methods.

We will attempt to identify the diamines which appear in the thermal degradation studies at 120 and 135°C using cation chromatography GC/MS methods. Once these peaks have been identified, we can determine their concentration and identify the pathway by which these compounds are formed.

We will perform more wetted wall column studies at a range of conditions including 80°C if possible with our current wetted wall configuration, and with different amine blends (other than 7 m MDEA/2 m PZ). In these studies, we are interested in determining the optimal amine blend from a rate standpoint.

Available online at www.sciencedirect.com

ScienceDirect

Energy Procedia 00 (2008) 000–000

Energy Procedia

www.elsevier.com/locate/XXX

GHGT-9

Catalysts and Inhibitors for MEA Oxidation

Andrew J. Sexton, Gary T. Rochelle*

The University of Texas at Austin, Department of Chemical Engineering, 1 University Station C0400, Austin, Texas 78712-0231

Elsevier use only: Received date here; revised date here; accepted date here

Abstract

Aqueous monoethanolamine (MEA) was subjected to oxidation by O_2/CO_2 at 55°C. Hydroxyethyl-formamide (HEF) and hydroxyethylimidazole (HEI) are the major oxidation products of MEA. Dissolved metals catalyze oxidation in the order copper > chromium/nickel > iron > vanadium. Inhibitors A, B and ethylenediaminetetracetic acid (EDTA) are effective degradation inhibitors. The addition of the expected inhibitors formaldehyde, formate or sodium sulfite had unintended effects on MEA losses. Total carbon and nitrogen analysis shows a greater than 90% closure of the material balance.

Keywords: Monoethanolamine; Oxidation; Degradation; Catalyst; Inhibitor

1. Introduction

Aqueous monoethanolamine (MEA) is the solvent of choice for CO_2 capture from flue gas because of its high capacity for CO_2 absorption and fast reaction kinetics [1]. In a typical aqueous absorption/stripping process, 7 m MEA is contacted with flue gas containing 1 to 10% CO_2 and 3 to 15% O_2 at 40 to 70°C to get a CO_2 loading of 0.45 to 0.5 mol/mol MEA. The CO_2 is stripped at 100-120°C to provide a lean loading of 0.2 to 0.4 mol CO_2/mol MEA. Solvent contaminated by degradation products is reclaimed from a slipstream.

Degradation of the solvent occurs by oxidation at absorber conditions and carbamate polymerization in the stripper [2]. Since most gas treating processes using alkanolamines have been operated in the absence of oxygen, oxidative degradation has not been quantified. Oxidative degradation is important because it can impact the environment and process economics and decrease equipment life due to corrosion.

1.1. Prior Work

Studies for the U.S. Navy [3-5] measured oxidation of amine solvents in the presence of 25 to 60 ppm dissolved iron. Chi and Rochelle [6] found that 0.0001 to 3.2mM dissolved iron produced 0.12 to 1.10mM/hr NH_3 from 7 m

* Corresponding author. Tel.: +1-502-350-1298; fax: +1-512-475-7824.
E-mail address: andres@che.utexas.edu.

MEA. Sexton [7] observed hydroxyethyl-formamide (HEF) and hydroxyethylimidazole (HEI) as important products of MEA oxidation with Fe catalyst.

V^{+5} and Cu^{+2} are corrosion inhibitors that can be used with aqueous MEA [8]. Blachly and Ravner [9] determined that Cu^{+2} at 10 ppm was even more effective than dissolved iron as an oxidation catalyst; 40 ppm Ni^{+2} was also effective. Goff [10] concluded that Cu^{+2} had a greater catalytic effect than Fe^{+2}; he also showed that the rate of NH_3 evolution is controlled by the rate of O_2 absorption into the amine when catalyzed by Cu^{+2} or Fe^{+2}.

Ethylenediaminetetracetic acid (EDTA) has been identified as an excellent chelator for copper and iron catalysts [11-13]. Fe is a known catalyst for EDTA oxidation [14]. Iminodiacetic acid (diglycine), glyoxylic acid and cyanate have all been identified as anionic degradation products of EDTA in the presence of UV and H_2O_2 [15].

Inhibitor A has proven to be effective with both iron and copper in aqueous MEA [10]. Na_2SO_3 is a known oxygen scavenger that is used in a range of applications varying from boiler feedwater treating to food packaging [16-18]. The kinetics of sulfite oxidation in aqueous solutions are known to be very fast, and the rate of oxidation is controlled by the rate of oxygen absorption.

Formaldehyde is an expected intermediate in the oxidative degradation of MEA [10,11]. Formate is an observed degradation product from the oxidation of formaldehyde. Since both of these products may compete with MEA for oxygen, they are suitable compounds to screen as degradation inhibitors. Although formaldehyde itself is considered toxic under the Clean Air Act [19], the presence of oxygen should oxidize the formaldehyde to formate, or it may react with MEA and oxygen to form hydroxyethyl-formamide.

Previous work by Sexton [7, 20] established that hydroxyethyl-formamide (HEF), 1-2-(hydroxyethyl)imidazole (HEI), formate, and ammonia are the major products of MEA degradation with catalysis by Fe^{+2}.

This goal of this study is to compare and contrast key liquid- and gas-phase oxidation products of MEA in the presence of these degradation catalysts and inhibitors. An oxygen consumption rate is calculated from product rates and their respective stoichiometries in order to determine whether degradation is kinetics controlled or mass transfer controlled by oxygen mass transfer. Additional details of this work and results for the oxidation of other amines are given by Sexton [20].

1.2. Experimental Apparatus

With low gas flow, oxygen mass transfer was achieved by vortex entrainment of 100ml/min of 98%O_2/2%CO_2 into 350mL of agitated amine solution controlled at 55°C. With high gas flow, 7.5l/min of air/N_2/2% CO_2 was sparged through 400mL of agitated aqueous amine controlled at 55°C. In both cases, the gas was presaturated with water at 55°C. Additional details on the apparatus are given by Sexton [7, 20].

1.3. Analytical Methods

Anionic degradation products were quantified using a Dionex IonPac AS15 Analytical Column and AG15 Guard Column. The mobile phase was KOH: 2mM from 0 to 17 minutes, ramping to 45mM, and held from 26 to 40 minutes. Water used for diluting the concentrated KOH was 18.2 MΩ*cm. MEA and cationic degradation products were quantified using two IonPac CS17 columns in series with a CSRS 4-mm suppressor. The mobile phase was 5mM methanesulfonic acid (MSA) from 0 to 7 minutes, 11mM at 7 minutes, then increased from 11mM to 39mM from 12 to 17 minutes, and held at 39mM until 20 minutes.

Nonionic degradation products were determined by HPLC with a Waters T3 C18 column using an evaporative light scattering detector (PL-ELS 2100). The nebulizer and evaporator were both set at 50°C with a N_2 flowrate of 1.6 SLM and a light source intensity of 85%. The method started with 1ml/min of 98% H_2O/2% acetonitrile (ACN) from 0-3 minutes, ramped to 80% H_2O/20% ACN from 3-15 minutes, and held until 20 minutes.

Total amide was determined by treating samples with NaOH and determining additional released organic acids by anion chromatography. However, this method gives systematically lower hydroxyethyl-formamide than direct HPLC analysis. Therefore it is only used for formamide when HPLC analysis is unavailable.

Volatile MEA and degradation products with high gas flow were determined by a gas-phase FTIR, a Temet Gasmet™ Dx-4000 held at 180°C. Amine solutions were loaded by sparging pure CO_2 with continuous weighing on a scale. Additional details on the analytical methods are given by Sexton [7, 20].

2. Results

Table 2 gives results at low gas flow rates. The total MEA loss is calculated from initial and final MEA as determined by cation IC; MEA loss rates less than 0.4mM/hr are too small to detect using this method. The total C and N in products was calculated without including formamide by IC or unknowns by HPLC. Total oxygen consumption from products was calculated by multiplying each product rate by its oxygen stoichiometry, shown in Table 1.

Table 1. Oxygen Stoichiometry for Important Liquid- and Gas-Phase Oxidative Degradation Products of MEA

Product	Stoichiometry (ν)
NH_3	0.0
Formaldehyde	0.25
Formic Acid	0.75
HEI	0.625
HEF	0.75
NO	1.25
CO_2	1.25
HNO_2	1.5
N_2O	2.0
Oxalic Acid	2.0

Table 2. Oxidative Degradation Product Rates (mM/hr), Low Gas Flow (7 m MEA, 55°C, 100cc/min 98%O_2/2%CO_2, 0.4 moles CO_2/mole MEA, 1400 RPM), 10-14 days

	Catalyst Effect				Successful Inhibitors					Unsuccessful Inhibitors			
Catalyst (mM)													
Fe	1			0.1		1	1	1	1	1		1	1
V		1											
Cr/Ni			0.6/0.1		0.6/0.1								
Cu				5							5		
Inhibitor (mM)													
Inhibitor A					100								
Inhibitor B						7.5							
EDTA							2	10	100				
CH_2O										500	500		
Na_2SO_3												100	
CH_2O_2													500
Results (mM/hr)													
MEA Loss	3.8	2.1	8.0	10.3	1.0	1.2	8.6	1.5	0.1	5.1	8.0	5.1	4.5
C in Products	6.3	1.6	5.3	20.0	0.0	0.1	3.8	0.7	0.0	5.8	14.6	5.4	4.5
N in Products	2.5	0.6	2.1	7.1	0.0	0.0	1.4	0.2	0.0	2.3	5.3	2.0	2.0
O_2 Consumption	1.9	0.7	1.8	5.6	0.0	0.2	0.9	0.2	0.0	1.7	3.6	1.6	1.6
HPLC (mM/hr)													
HEI	0.66	0.11	0.59	1.70	0.00	0.00	0.37	0.06	0.00	0.64	1.28	0.59	0.55
HEF	0.77	0.10	0.00	3.25	0.00	0.00	0.50	0.09	0.01	0.00	2.27	0.00	0.00
Total unknowns	2.28	0.49	2.91	1.49	0.00	0.00	0.53	0.10	0.06	2.64	0.96	2.87	2.40
Anion IC (mM/hr)													
Formate	0.29	0.06	0.29	0.73	0.00	0.04	0.05	0.06	0.01	0.22	0.36	0.08	0.14
Formamide	0.35	0.12	0.43	2.35	0.00	0.10	0.21	0.10	0.00	0.68	0.76	0.35	0.42
Oxamide	0.09	0.15	0.19	0.42	0.00	0.03	0.09	0.02	0.00	0.06	0.21	0.31	0.09
Nitrite	0.21	0.05	0.23	0.29	0.00	0.00	0.02	0.00	0.00	0.25	0.17	0.13	0.30
Derived Results													
N in solution (M)			4.14		4.77	4.77			4.91	4.52			4.24
C in solution (M)		10.00	9.82	8.73	5.00	5.00			9.47	9.44	9.54		9.53
N Imbalance (mM/hr)			3.31		0.00	0.09			0.00	1.26			0.19
C Imbalance (mM/hr)		2.88	10.15	0.00	1.91	2.15			0.00	2.79	1.1		2.65

Product rates (mM/hr) are calculated from the final sample analysis and the total reaction time. Amides were determined by both HPLC (HEF only) and anion IC (all general amides). However, the HPLC gives consistently

greater concentration for formamide and is believed to be more reliable. Therefore it has been used in all material balances. Concentrations for unknown peaks from HPLC were estimated assuming the calibration curve for HEI.

Nitrogen in solution was determined using Kjeldahl analysis; total organic carbon in solution was calculated using a Shimadzu TOC analyzer. The nitrogen imbalance is nitrogen unaccounted for after MEA nitrogen and product nitrogen concentrations are subtracted from total nitrogen in solution; the carbon imbalance is calculated in a similar manner.

Table 3 gives both liquid-phase and gas-phase product rates at high gas flow. For each volatile component, the continuous production rate is integrated over the entire experiment time and reported as an average rate (mM/hr). The overall MEA loss was calculated using cation chromatography and volatile MEA loss was calculated using FTIR. The difference between these two rates gave an MEA degradation loss rate. In 7 m MEA at low gas, the catalyst activity is in the order Fe/Cu > Cr/Ni > Fe > V. With Cu, the oxygen consumption rate is considerably higher than other catalyst systems, suggesting that oxygen mass transfer may be enhanced by reaction in the boundary layer. On the other hand, vanadium catalyzed systems exhibit lower degradation and oxygen consumption rates.

Table 3. Oxidative Degradation Product Rates (mM/hr), High Gas Flow (7 m MEA, 7.5 L/min 15%O_2/2%CO_2, α = 0.40, 1400 RPM), 7-10 days

Catalyst (mM)	**1 Fe**		**0.1 Fe / 5 Cu**	
Date	**7/08**	**4/08**	**11/08**	**5/08**
Results (mM/hr)				
MEA Loss	**5.8**	**3.8**	**3.5**	**5.3**
C in Products	**1.5**	**1.1**	**4.8**	**5.0**
N in Products	**2.0**	**2.0**	**3.5**	**4.0**
O_2 Consumption	**0.9**	**1.1**	**1.9**	**1.8**
HPLC (mM/hr)				
HEF	**0.00**	**0.00**	**0.87**	**0.91**
HEI	**0.00**	**0.00**	**0.23**	**0.29**
Unknown Peaks	**0.54**	**0.50**	**0.60**	**0.45**
Anion IC (mM/hr)				
Formate	**0.10**	**0.18**	**0.53**	**0.22**
Formamide	**0.16**	**0.49**	**0.92**	**1.05**
Oxamide	**0.01**	**0.10**	**0.05**	**0.11**
FTIR (mM/hr)				
NH_3	**1.83**	**1.69**	**1.69**	**1.97**
CO	**0.30**	**0.00**	**0.00**	**0.00**
N_2O	**0.00**	**0.16**	**0.16**	**0.14**
NO	**0.12**	**0.12**	**0.12**	**0.06**
C_2H_4	**0.24**	**0.00**	**0.00**	**0.00**
Formaldehyde	**0.09**	**0.02**	**0.02**	**0.01**
Acetaldehyde	**0.16**	**0.06**	**0.06**	**0.02**
MEA Volatile Loss	**2.5**	**3.2**	**3.2**	**1.9**
Derived Results				
N in solution (M)		**4.33**		**4.39**
C in solution (M)		**9.52**		**9.78**
N Imbalance (mM/hr)		**0.46**		**1.66**
C Imbalance (mM/hr)		**3.94**		**8.90**

Hydroxyethylimidazole, hydroxyethyl-formamide and formate are the most abundant degradation products at low gas. The production rate of HEF is almost an order of magnitude higher with Fe and Cu than with Fe; the production of HEI increases by a factor of three. This results in a carbon formation rate that is approximately three times greater, and an MEA loss rate that is more than double than when copper is absent from solution.

The major difference between the iron catalyzed experiment and the combined iron and copper catalyzed experiment at high gas is the increase in formate and HEF production. HEF production increases by factor of two when copper is added in the high gas apparatus. HEI is only detected at high gas in the presence of iron and copper.

Because ammonia is stripped at high gas rate, it is not available to produce HEI, which is present in much lower concentration than at low gas in the presence of Fe and Cu.

All other major degradation product formation rates, including ammonia, are similar between the two systems. This differs from the results by Goff [10] which indicate greater ammonia rates with copper.

Carbon and nitrogen formation rates in the experiment catalyzed by both chromium and nickel are approximately 15% lower than in the iron catalyzed experiment; most of this is accounted for by the reduced production of HEI. There is once again a noticeable shift from formate (and formamide) to oxalate production. However, measured MEA losses are 53% greater.

With the exception of the experiment performed in the presence of chromium and nickel, the carbon material balance ranges from 87% to 104%. Similarly, the nitrogen material balance ranges from 92% to 101% in these selected experiments.

The gap in the overall carbon and nitrogen material balances is attributed to peaks that still have not been identified using HPLC with ELSD. While HEF and HEI have been positively identified, some combination of five unknown peaks consistently shows up when degraded MEA samples are analyzed using HPLC-ELSD. Most degraded samples containing Fe only have at least 90% of raw peak area unidentified. On the other hand, only 18% to 52% of peak area remains unidentified for degradation experiments conducted in the presence of copper catalyst.

Estimating the unknown peaks as HEI reinforces prior data. Formation rates for the unknown HPLC peaks (using the HEI calibration curve) are greater in the presence of Fe or Cr/Ni than when Fe/Cu is present. Vanadium catalyzed systems exhibit the lowest HPLC production rate. This suggests that the formation of HEF and HEI is favored when Cu is present.

At high gas flow, 48% to 68% of the degraded MEA carbons have been accounted for by measured degradation products; 75% to 100% of the nitrogen loss has been accounted for in degradation products. Although the material balance is not closed, the gap is smaller for the experiments conducted in the presence of iron and copper. The carbon to nitrogen ratio ranges from 1.25:1 to 1.38:1 for this set of experiments.

Inhibitor A is an extremely effective oxidative degradation inhibitor for MEA systems in the presence of chromium and nickel (over a 99% reduction in the formation of all detectable products). Moreover, MEA loss rate was reduced by a factor of eight and is approaching the detection limits of the cation chromatography system.

Experimental results also show Inhibitor B to be extremely effective at inhibiting degradation in the presence of iron catalyst. Carbon and nitrogen-containing products are reduced by 97%, while MEA loss rates were reported in the range of the inhibited Cr/Ni system – only 25% the MEA loss rate of an uninhibited system catalyzed by iron.

Table 2 also details the effect of EDTA concentration on MEA oxidation catalyzed by iron. Both degradation product formation and MEA loss decrease as EDTA concentration is increased. This suggests that in high enough concentrations, EDTA is effective at chelating Fe and inhibiting the formation of observable oxidative degradation products.

Sodium sulfite, formaldehyde and formate were all ineffective as degradation inhibitors for the observed MEA systems. While observed products went down by approximately 15% to 20%, the MEA loss rate increased by about 30% over an iron catalyzed solution in the absence of sodium sulfite. Results from Table 2 also show the addition of formaldehyde had little impact on reducing product rates, and increased the MEA loss rate by about 30%.

The copper-catalyzed MEA system containing 500mM formaldehyde behaved quite similarly to the iron-catalyzed formaldehyde experiment. Hydroxyethyl-formamide is present at a 4:1 ratio with formate. Formate performs slightly better than formaldehyde in the presence of iron, but worse than a system in the absence of formate. Observed carbon and nitrogen products are 20 to 30% lower, but MEA losses are 20% higher.

Oxygen consumption rates range from 0.7 to 5.6mM/hr for low gas experiments performed in the absence of effective oxidative degradation inhibitors; mass transfer of oxygen into the interfacial layer of liquid determines the degradation rate for these low gas experiments. The presence of copper enhances mass transfer such that reaction is taking place in the boundary layer. Experiments performed in the presence of iron as well as a combination of chromium and nickel gave similar O_2 rates.

The low oxygen rate in the presence of vanadium suggests MEA degradation may not be completely mass transfer controlled in the presence of vanadium catalyst, as it approaches rates observed at inhibited conditions. Rates for experiments performed under inhibited conditions ranged from 0.0 to 0.9mM/hr; the degradation rate in these types of experiments is expected to be limited by reaction kinetics. At high gas, oxygen consumption ranged from 0.9 to 1.9 mM/hr. Rates increased by approximately 85% in the presence of copper and iron versus iron only.

3. Conclusions

When both iron and copper are present in solution, HEF, HEI and MEA losses increase by a factor of 3 compared to a system absent of iron. High gas experiments supported these observations. In terms of oxidative degradation potential: copper > chromium/nickel > iron > vanadium.

Experiments with low gas flow reveal that HEF and HEI are the major oxidation products of MEA. MEA systems catalyzed by 1mM vanadium produce much less formate (as well as formamide) and HEI, but more oxamide than systems catalyzed by iron. Overall, carbon and nitrogen formation rates were lower, as well as MEA losses.

Chromium and nickel, two metals present in stainless steel alloys, also catalyze the oxidative degradation of MEA. Observed carbon and nitrogen product rates are 20% lower than in an iron catalyzed system, while MEA losses are 55% greater. This suggests that chromium and nickel combined have a greater catalytic effect than iron by itself.

Data from experiments with high gas flow show that a combination of copper and iron creates more HEF (the major carbon-containing degradation product) and HEI than iron by itself. The presence of copper in aqueous MEA solution enhances the production of both formate and HEF, which experiments show is created from either the reaction of formaldehyde or a metal-formate complex with MEA.

Ammonia is the dominant nitrogen-containing degradation product at high gas. At high gas rate, NO_x is produced and stripped from the solution. On the other hand, at low gas rate where gas is not stripped from solution, NO_x is retained in the solution and oxidized to nitrite and nitrate. High gas flow experiments show that average ammonia production is independent of metal catalyst, which disagrees with Goff's findings.

Inhibitor A reduces the formation of known products by over 99% and cuts MEA losses by a factor of eight in Cr/Ni catalyzed systems; Sexton [21] previously showed the presence of 100mM Inhibitor A reduces the formation of known degradation products by 90% in an MEA system catalyzed by both iron and copper. In the presence of iron, Inhibitor B reduces product rates by 97% and MEA losses by 75%. Low gas experiments show that a 100:1 ratio of EDTA to Fe is necessary to sufficiently inhibit the oxidation of MEA. At this ratio, no observable MEA losses or oxidative degradation products are detected.

The addition of formaldehyde, formate or sodium sulfite had an unintended effect on MEA losses. They actually increased the rate at which MEA degraded. While observed products decreased, MEA losses increased by 20% to 30% in the presence of these potential inhibitors; the greater concentration of unidentified products offsets the decrease in observed products.

Under assumed mass transfer conditions in the low gas apparatus, calculated oxygen consumption ranges from 1.6 to 1.9mM/hr in all experiments performed in the presence of Fe and Cr/Ni, 3.6 to 5.6mM/hr for experiments performed in the presence of Cu, and 0.7mM/hr in the presence of V. Oxygen consumption rates were 0.2mM/hr or less under assumed inhibited conditions. The experiment performed at 2mM EDTA is in the region controlled by both kinetics and mass transfer.

Total carbon and nitrogen analysis shows that, with the exception of the low gas experiment performed in the presence of Cr and Ni catalyst, there is over a 90% material balance on all selected low and high gas flow experiments.

4. Acknowledgements

This work was supported by the Luminant Carbon Management Program. Experiments were completed with the assistance of Jang Lee, Ellie Doh, and Jon Mellin.

5. References

1. Kohl, A.; Nielsen, R. Gas Purification. 5th edition; Gulf Publishing Co.: Houston, 1997.
2. Rochelle, G. T.; Bishnoi, S.; Chi, S.; Dang, H.; Santos, J. "Research Needs for CO_2 Capture from Flue Gas by Aqueous Absorption/Stripping." DE-AF26-99FT01029; U.S. Department of Energy – Federal Energy Technology Center: Pittsburgh, PA, 2001.
3. Carbon Dioxide Absorbants. Girdler Corporation, Gas Processes Division, Louisville, KY, 1950.
4. Kindrick, R. C.; Atwood, K.; Arnold, M. R. "The Relative Resistance to Oxidation of Commercially Available Amines." Girdler Report No. T2.15-1-30, in Report: Carbon Dioxide Absorbents, Contract No. NObs-50023, by Girdler Corp., Gas Processes Division, Louisville, KY, for the Navy Department, Bureau of Ships, Washington, DC (Code 649P), 1950.
5. Kindrick, R. C.; Reitmweier, R. E.; Arnold, M. R. A Prolonged Oxidation Test on Amine Solutions Resistant to Oxidation. Girdler Report No. T2.15-1-31, in "Report: Carbon Dioxide Absorbents", Contract No. NObs-50023, by Girdler Corp., Gas Processes Division, Louisville, KY, for the Navy Department, Bureau of Ships, Washington, DC (Code 649P), 1950.
6. Chi, S.; Rochelle, G. T. Oxidative Degradation of Monoethanolamine. *Ind. & Eng. Chem. Res.* **2002**, 41(17): 4178-4186.
7. Sexton, A.; Rochelle, G. T. Reaction Products from the Oxidative Degradation of MEA. In Preparation for submission to *Ind. & Eng. Chem. Res.*, 2008.
8. Veawab, A.; Aroonwilas, A. Identification of Oxidizing Agents in Aqueous Amine-CO_2 Systems Using a Mechanistic Corrosion Model. *Corrosion Science* **2002,** 44(5), 967-987.
9. Blachly, C. H.; Ravner, H. The Effect of Trace Amounts of Copper on the Stability of Monoethanolamine Scrubber Solutions; NRL-MR-1482; U.S. Naval Research Laboratory: Washington, DC, 1963, 9 pp.
10. Goff, G. S. Oxidative Degradation of Aqueous Monoethanolamine in CO_2 Capture Processes: Iron and Copper Catalysis, Inhibition, and O_2 Mass Transfer. Doctoral Thesis, The University of Texas at Austin, 2005.
11. Chi, Q. S. Oxidative Degradation of Monoethanolamine. M.S. Thesis, The University of Texas at Austin, Austin, TX, 2000.
12. Goff, G. S. et al. Oxidative Degradation of Aqueous Monoethanolamine in CO_2 Capture Systems Under Absorber Conditions; Gale, J., et al., Eds. 6th International Conference on Greenhouse Gas Control Technologies, Kyoto, Japan, 2003. Elsevier: Oxford, 2003, 115-120.
13. Blachly, C. H.; Ravner, H. Studies of Submarine Carbon Dioxide Scrubber Operation: Effect of an Additive Package for the Stabilization of Monoethanolamine Solutions; NRL-MR-1598; U.S. Naval Research Laboratory: Washington, DC, March 1965.
14. Seibig, S.; et al. Kinetics of [FeII(EDTA)] Oxidation by Molecular Oxygen Revisited. New Evidence for a Multistep Mechanism. *Inorganic Chemistry* **1997**, 36(18), 4115-4120.
15. Sorensen, M.; Zurell, S.; Frimmel F. H. Degradation Pathway of the Photochemical Oxidation of Ethylenediaminetetraacetate (EDTA) in the UV/H_2O_2 Process. *Acta Hydrochim* **1998**, 26(2), 109-115.
16. Somogyi, L. P. Food Additives in Kirk-Othmer Encyclopedia of Chemical Technology, http://www.mrw.interscience.wiley.com/kirk/articles/foodfrie.a01/frame.html (Accessed January 2008).
17. White, J. C. Deaerator Providing Control of Physiochemical Oxygen Scavenging in Boiler Feedwaters; U.S. Patent Application 2001045396, 2001.
18. Hakka, L. E.; Ouimet, M. A. Recovery of CO_2 from Waste Gas Streams Using Amines as Absorbents; U.S. Patent Application 2004253159, 2004.
19. EPA Technology Transfer Network Air Toxics Website, The original list of hazardous air pollutants, http://www.epa.gov/ttn/atw/orig189.html (Accessed January 2008).
20. Sexton, A. PhD dissertation, The University of Texas at Austin, In preparation, 2008.
21. Sexton, A. "Oxidation Products of Amines in CO_2 Capture"; Greenhouse Control Technologies, Proceedings of the 8th International Conference on Greenhouse Gas Control Technologies; Trondheim, Norway, June 18-22, 2006.

Available online at www.sciencedirect.com

ScienceDirect

Energy Procedia 00 (2008) 000–000

Energy Procedia

www.elsevier.com/locate/XXX

GHGT-9

Thermal degradation of monoethanolamine at stripper conditions

Jason Davis[a] and Gary Rochelle[a,*]

[a]*Department of Chemical Engineering, The University of Texas at Austin, 1 University Station CO400, Austin, TX 78712*

Elsevier use only: Received date here; revised date here; accepted date here

Abstract

Thermal degradation of monethanolamine (MEA) is quantified as a function of initial amine concentration, CO_2 loading, and temperature over a range of expected stripper conditions in an amine absorber/stripper unit. The sum of the degradation products N,N'-di(2-hydroxyethyl)urea, 1-(2-hydroxyethyl)-2-imidazolidone, and N-(2-hydroxyethyl)ethylenediamine make up the majority of total MEA loss. The temperature dependent rate constant has an activation energy similar to diethanolamine (DEA) of 29 kcal/mole which corresponds to a quadrupling of the degradation rate when the stripper temperature is increased 17^{o}C. At 135^{o}C the degradation rate varies from 2.5 to 6% per week. Using speciation data from an Aspen® model of a stripper unit, losses in the packing are significant, but the majority of MEA loss occurs in the reboiler and reboiler sump. Thermal degradation is minor when the reboiler temperature is held below 110^{o}C.

Keywords: monoethanolamine; MEA; thermal degradation; carbon dioxide; solvent management; stripping

1. Introduction

Monoethanolamine (MEA) is the state of the art solvent being considered for carbon dioxide removal via amine absorption/stripping due to its low cost of production and relative availability, yet there is very little published data on thermal degradation rates of MEA at stripper conditions. In natural gas treating, this problem has been controlled by maintaining low concentrations of amine and carbon dioxide, and operating the stripper at pressures slightly above atmospheric in order to keep the reboiler temperature as low as possible.

Oyenekan [1, 2] established that the energy requirements for the stripper and compressor can be reduced by operating the stripper at elevated pressures with high capacity solvents. This operational method utilizes thermal compression to pressurize the CO_2 stream prior to the compressor, thereby reducing energy and capital costs associated with the compressor. The elevated pressure increases the ratio of CO_2 to water that is evolved from the

* Corresponding author. Tel.: 1-512-471-7230; fax: +1-512-471-7060.
E-mail address:gtr@che.utexas.edu

stripper making the steam used in the reboiler a more efficient use of energy. The problem with elevated pressure and temperature is that it increases thermal degradation rates. In order to better understand the balance between energy optimization and solvent make-up costs, a model for amine thermal degradation needs to be established.

Polderman [3] describes the mechanism for thermal degradation of MEA by carbamate polymerization. In the absorber, MEA associates with CO_2 to form MEA carbamate as illustrated below.

This reaction is normally reversed in the stripper, but in some cases the MEA carbamate will cyclize to form 2-oxazolidone, which is also a reversible reaction, as shown below.

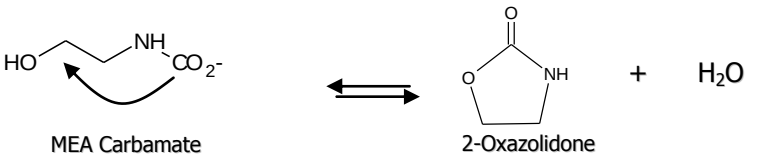

Yazvikova [4] found that MEA carbamate can also react with a free MEA molecule and irreversibly dehydrolize to form N,N'-di(2-hydroxyethyl)urea[2].

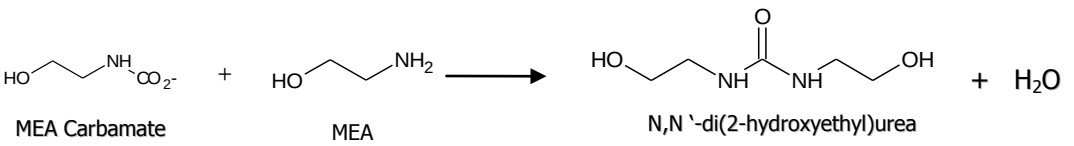

The former product, 2-Oxazolidone, can then react with another molecule of MEA to form 1-(2-hydroxyethyl)-2-imidazolidone which is sometimes referred to as HEIA.

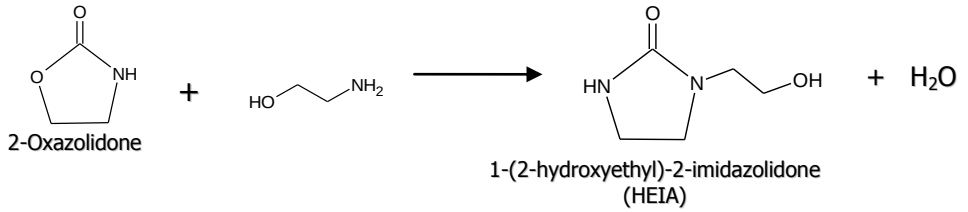

HEIA can then be hydrolyzed to form N-(2-hydroxyethyl)-ethylenediamine or HEEDA.

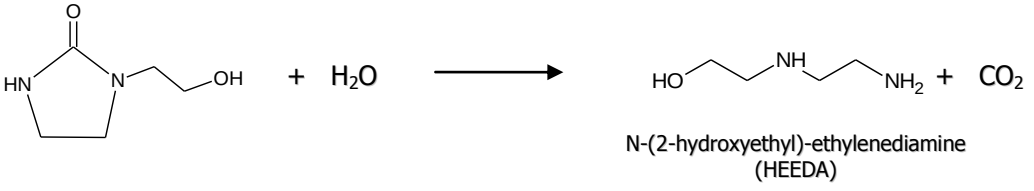

These four species (2-oxazolidone, dihydroxyethylurea, HEIA and HEEDA) plus further polymerization products are believed to be the main products of thermal degradation. The rate of formation of these products is a function of temperature (faster kinetics), CO_2 loading (more carbamate present), and MEA concentration.

Thermal degradation of diethanolamine has been studied by Kennard and Meisen [5, 6]. They found that the first order rate constant for DEA at temperatures from 90 to 170°C was linear on an Arrhenius plot and using the slope of this line, an activation energy of 29 kcal/mol is found. The reaction mechanism is similar to MEA and was found to form a DEA analog for the oxazolidone, urea, and HEEDA.

2. Experimental

Previous literature on thermal degradation of amines used a stirred reactor with intermittent sampling to quantify amine losses. The problem with this design is that in order to achieve a reasonable experiment time, elevated temperatures and CO_2 pressures were used to increase the degradation rate and only one concentration of amine and carbon dioxide could be tested at a time. In this work a set of 10mL stainless steel reactors were constructed and placed in a set of forced convection ovens set at temperatures ranging from 100 – 150°C. Multiple reactors were filled with the same solution and removed at set times over several months and an amine loss profile was constructed from the data. In this way many different amines, amine concentrations, CO_2 loadings, and temperatures were run at the same time yielding a large data set at reasonable operating conditions.

Amine solutions were made and loaded with CO_2 gravimetrically by bubbling pure CO_2 through the solution until the desired concentration was reached. Five to ten sample reactors were filled with 10mL of identical starting solution leaving a small amount of headspace, closed and tightened to Swagelok specifications and placed in a forced convection oven. Samples were removed at specified time intervals ranging from several days to several months and cooled to room temperature. The samples were then transferred to glass vials and a portion was diluted with deionized water for analytical testing. The samples were analyzed using cation ion chromatography to measure the disappearance of MEA and the appearance of ionic degradation products such as HEEDA. HPLC with an evaporative light scattering detector was used to measure nonionic species such as MEA urea and HEIA. Unknowns were identified using known addition spiking on IC and HPLC and by mass spectrometry.

For these MEA experiments the initial amine concentration was varied from 15 to 40wt% MEA in a CO_2 free solution, the CO_2 loading was varied from 0.2 to 0.5 moles CO_2 per mole of amine, and the temperature was varied from 100°C (an atmospheric stripper) to 150 °C which would represent a stripper at an elevated pressure of ~8 atm.

3. Results and Discussion

Figure 1 shows the effects of amine concentration, CO_2 loading, and temperature on amine loss. The points represent actual data points collected from individual sample reactors, and the curves represent an empirical fit of all the data over the entire range of operating conditions.

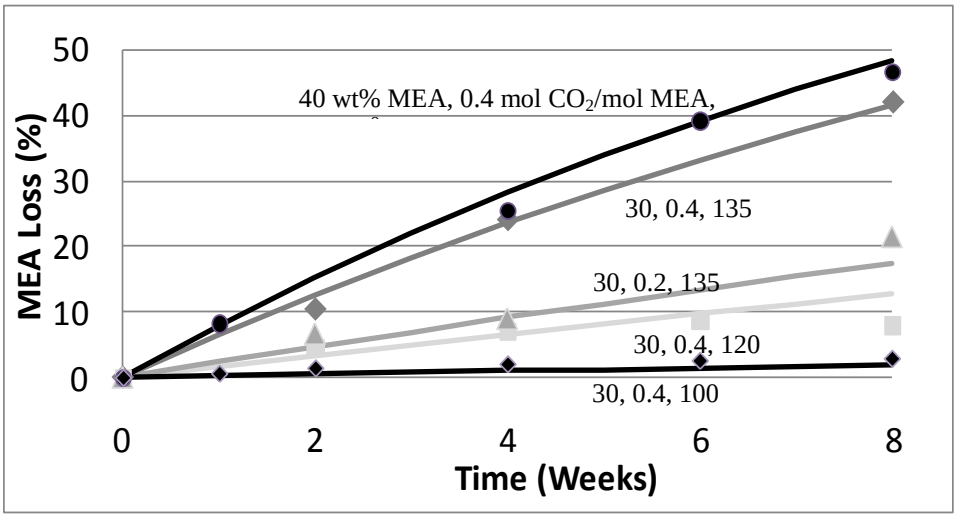

Figure 1. MEA loss over time as a function of MEA concentration, CO_2 loading and temperature

30 wt % MEA with a loading of 0.4 moles CO_2 per mole MEA at a temperature of 135°C will be used as the base case for this comparison. The bottom two curves represent a similar solution held at 120°C and 100°C. From this data, it can be concluded that the temperature dependent rate constant has an activation energy of 29 kcal/mol which corresponds to roughly quadrupling the degradation rate every 17°C or approximately every time the pressure of the stripper is doubled. This activation energy is equivalent to the activation energy found for DEA using the data provided by Kennard and Meisen.

Decreasing the loading is roughly a first order effect since reducing the loading from 0.4 to 0.2 corresponds to a similar decrease in degradation rate. Increasing the concentration from 30 to 40 wt % shows an effect that is slightly more than first order since the data does not collapse using this scale. In practice, increasing the concentration will also increase the reboiler temperature due to the elevated boiling point of solution assuming constant pressure. Although this temperature increase will be small, the overall increase in thermal degradation can be significant due to the strong temperature dependence discussed earlier.

3.1 Degradation Product Formation

MEA concentration was measured using cation ion chromatography and compared to the original undegraded MEA solution. For experiments with less than 5% total amine loss, the sum of the HEIA, HEEDA, and MEA urea is used to represent the total amine loss since experiments have shown that at low total degradation, these three products give a good mass balance with the total MEA loss. Table 1 shows the MEA and HEIA concentrations for 7 m MEA (30 wt %) at varying temperature and CO_2 loading.

Table 1. MEA and degradation product concentration (molality) after a given period of time based on CO_2 loading (moles CO_2/mole MEA) and temperature (°C) from a 7 m MEA solution.

Temp	Initial CO_2 Loading	MEA 2 weeks	MEA 4 weeks	MEA 8 weeks	HEIA 8 weeks	HEEDA 8 weeks	MEA Urea 8 weeks
100	0.2	6.94	6.92	6.88	0.03	NA	0.04
100	0.4	6.90	6.85	6.79	0.05	NA	0.05
100	0.5	6.90	6.84	6.77	0.05	NA	0.06
120	0.2	6.9	6.9	6.7	0.15	0.03	0.04
120	0.4	6.7	6.5	6.4	0.50	0.05	0.08
120	0.5	6.7	6.4	5.9	0.43	0.05	0.06
135	0.2	6.5	6.4	5.5	0.28	0.25	0.03
135	0.4	6.3	5.3	4.1	0.7	0.17	0.03
135	0.5	5.5	4.6	3.3	0.7	0.11	0.02
150	0.4	3.7	1.4	0.8	NA	NA	NA

Since it takes two molecules of MEA to form one molecule of HEIA, HEIA is a major degradation product totaling a large percentage of the total MEA loss at all temperatures. The drastic effect of temperature can also be seen as the total amine loss increases from 3% to 89% by increasing the temperature 50°C. One discrepancy in the data is the 8 week data point of the 120°C data at a loading of 0.4. The HEIA concentration appears to be larger than the total MEA loss since HEIA formation requires two molecules of MEA. The MEA concentration was found to be higher than the empirical model predicted concentration of 6.1m and the HEIA concentration was higher than expected.

Figure 2 shows the formation of degradation products as a percentage of total MEA loss. The black points represent measured MEA loss at the given times and overall curve is the sum of the degradation products.

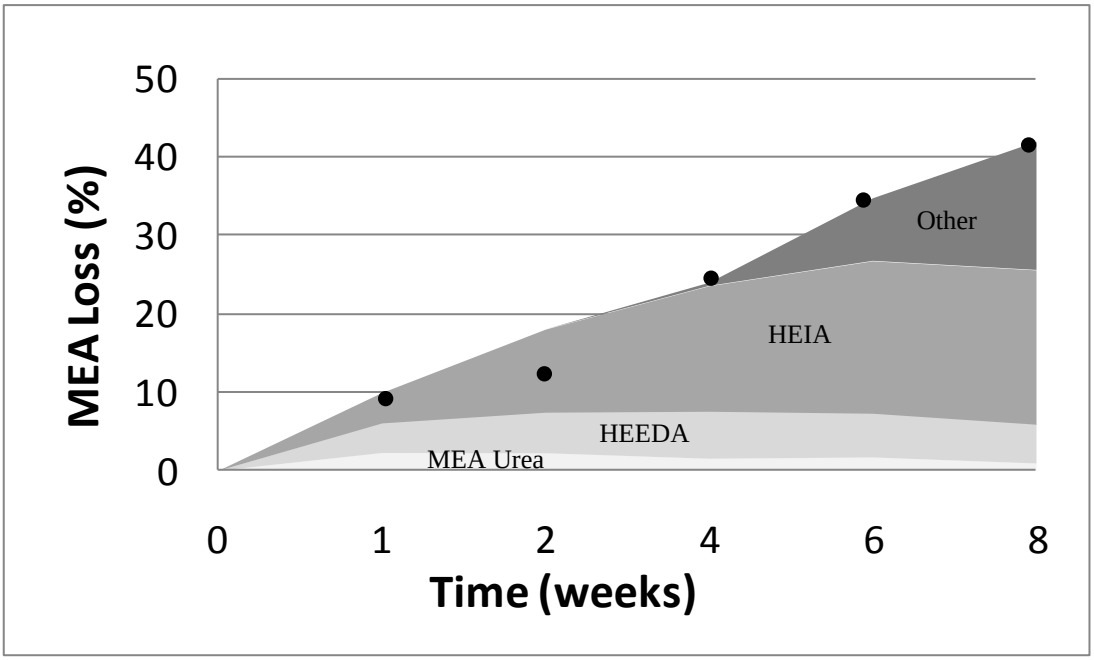

Figure 2. MEA degradation products as a sum of total MEA degradation in a 30 wt % MEA solution with a loading of 0.4 moles CO_2 per mole MEA held at 135°C.

The MEA urea appears in measurable quantities by HPLC in a very short time and maintains a steady concentration relative to the concentration of MEA. HEEDA and HEIA appear relatively close together, but the HEEDA reaches a pseudo-equilibrium with the MEA concentration and then decreases over time as the MEA decreases. The HEIA continues to increase after the HEEDA concentration has reached its maximum suggesting it is a stable product and not an intermediate for HEEDA production. The other products listed represent polymeric products that form when MEA reacts with HEEDA carbamate to continue the carbamate polymerization reaction and other side reactions. The sum of these products matches the overall MEA product loss well until significant degradation has occurred. For this reason, it is reasonable to assume the total amine loss can be measured by summing these degradation products at low reaction times. This allows for the measurement of degradation rates at short times and can decrease degradation experiment times and should allow for measurements of thermal degradation losses in short time pilot plant campaigns of MEA.

3.2 HEIA and HEEDA

Because the HEIA appeared to be a stable product, it was hypothesized that HEEDA is the precursor to HEIA and not the other way around as proposed by Polderman. Several sample reactors were filled with CO_2 loaded HEEDA, a blend of HEEDA and MEA, HEIA, and a blend of HEIA and MEA then placed in ovens set at 135°C. It was found that HEEDA converted to HEIA in stoichiometric quantities to the CO_2 concentration very rapidly in both the HEEDA and MEA/HEEDA blend, but HEIA did not convert to HEEDA in appreciable quantities until very long hold times. This leads us to believe that HEIA is formed from HEEDA carbamate and because the HEIA was well conserved over time, that it is a stable product. HEEDA also was found to degrade to polymeric products as found by ion chromatography.

3.3 MEA Urea Formation

MEA urea was found in appreciable quantities by HPLC in degraded MEA samples. MEA urea was found in measurable quantities at very short times and after an initial lag period, tracked the MEA concentration for the remainder of the experiment. Sample containers of 50 wt % oxazolidone in water were placed in the forced

convection ovens and taken out after several minutes to several hours. The oxazolidone converted to large quantities of the MEA urea. It is unclear if this urea is formed directly from oxazolidone or if the oxazolidone first reverts to MEA and then proceeds to the urea. Further experiments with the MEA urea will be conducted to test if this is an intermediate to further degradation products or if it just forms an equilibrium with MEA and remains in solution as such.

3.4 Degradation in the Stripper

The temperature and composition profile of a stripper taken from an Aspen Plus® simulation were used in conjunction with this work in order to determine where in the stripper thermal degradation occurs. The system was modeled using a 5 m MEA solution (~24 wt %) with a rich loading 0.45, lean loading of 0.37 and a pressure of 1.6 atm with a reboiler temperature of 108°C. It was assumed that there is 5% liquid hold-up in the packing and the sump volume is equal to the liquid hold-up in the packing. It was found that two-thirds of the total degradation occurred in the reboiler sump where the temperature was the highest and one-third occurred in the stripper packing where the CO_2 loading was highest. The total loss of MEA was found to be 80 g/ton of CO_2 under these conditions. Increasing the reboiler temperature by 20°C increased the loss to 540 g/ton CO_2. At a price of $1.10/lb of MEA, this gives a make-up cost of $0.19/ton CO_2 at the lower temperature and $1.31/ton CO_2 at the higher temperature. Further cost considerations that need to be taken into account include the cost of reclaiming and the cost of waste disposal. If thermal reclaiming is used it could drastically increase the total MEA degradation since this will be performed at higher temperatures in order to boil off the MEA.

4. Conclusions

MEA degrades in the presence of CO_2 at expected stripper temperatures. The temperature dependent rate constant has an activation energy equivalent to DEA of approximately 29 kcal/mol which corresponds to a quadrupling of the thermal degradation rate with a 17°C increase in temperature or a doubling of the stripper pressure. At 135°C the degradation rate is 2.5 to 6% per week. Loading has a first order effect and amine concentration has a slightly more than first order effect on the degradation rate.

The sum of HEIA, HEEDA and MEA make up the majority of total MEA loss in degradation experiments with less than 20% total MEA loss, and can be used to approximate MEA loss in short time experiments. Polymeric products that will form from the reaction of HEEDA with MEA do not appear in appreciable quantities until very long hold times and not until a large amount of HEIA is present.

HEIA is formed from HEEDA instead of Polderman's reaction mechanism which had this reversed. HEIA does not behave like an intermediate and is the most stable and abundant degradation product in highly degraded samples. HEEDA and MEA urea were found in measurable quantities that once established, track the MEA concentration throughout the remainder of the experiment.

MEA make-up costs from degradation in the stripper are low at temperatures below 110°C, but can become significant if the pressure in the stripper is increased in order to take advantage of thermal compression as suggested by Oyenekan. Further modeling and cost estimates need to be performed in order to optimize this balance between solvent make-up costs and energy requirements.

5. References

1. B.A. Oyenekan, G.T. Rochelle (2007). "Alternative stripper configurations for CO_2 capture by aqueous amines." *AIChE J.* **53**(12): 3144-3154.
2. B.A. Oyenekan, G.T. Rochelle (2006). "Energy performance of stripper configurations for CO2 capture by aqueous amines." *Ind. & Eng. Chem. Res.* **45**(8): 2457-2464.
3. L.D. Polderman, C.P. Dillon, *et al.* (1955). "Why monoethanolamine solution breaks down in gas treating service." *Proc. Gas Conditioning Conf*: 49-56.

4. N.V. Yazvikova, L.G. Zelenskaya, *et al.* (1975). "Mechanism of side reactions during removal of carbon dioxide from gases by treatment with monoethanolamine." *Z. Prik. Khim.* **48**(3): 674-676.
5. A. Meisen, M.L. Kennard (1982). "DEA degradation mechanism." *Hydrocarbon Processing, Intl Ed.* **61**(10):105-108.
6. M.L. Kennard, A. Meisen (1985). "Mechanisms and kinetics of diethanolamine degradation." *Ind. Eng. Chem. Fund.* **24**: 129-140.

Available online at www.sciencedirect.com

ScienceDirect

Energy Procedia 00 (2008) 000–000

Energy Procedia

www.elsevier.com/locate/XXX

GHGT-9

Absorption and desorption rates of carbon dioxide with monoethanolamine and piperazine

Ross Dugas[a], Gary Rochelle[a,*]

[a]*Department of Chemical Engineering, The University of Texas at Austin, 1 University Station C0400, Austin, TX 78712, USA*

Elsevier use only: Received date here; revised date here; accepted date here

Abstract

CO_2 absorption/desorption was measured in a wetted wall column at 40 and 60˚C with 7, 9, 11, and 13 m monoethanolamine (MEA) and 2, 5, 8, and 12 m piperazine (PZ) at various CO_2 loadings. 8 m PZ has a 75% greater CO_2 capacity than 7 m MEA. CO_2 absorption and desorption is 2–3 times faster with PZ than with MEA at equivalent CO_2 partial pressure. The CO_2 flux normalized by the liquid side partial pressure driving force, k_g', for both MEA and PZ is practically independent of temperature and amine concentration over the range of these experiments when represented as a function of the equilibrium partial pressure at 40˚C. Normalized flux decreases a factor of 10 as the equilibrium partial pressure at 40˚C increases from 100 to 10000 Pa.

Keywords: carbon dioxide; monoethanolamine; piperazine; absorption; desorption; rates; partial pressure; capacity

1. Introduction

CO_2 absorption and desorption rates are important in CO_2 capture since they can affect both capital and operating costs. Faster solvents can reduce the amount of packing required in the absorber and stripper and can also achieve a closer approach to equilibrium in the absorber, saving energy in the stripper.

CO_2 absorption rates into highly loaded, highly concentrated monoethanolamine (MEA) solutions have been measured by Aboudheir [1] and Dang [2]. Absorption rates in CO_2 loaded dilute piperazine (PZ) have been measured by Bishnoi [3]. CO_2 partial pressures in loaded MEA and PZ solutions at absorber temperatures have been measured by Hilliard [4], Jou [5], Dang [2], Bishnoi [3] and Ermatchkov [6].

Carbon dioxide absorption and desorption rates for 7, 9, 11, and 13 m MEA and 2, 5, 8, and 12 m PZ were measured in a wetted wall column at 40 and 60˚C. For each amine concentration about 4 CO_2 loadings were tested.

* Corresponding author. Tel.: 512-471-7230; fax: 512-471-7060
E-mail address: gtr@che.utexas.edu.

The CO_2 loadings represent the expected range of CO_2 loading in a CO_2 capture system for a coal-fired power plant. The equilibrium CO_2 partial pressure and liquid film mass transfer coefficients were measured at each condition.

2. Experimental Apparatus

The wetted wall column countercurrently contacts an aqueous amine solution with N_2/CO_2 on the surface of a stainless steel rod with a known surface area. Several researchers (Cullinane [7], Al-Juaied [8], Bishnoi [3], Dang [2]) have made rate and CO_2 partial pressure measurements with this equipment. A schematic of the overall wetted wall column is shown in Figure 1. A more detailed view of the reaction chamber is shown in Figure 2.

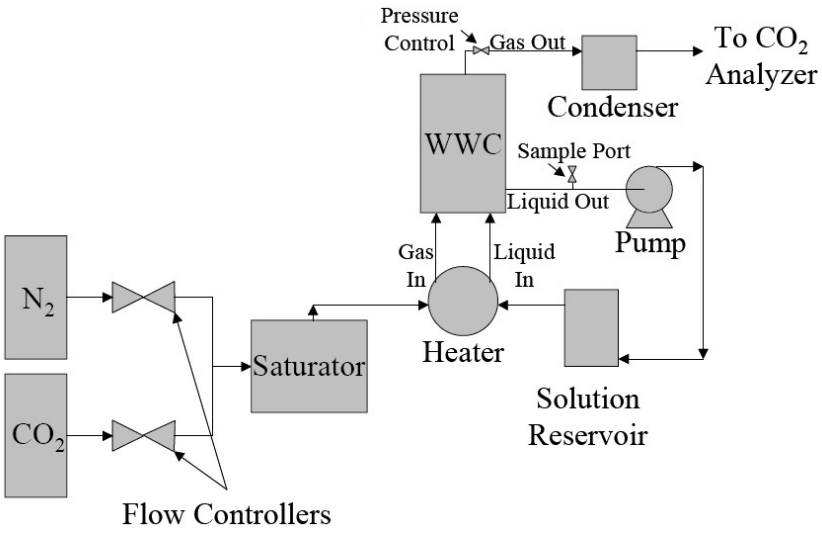

Figure 1. Schematic of the Wetted Wall Column

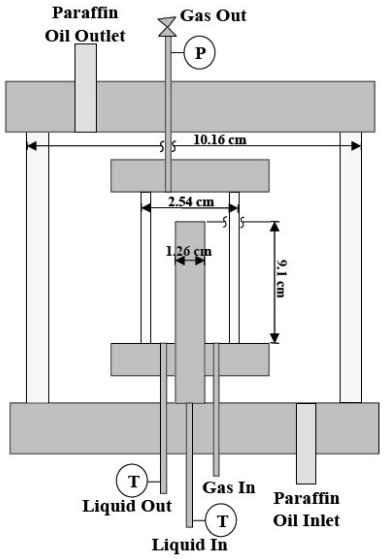

Figure 2. Schematic of the Wetted Wall Column Reaction Chamber

Nitrogen and carbon dioxide are mixed using mass flow controllers to create a simulated flue gas of known concentration. The gas is saturated and heated at the experimental temperature before entering the wetted wall column reaction chamber. In the chamber the gas countercurrently contacts the falling amine solution film on the surface of the stainless steel rod. CO_2 is either absorbed or desorbed into the gaseous phase. The outlet flue gas is dried using a condenser and $CaSO_4$ desiccant. The dry flue gas is analyzed by a Horiba CO_2 analyzer accurate to 0.5% of full scale. The Horiba analyzers have ranges of 0–500, 1000, 5000 ppm and 0–1, 2, 10, 20 mol%. Since the flow rate of gas, inlet and outlet CO_2 concentration and contact area for reaction are known, the flux and resultant kinetics can be determined. By testing inlet CO_2 concentrations that result in absorption and desorption, the equilibrium partial pressure can be bracketed and determined.

The wetted wall column can be operated from atmospheric pressure up to 100 psig, or 7 atmospheres gauge. Gas and liquid flow rates are typically 4–6 standard L/min and 0.18–0.24 L/min, respectively.

3. Results and Discussion

CO_2 absorption and desorption experiments in the wetted wall column are conducted using 6 inlet CO_2 partial pressures for each solvent condition. The flux of CO_2 is directly related to the log mean CO_2 partial pressure driving force, assuming plug flow for the gas. The equilibrium partial pressure is obtained by iterating to the zero flux partial pressure. The slope of the curve fitted line is equal to the overall mass transfer coefficient K_G. The overall mass transfer coefficient can be converted to the liquid film mass transfer coefficient, k_g', by using the series

resistance relationship (Equation 1) and a correlation [9] for the gas film mass transfer coefficient, k_g. Each set of 6 CO_2 absorption or desorption experiments, as shown in Figure 3, results in one k_g' value. Obtained k_g' values are a function of both the reaction kinetics and the diffusion of reactants and products, characterized by k_l^o. The k_g' rate plots (Figures 7–9) include physical mass transfer resistance but k_l^o estimations [9] are included in Tables 1 and 2. The diffusion coefficient of CO_2 in solution is calculated via the N_2O analogy. Diffusion coefficients in water were obtained from Versteeg [10]. N_2O diffusion rates in amines were obtained from Cullinane [9].

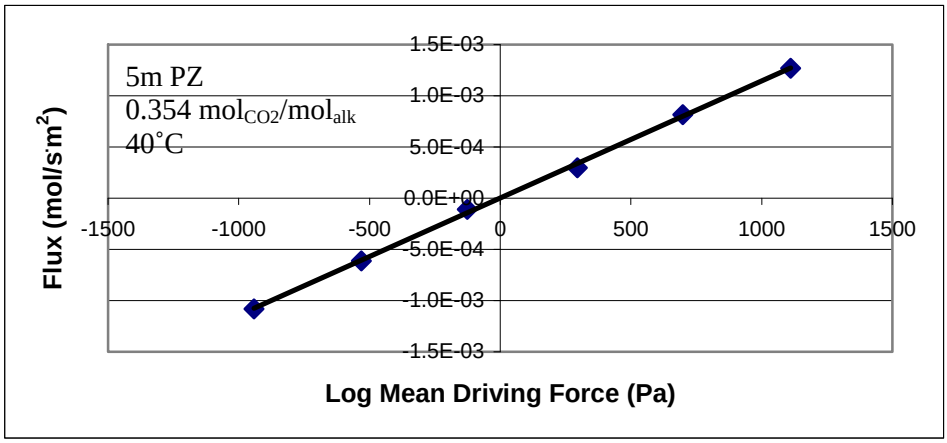

Figure 3. Flux-Driving Force Dependence for 5 m PZ, 0.354 mol_{CO2}/mol_{alk}, 40˚C

$$\frac{1}{K_G} = \frac{1}{k_g} + \frac{1}{k_g'} \tag{1}$$

The measured CO_2 partial pressure and rate data for MEA and PZ are listed in Tables 1 and 2, which include loaded amine solutions at expected conditions for CO_2 capture from coal-fired power plants. All experimental runs are less than 50% gas film controlled. 12 m PZ solution was too viscous at 40˚C to use in the wetted wall column. 12 m PZ near 0.4 loading at 60°C was not tested because of solid precipitation.

Table 1. CO_2 Partial Pressure and Rate Data for 7, 9, 11, and 13 m MEA Solutions at 40 and 60˚C

MEA	Temp	CO_2 Loading	P_{CO2}	Q_{Liq}	k_l^o	k_g'
m	C	mol/mol_{alk}	Pa	mL/s	m/s	$mol/s \cdot Pa \cdot m^2$
7	40	0.252	15.7	3.2	7.5E-05	3.34E-06
		0.351	77	3.2	6.4E-05	1.40E-06
		0.432	465	3.1	6.3E-05	7.66E-07
		0.496	4216	3.1	6.5E-05	3.47E-07
	60	0.252	109	3.2	9.0E-05	2.92E-06
		0.351	660	3.2	8.0E-05	1.70E-06
		0.432	3434	3.1	7.9E-05	9.28E-07
		0.496	16157	3.1	7.9E-05	3.76E-07
9	40	0.231	10.4	3.3	7.2E-05	-
		0.324	34	3.1	6.3E-05	1.86E-06
		0.382	107	3.1	6.1E-05	1.40E-06
		0.441	417	3.1	5.9E-05	8.36E-07
		0.496	5354	3.0	5.9E-05	3.02E-07
	60	0.231	61	3.3	8.3E-05	3.80E-06
		0.324	263	3.1	7.7E-05	2.44E-06
		0.382	892	3.1	7.4E-05	1.47E-06
		0.441	2862	3.1	7.3E-05	9.57E-07
		0.496	21249	3.0	7.0E-05	3.24E-07

MEA	Temp	CO_2 Loading	P_{CO2}	Q_{Liq}	k_l^o	k_g'
m	C	mol/mol_{alk}	Pa	mL/s	m/s	$mol/s \cdot Pa \cdot m^2$
11	40	0.261	14.0	3.2	6.0E-05	3.36E-06
		0.353	67	3.1	5.5E-05	1.76E-06
		0.428	434	3.1	5.2E-05	7.14E-07
		0.461	1509	3.1	5.1E-05	4.34E-07
	60	0.261	96	3.2	7.4E-05	3.35E-06
		0.353	634	3.1	6.7E-05	1.80E-06
		0.428	3463	3.1	6.4E-05	8.71E-07
		0.461	8171	3.1	6.3E-05	5.02E-07
13	40	0.252	12.3	3.2	5.4E-05	3.08E-06
		0.372	84	2.7	4.7E-05	1.28E-06
		0.435	491	3.1	4.7E-05	6.96E-07
		0.502	8792	3.1	4.5E-05	1.62E-07
	60	0.252	100	2.7	6.4E-05	2.98E-06
		0.372	694	2.7	5.8E-05	1.54E-06
		0.435	3859	3.1	5.7E-05	7.56E-07
		0.502	29427	2.9	5.5E-05	1.93E-07

Table 2. CO_2 Partial Pressure and Rate Data for 2, 5, 8, and 12 m PZ Solutions at 40 and 60˚C

PZ	Temp	CO_2 Loading	P_{CO2}	Q_{Liq}	k_l^o	k_g'
m	C	mol/mol_{alk}	Pa	mL/s	m/s	$mol/s \cdot Pa \cdot m^2$
2	40	0.240	96	3.0	9.0E-05	3.32E-06
		0.316	499	3.0	9.0E-05	2.04E-06
		0.352	1305	3.0	8.9E-05	1.39E-06
		0.411	7127	3.0	9.0E-05	5.55E-07
	60	0.240	559	3.0	1.1E-04	3.33E-06
		0.316	2541	3.0	1.1E-04	2.06E-06
		0.352	5593	3.0	1.1E-04	1.38E-06
		0.411	25378	3.0	1.0E-04	3.84E-07
5	40	0.226	65	3.6	6.0E-05	4.39E-06
		0.299	346	3.6	5.7E-05	2.57E-06
		0.354	1120	3.5	5.4E-05	1.69E-06
		0.402	4563	3.5	5.3E-05	7.93E-07
	60	0.226	385	3.6	7.4E-05	4.75E-06
		0.299	1814	3.6	7.0E-05	2.62E-06
		0.354	5021	3.5	6.6E-05	1.80E-06
		0.402	17233	3.3	6.2E-05	6.59E-07

PZ	Temp	CO_2 Loading	P_{CO2}	Q_{Liq}	k_l^o	k_g'
m	C	mol/mol_{alk}	Pa	mL/s	m/s	$mol/s \cdot Pa \cdot m^2$
8	40	0.231	68	4.0	3.8E-05	4.27E-06
		0.305	530	3.1	3.5E-05	1.98E-06
		0.360	1409	3.7	3.7E-05	1.14E-06
		0.404	8153	3.7	3.6E-05	3.53E-07
	60	0.231	430	3.5	5.1E-05	4.41E-06
		0.305	2407	3.1	4.7E-05	2.02E-06
		0.360	7454	3.5	4.7E-05	9.57E-07
		0.404	30783	3.7	4.6E-05	3.20E-07
12	60	0.231	331	4.0	3.6E-05	4.19E-06
		0.289	1865	3.9	3.4E-05	1.85E-06
		0.354	6791	3.9	3.1E-05	7.73E-07

Figure 4 shows the comparison of the obtained CO_2 partial pressure data with literature values for MEA solutions at 40 and 60˚C. Both Hilliard [4] and Jou [5] used equilibrium cell that recirculate the gas phase through the amine solvent to achieve equilibrium. The filled points represent the CO_2 partial pressures obtained using the wetted wall column from each series of 6 absorption or desorption runs.

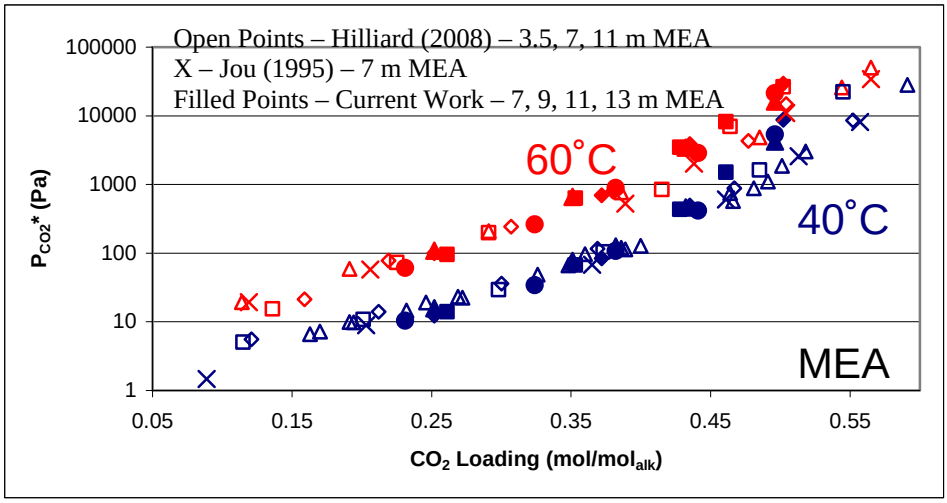

Figure 4. CO_2 Partial Pressure Data for Monoethanolamine Solutions at 40 and 60˚C

Below 0.45 loading the data with our wetted wall column match the data of Hilliard [4] and Jou [5]. However, above 0.45 loading the new data are higher and seem to be a function of amine concentration.

The measured CO_2 partial pressure in piperazine solution is comparable to the results of Hilliard [4] and Ermatchkov [6] (Figure 5).

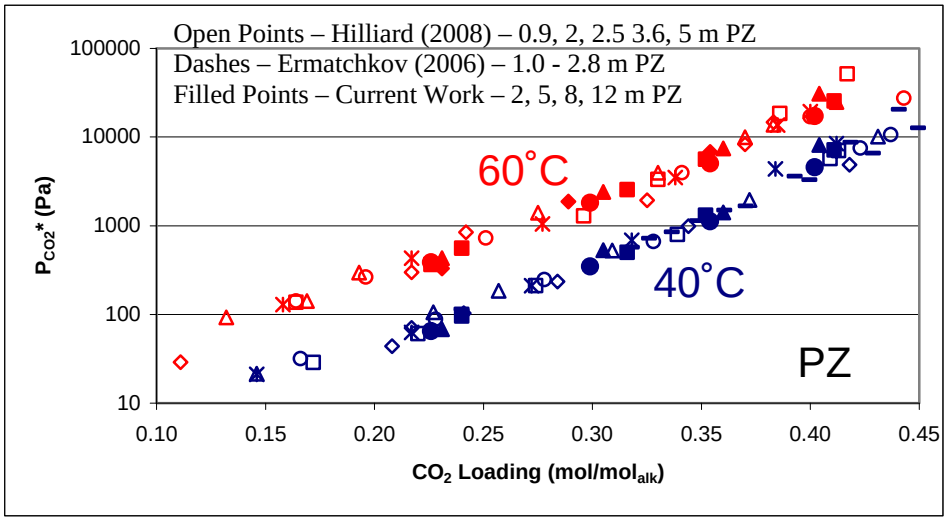

Figure 5. CO_2 Partial Pressure for Piperazine Solutions at 40 and 60˚C

When represented as a function of CO_2 loading the equilibrium CO_2 partial pressure of both MEA and PZ solutions is not a function of amine concentration. Therefore more concentrated solution will always have a greater CO_2 capacity. In an absorption/stripping process solvent compositions with greater capacity will result in lower solvent flow rates and likely significant energy savings due to a reduction in the sensible heat energy requirement in the stripper.

Figure 6 shows the working capacity for CO_2 as moles CO_2/(kg H_2O+amine), which will be most directly related to the sensible heat requirement. Heat capacity data [4] as well as empirical pilot plant data suggest that the presence of CO_2 does not affect the heat capacity. The CO_2 capacity is based on the difference in the CO_2 solubility between the lean and rich solutions of the absorber. Figure 6 assumes a rich solution with an equilibrium partial pressure of 5 kPa at 40˚C which is representative of approximately 40% approach to equilibrium with an inlet coal fired flue gas. Figure 6 gives capacity as a function of the partial pressure of CO_2 at the lean loading, which would depend on stripper design and optimization.

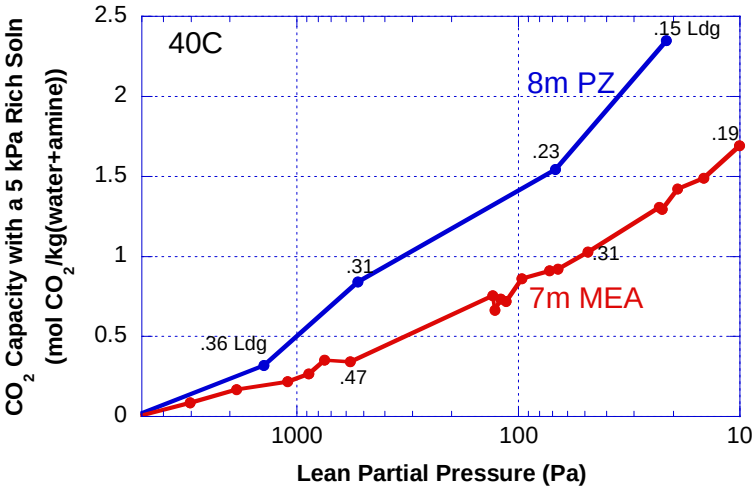

Figure 6. CO_2 Capacity of 8 m PZ and 7 m MEA at 40˚C, Assuming a 5 kPa rich Solution

Regardless of the selected lean CO_2 partial pressure, 8 m PZ seems to demonstrate an approximately 75% increase in the CO_2 capacity over 7 m MEA. This increase is mostly due to the greater amine concentration and the fact that piperazine has 2 active amines groups per molecule.

In this paper CO_2 mass transfer rates are reported as the flux divided by the liquid side driving force in partial pressure, k_g'. k_g' is the liquid film mass transfer coefficient in gas film units. It is expected that mass transfer rates in these systems will be dominated by the mechanism of pseudo-first order reaction with diffusion in the boundary layer given by Equation 2.

$$k_g' \approx \frac{\sqrt{k_2[Am]D_{CO2}}}{H_{CO2}} \tag{2}$$

The k_g' basis simplifies rate comparisons by reporting the mathematically obtained group of terms as an effective mass transfer coefficient. Henry's constant, H_{CO2}, increases with temperature [10] and amine concentration [11]. The diffusion coefficient, D_{CO2}, increases with temperature and decreases with amine concentration. The concentration of free amine will increase with amine concentration. The rate constant will increase with temperature and may also be a function of the ionic strength environment.

The results from the wetted wall column suggest that when k_g' is represented as a function of the P_{CO2} (or CO_2 loading) at 40˚C, k_g' does not depend on temperature or amine concentration. This empirical result suggests that the parameters in Equation 2 vary in such a way that their individual variance with temperature and amine concentration cancel.

The lack of temperature dependence on k_g' can be seen in Figure 7 which compares the current work at 7 m MEA to data obtained by Aboudheir [1] and Dang [2].

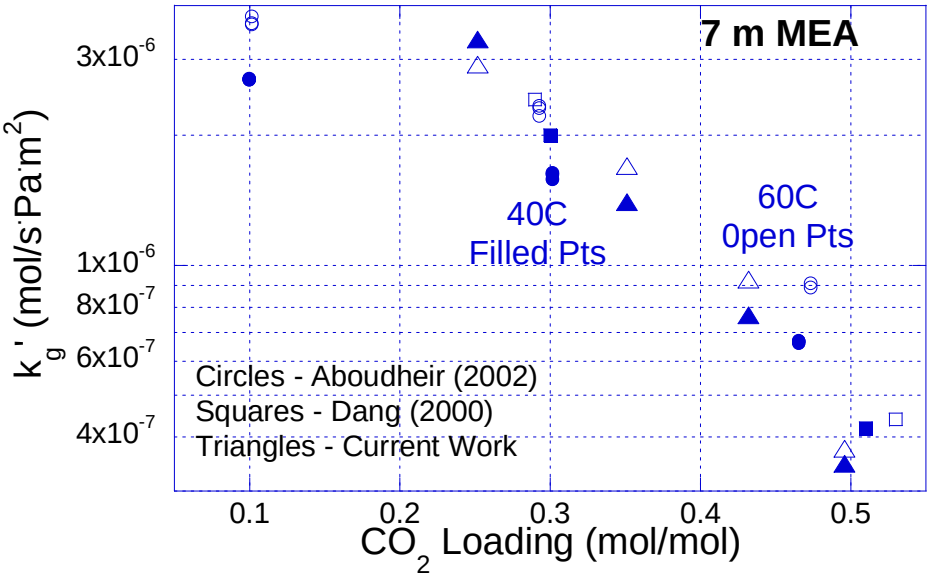

Figure 7. CO_2 Absorption Rate Data for 7 m MEA at 40 and 60˚C

Aboudheir used a laminar jet absorber. Dang used the same wetted wall column as in this work. The diffusion of reactants and products may explain why Aboudheir data at low loading do not follow the trend.

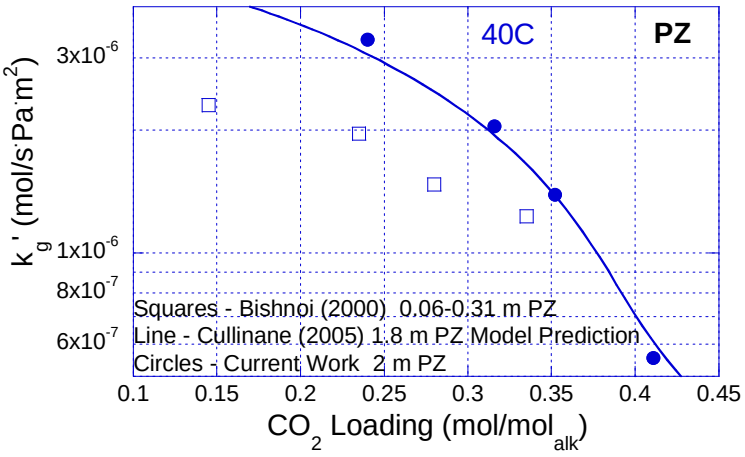

Figure 8. CO_2 Absorption Data for Piperazine at 40˚C.

Figure 8 compares 2 m PZ data to very dilute piperazine data obtained by Bishnoi [3]. These points probably fall below 2 m PZ since the amine concentration is so low. The predicted 1.8 m PZ rate curve by Cullinane uses rate constants determined by the regression of K^+/PZ data [9].

Figure 9 plots k_g' versus the equilibrium partial pressure of the solution at 40˚C to show that temperature and the amine concentration do not significantly affect k_g' values for MEA or PZ solutions at 40 and 60˚C. For both MEA and PZ solutions, k_g' is reduced drastically with an increase in equilibrium partial pressure, representative of CO_2 loading. This is mostly due to a decrease in free amine at higher CO_2 loading. CO_2 reaction rates for PZ are about 2–3 times faster than with MEA at comparable CO_2 partial pressures. The 12 m PZ points at 60˚C are not included in Figure 9 since the equilibrium partial pressures of the solutions were not able to be verified at 40˚C due to viscosity limitations.

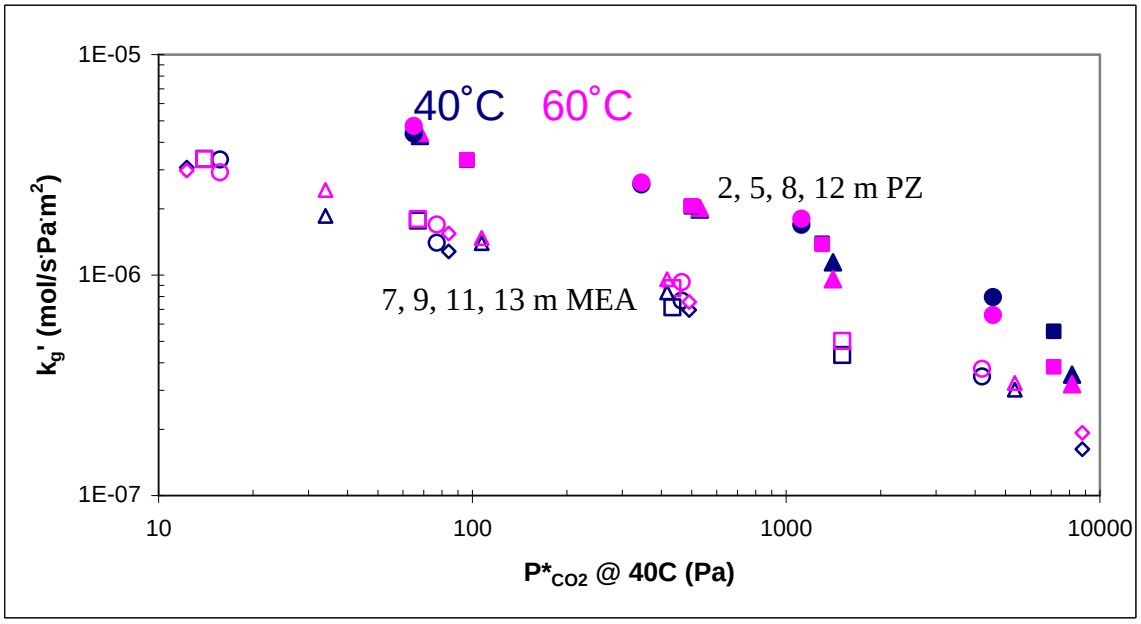

Figure 9. Absorption/Desorption Rates for CO_2 in MEA and PZ Solutions Plotted Versus the Equilibrium Partial Pressure at 40˚C

Since k_g' is essentially independent of amine concentration, more concentrated amine solutions should have lower energy requirements for CO_2 capture. Corrosion, degradation, viscosity, solubility, packing wetting or heat transfer concerns could limit the amine concentration in industrial operation.

4. Conclusions

CO_2 partial pressure and rate data from MEA and PZ wetted wall column experiments agreed very well with literature values. CO_2 partial pressure data for MEA solutions showed a small deviation at loadings higher than 0.45. Rate variations from literature reported values can be explained by mass transfer phenomenon.

8 m PZ has a 75% greater operational CO_2 capacity than 7 m MEA. CO_2 reaction rates for PZ were shown to be 2–3 times faster than MEA solutions. Despite the fact that k_g' incorporates terms which are strongly temperature and amine concentration dependent, k_g' is essentially independent of temperature and amine concentration at 40 and 60˚C.

5. References

1. A.A. Aboudheir (2002). Kinetics, Modeling, and Simulation of Carbon Dioxide Absorption into Highly Concentrated and Loaded Monoethanolamine Solutions. Chemical Engineering. Regina, Saskatchewan, Canada, University of Regina. Ph.D.: 364.
2. H. Dang and G.T. Rochelle (2003). "CO_2 Absorption Rate and Solubility in Monoethanolamine/Piperazine/Water," *Separation Sci & Tech*, 38(2): 337–357.
3. S. Bishnoi and G.T. Rochelle (2000). "Absorption of Carbon Dioxide into Aqueous Piperazine: Reaction Kinetics, Mass Transfer and Solubility." *Chem. Engr. Sci*, 55: 5531–5543.
4. M.D. Hilliard (2008). A Predictive Thermodynamic Model for an Aqueous Blend of Potassium Carbonate, Piperazine, and Monoethanolamine for Carbon Dioxide Capture from Flue Gas. Chemical Engineering. Austin, The University of Texas at Austin. Ph.D.: 1025.
5. F.-Y. Jou, A.E. Mather, *et al.* (1995). "The Solubility of CO_2 in a 30 Mass Percent Monoethanolamine Solution." *Can. J. Chem. Eng*, 73(1): 140–147.
6. V. Ermatchkov, A. Perez-Salado Kamps, *et al.* (2006). "Solubility of Carbon Dioxide in Aqueous Solutions of Piperazine in the Low Gas Loading Region." *J. Chem. & Eng. Data*, 51(5): 1788–1796.
7. J.T. Cullinane and G.T. Rochelle (2006). "Kinetics of Carbon Dioxide Absorption into Aqueous Potassium Carbonate and Piperazine." *Ind. & Eng. Chem. Res*, 45(8): 2531–2545.
8. M. Al-Juaied and G.T. Rochelle (2006). "Absorption of CO_2 in Aqueous Blends of Diglycolamine and Morpholine." *Chem. Eng. Sci*, 61(12): 3830–3837.
9. J.T. Cullinane (2005). Thermodynamics and Kinetics of aqueous piperazine with potassium carbonate for carbon dioxide absorption. Chemical Engineering. Austin, TX, The University of Texas at Austin: 295.
10. G.F. Versteeg, L.A.J. Van Dijck, *et al.* (1996). "On the Kinetics Between CO_2 and Alkanolamines Both in Aqueous and Non-aqueous Solutions. An Overview." *Chem. Eng. Comm*, 144: 113–158.
11. G.J. Browning and R.H. Weiland (1994). "Physical Solubility of Carbon Dioxide in Aqueous Alkanolamine via Nitrous Oxide Analogy." *J. Chem. & Eng. Data*, 39: 817–822.

Available online at www.sciencedirect.com

ScienceDirect

Energy Procedia 00 (2008) 000–000

Energy Procedia

www.elsevier.com/locate/XXX

GHGT-9

Influence of viscosity and surface tension on the effective mass transfer area of structured packing

Robert E. Tsai[a], A. Frank Seibert[a], R. Bruce Eldridge[a], and Gary T. Rochelle[a,*]

[a]*Department of Chemical Engineering, The Separations Research Program, The University of Texas at Austin, Austin, Texas 78712, USA*

Elsevier use only: Received date here; revised date here; accepted date here

Abstract

The effective mass transfer area (a_e) of three structured packings (Mellapak 250Y, Mellapak 500Y, and Flexipac 1Y) was measured via chemical absorption in a 0.427 m ID column as a function of liquid load (1-30 gpm/ft^2 or 2.4-73.2 m^3/m^2·h), liquid viscosity (1-15 mPa·s), and surface tension (30-72 mN/m). Viscosity had no effect and surface tension had only a weak effect on the effective area. The ratio of effective area to specific surface area (a_e/a_p) was correlated as a function of the liquid Weber and Froude numbers within limits of ±15% for the entire experimental database:

$$\frac{a_e}{a_p} = 1.198\left[\left(We_L\right)\left(Fr_L\right)^{-1/3}\right]^{0.121}$$

Keywords: CO_2 absorption; structured packing; packed column; effective area; viscosity; surface tension

1. Introduction

Packed columns are commonly used in absorption and stripping processes to provide efficient gas-liquid contacting. A reliable model for the effective mass transfer area (a_e) of the packing is important for design and analysis of these systems. It is especially critical for CO_2 capture by amine absorption, because the CO_2 absorption rate typically becomes independent of conventional mass transfer coefficients (k_G or k_L^0) but remains directly proportional to the effective area.

Wang et al. [1] provided a comprehensive review of the numerous packing area correlations in the literature. None have been shown to be truly predictive over a wide range of conditions. Different and sometimes even contradictory effects of viscosity and surface tension on the effective area are predicted. The various amine solvents

* Corresponding author. Tel.: +1-512-471-7230; fax: +1-512-471-7824.
E-mail address: gtr@che.utexas.edu.

that are being considered for CO_2 capture have a range of viscosities and surface tensions [2-4], and therefore, a dependable model is needed to predict these effects.

The influence of liquid viscosity and surface tension on the effective mass transfer area of structured packing was determined by absorption of CO_2 into dilute caustic solution. With excess free hydroxide, the concentration of bicarbonate (HCO_3^-) is negligible, and the overall reaction may be written as:

$$CO_2(aq) + 2OH^- \rightarrow CO_3^{2-} + H_2O \quad (1)$$

The reaction can be considered as practically irreversible, with a rate expression given by equation 2.

$$r = k_{OH^-}[OH^-][CO_2] \quad (2)$$

When CO_2 partial pressures are low and hydroxide ion is present in relative excess, the reaction can be treated as pseudo-first-order. Equation 2 consequently simplifies to:

$$r \cong k_1[CO_2] \quad (3)$$

2. Experimental

2.1 Packed column

The packed column had an outside diameter of 0.46 m, an inside diameter of 0.427 m, and a 3-m packed height. Operation was countercurrent, with ambient air entering below the packing bed and flowing upward through the tower. The liquid (typically 0.75 m^3 inventory) was pumped in a closed loop and was distributed at the top of the column using a pressurized fractal distributor with 108 drip points/m^2. See Tsai et al. [5] for more details.

2.2 Wetted-wall column (WWC)

The wetted-wall column (WWC) was a bench-scale gas-liquid contactor with a known interfacial area (38.52 cm^2) that was used to measure the kinetics of various systems. The apparatus has previously been used and described by Bishnoi and Rochelle [6], Cullinane and Rochelle [7], and Tsai et al. [5].

2.3 Supplementary equipment

The goniometer (ramé-hart Inc., model #100-00) included an adjustable stage, a syringe support arm, a computer-linked camera for live image display, and a light source. This system was used with FTA32 Video 2.0 software (developed by First Ten Angstroms, Inc.) to make surface tension measurements via pendant drop analysis.

A Physica MCR 300 rheometer (Anton Paar, USA) equipped with a cone-plate spindle (CP 50-1) was used for viscosity measurements. Temperature was regulated (± 0.1°C) with a Peltier unit (TEK 150P-C) and a Julabo F25 water bath unit (for counter-cooling). Measurement profiles typically consisted of a logarithmically ramped shear rate (100-500 s^{-1}), with a minimum of 10 points taken at 15 second intervals.

2.4 Chemical reagents

A nonionic surfactant, Tergitol NP-7 (Dow), was used to reduce the surface tension of solutions. POLYOX WSR N750 (Dow) – essentially, poly(ethylene oxide) with a molecular weight of 300,000 – was employed as a viscosity enhancer. With both of these reagents, suppression of foam was found to be necessary, particularly during packed column experiments. Dow Corning Q2-3183A antifoam was utilized for this purpose.

3. Results and Discussion

3.1 Theoretical analysis of data

The performance of both the WWC and the packed column was modeled by series resistance (equation 4). The overall mass transfer resistance is the sum of the gas- and liquid-side resistances.

$$\frac{1}{K_G} = \frac{1}{k_G} + \frac{1}{k_g'} \tag{4}$$

For the WWC, the overall mass transfer coefficient (K_G) was determined from the CO_2 flux and the partial pressure driving force. The gas-side mass transfer coefficient (k_G) was a function of physical properties and was calculated using a correlation that was developed by absorption of SO_2 into NaOH solution, an entirely gas-film controlled process [6]. K_G and k_G were used to calculate k_g', which has been defined as a liquid-side mass transfer coefficient expressed in terms of a CO_2 partial pressure driving force.

$$N_{CO_2} = k_g'\left(P^i_{CO_2} - P^*_{CO_2}\right) = k_g' P^i_{CO_2} \tag{5}$$

In equation 5, P^*_{CO2} is zero because of the irreversibility of the CO_2-NaOH reaction. Under the assumption of pseudo-first-order conditions, surface renewal theory may be used to present the flux as [8]:

$$N_{CO_2} = k_L^0\sqrt{1 + \frac{k_1 D_{CO_2,L}}{\left(k_L^0\right)^2}}\,\frac{P^i_{CO_2}}{H_{CO_2}} = k_L^0\sqrt{1+Ha^2}\,\frac{P^i_{CO_2}}{H_{CO_2}} \tag{6}$$

Ha^2 was on the order of 10^2 in the WWC, so equation 6 was simplified to:

$$N_{CO_2} = \frac{\sqrt{k_1 D_{CO_2,L}}}{H_{CO_2}} P^i_{CO_2} \tag{7}$$

Thus, from equations 5 and 7, we have the following theoretical expression for k_g'.

$$k_g' = \frac{\sqrt{k_1 D_{CO_2,L}}}{H_{CO_2}} = \frac{\sqrt{k_{OH^-}[OH^-] D_{CO_2,L}}}{H_{CO_2}} \tag{8}$$

Measured k_g' values were compared with calculated ones, evaluated using literature values for the terms in equation 8. The correlations for the diffusion coefficient ($D_{CO2,L}$), Henry's constant (H_{CO2}), and reaction rate constant (k_{OH-}) were based on the work of Pohorecki and Moniuk [9].

For the packed column experiment, gas-side resistance was intentionally limited by using dilute caustic solution (0.1 kmol/m^3) and operating at high superficial air velocities (0.6, 1.0, or 1.5 m/s). This resistance was estimated to account for 1% of the overall mass transfer resistance, with k_G calculated from the correlation of Rocha et al. [10]. The $1/k_G$ term in equation 4 was ignored, and K_G was assumed to be equal to k_g'. This approximation enabled the effective area (a_e) to be determined by separating it from the volumetric mass transfer coefficient, $K_G a_e$.

$$a_e = \frac{u_G \ln\left(\frac{y_{CO_2,in}}{y_{CO_2,out}}\right)}{ZK_G RT} \approx \frac{u_G \ln\left(\frac{y_{CO_2,in}}{y_{CO_2,out}}\right)}{Zk_g' RT} = \frac{u_G \ln\left(\frac{y_{CO_2,in}}{y_{CO_2,out}}\right)}{ZRT} \cdot \frac{H_{CO_2}}{\sqrt{k_{OH^-}[OH^-] D_{CO_2,L}}} \tag{9}$$

k_g' was calculated with equation 8, although the $Ha^2 >> 1$ approximation was weaker in these experiments. Ha^2 was around 15 in the worst case scenario, with k_L^0 estimated from the correlation of Rocha et al. [10].

3.2 Results with the wetted-wall column (WWC)

The WWC had two purposes. First, it was used to validate the baseline CO_2-NaOH kinetics – that is, k_g' calculated using the equations of Pohorecki and Moniuk [9]. Second, it was employed to test for potential impacts of the property-modifying additives (Tergitol NP-7 or POLYOX WSR N750) on k_g'. The WWC results are summarized in Table 1, expressed as a normalized k_g' (experimental k_g' / calculated k_g').

Table 1. Summary of WWC results

Test system	Approx. μ_L and/or σ	Number of data points	Normalized k_g'
0.1 kmol/m^3 NaOH	0.75 mPa·s, 72 mN/m	111	1.10 ± 0.09
0.1 kmol/m^3 NaOH + 125 ppm$_v$ Tergitol NP-7 + 50 ppm$_{w/v}$ Dow Corning Q2-3183A antifoam	30 mN/m	32	1.08 ± 0.07
0.1 kmol/m^3 NaOH + 1.25 wt % POLYOX WSR N750	7.5 mPa·s	10	0.91 ± 0.05

The baseline measurements gave values of flux (k_g') that were 10% higher than predicted by the parameters from Pohorecki and Moniuk [9]. Nevertheless, the disparity was not believed to be drastic enough to reject the use of their correlations. The "Pohorecki" k_g' was therefore assumed to be applicable in the interpretation of the packed column results. There was no statistically confirmable impact of surfactant and antifoam, implying that the same k_g' could be applied for this system as well. Possible explanations for this result are discussed in Tsai et al. [5]. The effect of POLYOX WSR N750 was rather interesting. Given the fairly low concentration of polymer, one would not anticipate any major effects on k_{OH^-} or H_{CO2} [11]. A ten-fold viscosity increase would, however, be expected to cause an equivalent decrease in the diffusion coefficient, which consequently would reduce k_g' by a factor of 3. This was clearly not the case, as the data exhibited only a minor depression in k_g' relative to the baseline. A survey of the literature revealed that this result was, in fact, quite justifiable. Several different studies have confirmed a unique feature of dilute, aqueous polymer solutions: limited influence on the diffusivity of small molecules like CO_2. Komiyama and Fuoss [12] postulated that while the bulk viscosity of a solution might be enhanced by entanglement of long polymer chains, considerable freedom should still exist for the localized movement of chain segments and of small molecules around these segments. In other words, the local viscosity should be significantly lower than the bulk viscosity, and thus, the CO_2 diffusion rates in polymer solutions and in pure solutions should not differ too much. Lohse et al. [13] measured CO_2 diffusion in aqueous polymer solutions and correlated their results in the form of equation 10. The subscripts 0 and P respectively refer to pure solution and polymer.

$$\frac{D_{CO_2,L}}{D_{CO_2,0}} = \left(\frac{\mu_L}{\mu_0} \right)^{-3.7\sqrt{\frac{M_0}{M_P}}} \tag{10}$$

The WWC data displayed a somewhat larger reduction in k_g' than that predicted by equation 10, but they were still in far better agreement with the "polymer" theory than with the "standard" theory (inverse 1:1 relationship of diffusivity-viscosity). Equation 10 was concluded to be valid, and for the packed column experiments conducted with POLYOX WSR N750, the diffusion coefficient in equation 8 was modified accordingly.

The WWC tests with POLYOX did not include antifoam (Table 1). Additional experiments will be performed that incorporate this additive; however, for the moment, its presence has been assumed to have no influence on k_g'.

3.3 Mass transfer area measurements

One of the packings characterized in this work was Sulzer Mellapak 250Y, a standard high capacity structured packing (a_p = 250 m^2/m^3). The data could not be differentiated with respect to air velocity (0.6, 1.0, or 1.5 m/s) and are plotted in Figure 1.

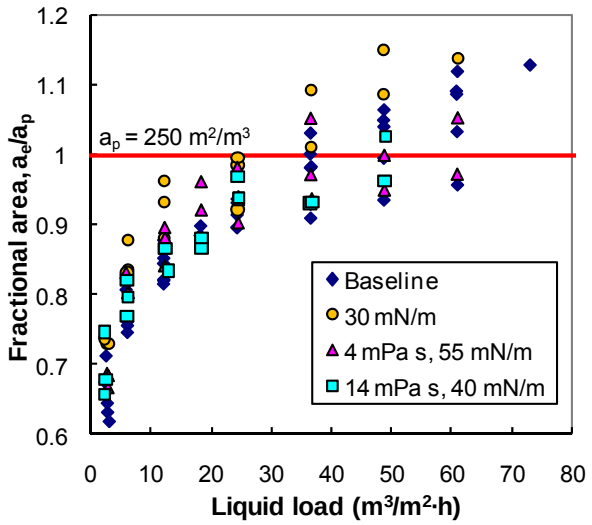

Figure 1. Fractional area data for Mellapak 250Y.

Tests with Tergitol NP-7 or POLYOX WSR N750 required antifoam, which was generally used in quantities no greater than 100 $ppm_{w/v}$. It was not possible to increase viscosity without also affecting surface tension because of the POLYOX WSR N750 itself, as well as the antifoam; hence the reduced surface tensions of the viscous systems. The fractional areas for Mellapak 250Y were quite high, indicating the surface area was being well utilized. Lowering the surface tension to 30 mN/m appeared to result in a marginal increase in the measured area, but this could not be definitively concluded, given the inherent experimental error (~10%). Viscosity had no impact on the effective area. Thus, it would seem that the mass transfer area of Mellapak 250Y is relatively insensitive to physical property variations. This is in contrast to a high surface area packing such as Mellapak 500Y, where surface tension appears to play a significant role,

likely because of the greater prominence of capillary phenomena (i.e. liquid pooling and bridging) [5,14].

3.4 Global model

The current experimental database consists of three different structured packings (Mellapak 250Y, Mellapak 500Y, and Flexipac 1Y), tested over a range of liquid viscosities (1-15 mPa·s) and surface tensions (30-72 mN/m). The relevant physical dimensions of the packings are provided in Table 2.

Table 2. Packing parameters

Packing	Specific area, a_p (m^2/m^3)	Wetted perimeter (in cross-sectional slice), L_p (m)
Sulzer Mellapak 250Y (M250Y)	250	15.456
Sulzer Mellapak 500Y (M500Y)	500	35.305
Koch-Glitsch Flexipac 1Y (F1Y)	410	30.228

An attempt was made to correlate the entire database in the form of dimensionless groups. It has been our experience that below the flooding limit, gas properties (e.g. superficial velocity) have no impact on the effective area of structured packing. The modeling effort was therefore based solely on liquid parameters. The characteristic length, δ, was defined as the thickness of the liquid film on the packing surface. Likewise, the liquid velocity, u_L, was a calculated average film velocity. The "classical" equations for film flow on an inclined flat plate, as presented by Bird et al. [15] (among others), were assumed to apply. The film thickness equation is expressed below.

$$\delta = \sqrt{\frac{3u_L\mu_L}{\rho_L g \sin\alpha}} = \sqrt[3]{\frac{3\mu_L}{\rho_L g \sin\alpha}\frac{Q}{L_p}} \tag{11}$$

It was found that the data aligned quite well when plotted as a function of $(We_L)(Fr_L)^{-1/3}$, as shown in Figure 2. Practically all of the points fall within 15% of the regressed correlation (equation 12).

$$\frac{a_e}{a_p} = 1.198\left[(We_L)(Fr_L)^{-1/3}\right]^{0.121} = 1.198\left[\frac{\rho_L}{\sigma} g^{1/3}\left(\frac{Q}{L_p}\right)^{4/3}\right]^{0.121} \tag{12}$$

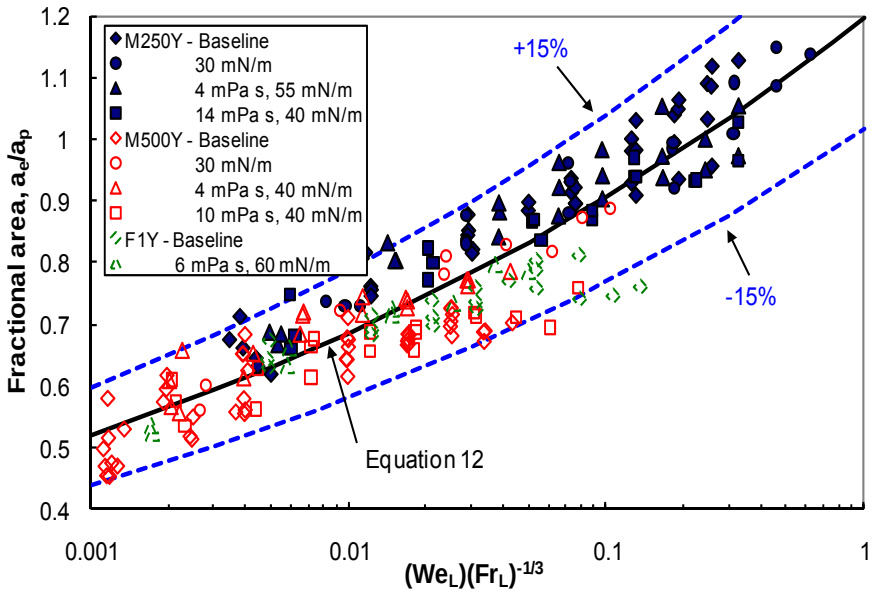

Figure 2. Structured packing mass transfer area database, compared with global correlation (equation 12).

An expansion of $(We_L)(Fr_L)^{-1/3}$ to individual physical parameters reveals that the effective area is predicted to be most strongly tied to the liquid flow rate and packing geometry. Liquid density and surface tension are significant as well, although the correlation fails to capture the distinct surface tension/geometry relation that has been observed [5]. Viscosity is notably absent from equation 12, which is consistent with our current findings. There is also no predicted effect of corrugation angle, which has been held constant (45°) in the tests performed thus far.

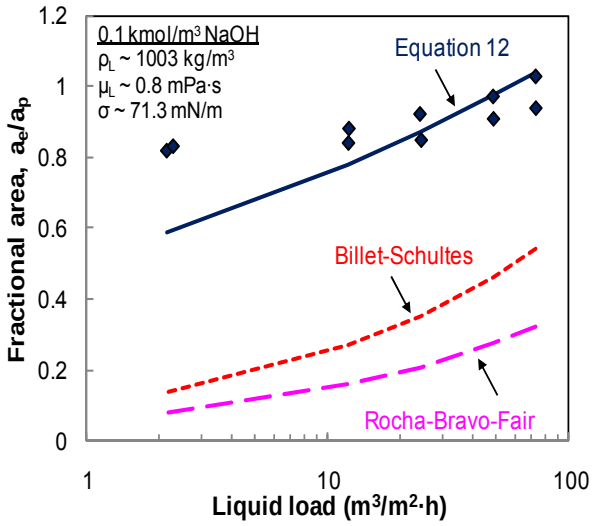

Figure 3. Comparison of prototype 250-series packing data (points) with models. $a_p = 250$ m^2/m^3; $L_p = 15.921$ m.

The Separations Research Program (SRP) at the University of Texas has compiled a large database of effective area measurements. Figure 3 presents results obtained with a non-perforated 250-series structured packing using a gravity-fed orifice pipe liquid distributor with 430 drip points/m^2. The data are compared with the predictions from equation 12 and two widely used models: Rocha-Bravo-Fair [10] and Billet-Schultes [16]. Equation 12 matches the data well, especially at the higher liquid loads. One would expect the packing surface to be well wetted at high liquid loads, on account of the relatively open geometry. However, even near 80 m^3/m^2·h, both Rocha-Bravo-Fair and Billet-Schultes predict fractional areas far from unity. It is worth noting that the literature models were primarily inferred from distillation data, generally consisting of systems with very low surface tensions. Furthermore, validation was strictly with overall mass

transfer results (e.g. $K_G a_e$); a_e itself was not independently verified. Caution should be exercised when modeling the effective area of structured packing with these correlations at high surface tensions.

4. Conclusions

Rates of absorption of CO_2 into 0.1 kmol/m^3 NaOH were measured. The value of k_g' was found to be 10% greater than predicted by the correlation of Pohorecki and Moniuk [9]. Use of their correlation was nevertheless believed to be acceptable. The addition of Tergitol NP-7 surfactant (125 ppm_v) and Dow Corning Q2-3183A (50 $ppm_{w/v}$) antifoam did not appreciably affect k_g'. The presence of POLYOX WSR N750 (1.25 wt %) only resulted in a small depression in k_g', which was actually in close agreement with the theory discussed in the literature.

The effective mass transfer areas of three structured packings (Mellapak 250Y, Mellapak 500Y, and Flexipac 1Y) were measured via absorption of CO_2 into caustic solution. No dependence on liquid viscosity (1-15 mPa·s) was observed. Surface tension was found to be important for M500Y but not for M250Y; the interfacial area of M500Y increased significantly when surface tension was lowered to 30 mN/m. The mass transfer area database was represented well (±15%) by the correlation that was regressed as a function of $(We_L)(Fr_L)^{-1/3}$.

5. Acknowledgment

This work was supported by the Luminant Carbon Management Program. We are grateful to Sulzer Chemtech and Koch-Glitsch for providing the packing materials for this research. We acknowledge Dow and Dow Corning for their donations as well. We also recognize the contributions of J. Christopher Lewis, Andreas Kettner, Peter Schultheiss, and the SRP staff members to this work.

6. Nomenclature

a_e = effective area of packing, m^2/m^3
a_p = specific surface area of packing, m^2/m^3
D_{CO2} = diffusivity of CO_2, m^2/s
g = gravitational constant, m/s^2
H_{CO2} = Henry's constant of CO_2, m^3·Pa/kmol
K_G = overall gas-side mass transfer coefficient, kmol/m^2·Pa·s
k_1 = pseudo-first-order reaction rate constant, s^{-1}
k_G = gas-side mass transfer coefficient, kmol/m^2·Pa·s
k_g' = liquid-side mass transfer coefficient, kmol/m^2·Pa·s
k_L^0 = physical liquid-side mass transfer coefficient, m/s
k_{OH-} = second-order reaction rate constant, m^3/kmol·s
L_p = wetted perimeter in cross-sectional slice of packing, m
M = molecular weight, kg/kmol
N_{CO2} = molar flux of CO_2, kmol/m^2·s
P^*_{CO2} = equilibrium partial pressure of CO_2, Pa
P^i_{CO2} = partial pressure of CO_2 at gas-liquid interface, Pa
Q = volumetric flow rate, m^3/s
R = ideal gas constant, m^3·Pa/kmol·K
r = chemical reaction rate, kmol/m^3·s
T = absolute temperature, K
u = velocity, m/s
$y_{CO2,in/out}$ = mole fraction of CO_2 at inlet/outlet
Z = packed height, m

Greek Symbols

α = corrugation angle (with respect to the horizontal), deg
δ = film thickness, m
μ = viscosity, Pa·s
ρ = density, kg/m^3
σ = surface tension, N/m

Subscripts

G = gas phase
L = liquid phase

Dimensionless Groups

a_f = fractional area of packing, a_e/a_p
Fr = Froude number, $u^2/g{\cdot}\delta$
Ha = Hatta number, $(k_1 D_{CO2,L})^{0.5}/k_L{}^0$
We = Weber number, $\rho u^2 \delta/\sigma$

7. References

1. G.Q. Wang, X.G. Yuan, and K.T. Yu, Review of Mass-Transfer Correlations for Packed Columns, *Ind. Eng. Chem. Res.* 44 (2005) 8715.
2. R.H. Weiland, J.C. Dingman, D.B. Cronin, and G.J. Browning, Density and Viscosity of Some Partially Carbonated Aqueous Alkanolamine Solutions and Their Blends, *J. Chem. Eng. Data* 43 (1998) 378.
3. G. Vázquez, E. Alvarez, J.M. Navaza, R. Rendo, and E. Romero, Surface Tension of Binary Mixtures of Water + Monoethanolamine and Water + 2-Amino-2-methyl-1-propanol and Tertiary Mixtures of These Amines with Water from 25°C to 50°C, *J. Chem. Eng. Data* 42 (1997) 57.
4. A. Henni, J.J. Hromek, P. Tontiwachwuthikul, and A. Chakma, Volumetric Properties and Viscosities for Aqueous AMP Solutions from 25°C to 70°C, *J. Chem. Eng. Data* 48 (2003) 551.
5. R.E. Tsai, P. Schultheiss, A. Kettner, J.C. Lewis, A.F. Seibert, R.B. Eldridge, and G.T. Rochelle, Influence of Surface Tension on Effective Packing Area, *Ind. Eng. Chem. Res.* 47 (2008) 1253.
6. S. Bishnoi and G.T. Rochelle, Absorption of Carbon Dioxide into Aqueous Piperazine: Reaction Kinetics, Mass Transfer and Solubility, *Chem. Eng. Sci.* 55 (2000) 5531.
7. J.T. Cullinane and G.T. Rochelle, Kinetics of Carbon Dioxide Absorption into Aqueous Potassium Carbonate and Piperazine, *Ind. Eng. Chem. Res.* 45 (2006) 2531.
8. P.V. Danckwerts, *Gas-Liquid Reactions*, McGraw-Hill Book Company, New York, 1970.
9. R. Pohorecki and W. Moniuk, Kinetics of Reaction between Carbon Dioxide and Hydroxyl Ions in Aqueous Electrolyte Solutions, *Chem. Eng. Sci.* 43 (1988) 1677.
10. J.A. Rocha, J.L. Bravo, and J.R. Fair, Distillation Columns Containing Structured Packings: A Comprehensive Model for Their Performance. 2. Mass-Transfer Model, *Ind. Eng. Chem. Res.* 35 (1996) 1660.
11. E. Rischbieter, A. Schumpe, and V. Wunder, Gas Solubilities in Aqueous Solutions of Organic Substances, *J. Chem. Eng. Data* 41 (1996) 809.
12. J. Komiyama and R.M. Fuoss, Conductance in Water-Poly(vinyl alcohol) Mixtures, *Proc. Natl. Acad. Sci. U.S.A.* 69 (1972) 829.
13. M. Lohse, E. Alper, G. Quicker, and W.D. Deckwer, Diffusivity and Solubility of Carbon Dioxide in Diluted Polymer Solutions, *AIChE J.* 27 (1981) 626.
14. C.W. Green, J. Farone, J.K. Briley, R.B. Eldridge, R.A. Ketcham, and B. Nightingale, Novel Application of X-ray Computed Tomography: Determination of Gas/Liquid Contact Area and Liquid Holdup in Structured Packing, *Ind. Eng. Chem. Res.* 46 (2007) 5734.

15. R.B. Bird, W.E. Stewart, and E.N. Lightfoot, *Transport Phenomena* (2nd ed.), John Wiley & Sons, Inc., New York, 2002.
16. R. Billet and M. Schultes, Predicting Mass Transfer in Packed Columns, *Chem. Eng. Technol.* 16 (1993) 1.

Available online at www.sciencedirect.com

ScienceDirect

Physics Procedia 00 (2008) 000–000

Physics Procedia

www.elsevier.com/locate/XXX

GHGT-9

Modeling CO_2 Capture with Aqueous Monoethanolamine

Jorge M Plaza[a], David Van Wagener[a], Gary T. Rochelle[a,*]

[a]*Department of Chemical Engineering, The University of Texas at Austin, 1 University Station C0400, Austin, TX 78712, USA*

Elsevier use only: Received date here; revised date here; accepted date here

Abstract

Hilliard [1] completed several thermodynamic models in Aspen Plus®® for modeling CO_2 removal with amine solvents, including MEA-H_2O-CO_2. This solvent was selected to make a system model for CO_2 removal by absorption/stripping. Both the absorber and the stripper used RateSep™ to rigorously calculate mass transfer rates. The accuracy of the new model was assessed using a recent pilot plant run with 35 wt % MEA. Absorber loadings and removal were matched and the temperature profile was approached within 5°C. An average 3.8% difference between measured and calculated values was achieved in the stripper. A three-stage flash configuration which efficiently utilizes solar energy was developed. It reduces energy use by 6% relative to a simple stripper. Intercooling was used to reach 90% removal in the absorber at these optimized conditions.

Keywords: Kinetics; Absorption; Stripping; Carbon dioxide; MEA; modeling

1. Introduction

CO_2 capture by amine absorption and stripping is currently considered the most feasible option for the removal of carbon dioxide from coal- and natural gas- fired power plants. Monoethanolamine (MEA) is the proven solvent for this application. Previous models have been developed for this system. Freguia [2] developed a model using AspenPlus® Ratefrac™ that incorporated kinetic work by Dang [3] and modified VLE by Austgen [4] to include work by Jou et al. [5]. Ziaii [6] used AspenPlus®. RateSep™ with the thermodynamic framework by Freguia and approximated Aboudheir [7] kinetics. This paper presents results with a new MEA model that uses a rigorous thermodynamic model developed by Hilliard [1] and kinetics extracted from values obtained by Aboudheir [7] with a laminar jet. The model was developed with the AspenPlus®. Ratesep™ framework and was validated with a pilot plant run with 35 wt % MEA. Additionally, an innovative stripper configuration was optimized and its corresponding absorber was specified.

2. Thermodynamic model

The absorber and stripper models use the thermodynamic representation by Hilliard [1]. Hilliard used the electrolyte nonrandom two-liquid (e-NRTL) activity coefficient model in Aspen Plus® to develop a rigorous and consistent thermodynamic representation of mixtures of MEA – H_2O – CO_2. His model differs from previous models in that it represents additional data on amine vapor pressure, enthalpies of absorption, heat capacity, and NMR speciation. This framework uses Gibbs free energy and enthalpy values within Aspen Plus® to maintain thermodynamic consistency.

3. Absorber MEA model and validation

Kinetics are based on selected measurements of CO_2 absorption by Aboudheir [7] in a laminar jet. These data were used to evaluate the forward rate constants for the formation of carbamate using Aspen Plus®® RateSep™. An absorber model was set up using the Hilliard thermodynamic model and kinetics were represented using two reversible reactions:

* Corresponding author. Tel.:1-512-471-7230; fax:1-512-471-7060.
E-mail address: gtr@che.utexas.edu

$$2\ MEA + CO_2 \leftrightarrow MEAH^+ + MEACOO^- \quad (1)$$

$$forward\ rate\left(\frac{kmol}{m^3-s}\right) = 5.31e9\ exp\left(-\frac{14610}{8.314}\right) a_{MEA}^2 a_{CO_2} \quad (1a)$$

$$Reverse\ rate\left(\frac{kmol}{m^3-s}\right) = 4.75e5\ exp\left(-\frac{102740}{8.314}\right) a_{MEACOO^-} a_{MEAH^+} \quad (1b)$$

$$MEA + CO_2 + H_2O \leftrightarrow HCO_3^- + MEAH^+ \quad (2)$$

$$forward\ rate\left(\frac{kmol}{m^3-s}\right) = 9026\ exp\left(-\frac{49000}{8.314}\right) a_{MEA} a_{CO_2} \quad (2a)$$

$$Reverse\ rate\left(\frac{kmol}{m^3-s}\right) = 2917\ exp\left(-\frac{114250}{8.314}\right) \frac{a_{HCO_3^-} a_{MEAH^+}}{a_{H_2O}} \quad (2b)$$

The bicarbonate reaction (2) rate constants were evaluated using data at 25°C for reaction of tertiary amines and CO_2. This data was correlated with the base dissociation constant (pK_b) in Rochelle [8]. The values of the reaction constant for tertiary amines were fit as a function of pK_b.and the forward rate constant for MEA (pK_b=4.45) was extracted from this fit and converted to an activity/mole fraction basis with the activity coefficients from the Hilliard model. The energy of activation was approximated using data for MDEA (49 kJ/gmol) [8]. The forward reaction rate constant for the bicarbonate reaction was calculated with the conditions defined by the data set selected from Aboudheir and then used along with the equilibrium constants to determine the reverse rates for the bicarbonate reaction.

Nine points from Aboudheir [7] were used to determine the forward carbamate formation rate (1a). Three at 313 K (40°C), loading of 0.2767 and the rest at 333 K (60°C), with loadings of 0.1104 and 0.2819. A laminar jet was modeled in Aspen Plus® using the bicarbonate constants and thermodynamics from Hilliard [1]. Density, viscosity, thermal conductivity, and surface tension of the MEA – H_2O – CO_2 system, along with carbon dioxide diffusivity in water, were corrected based on work by Aspen Technology, Inc. [9]. Initially the energy of activation was set to zero and the reported flux by Aboudheir was matched by changing the pre-exponential factor in the power law. The resulting rate constants were averaged among the same temperature and loading conditions and then regressed to obtain values for the pre-exponential factor and activation energy. The activity of MEA was squared to represent apparent effects of changes in loading.

4. Pilot plant model validation

The proposed model was adjusted to match experimental data from a pilot plant run with 9 m MEA at the University of Texas at Austin [10] using the parameter estimation tool in Aspen Plus® 2006.5.

4.1 Absorber Model Validation

The operating mode was similar to that reported by Chen [10], but the air was not recycled back to the absorber. The absorber packing (Flexipac 1Y) was modeled with 12 equal stages using the countercurrent flow model. The liquid mass transfer film was represented with 16 segments. The interfacial area was calculated using a new correlation developed by Tsai [11]. Heat loss was neglected.

The variables and parameters used for the reconciliation and their chosen standard deviations along with the resulting model predictions are presented in Table 1. The only manipulated model parameter was the interfacial area factor which corrected the calculated interfacial area. High standard deviations (20°C) were specified for the outlet gas and the top column temperatures because they were considered less reliable. The water (water – Lean) and CO_2 content (CO_2 – Lean) of the lean feed were treated as reconcilable experimental values. The resulting values give a lean loading of 0.365 which is 1% greater than the measured value (0.36). Figure 1 compares the resulting model temperature profiles with the experimental results. The point at a relative position of -0.1 represents a measurement downstream of the column.

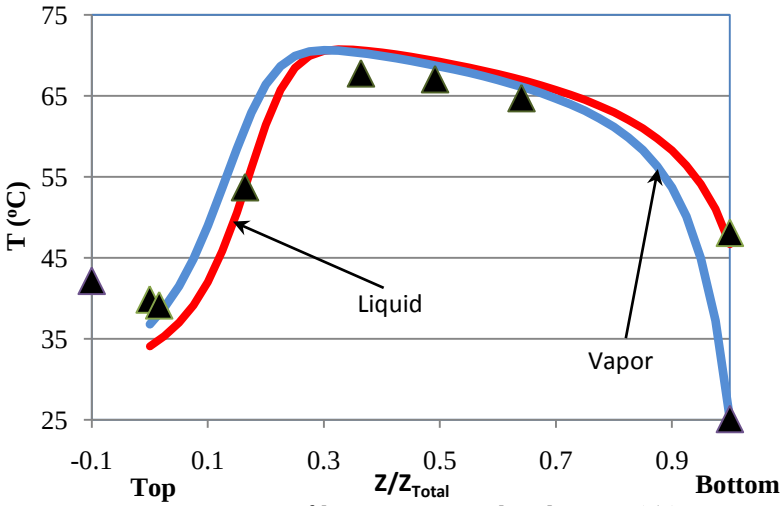

Figure 1: Temperature profiles. 9 m MEA pilot plant run (▲) measured (—) reconciled

The reconciled flow rates, compositions, and the CO_2 removal are within 1 to 6% reported values, reflecting moderate adjustments to close the mass balance. CO_2 removal and other pilot plant measurements were matched by adjusting the wetted area prediction of the Tsai model by a factor of 0.82.

4.2 Stripper Model

This Aspen Plus® simulation work assumes equilibrium reactions in the stripper. The RateSep™ tool rigorously calculates the heat and mass transfer for each stage of the simple stripper. The packing mass transfer model by Onda [12]was used to estimate liquid mass transfer coefficients and area of packing. The reboiler was modeled as equilibrium. The necessary pumps and intercooled vapor compression were included, except for the pilot plant which did not require a compressor.

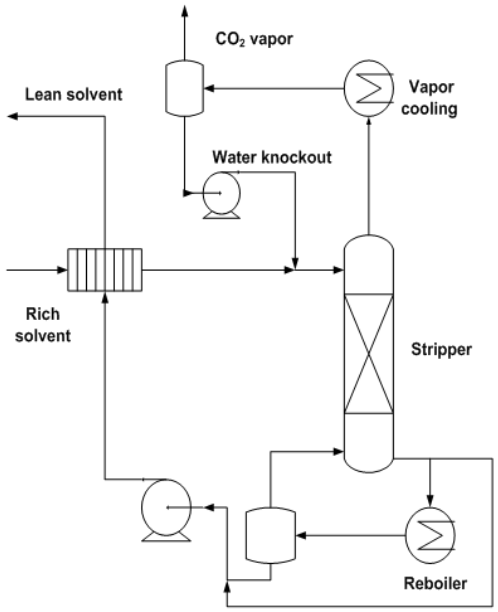

Figure 2: PFD of Pilot Plant Stripper

Table 1: Pilot Plant Reconciliation, 9 m MEA, 6.10 m absorber packing, 0.43 m Diameter

Variable	Pilot Plant Value	Specified deviation	Reconciled Value	Actual Deviation (%)
Area Factor	1.0	----	0.816	----
Rich ldg (mol CO_2/mol MEA)	0.48	1%	0.469	2.3
Inlet Gas (mol/hr)	34572	5%	33346	3.5
Y_{CO2} – In	0.119	5%	0.1192	0.0
Y_{CO2} – Out	0.047	5%	0.0501	5.7
T_G – In (°C)	25.1	1	25.1	0
T_G – Out (°C)	42.2	20	46.1	3.9
T_L – In (°C)	39.9	4	38.2	1.7
T_L – Out (°C)	44.9	4	46.7	1.8
Column T (°C)				
Top	39.2	20	34.8	4.4
T1	53.7	2	53.8	0.1
T2	67.8	2	70.8	3.0
T3	67.1	2	69.4	2.3
T4	64.7	2	67.0	2.3
Bottom	48.1	3	46.7	1.4
Water – Lean (mol/hr)	143600	0.5%	143700	0.1
CO_2 – Lean (mol/hr)	8202	2%	8307	1.3
CO_2 Removal (%)l	60.0	1%	59.9	0.2

A nonconventional stripper section was used to simulate the reboiler configuration of the pilot plant. The reboiler was configured to heat only a fraction of the sump drawoff (Figure 2). The column is identical to the absorber, containing 20 feet of packing (CMR#2) with a 16.8 inch diameter. The pilot plant provided data for various points in the process, but several crucial values were unknown. For example, the split ratio of lean amine flow was not manipulated or measured, and it could not be calculated.

A three-stage flash configuration was developed for the stripper (Figure 3). Unlike configurations with reboilers, a countercurrent heat exchanger is used to preheat the rich stream exiting the cross heat exchanger before the stripping equipment. Preheating results in higher stripping temperatures, which yields greater CO_2 selectivity. High stripping temperatures were previously avoided to reduce the risk of thermal degradation of the solvent. However, if thermal degradation is not an issue for new solvents, it would be preferable to use higher temperatures. Additionally, by using a countercurrent exchanger to heat the rich stream, a solar energy source with a variable heating temperature is expected to operate more efficiently. The flash assumes chemical and thermal equilibrium. The stripper was sized to remove CO_2 from a 500 MW coal-fired power plant with 90% carbon removal. A 5° cold side approach was specified on the cross heat exchanger, and a 10° LMTD driving force was specified for all other heat exchangers.

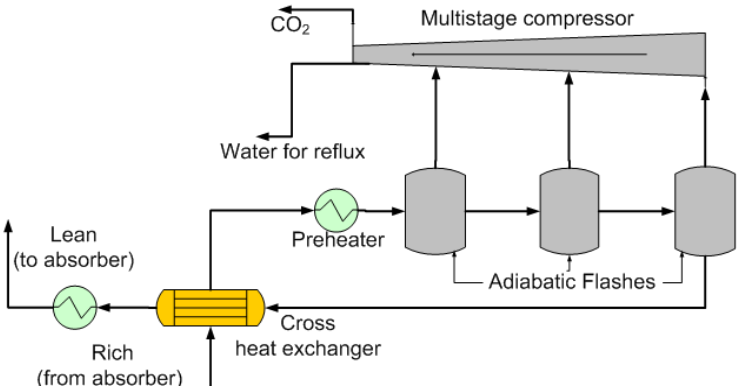

Figure 3: Three-stage flash for stripping; compressor intercooled at each suction to 40°C

$$W_{eq} = 0.75 * Q * \left(\frac{T_{heating} - T_{sink}}{T_{heating}}\right) + \sum W_{pump\ /comp} \quad (3)$$

$$W_{eq} = 0.75 * Q * \left(\frac{(T_f - T_o) - T_{sink}\left(\frac{T_f}{T_o}\right)}{T_f - T_o}\right) + \sum W_{pump\ /comp} \quad (4)$$

The stripper performance of all simulations was evaluated using equivalent work, which calculates the total electrical energy usage of a power plant. The standard form is shown in equation 3, and this equation was integrated when a variable temperature energy source (solar heat) was used in the three-stage flash configuration (equation 4). This variable temperature source had an inlet temperature of T_o and an outlet temperature of T_f.

4.3 Stripper Model Validation

The October, 2007 pilot plant run using 9 m MEA was also evaluated using the stripper model. Table 2 summarizes important data and calculations from the process. There were six thermocouples in the column at various heights, each indicated by *Temperature i* in Table 2.

Data regressions were initially used in Aspen Plus® in an attempt to reconcile the results, but all regressions failed to produce close agreement. The best solution was determined to be adjusting heat duties in selected stages within the column to simulate heat loss. Pilot plant results did not include a profile of heat loss in the column, so it was specified to match column temperatures. The split ratio in the reboiler and its duty were adjusted to match the reboiler temperature and lean loading. Figure 4 displays the column profile as a function of stage for the plant data, the initial Aspen calculation, and the final Aspen calculation with a matched temperature profile by adjusting to loss. The agreement between the values in Table 2 demonstrates that the CO_2 removal at the pilot plant was verified with the model. The simulation predicted a nearly identical reboiler duty, and the heat loss was only 12% greater than the calculated heat loss at the pilot plant. The average variation between measured and calculated values was 3.8%.

Table 2: Stripper Pilot Plant Results

Variable	Pilot Plant	Aspen Plus®	Variable	Pilot Plant	Aspen Plus®
Lean stream			*Column data*		
T (°C)	44.9	44.9	T 1 (°C)	87.6	86.7
Flow (kg/min)	73.3	70.9	T 2 (°C)	86.3	86.3
Ldg (mol/mol)	0.36	0.36	T 3 (°C)	87.9	87.9
Rich stream			T 4 (°C)	90.4	90.4
T (°C)	50.2	50.4	T 5 (°C)	91.0	91.0
Flow (kg/min)	70.6	69.0	T 6 (°C)	95.3	95.3
Ldg (mol/mol)	0.48	0.48	Reboiler T (°C)	102.7	102.7
Heat exchanger Ts			Q (kW)	143.0	143.3
Lean in (°C)	44.9	44.9	Q loss (kW)	22.6	24.9
Lean out (°C)	91.6	93.1	Sump T (°C)	98.2	97.8
Rich in (°C)	98.6	99.7	Column P, bot (kPa)	105.0	105.0
Rich out (°C)	50.2	50.4	ΔP, top (kPa)	0.14	0.14
Performance			ΔP, bot (kPa)	0.15	0.15
Eq Work (kJ/mol CO_2)	-	41.2	Outlet vapor T (°C)	87.4	87.0
			Packing ht (m)	6.10	1.52

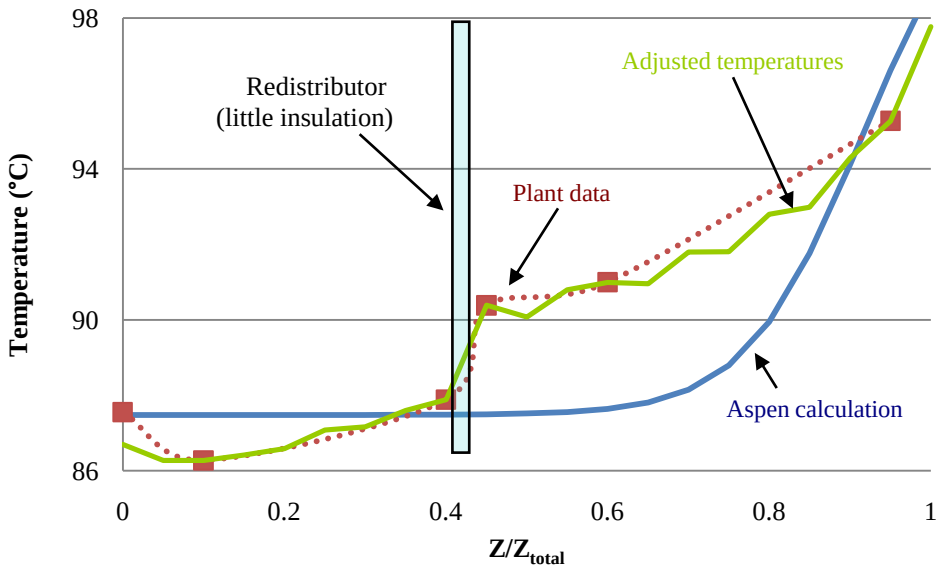

Figure 4: Temperature Profiles in Pilot Plant and Aspen Simulation (Stripper). Rich loading = 0.48, 63% removal. "Aspen calculation": no heat loss, 75% split to reboiler, 20 ft CMR NO-2P packing. "Adjusted temperatures": 5 ft CMR NO-2P packing, heat loss adjusted to match T profile.

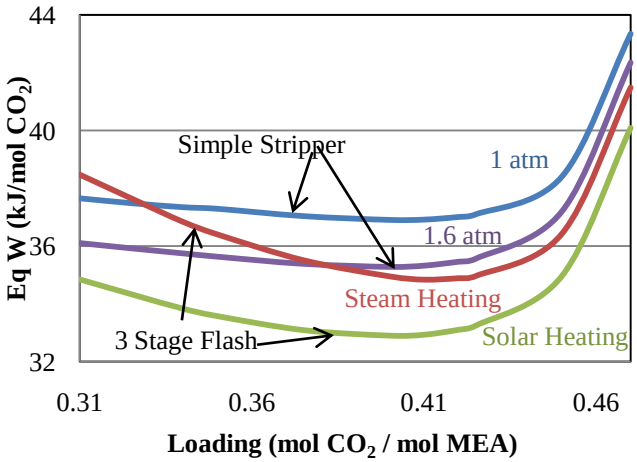

Figure 5: Equivalent work response to lean loading. 9 m MEA, 0.495 rich loading, 0.40 lean loading, 5°C cross exchange cold side temperature approach, 10°C driving force in reboiler/preheater, compression to 5MPa

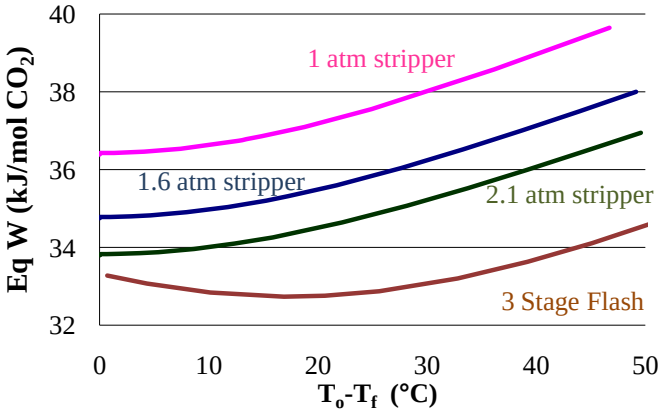

Figure 6: Equivalent work response to heating fluid temperature difference. 9 m MEA, 0.495 rich loading, 0.40 lean loading, 5°C cross exchange cold side temperature approach, 10°C driving force in reboiler/preheater, compression to 5MPa.

5 Optimization case study

5.1 Improving Stripper Performance

The three-stage flash configuration was run with 9 m MEA, and a constant rich loading of 0.495 was used corresponding approximately to 5 kPa P^*_{CO2} in the absorber. The lean loading was optimized to minimize the total equivalent work. The equivalent work for various conditions was compared against the equivalent work for a similar system of conditions for a simple stripper, both atmospheric and 1.6 atm columns. The three-stage flash and simple stripper configurations responded differently to changes in lean loading; however, both configurations yielded an optimum lean loading of 0.40. Figure 5 displays the equivalent work response to lean loading for four scenarios: solar-heated, three-stage flash with an exiting lean pressure of 110 kPa, steam-heated, three-stage with an exiting lean pressure of 110 kPa, the baseline simple stripper configuration with steam heat operating at both 1 atm and 1.6 atm.

The 1.6 atm simple stripper was considered to be the most appropriate comparison to the three-stage flash because the maximum temperatures of these configurations were relatively equal: at the optimized lean loading the highest temperature was

105°C. Whether using solar or steam heating, the three-stage flash required less energy than the 1.6 atm simple stripper. The three-stage flash with solar heating required 2.0 kJ/mol CO_2 less energy than the 1.6 atm stripper. The difference in performance using steam and solar heating for all simple strippers and the three-stage flash was investigated (Figure 6). The y-intercepts represent steam heating with a constant heating temperature, and the rest of the curves demonstrate the change in energy consumption when varying the ΔT with a constant 10°C LMTD. The trends demonstrate that the three-stage flash is always an improvement over the simple stripper, but it performs best with solar heating. A reboiled stripper would not benefit from solar heating.

5.2 Absorber Design

An absorber was specified based on the optimum flow and loading conditions defined by the stripper (Table 3). The absorber requirements were to obtain the maximum removal matching the lean and rich loadings. Three absorber configurations were analyzed: no intercooling, middle, and optimum intercooling. Intercooling was evaluated in the model by specifying a stage liquid temperature to 40°C (using cooling water). Intercooling was set in the middle of the absorber and at an optimum defined by the position of the intercooled stage that gave the minimum packing height. Initially 90% removal of CO_2 was specified. However, the simple absorber presented a pinch at the bottom of the column that made it impossible to reach this value. The gas inlet flow was increased to 11 kmol/s in a second case reaching 50% removal to match the rich loading with the simple absorber.

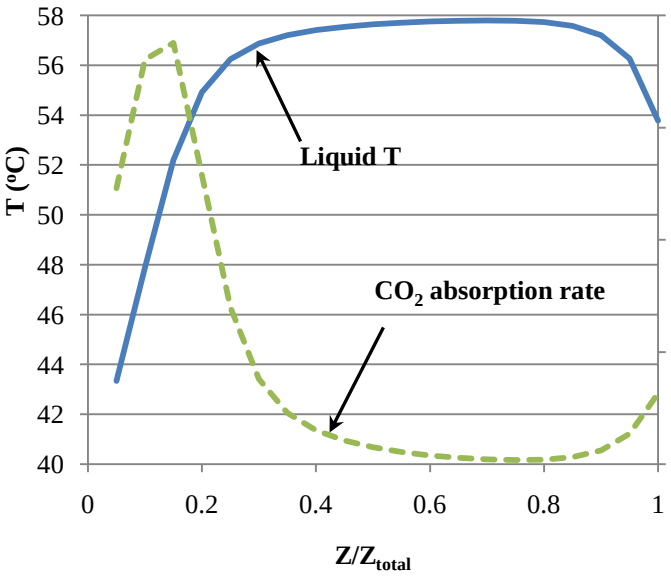

Figure 7: Temperature and absorption rate profiles of an absorber column with no intercooling. 15 m packing 84.7% CO_2 removal, rich loading = 0.489.

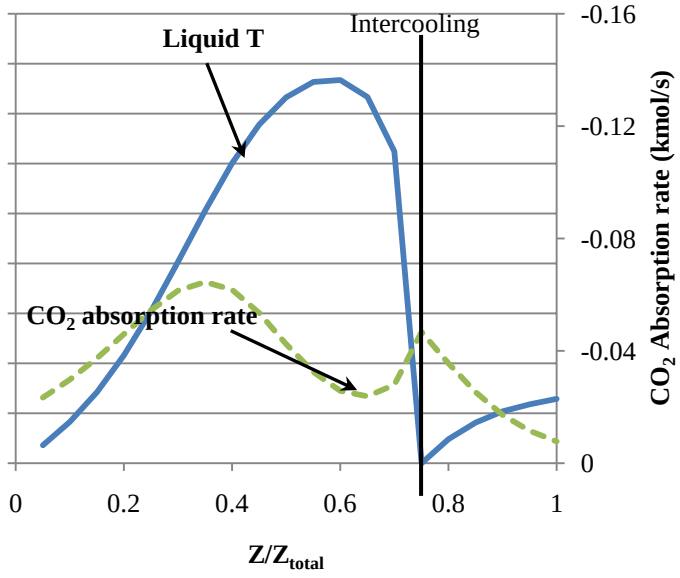

Figure 8: Temperature and absorption rate profiles of an intercooled column with 5.16 m of packing. 90% removal.

Table 3: Defined specifications for absorber design

Lean stream		*Gas inlet*	
T(°C)	40	T (°C)	40
Pressure (kPa)	101.1	P (kPa)	101.1
Flow (kmol/s)	57.6	Flow (kmol/s)	6.1
Ldg (mol CO_2/mol MEA)	0.40	Y_{CO2}	0.133
Rich stream		Y_{H2O}	0.066
Ldg (mol CO_2/mol MEA)	0.495	$Y_{N2/O2}$	0.81
Column Specifications			
Dia. (m) 80% flooding	11.4	Packing	Flexipac 1Y

Table 4 shows the results for each case. Temperature and CO_2 profiles for the simple absorber with 15m of packing and an optimized intercooling for 90% removal (Figures 7 & 8) are also included.

The rich and lean loading from the stripper were matched using an intercooled absorber. The simple absorber is limited by a mid-column absorption pinch that coincides with the temperature bulge. Intercooling breaks the pinch and reduces the temperature bulge, increasing the performance of the absorber. Results show that optimum placing of the intercooling stage is capable of reducing packing height by 15%.

Table 4: Absorber results

Removal	Intercooling	Packing Height (m)
90%	None	Infeasible
	Mid column	6.07
	Optimized	5.16
50%	None	18
	Mid column	2.62
	Optimized	2.34

6 Conclusions

Reconciled pilot plant data show the proposed absorber model is capable of simulating operation of the absorber. Loadings and removal were around 1% off the measured value. Temperature profiles are 2 to 8^{o}C off the reported values. This may correspond to the unaccounted heat losses.

The stripper pilot plant data was matched with an average deviation of 3.8% by specifying heat duties to account for heat loss.

The three-stage flash was developed as an alternate stripper configuration which efficiently utilizes solar energy, improving stripper performance by 6%.
Intercooling increased the performance of the absorber allowing 90% removal. Optimum placement of the intercooled stage can reduce packing height by 13%.

7 Acknowledgements

This work was supported by the Luminant Carbon Management Program. AspenTech provided Aspen Plus® with RateSep™. Special assistance was provided by Chau-Chyun Chen of AspenTech.

8 References

1. Hilliard, M.D. A Predictive Thermodynamic Model for an Aqueous Blend of Potassium Carbonate, Piperazine, and Monoethanolamine for Carbon Dioxide Capture from Flue Gas,. Ph.D Dissertation, The University of Texas at Austin, Austin, Texas, 2008.
2. Freguia, S.,G.T. Rochelle, Modeling of CO2 capture by aqueous monoethanolamine. *Aiche J* **2003,** 49, (7), 1676-1686.
3. Dang, H. CO_2 Absorption Rate and Solubility in MEA/PZ/H_2O. Masters Thesis, The University of Texas at Austin, Austin, TX, 2000.
4. Austgen, D.M.,G.T. Rochelle,X. Peng,C.C. Chen, Model of Vapor Liquid Equilibria for Aqueous Acid Gas Alkanolamine Systems Using the Electrolyte NRTL Equation. *Ind Eng Chem Res* **1989,** 28, (7), 1060-1073.
5. Jou;, F.-Y.,F.D. Otto;,A.E. Mather, Vapor-Liquid Equilibrium of Carbon Dioxide in Aqueous Mixtures of Monoethanolamine and Methyldiethanolamine. *Ind. Eng. Chem. Res.* **1994,** 33, (8), 2002-2005.
6. Fisher, K.S.,K. Searcy,G.T. Rochelle,S. Ziaii,C. Schubert *Advanced Amine Solvent Formulations and Process Integration for Near-Term Capture Success.*; DE-FG02-06ER84625; U.S. Department of Energy: 2007.
7. Aboudheir, A. Kinetics Modeling and Simulation of Carbon Dioxide Absorption into Highly Concentrated and Loaded Monoethanolamine Solutions. Ph.D. Dissertation, University of Regina, Regina, 2002.
8. Rochelle, G.,S. Chi,H. Dang,J. Santos *Research Needs for CO_2 Capture from Flue Gas by Aqueous Absorption/Stripping*; U.S. Department of Energy - Federal Energy Technology Center: Austin, TX, January 17, 2001, 2001.
9. Huiling;, Q.,C.C. Chen *Internal Report: Modeling Transport Properties of CO_2 Capture Systems with Aqueous Monoethanolamine Solution*; Aspen Technology, Inc: 2008.
10. Chen, E. Carbon Dioxide Absorption into Piperazine Promoted Potassium Carbonate using Structured Packing. Ph.D. Dissertation, The University of Texas at Austin, Austin, Tx, 2007.
11. Tsai, R.,F. Seibert,B. Eldridge,G.T. Rochelle In *Influence of Viscosity and Surface Tension on the Effective Mass Transfer Area of Structured Packing*, 9th International Conference on Greenhouse Gas Control Technologies, Washington D.C. , 2008; Elsevier: Washington D.C. , 2008.
12. Onda, K., H. Takeuchi, et al. , Mass transfer coefficients between gas and liquid phases in packed columns. *Journal of Chemical Engineering of Japan* **1968,** 1 (1), 6.

Available online at www.sciencedirect.com

ScienceDirect

Energy Procedia 00 (2008) 000–000

Energy Procedia

www.elsevier.com/locate/XXX

GHGT-9

Solvent reclaiming by crystallization of potassium sulfate

Qing Xu[a], Gary T. Rochelle[a,*]

[a]*Dept. of Chemical Engineering, University of Texas at Austin, Austin, TX 78712, USA*

Elsevier use only: Received date here; revised date here; accepted date here

Abstract

Residual SO_2 accumulates as sulfate in aqueous amine used for CO_2 capture from coal-fired power plants. This paper reports research results on a new process to remove this sulfate by crystallization of K_2SO_4. The K_2SO_4 solubility in CO_2 loaded aqueous amine solutions was measured and correlated with an empirical relationship and with the electrolyte-NRTL model in AspenPlus®. The volume median particle size of K_2SO_4 by continuous crystallization ranges from 90 to 340 μm. A case study of the new reclaiming process was done in AspenPlus® and the total estimated cost to remove sulfate is about \$1.1/ton CO_2.

Key Words: Potassium sulfate; crystallization; reclaiming; sulfate removal.

1. Introduction

One side reaction in CO_2 capture when using amine-based treatment is the generation of sulfate from SO_2. Generally, there are two places where sulfate can be removed: the polishing scrubber before CO_2 absorption and solvent reclaiming after stripping. The accumulated sulfate in the system must be maintained below a critical level where the aqueous monoethanolamine (MEA) or piperazine (PZ) still has adequate capacity for CO_2 capture. The amount of sulfate removed by the polishing scrubber can be adjusted so that the total cost is minimized.

Three methods have been commercially used for solvent reclaiming: distillation (thermal reclaiming), electrodialysis, and ion exchange. Electrodialysis and ion exchange remove only ionic impurities, while distillation removes all the impurities but causes thermal degradation and consumes more energy. All of these methods generate considerable amount of diluted or concentrated waste [1].

In this study potassium hydroxide is added to precipitate potassium sulfate solids. This solvent reclaiming process may reduce the cost and solve energy and waste problems in existing reclaiming processes. This paper represents results in three specific areas: thermodynamics, continuous crystallization, and simulation.

* Corresponding author. Tel.: +1-512-471-7230; fax: +1-512-471-7060.
E-mail address: gtr@che.utexas.edu.

2. Thermodynamics – solubility measurement and interaction parameter regression

2.1 Theory

Sulfate solubility in organic aqueous solution (ammonia, ethyl alcohol, ethylene glycol, sugar, etc.) decreases with greater organic concentration and lower temperature [7]. MEA and PZ are organic solvents, and the K_2SO_4 solubility in these aqueous amine solutions is expected to be lower than that in the aqueous solution. However CO_2 loading which increases ionic concentrations as carbamate and protonated amine should increase sulfate solubility.

Under normal conditions, in aqueous electrolyte solutions the concentration of the electrolyte has a significant impact on the electrical conductivity [8]. The ionic strength is a function of the concentration of all ions in the solution: $I = \frac{1}{2}\sum_{i=1}^{n} c_i z_i^2$. Where c_i is the concentration if ion i and z_i is the charge number of that ion. Conductivity can be measured and reflects the electrolyte concentration changes in the solution, while ionic strength represents both the ion concentration and the charge numbers. In this study, CO_2 concentration contributes the most to ionic strength.

2.2 Experimental

In method 1, the conductivity of 50 g of loaded, agitated solution was measured as 0.1-0.4 g K_2SO_4 was sequentially added until the solution was saturated. Then an excess of K_2SO_4 was added to the solution and the final conductivity was recorded. Conductivity was correlated with K_2SO_4 concentration and extrapolated to obtain the K_2SO_4 saturation concentration. In modifications of this procedure, KOH or H_2SO_4 was added to the solution before the additions of K_2SO_4. These experiments were conducted at room temperature and at 40ºC.

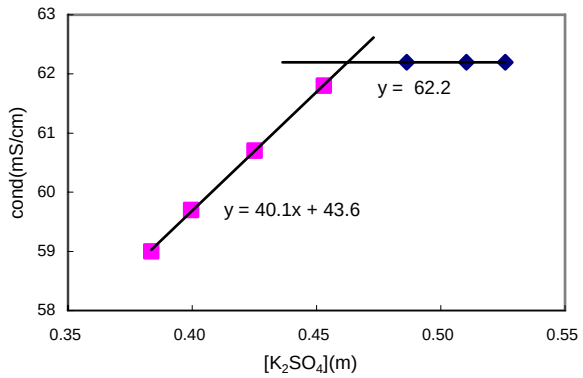

Fig. 1. Conductivity Dependence on Concentration
7 m MEA, $[CO_2]_t$=2.8 m, T=40 ºC

Method 2 was used with high CO_2 loading at relatively high temperature. Instead of adding solid K_2SO_4 to change the concentration of K_2SO_4, 2.0-3.5 mL of loaded solution was sequentially added to the system through a Brinkmann® bottletop buret, and conductivity was measured with each addition. In the beginning, the solution was over-saturated with solids, and then became diluted. Conductivity was correlated with K_2SO_4 concentration and extrapolated to obtain the K_2SO_4 saturation concentration. These experiments were conducted at 80ºC.

A total inorganic carbon analyzer was used to analyze CO_2 concentration change before and after experiments. pH titration was used to analyze amine concentration before and after experiments.

2.3 Results and Discussion

Fig. 1 shows how conductivity is used to determine solubility. The intersection of the curves is the saturation point, and solubility of K_2SO_4 is calculated from the two equations. The results are listed in Table 2. These data are represented by the empirical correlation:

$$\ln Ksp_{calc}(\text{Emp.}) = 7.82 \cdot I^{0.2} - 0.37([\text{eq.amine}], \text{m}) - \frac{2273.4}{T(K)} - 1.445 \qquad (1)$$

where I is the ionic strength, $[\text{eq.amine}] = [\text{MEA}] + 2 \cdot [\text{PZ}]$ and $Ksp = ([K^+], \text{m})^2 \cdot ([SO_4^{-2}], \text{m}) \cdot$

Ksp_{calc}/Ksp(Emp.) is a measure of how well the empirical model predicts the K_2SO_4 solubility. K_2SO_4 solubility increases with greater ionic strength and temperature and decreases with greater amine concentration. Thus higher CO_2 loading increases K_2SO_4 solubility by increasing ionic strength of the aqueous amine solution.

2.4 Aspen parameter regression

The Data Regression System in Aspen Plus® was used to determine the interaction parameters in the electrolyte-NRTL model from all of the experimental data on K_2SO_4 solubility. τ is the energy parameter, one of the electrolyte-NRTL parameters, for molecule-molecule, molecule-electrolyte, and electrolyte-electrolyte pairs [2]. The values of τ are used in the activity coefficient calculation in the electrolyte-NRTL activity coefficient model. For electrolyte-molecule pair parameters, the temperature dependency relations are as follows:

$$\tau_{ca,B} = C_{ca,B} + \frac{D_{ca,B}}{T} + E_{ca,B}\left[\frac{T^{ref} - T}{T} + \ln\frac{T}{T^{ref}}\right] \quad (2)$$

$$\tau_{B,ca} = C_{B,ca} + \frac{D_{B,ca}}{T} + E_{B,ca}\left[\frac{T^{ref} - T}{T} + \ln\frac{T}{T^{ref}}\right] \quad (3)$$

where B is the solvent molecule, ca is electrolyte pair c and a, and T^{ref} is 298.15K.

Table 1: Regressed Parameters for the Electrolyte-NRTL Model

Component	Value	St.dev.
$H_2O/(K^+,MEACOO^-)$	6.76	1.8
$H_2O/(MEA^+,SO_4^{-2})$	7.15	1.6
$MEA/(MEA^+,SO_4^{-2})$	13.68	8.0
$(K^+,SO_4^{-2})/MEA$	-1.57	1.1
$MEA/(K^+,SO_4^{-2})$	7.59	1.4
$H_2O/(K^+,HCO_3^-)$	14.76	1.0
$MEA/(K^+,HCO_3^-)$	15.41	31
$(K^+,OH^-)/MEA$	2.75	5.0
$MEA/(K^+,OH^-)$	-3.04	1.4

In Aspen Plus®, the solubility of K_2SO_4 is represented by $\ln(Ksp) = A + B/T + C\cdot\ln(T)$; T is in Kelvin. A, B, and C were regressed from K_2SO_4 solubility data in water (Söhnel, 1985 [3]). The regressed values for A, B, and C are 265.7, -14954, and -40.7, and the standard deviations are 1.8, 85, and 0.3, respectively. Starting with these values and with 30 other values of C, D, and E regressed by Hilliard (2008) [4] for MEA-H_2O-CO_2, values were regressed for τ parameters including the additional components K^+ and SO_4^{-2}. The data regression includes data reported above in MEA with and without CO_2 and data in water by Söhnel (1985) [3]. Data with CO_2 loading were regressed with a higher weight since most parameters are affected by CO_2. The result uses only C parameters and is given in Table 1.

The other τ parameters were set to default values [2]. Then the parameter set of 9 regressed values and default values was developed; this set is expected to simulate the interaction between ion pairs and molecules within certain condition ranges.

2.5 Test of the Model

The electrolyte-NRTL model in Aspen Plus®, with the developed parameters in Table 1, was used in a series of flash simulations. Each of the experimental conditions was used to get the activity coefficients and mole fractions of K^+ and SO_4^{-2}, as well as Ksp_{calc}/Ksp(Aspen).

$$\frac{Ksp_{calc}}{Ksp}(\text{Aspen}) = \frac{Ksp_{calc}}{Ksp(T)} = \frac{x^2(K^+)\cdot\gamma^2(K^+)\cdot x(SO_4^{2-})\cdot\gamma(SO_4^{2-})}{A + B/T + C\cdot\ln(T)} \quad (4)$$

The Ksp_{calc}/Ksp(Aspen) in Table 2 illustrates that the regression is not accurate at high amine concentration and high CO_2 loading. Temperature has no obvious effect on the accuracy of the prediction.

Table 2: Potassium Sulfate Solubility and Prediction by Empirical Model and Aspen Model

T	Concentration(m)				Ksp_{calc}/Ksp		T	Concentration(m)				Ksp_{calc}/ Ksp	
(°C)	K^+	SO_4^{-2}	CO_2	Amine	Emp.	Aspen	(°C)	K^+	SO_4^{-2}	CO_2	Amine	Emp.	Aspen
in water *							24	0.76	0.38	5.5	11	0.81	N/A
20	1.27	0.63	0	0	0.72	0.78	40	0.89	0.44	5.5	11	0.80	15.2
25	1.38	0.69	0	0	0.75	1.26	40	0.42	0.21	2.2	11	1.17	1.37
30	1.48	0.74	0	0	0.78	0.59	40	0.95	0.30	4.4	11	0.58	9.46
40	1.70	0.85	0	0	0.84	0.70	40	0.33	0.17	1.1	11	0.85	1.57
50	1.90	0.95	0	0	0.93	0.39	40	0.31	0.16	0.55	11	0.49	2.68
60	2.11	1.05	0	0	1.03	0.87	40	0.68	0.49	4.4	11	0.87	10.1
70	2.30	1.15	0	0	1.15	0.67	80	1.25	0.62	5.5	11	0.78	8.48
80	2.47	1.23	0	0	1.30	0.62	80	1.20	0.42	4.4	11	0.68	4.10
0 loading MEA							80	0.99	0.65	4.4	11	0.84	5.05

T	Concentration(m)				Ksp_{calc}/Ksp		T	Concentration(m)				Ksp_{calc}/ Ksp	
(°C)	K^+	SO_4^{-2}	CO_2	Amine	Emp.	Aspen	(°C)	K^+	SO_4^{-2}	CO_2	Amine	Emp.	Aspen
22	1.34	0.67	0	0	0.71	1.04					PZ		
45	1.80	0.90	0	0	0.89	0.99	25	0.54	0.27	2	4	1.14	N/A
40	0.23	0.12	0	3.5	4.03	N/A	23	0.72	0.36	4	4	1.53	N/A
24	0.21	0.10	0	7	0.95	2.90	40	0.44	0.22	1.9	5	1.23	N/A
40	0.25	0.12	0	7	1.03	2.49	40	0.78	0.39	4.2	5	0.97	N/A
80	0.44	0.22	0	7	0.91	1.73	40	0.34	0.17	8	10	0.83	N/A
24	0.09	0.04	0	11	1.08	0.19	40	0.34	0.17	4.8	8	1.26	N/A
25	0.12	0.06	0	11	0.59	N/A	40	0.32	0.16	6.4	8	2.76	N/A
80	0.20	0.10	0	11	0.79	0.47	40	0.42	0.21	0.8	4	1.04	N/A
40	0.10	0.05	0	11.4	1.00	0.14	80	0.51	0.25	4.8	8	0.95	N/A
				MEA			80	0.55	0.28	6.4	8	1.35	N/A
24	0.84	0.22	2.8	7	1.24	1.73					MEA/PZ		
40	0.62	0.31	1.4	7	1.11	0.53	23	0.77	0.38	5.5	7/2	0.76	N/A
40	0.91	0.46	2.8	7	1.09	1.18	24	0.35	0.17	2.2	7/2	1.32	N/A
40	0.74	0.19	1.4	7	0.94	0.50	40	0.83	0.42	5.5	7/2	0.94	N/A
40	0.61	0.46	1.4	7	1.06	0.72	40	0.74	0.37	2.2	3.7/0.8	2.37	N/A
40	0.70	0.17	1.4	7	1.10	0.40	40	0.59	0.12	2.2	7/2	0.84	N/A
42	0.93	0.46	2.8	7	1.09	1.17	40	0.43	0.37	2.2	7/2	0.85	N/A
40	0.44	0.22	0.7	7	1.20	0.56	40	0.26	0.13	1.1	7/2	1.63	N/A
40	0.43	0.22	0.35	7	0.77	1.22	40	0.64	0.32	3.9	7/2	0.96	N/A
80	1.35	0.68	2.8	7	1.03	0.70	80	1.04	0.52	5.5	7/1	1.22	N/A
80	0.94	0.62	1.4	7	1.05	0.39	80	0.94	0.47	3.9	7/2	0.83	N/A
				MEA			80	0.67	0.34	2.2	7/2	0.84	N/A
24	0.69	0.34	5.5	11	1.05	13.9	40	0.43	0.37	2.2	7/2	0.85	N/A

*: data in water by Söhnel, 1985 [3].

Fig. 2 gives the prediction of K_2SO_4 solubility in MEA solution at 40ºC using both empirical and Aspen models. The squares and triangles are from experiment data, solid lines are from the empirical model, and dashed lines are from the Aspen model. The empirical model fairly predicts all the data points; while the Aspen model is off for 11 m MEA at high CO_2 loading.

3. Continuous Crystallization

3.1 Experimental

The apparatus is shown in Fig. 3. K_2SO_4 was crystallized continuously in a stirred reactor fed with loaded amine solution and KOH. The amine feed included CO_2 and enough K_2SO_4 to be close to K_2SO_4 saturation. Sulphuric acid was added to the amine feed to adjust SO_4^{-2}/K^+. The KOH feed was 29.6 wt % or 43.5 wt % aqueous KOH. The feeds were preheated by going through the water bath and pumped into a jacketed beaker. An agitator or magnetic stir bar was used for agitation. The electrical conductivity and temperature of the solution were measured. The volume of the reactor was 200 mL or 50 mL, and the residence time varied from 3 min to 20 min. The liquid level was controlled by adjusting the slurry pump. Slurry samples were collected during the last 2 residence times. It is assumed that the system gets to steady state around 8-10 residence times. Gravity filtration and vacuum filtration were used for a primary separation, and then the filtered sample was dried in an oven at 105ºC. The weights before and after drying were recorded. A dry sample of solids was dispersed into saturated K_2SO_4 aqueous solution by a sonicator. The size distribution was determined by a Malvern® mastersizer. SEM and light microscopy images were taken to show

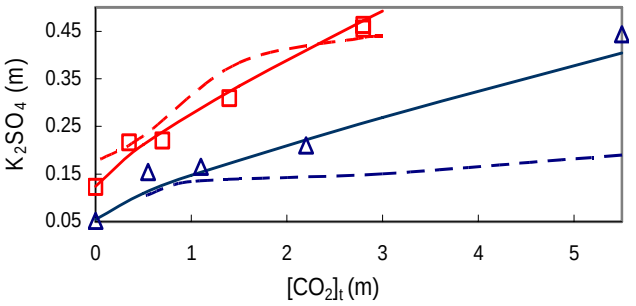

Fig. 2. Prediction of K_2SO_4 solubility in MEA solution at 40ºC

crystal habit, shape and surface, as well as to verify the mean crystal size result of the mastersizer. X-ray diffraction was used to test the purity of the solid product. Settling rate was measured for selected samples from the reactor after experiments.

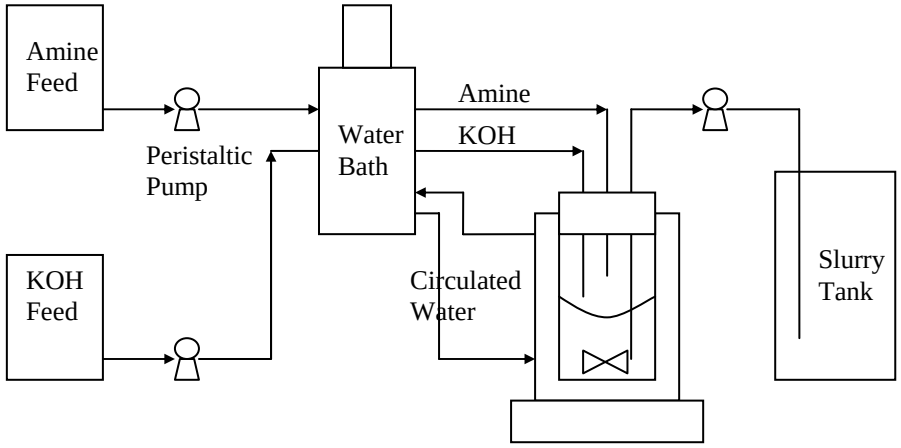

Fig. 3. Continuous crystallization apparatus

3.2 Results and Discussion

Table 3 gives the conditions for each run and the resulting particle size represented as the volume median size and as the moisture content in the filter cake. The volume median particle size varies from 90 to 340 μm with residence times of only 3 to 20 minutes. The solids filter easily and settle rapidly. It appears that greater particle sizes result from greater T, longer residence time, reduced SO_4^{-2}/K^+, and reduced amine concentration. There appeared to be no effect of additives. CO_2 loading is defined as: $\alpha = \frac{[CO_2]_t}{[\text{eq.amine}] - 2\cdot[H_2SO_4]}$

Table 3: Continuous Crystallization of Potassium Sulfate

T	Agitation	τ	Concentration (m)		CO_2	KOH	SO_4^{-2}/K^+	Volume Median Particle size (μm)*			Initial Settling Rate
°C	RPM	min	MEA	SO_4^{-2}	ldg.	wt%		L_1	L_2	L_3	cm/min
25	420**	20	7	1	0.4	29.6	0.77	234	300	N/A	N/A
60	380	10	7	1	0.4	43.5	0.41	202	300	N/A	N/A
40	380	10	7	1.52	0.4	43.5	1.1	194	100-150	150	7.1
40	380	10	7	1.52	0.4	43.5	0.63	305	100-150	100-150	N/A
40	380	3	7	1.52	0.4	43.5	1.1	90	50	50	5.1
40	380	20	7	1.52	0.4	43.5	1.1	334	100-150	125-150	4.0
40	870	10	7	1.52	0.4	43.5	1.1	225	30-50	50	1.4
40	250	10	7	1.52	0.4	43.5	1.1	158	100-150	N/A	2.2
40	380	10	11	1.67	0.31	43.5	1	172	30	N/A	N/A
25	750**	20	11	1	0.4	29.6	0.34	339	250-300	N/A	N/A
40	380	10	8(PZ)	0.63	0.40	43.5	0.21	194	100-150	150	N/A
40	380	10	7/2(PZ)	1.67	0.30	43.5	1.1	209	30-50	N/A	2.5
40	380	10	7[a]***	1.52	0.4	43.5	1.1	207	100-150	100	N/A
40	380	10	7[b]	1.52	0.4	43.5	1.1	317	150-200	N/A	4.1
40	380	10	7[c]	1.52	0.4	43.5	1.1	245	100-150	150+	N/A
60	380	10	7[d]	1	0.4	43.5	0.37	218	N/A	N/A	N/A

*: L_1 is from mastersizer®; L_2 is the greatest length inside one image by light microscope; L_3 is the greatest length inside one image by SEM.
**: An overhead stirrer was used while a one-inch magnetic stir bar was used in the others. RPM is given in the manuals for certain speed settings.

***: Additives: a: 0.1mM Fe^{+2}, 0.1mM Cu^{+2}, 100mM inhibitor A; b: mole ratio HEEDA/MEA=0.05, mass ratio HEIA/MEA=0.02; c: 0.1mM Fe^{+2}, 0.1mM Ni^{+2}, 0.1 mM Cr^{+2}; d: <1mM Fe^{+2}.

Figs. 4 and 5 show typical images of K_2SO_4 crystals under SEM and light microscopy, respectively. Therefore big crystals can be formed under the experimental condition range and are easily separated. This indicates the feasibility of reclaiming amine solvent by K_2SO_4 crystallization.

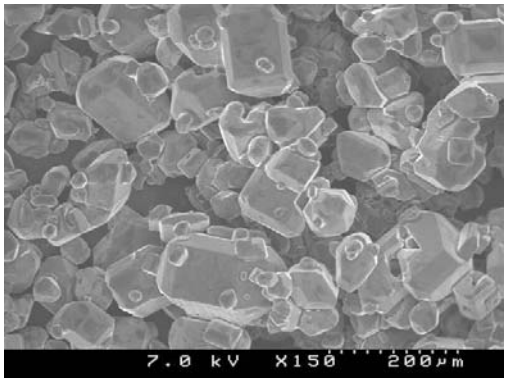

Fig. 4. K_2SO_4 Crystals under SEM
From exp. with 0.1mM Fe^{+2}, 0.1mM Ni^{+2}, 0.1 mM Cr^{+2}.

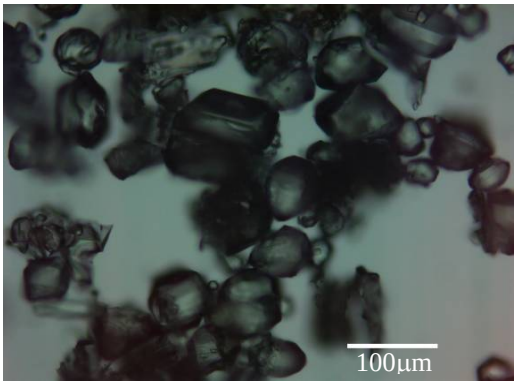

Fig. 5. K_2SO_4 Crystals under Light Microscope
From exp. with 7m MEA, 0.4 loading, SO_4^{-2}/K^+=0.63.

4 Material and Energy Balances and Cost Estimation

4.1 Process Simulation Description

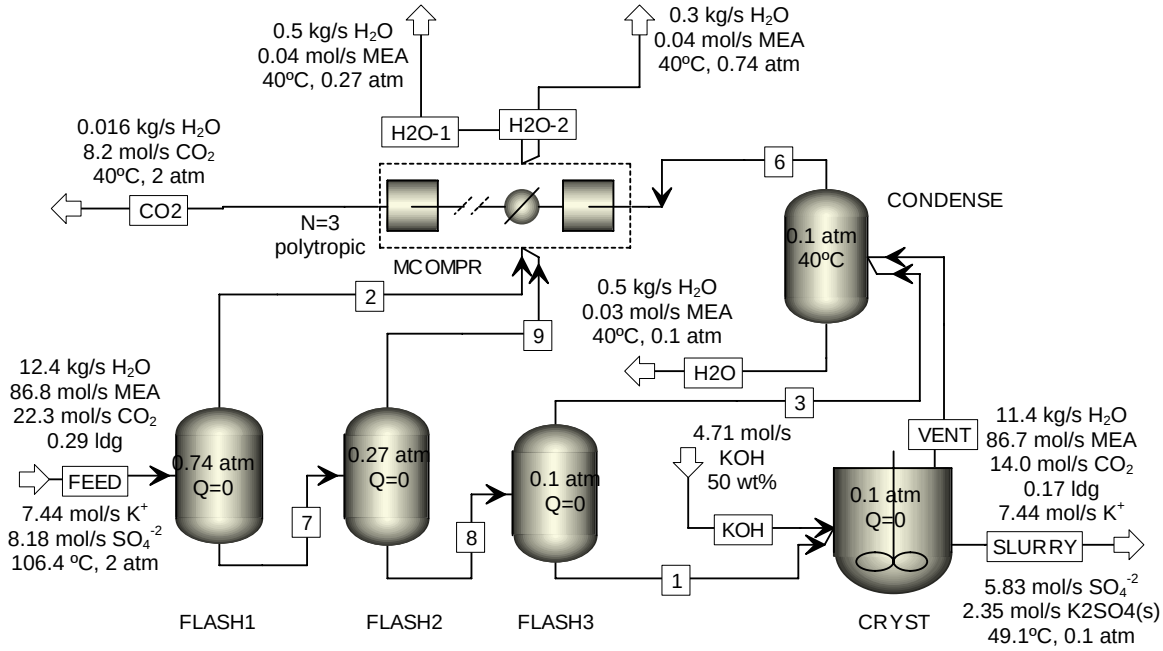

Fig. 6. Reclaiming Process by K_2SO_4 Crystallization

Fig. 6 shows AspenPlus® modelling results for a reclaiming process using K_2SO_4 crystallization. The base case is a 500 MW power plant [5]. The flue gas contains 12.38% CO_2 and 100 ppm SO_2 and the CO_2 removal rate is 90%. A sub-stream from the bottom of stripper is fed into the reclaiming system. The flow rate is adjusted to avoid any sulfate accumulation in the solvent, that is, to remove all sulfate in flue gas. In flash 1, 2, and 3, CO_2 and water evaporate to concentrate the solution and the pressure drops to about 0.1 atm. The pressures of the crystallizer and condenser were set to be equal to that of flash 3. 50 wt% KOH is fed into the crystallizer to precipitate extra sulfate. Water is condensed from vapor (stream 2, 9, 3 and vent) by the condenser and the cooling system inside the multi-compressor. Through the multistage compressor, vapor is compressed to 2 atm, which is the same as that from the top of the stripper. Slurry is further separated and clear liquid is pumped back to the absorber-stripper system. The flow rate of the KOH stream is adjusted to make potassium flow rates equal in the feed and liquid phase of the slurry. Make-up water is needed to dilute the slurry so that it can be pumped to the absorber. Through this process, sulfate is removed, part of CO_2 is separated and compressed, and energy is lost through the cooling down of inlet stream and compression of CO_2.

4.2 Results and discussion

Conditions of important blocks and streams are shown in Fig. 6. The net duty of the condenser is 1.21E6 Watt, while cooling duty and net work of the multi-stage compressor are 2.15E6 and 7.06E4 Watt. According to Hilliard [4] the average heat capacity of the inlet feed between 40-120ºC is 3.54 kJ/(kgK), thus the equivalent work that is lost from the main stream in this process is:

$$\begin{aligned} Weq_1 &= m \cdot 0.75 * \int_{49.1+273.15}^{106.4+273.15} \frac{T - T_{ref}}{T} \cdot CpdT \\ &= 19.76 kg/s \cdot 0.75 \cdot 3.54 kJ/(kg.K) \cdot \int_{322.25}^{379.55} (1 - \frac{313.15}{T}) dT \\ &= 3.17E5(Watt) \end{aligned}$$

The equivalent work that benefits from compressed CO_2 is:

$$Weq_2 = 8.2(mol\ CO_2/s) \cdot 15(kJ/mol\ CO_2) = 123(\text{kJ/s}) = 1.23E5(Watt)$$

The total equivalent work that is lost in this process per mole sulfate removed is:

$$\begin{aligned} Weq &= (Weq_1 + W_{compr} - Weq_2) / (\text{moles of } K_2SO_4 \text{ in slurry}) \\ &= (3.17E5 + 7.06E4 - 1.23E5) Watt / 2.35 mol/s \\ &= 1.126E5\ \text{J}/mol\ K_2SO_4 \end{aligned}$$

Knowing the ratio of CO_2 to SO_2 in the flue gas and a typical electricity cost, the cost of sulfate removal in dollars per ton CO_2 can be calculated using the following formula:

$$\text{Energy cost} = \frac{112.6kJ}{mol\ SO_2} \cdot \frac{1E-4 mol SO_2}{12.38\% mol\ CO_2 \cdot 90\%} \cdot \frac{molCO_2}{44.01g} \cdot \frac{1E6g}{ton} \cdot \frac{MWhr}{3.6E6kJ} \cdot \frac{60\$}{MWhr} = 0.038\ \$/ton CO_2$$

The energy cost is very low. The chemical cost can be calculated based on the assumption that K_2SO_4 can be sold as fertilizer. (Prices used are from Aug. 2006 [6]: caustic potash liq. 45% \$15.6/100 lb; \$200/ton K_2SO_4 fertilizer, which are \$0.043 and \$0.017 per mole potassium, respectively).

$$\$/\text{mol } SO_2 = 2 \cdot (0.043 - 0.017) = 0.051 \$/mol\ SO_2$$

The dollar cost per ton of CO_2 can be calculated using this formula:

$$\text{Chemical cost} = \frac{\$0.051}{mol\ SO_2} \cdot \frac{1E-4 mol SO_2}{12.38\% mol\ CO_2 \cdot 90\%} \cdot \frac{molCO_2}{44.01g} \cdot \frac{1E6g}{ton} = 1.040\ \$/ton CO_2$$

Total cost=0.038+1.040=1.078 (\$/ton CO_2)

According to this case study, the cost of sulfate removal is about \$1.1 per ton CO_2. This is very low compared with CO_2 capture cost without solvent reclaiming, which is about \$55-67 per ton CO_2 [5]. There are also environmental advantages over the other 3 reclaiming processes: little waste solution is generated and the by-product K_2SO_4 can be used as fertilizer.

5. Conclusion

A new reclaiming process was developed to remove sulfate from amine solvent. Experiments of K_2SO_4 solubility measurement were performed at 25ºC to 80ºC with 0 to 0.5 moles CO_2/equivalent amine in aqueous solutions of 3.5 to 11 m MEA, 4 to 10 m PZ, and 7 m MEA/2 m PZ. The K_2SO_4 solubility varies from 0.04 to 0.9 m, and the Ksp varies from 0.4 to 3.1. A typical lean solution of 7 m MEA with 0.4 CO_2 dissolves as much as 0.46 m of K_2SO_4. An empirical model was correlated for data prediction: $\ln Ksp_{calc}(\text{Emp.}) = 7.82 \cdot I^{0.2} - 0.37([\text{eq.amine}], \text{m}) - \frac{2273.4}{T(K)} - 1.445 \cdot$ This shows that K_2SO_4 solubility increases with greater CO_2 concentration and temperature and decreases with greater amine concentration. An interaction parameter model using Aspen Plus® was developed with 9 parameters for the electrolyte-NRTL model.

By adding 29.6 wt % or 43.5 wt % KOH to 7 and 11 m MEA, 8 m PZ, and 2 m MEA/7 m PZ, with SO_4^{-2}/K^+ from 0.3 to 1.1 and 0.6 to 1.7 m SO_4^{-2}, at 25, 40, and 60ºC, with residences time of 3 min, 10 min, and 20 min, agitation rates from 250 to 870 RPM, with or without additives (Fe^{+2}, Cr^{+2}, Cu^{+2}, Ni^{+2}, HEEDA, HEIA, inhibitor A, etc.), K_2SO_4 was crystallized continuously and the results show that big crystals with a volume median particle size of 90-340 μm can form and solid-liquid separation is easy to achieve.

A case study of a 500 MW power plant was done by process simulation in Aspen Plus®. Estimated energy and chemical costs show that the total cost to remove sulfate in that case would be $1.1 per ton CO_2, which is very acceptable. The waste generation is very small compared with the other reclaiming processes.

Based on all the above results the reclaiming by potassium sulfate crystallization is a good option for solvent reclaiming in post-combustion CO_2 capture.

6. Acknowledgements

The work was supported by the Luminant Carbon Management Program. Martin Metzner assisted in experimental measurements.

References

1. A. L. Cummings, G. D. Smith, D. K. Nelsen, *Advances in amine reclaiming – why there is no excuse to operate a dirty amine system*, Laurance Reid Gas Conditioning Conference, 2007(227-244).
2. Aspen Plus® help: Electrolyte-NRTL model and activity coefficient model. Aspen Plus® 2006.5.
3. O. Söhnel, P. Novotny, *Densities of aqueous solutions of inorganic substances*, Elsevier, Amsterdam, 1985.
4. M. Hilliard, Ph.D. dissertation, *A predictive thermodynamic model for an aqueous blend of potassium carbonate, piperazine, and monoethanolamine for carbon dioxide capture from flue gas*, The University of Texas at Austin (2008).
5. K. S. Fisher, G. T. Rochelle, C. Schubert, *Advanced amine solvent formulations and process integration for near-term CO_2 capture success*, final report to DOE, 2007.
6. ICIS students: chemical market reporter, Aug 28, 2006. http://www.icis.com/StaticPages/p-s.htm#P
7.W. F. Linke, *Solubilities of inorganic and metal organic compounds*, volume II, 4th ed, American Chemical Society, 1965(301-325).
8. A. L. Horvath, *Handbook of aqueous electrolyte solutions*, Ellis Horwood Limited, 1985 (250-253).

Available online at www.sciencedirect.com

ScienceDirect

Energy Procedia 00 (2008) 000–000

Physics Procedia

www.elsevier.com/locate/XXX

GHGT-9

Carbon dioxide capture with concentrated, aqueous piperazine

Stephanie A. Freeman[a], Ross Dugas[a], David Van Wagener[a], Thu Nguyen[a], and Gary T. Rochelle[a,*]

[a]*Department of Chemical Engineering, The University of Texas at Austin, 1 University Station C0400, Austin, TX,78712 USA*

Elsevier use only: Received date here; revised date here; accepted date here

Abstract

Concentrated, aqueous piperazine (PZ) has been investigated as a novel amine solvent for carbon dioxide (CO_2) absorption. The CO_2 absorption rate with aqueous PZ is more than double that of 7 m MEA and volatility at 40°C ranges from 10 to 19 ppm. Thermal degradation is negligible in concentrated PZ solutions up to a temperature of 150°C, a significant advantage over MEA systems. Oxidative degradation of concentrated PZ solutions is appreciable in the presence of copper (4 mM), but negligible in the presence of chromium (0.6 mM), nickel (0.25 mM), iron (0.25 mM), and vanadium (0.1 mM). Initial system modeling suggests that 8 m PZ will use 5 to 10 % less energy than 7 m MEA. The fast kinetics and low degradation rates suggest that concentrated PZ has the potential to be a preferred solvent for CO_2 capture.

Keywords: carbon dioxide; CO_2 capture; piperazine; amine degradation; absorption; stripping

1. Introduction

The increase in the anthropogenic carbon dioxide (CO_2) concentration in the atmosphere over the past few decades is known to be part of the cause of global warming. A large impact on CO_2 emissions can be made by targeting large point sources such as coal-fired power plants. Amine based absorption and stripping systems have been studied for CO_2 capture from coal-fired power plants and have shown the most promise for effective CO_2 control. Traditional amines such as monoethanolamine (MEA) and amine blends such as potassium carbonate/piperazine (PZ) and methyldiethanolamine (MDEA)/PZ have been investigated extensively for this application[1-3].

PZ is a diamine that has previously been studied as a promoter for amine systems to improve kinetics, such as MDEA/PZ or MEA/PZ blends. The concentration of PZ when used as a promoter has been between low, between 0.5 to 2.5 m PZ, because PZ is not highly soluble. Given the nature and magnitude of absorption/stripping systems, any possibility of precipitation ruled out PZ for use at concentrations above its room temperature solubility. Additionally, the boiling point of PZ (146.5°C) is lower than that of MEA (170°C), indicating the possibility for higher volatility. Recent work has indicated that the volatility of PZ is comparable to that of MEA due to the non-ideality of PZ in solution. Increasing the concentration of PZ in solution allows for increased solvent capacity and faster kinetics.

PZ has been studied as a solvent for absorption/stripping systems for the removal of CO_2 from the flue gas of coal-fired power plants. The current work examines solid solubility, oxidative degradation, and thermal degradation of concentrated aqueous PZ solutions. Additionally, extensive work on the kinetics of the absorption of CO_2 into PZ is reported. Finally, preliminary modeling work indicates that stripper performance with a concentrated PZ solvent is comparable to MEA systems.

* Corresponding author. Tel.: +1-512-471-7230; fax: +1-512-471-7060.
E-mail address: gtr@che.utexas.edu.

2. Materials and Methods

2.1 Solution Preparation

Aqueous piperazine solutions were created by heating anhydrous piperazine (99% pure, Fluka) with water until the solid crystals melted into a solution. The warm solution was transferred to a glass cylinder with a CO_2 gas sparger and the cylinder was placed on a scale. The scale was used to gravimetrically add CO_2 to achieve the desired loading.

2.2 CO_2 Loading through Total Inorganic Carbon (TIC)

The concentration of CO_2 in solution was determined by total inorganic carbon analysis [2]. The sample is diluted and then acidified in 30 wt% phosphoric acid to release aqueous CO_2, carbamate, and bicarbonate species as gaseous CO_2. The CO_2 is carried through an infrared analyzer with nitrogen. The resulting analyzer peaks are integrated and correlated to CO_2 concentrations using a 1000 ppm K_2CO_3/$KHCO_3$ standard inorganic carbon solution. CO_2 loading is reported as moles CO_2/mole alkalinity or moles CO_2/equiv PZ, where 2 moles alkalinity/mole PZ is the conversion factor.

2.3 Amine Titration

The concentration of piperazine in solution was determined using acid titration [2]. An automatic Titrando series titrator with automatic equivalence point detection was used (Metrohm USA). The 300X diluted sample was titrated with 0.1 N H_2SO_4 to a pH of 2.4. The amount of acid needed to reach the equivalence point at a pH of 3.9 was used to calculate the total amine concentration in solution.

2.4 Viscosity Measurements

Viscosity was measured using a Physica MCR 300 cone and plate rheometer (Anton Paar). The apparatus allows for precise temperature control for measuring viscosity at temperatures ranging from 20 to 70°C. To determine viscosity, the angular speed of the top disk (cone) is increased from 100 to 1000 s^{-1} over a period of 100 seconds and the shear stress exerted by the solution is measured every 10 seconds. Reported viscosities are averages of these 10 individual measurements.

2.5 Oxidative Degradation

Oxidative degradation experiments were performed in a low gas flow agitated reactor fed with 100 mL/min of a saturated 98%/2% O_2/CO_2 gas mixture [4]. The reactor is a 500-mL jacketed reactor is filled with 350 mL of solvent. The jacket contains circulated water maintained at 55°C. The reactor is agitated at 1400 rpm to increase the mass transfer of oxygen into the solution. The reactor is operated continuously for 3-5 weeks, depending on the experiment. Liquid samples are taken every two days and water is added to maintain the water balance on the reactor contents. The liquid samples were analyzed for PZ and degradation products by cation and anion chromatography.

2.6 Vapor-Liquid Equilibrium

CO_2 solubility and amine volatility were measured in a batch equilibrium cell with gas recycle through a hot gas FTIR [2]. The cell was a jacketed, glass reactor where temperature is controlled within 1°C. The inlet gas is sparged from the bottom of the reactor and there is additional mechanical agitation to enhance mass transfer. The gas in the headspace of the reactor is continuously sampled by an FT-IR. The gas leaves the reactor and passes through a mist eliminator and into a sample line heated to 180°C. The heated gas stream is then analyzed by the multi-component FTIR analyzer.

2.7 Thermal Degradation

Thermal bombs were constructed from $^1/_4$ or $^3/_8$-inch stainless steel tubing with two swagelock end caps [5]. Bombs were filled with 2 or 10 mL of PZ solution, sealed, and placed in forced convention ovens at various temperatures. Bombs were removed from the ovens each week and the contents were analyzed for degradation products, remaining amine concentration, and CO_2 loading. Amine losses are reported as a fraction of the initial amine that is remaining after the indicated time period as analyzed using cation ion chromatography (IC).

2.8 Wetted Wall Column Operation

The wetted wall column counter-currently contacts an aqueous piperazine solution with a saturated N_2/CO_2 stream on the surface of a stainless steel rod with a known surface area [3, 6]. The wetted wall column can either perform absorption or desorption of CO_2 depending on the inlet CO_2 partial pressure of gas phase. By bracketing CO_2 partial pressures that result in absorption and desorption, the equilibrium partial pressure of the solution can be determined.

The gas flow rate entering the wetted wall column is controlled via mass flow controllers. Inlet and outlet CO_2 concentrations are measured by Horiba CO_2 analyzers. As Equation 1 shows, the calculated CO_2 flux divided by the CO_2 partial pressure driving force provides an overall mass transfer coefficient for the experiment (K_G). The overall mass transfer coefficient is related to the liquid and gas phase mass transfer coefficients via a series resistance relationship shown in Equation 2.

$$\text{Flux} = K_G\left(P_{CO_2,\text{bulk}} - P^*_{CO_2}\right) \quad \text{Eqn. 1}$$

$$\frac{1}{K_G} = \frac{1}{k_g} + \frac{1}{k_g'} \quad \text{Eqn. 2}$$

The gas phase mass transfer coefficient, k_g, is correlated to experimental conditions and is a strong function of the geometry of the apparatus. The liquid film mass transfer coefficient, k_g', quantifies how fast the solution will absorb or desorb CO_2.

3. Results

3.1 Solid Solubility

The solid solubility of PZ was studied over a range of PZ concentration, CO_2 loading, and temperature. Solutions were prepared to cover the desired solution properties and were allowed to equilibrate at each condition with stirring before solubility observations were made. The transition temperature of 8 and 10 m PZ solutions over a range of CO_2 loading is shown in Figure 1. The transition temperature is the temperature at which a liquid solution will first precipitate when cooled slowly. The approximate temperature ramp for all transitions was 1°C every 5 minutes. The two dashed lines at rich loadings in Figure 1 represent soluble PZ solutions indicating that the solubility envelope extends at least this far. The transition temperature of unloaded PZ solutions ranging from 1.0 to 40 m PZ is shown in Figure 2.

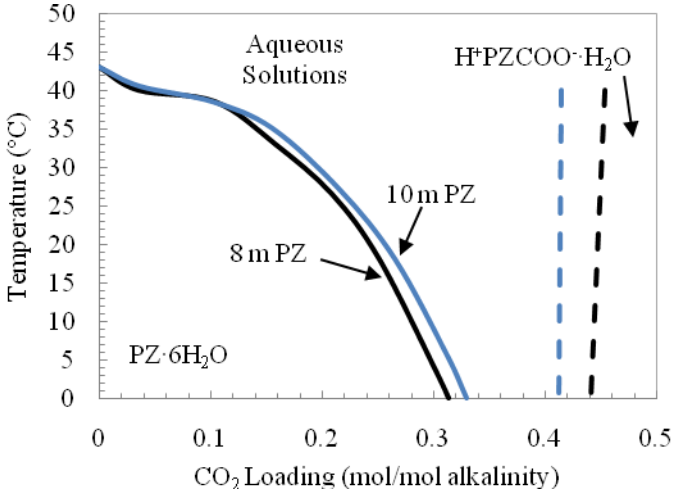

Figure 1: Solid-Liquid Transition Temperatures for Aqueous Piperazine

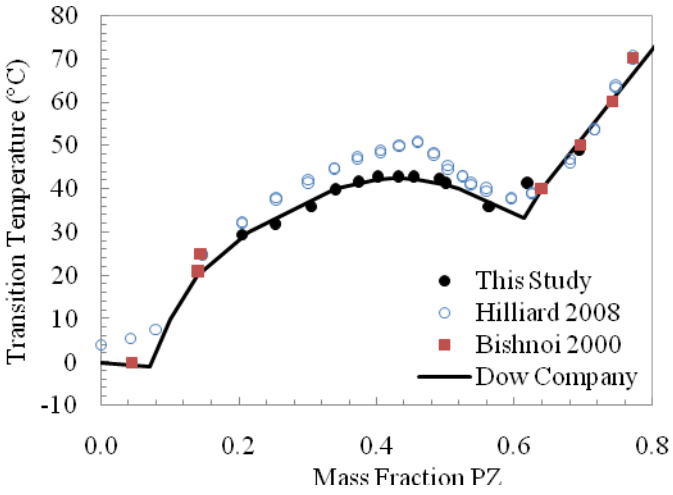

Figure 2: Comparison of Solid Solubility for Aqueous Piperazine Solutions [1, 2, 7]

The data from this study shows a eutectic point around 60 wt% PZ that was observed in the other data sources as well [2, 7]. For 8 m PZ, a CO_2 loading of approximately 0.25 mol CO_2/mol alkalinity is required to maintain a liquid solution without precipitation at room temperature (20°C). In addition, the solubility of PZ at 20°C is 14 wt% PZ, which corresponds to 1.9 m PZ.

3.2 Viscosity

The viscosity of aqueous PZ solutions has been measured from 0.20 to 0.45 moles CO_2/mole alkalinity, 2 m PZ to 20 m PZ, and 25°C to 60°C. The viscosity of 8 and 10 m PZ is compared with other amines in

Figure 3. The amine concentration is plotted in units of moles alkalinity per kg of water in order to compare mono- and diamines on the same basis. All of the viscosities are at 40°C and at the rich loading of the system (0.3 mol CO_2/equiv Amine for MDEA and MDEA/PZ; 0.4 mol CO_2/equiv Amine for PZ and DGA; 0.5 mol CO_2/equiv Amine for MEA).

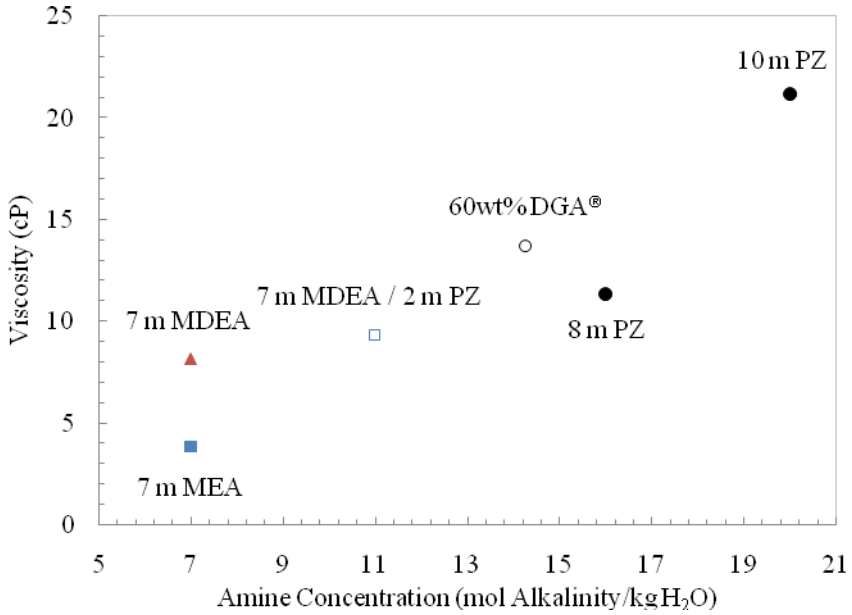

Figure 3: Viscosity of Amine Solutions at Typical Rich Loading, 40°C [8, 9]

Comparison of the viscosity on this basis shows how the amine basic groups affect overall viscosity. As the concentration of basic groups increases, the viscosity increases in a linear direction. The viscosity of 8 m PZ is higher than that of 7 m MEA, but as compared to 60 wt % DGA®, the viscosity of PZ is lower for a higher alkalinity. DGA® solutions at 60 wt % are successfully used in natural gas treating [10].

3.3 Oxidative Degradation

Heavy metals are known to catalyze the oxidative degradation of amines [11]. The results of oxidative degradation of concentrated PZ in the presence of several dissolved metals are shown in Table 1. The experiments simulated four scenarios: (1) leaching of stainless steel metals, (2) addition of a copper-based corrosion inhibitor, (3) addition of a vanadium-based corrosion inhibitor (low concentration), and (4) addition of a copper-based corrosion inhibitor and proprietary inhibitor "A".

Table 1: Oxidative Degradation of PZ and MEA at 55°C (100 ml min of 98% O_2/2% CO_2, 350 mL solution)

Case	Solution (m)	Heavy Metals (mM)	Rate of Formation (mM/hr)			
			Formate	Formamide	EDA	Amine
-	7 MEA	1.0 Fe	0.29	0.35	-	-3.8
1	10 PZ	0.6 Fe^{2+}, 0.25 Cr^{3+}, 0.25 Ni^{2+}	0.005	0.007	0	-1.1
2	10 PZ	4.0 Cu^{2+}	0.14	0.24	0.43	-3.0
3	8 PZ	0.1 Fe^{2+}, 0.1 V^{4+}	0.006	0.013	0	-0.8
4	8 PZ	4.0 Cu^{2+}, 0.1 Fe^{2+}, 100 "A"	0.011	0.016	0.009	-1.1

Oxidative degradation of concentrated PZ was found to be four times slower than that of MEA in the presence of stainless steel metals (Fe^{2+}, Cr^{3+}, and Ni^{2+}) and a low concentration of vanadium. As with MEA solutions, PZ was determined to be highly susceptible to oxidative degradation in the presence of Cu^{2+} [12]. The primary degradation products were found to be ethylenediamine (EDA), formate, oxalate, and N-formylpiperazine, the amide of formate and PZ (denoted as Formamide in the table). The N-formylpiperazine concentration was not measured directly, but inferred from formate production through the basic reversal of the N-formylpiperazine formation reaction. Also, as with MEA, Inhibitor "A" was able to vastly reduce this degradation to levels comparable with the stainless steel and vanadium cases [12].

3.4 Thermal Degradation

Thermal degradation was investigated in PZ solutions at slightly above stripper temperature (135°C) and much higher than stripper temperatures (150°C and 175°C). The thermal degradation results are shown in Table 2. Experiments ranged from 4 to 12 weeks in length.

Table 2: Thermal Degradation of PZ and MEA [5]

Solvent	CO_2 Loading (mol/mol alkalinity)	Temperature (°C)	Amine Loss (% per week)
7 m MEA	0.4	135	5.3%
10 m PZ	0.3	135	0.25%
7 m MEA	0.4	150	11%
10 m PZ	0.3	150	0.8%
8 m PZ	0.3	175	8.0%

PZ thermal degradation was determined to be negligible at 135 and 150°C as compared to 7 m MEA. At 175°C, 32% of the PZ was degraded in 4 weeks. EDA was observed as a thermal degradation product at 175°C but not at lower temperatures. Addition of 5.0 mM Cu^{2+}/0.1 mM Fe^{2+}, 5.0 mM Cu^{2+}/0.1 mM Fe^{2+}/100 mM Inhibitor "A", and 0.6 mM Cr^{3+}/0.25 mM Fe^{2+}/0.25 mM Ni^{2+} did not affect degradation rates at 175°C.

3.5 CO_2 Solubility

The measured solubility of CO_2 in 2 m to 8 m PZ solutions is in given in Figure 4 and compared to previous studies [2, 13].

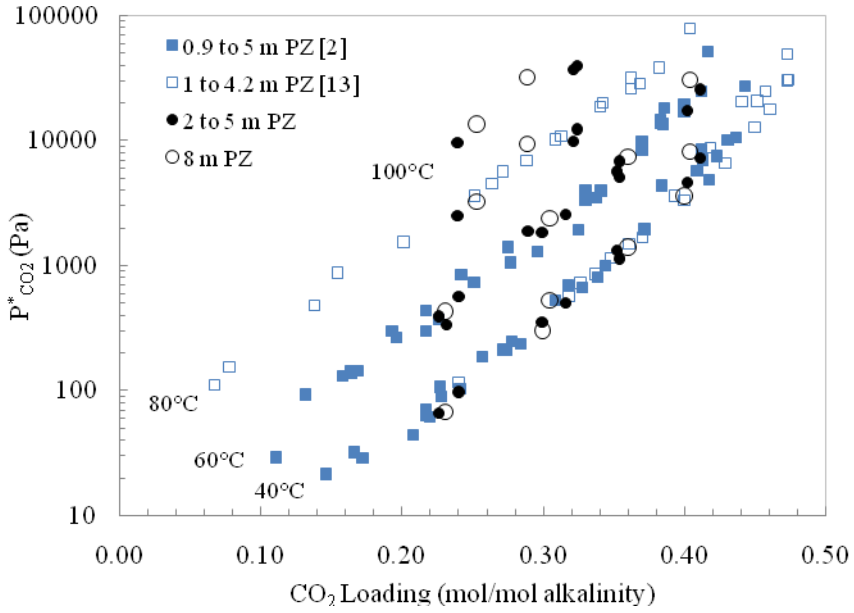

Figure 4: CO_2 Solubility in Aqueous PZ Solutions [2, 13].

The CO_2 solubility of concentrated, aqueous PZ solutions follows the trends found previously for lower concentration PZ solutions at 40 and 60°C. CO_2 solubility is known to not be a strong function of amine concentration and this is confirmed for high concentration PZ solutions [2]. At 40°C, 8 m PZ provides a working capacity of 0.73 moles/kg (PZ+H_2O), which is calculated based on a change in the equilibrium CO_2 partial pressure from 7.5 kPa (loading of 0.415 mol CO_2/mol alkalinity) to 0.75 kPa (0.33 mol CO_2/mol alkalinity). For 7 m MEA at 40°C, the working capacity is 0.43 moles CO_2/kg (MEA+H_2O) based on a change in the equilibrium partial pressure of CO_2 from 5 kPa (0.53 mol CO_2/mol alkalinity) to 0.5 kPa (0.45 mol CO_2/mol alkalinity). The selected range of CO_2 loading for the 8 m PZ solution falls within the solubility envelope established in Figure 1 and 2.

3.6 Kinetics of CO_2 Absorption in PZ Solutions

The kinetics of the CO_2 absorption into concentrated aqueous PZ was studied in a wetted wall column. The measured liquid-side mass transfer coefficient based on a gas side driving force, k_g', is shown compared to 7 m MEA in

Figure 5 for 40°C and 60°C. Data at 60°C are plotted versus the equilibrium partial pressure of CO_2 if the solution were at 40°C for comparison purposes.

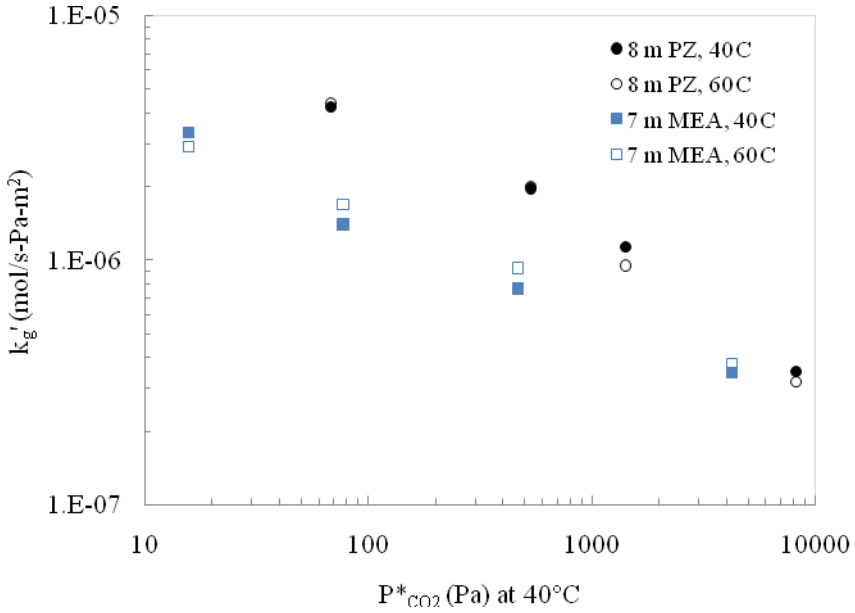

Figure 5: Comparison of Mass Transfer Coefficients in PZ and MEA [6].

As demonstrated in Figure 5, the normalized flux, k_g', for 8 m PZ is 2 to 3 times greater than for 7 m MEA. For example, at 40°C and an equilibrium CO_2 partial pressure of 500 Pa, the k_g' for 8 m PZ and 7 m MEA are 1.98 x 10^{-6} and 7.66 x 10^{-7} mol/s-Pa-m^2, respectively. This demonstrates that the kinetic rate of concentrated PZ is over twice as fast as MEA at 40°C. The same trend is observed for the data at 60°C.

3.7 Volatility of PZ Solutions

The volatility of PZ was measured in the equilibrium cell with hot gas FTIR. The volatility of 8 m PZ solutions is compared to that of 5 m PZ and 7 m MEA in Figure 6. The volatility of each solution is normalized by the PZ concentration for comparison purposes.

At 40°C, the normalized volatility of PZ solutions is the same as the normalized volatility of MEA solutions. It was anticipated that PZ would have a higher volatility than MEA because the boiling point of PZ, 146°C, is lower than that of MEA, 170°C. However, the volatility of PZ is comparable at 40°C. Initial modeling of PZ systems demonstrates this effect as a greatly reduced activity coefficient for PZ [2]. At 40°C, PZ volatility varies from 10 to 19 ppm at atmospheric pressure.

3.8 Estimated Energy Requirement

Thermodynamic models for MEA and PZ were developed by Hilliard, and the PZ model was modified for concentrated solutions [2]. The stripper section of an absorber/stripper system for CO_2 removal was simulated for 8 m PZ and compared with 7 m MEA. These simulations included a simple stripper with CO_2 compression to 5 MPa, a 5°C cold side temperature approach for the cross heat exchanger, and a 10°C approach for the reboiler. For all cases, 15 m of CMR NO-2P packing was used with an 80% approach to flood. The rich stream for each case assumed a P^*_{CO2} at the absorber temperature of 40°C. One PZ case assumed a higher P^*_{CO2} due to the faster rates of PZ expected in the absorber. Equivalent work, W_{eq}, is calculated as shown in equation 3 using the stripper reboiler duty, Q, total pumping work, W_{pump}, and total CO_2 compression work to achieve 50 atm, W_{comp}.

$$W_{eq} = 0.75\,Q\left(\frac{T_{reboiler} - T_{sink}}{T_{reboiler}}\right) + W_{pumps} + W_{comp} \qquad \text{Eqn. 3}$$

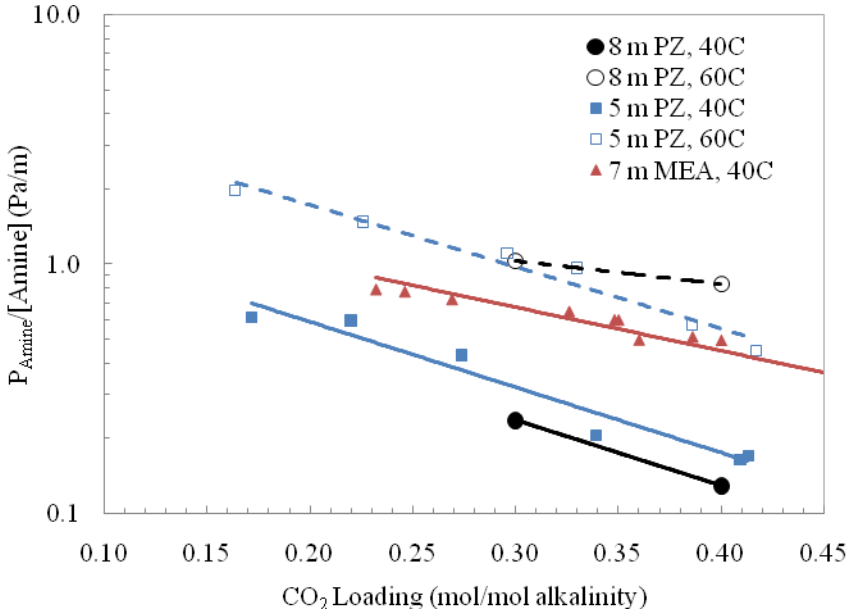

Figure 6: PZ and MEA Volatility Normalized to Amine Concentration.

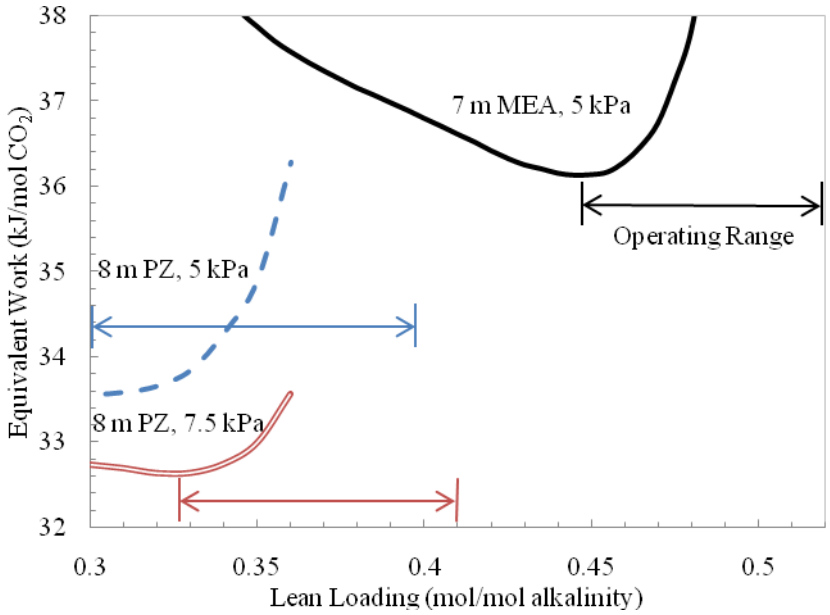

Figure 7: Equivalent Work Requirement for Simple Stripper with 5°C Approach and Rich CO_2 Equilibrium Partial Pressure of 5 or 7.5 kPa

Each system was simulated at their optimum lean loadings and the baseline system, 7 m MEA, had an equivalent work of 36.1 kJ/mol CO_2. The two 8 m PZ systems modeled at a 5.0 or 7.5 kPa rich equilibrium CO_2 partial pressure had minimum equivalent works of 33.5 kJ/mol CO_2 and 32.6 kJ/mol CO_2, respectively. The PZ system with the lower rich P^*_{CO2}, 5 kPa, was less efficient than the system with 7.5 kPa P^*_{CO2}, but was better than the 7 m MEA case with an equivalent rich loading. The increased capacity of PZ improved its performance over the baseline, despite a lower ΔH_{abs}.

4. Conclusions

Concentrated, aqueous solutions of PZ have shown promise for improved solvent performance in absorption/stripping systems for CO_2 capture. For 8 m PZ, a CO_2 loading of approximately 0.25 mol CO_2/mol alkalinity is required to maintain a liquid solution without precipitation at room temperature (20°C). Additionally, the solubility of PZ at 20°C is approximately 14 wt% PZ, or 1.9 m PZ. The volatility of 8 m PZ systems was found to be between 10.2 and 18.7 ppm PZ at 40°C, which is comparable to 7 m MEA solutions.

Oxidative degradation of concentrated PZ has been shown to be four times slower than 7 m MEA in the presence of the combination of Fe^{2+}, Cr^{3+}, and Ni^{2+} and Fe^{2+} and V^{4+}. In the presence of copper-based corrosion inhibitors, oxidative degradation is an issue but can be drastically reduced with the use of Inhibitor "A". Concentrated PZ is resistant to thermal degradation up to 150°C but does degrade at 175°C, losing 32% of the PZ over 2 weeks. The resistance of PZ to thermal degradation allows for the possibility of higher pressure strippers to improve energy performance.

Kinetic measurements have shown that the rate of CO_2 absorption into 8 m PZ is more than twice that of 7 m MEA at 40°C and nearly double at 60°C. The working capacity of an 8 m PZ solution is 0.73 mol CO_2/(kg PZ + H_2O), nearly double that of 7 m MEA. Initial modeling of the stripper section indicate that the equivalent work required for stripping of an 8 m PZ solution will be approximately 5-10% lower than that of 7 m MEA.

The rapid rate of CO_2 absorption, low degradation rate, and low predicted equivalent work indicate that 8 m PZ solutions are an attractive option for CO_2 capture in absorption/stripping systems.

5. Acknowledgements

The Luminant Carbon Management Program provided support for this research.

6. References

1. S. Bishnoi, Carbon Dioxide Absorption and Solution Equilibrium in Piperazine Activated Methyldiethanolamine. The University of Texas at Austin, Austin, TX, 2000.
2. M.D. Hilliard, A Predictive Thermodynamic Model for an Aqueous Blend of Potassium Carbonate, Piperazine, and Monoethanolamine for Carbon Dioxide Capture from Flue Gas. The University of Texas at Austin, Austin, TX, 2008.
3. J.T. Cullinane and G.T. Rochelle, "Thermodynamics of aqueous potassium carbonate, piperazine, and carbon dioxide." *Fluid Phase Equilibria*. 227(2) (2005) 197-213.
4. A. Sexton, "Catalysts and inhibitors for MEA oxidation." Presentation at GHGT-9, Washington D.C., 2008.
5. J. Davis, "Thermal degradation of monoethanolamine at stripper conditions." Presentation at GHGT-9, Washington D.C., 2008.
6. R. Dugas, "Absorption and desorption rates of carbon dioxide with monoethanolamine and piperazine." Presentation at GHGT-9, Washington D.C., 2008.
7. Brochure, Dow Chemical Company, *Ethyleneamines*; August, 2001 p 48.
8. Brochure, Diglycolamine® Agent - Product Information, *Diglycolamine® Agent - Product Information*; 2005 p 60.
9. F. Closmann, "MDEA/piperazine as a solvent for CO_2 capture." Presentation at GHGT-9, Washington D.C., 2008.
10. M.A. Al-Juaied, Carbon Dioxide Removal from Natural Gas by Membranes in the Presence of Heavy Hydrocarbons and by Aqueous Diglycolamine®/Morpholine. The University of Texas at Austin, Austin, TX, 2002.
11. G.S. Goff and G.T. Rochelle, "Monoethanolamine degradation: O_2 mass transfer effects under CO_2 capture conditions." *Ind. Eng. Chem. Res.* 43(20) (2004) 6400-6408.
12. G.S. Goff and G.T. Rochelle, "Oxidation inhibitors for copper and iron catalyzed degradation of monoethanolamine in CO_2 capture processes." *Ind. Eng. Chem. Res.* 45(8) (2006) 2513-2521.
13. V. Ermatchkov, A.P.S. Kamps, D. Speyer, and G. Maurer, "Solubility of carbon dioxide in aqueous solutions of piperazine in the low gas loading region." *J Chem. Eng. Data* 51(5) (2006) 1788-1796.

Available online at www.sciencedirect.com

ScienceDirect

Energy Procedia 00 (2008) 000–000

Energy Procedia

www.elsevier.com/locate/XXX

GHGT-9

Dynamic operation of amine scrubbing in response to electricity demand and pricing

Sepideh Ziaii[a], Stuart Cohen[b], Gary T. Rochelle[a,]*, Thomas F. Edgar[a], Michael E. Webber[b]

[a]*Chemical Engineering Department, University of Texas, Austin, Texas 78712, USA*
[b]*Mechanical Engineering Department, University of Texas, Austin, Texas 78712, USA*

Elsevier use only: Received date here; revised date here; accepted date here

Abstract

This paper examines dynamic operation of CO_2 capture with absorption/stripping using 7 m MEA, where the absorber is operated at full capacity with the stripper at reduced load. Depending on the cost of CO_2 emissions, doing so in response to variations in electricity demand could improve annual profit by $10-$100 million or more at facilities with CO_2 capture. Dynamic scenarios were simulated with a controlled, constant ratio of heat rate and solvent rate. With an 80% load reduction, scenarios that turn off and on affect stripper performance slightly and reach the steady state in about 90 and 18 minutes respectively.

Keywords: CO_2 capture; dynamics; modeling; absorption; stripping

1. Introduction

Most analyses of CO_2 capture systems assume continuous operation at a full-load operating condition where the energy requirement for CO_2 capture and associated electricity production costs remain constant over plant lifetime. For a coal-fired power plant using post-combustion amine absorption/stripping for CO_2 removal, full-load CO_2 capture could reduce net energy output by 11-40% from that of an equivalent gross size plant without CO_2 capture [1, 2]. The bulk of this energy requirement is a consequence of the heat used for solvent regeneration and the work required to compress CO_2 to pipeline pressures for transport to a storage site. In a typical design, about 50% of the steam is extracted between the intermediate and low-pressure turbines, expanded in a let-down turbine that runs the CO_2 compression train, and then sent to the stripper column for solvent regeneration (see Figure 3) [3]. The resulting increase in production costs, coupled with the high capital costs of CO_2 removal equipment, greatly hinder the economic viability of CO_2 capture.

In contrast to static analyses, this paper examines the process feasibility and electric grid implications of flexible CO_2 capture operation. A post-combustion system can be operated flexibly by redirecting some or all of the steam being used for CO_2 capture back to the low-pressure turbine in order to increase power output when desired. Doing so allows stripping and compression systems to operate at reduced load, and while additional CO_2 may be vented during part or zero-load operation, sufficient solvent storage could allow continued CO_2 capture in the absorber [4].

Previous work has shown that by operating CO_2 capture at low or zero-load during annual peak electric grid demand, the need to spend billions of dollars of capital costs to replace the capacity lost to CO_2 capture energy requirements can be avoided. A

* Corresponding author. Tel.: +1-512-471-7230; fax: +1-512-471-7060.
E-mail address: gtr@che.utexas.edu.

study of the Electric Reliability Council of Texas (ERCOT) electric grid finds that the infrequency of annual peak electricity demand allows these capital savings to be achieved with less than 100 hours of zero-load operation throughout an entire year, so that CO_2 reductions are near those achieved with continuous operation even if CO_2 is vented when it is not removed [5]. Flexible CO_2 capture could increase plant output range and improve the ability of a plant to perform profitable grid reliability services [4]. By giving a plant operator the option to choose a desired CO_2 capture operating condition based on current market conditions such as fuel prices, CO_2 prices, and electricity demand, flexible CO_2 capture can be utilized to operate more economically than if capture systems are restricted to continuous, full-load operation.

2. Modeling flexible CO_2 capture in the ERCOT electric grid

A model of the ERCOT electric grid was created using MATLAB software and used to investigate how flexible CO_2 capture in response to hourly variations in electricity demand will affect performance, economics, and CO_2 emissions at power plants running CO_2 capture and in the electric grid as a whole.

Historic load and electric grid conditions were used from 2006 to perform calculations for a one-year period. In 2006, installed capacity in ERCOT included about 20% coal, 72% natural gas, and 6% nuclear-based generation, with additional capacity from wind, hydroelectric, and other sources. Lower electricity production costs allow coal and nuclear-based plants to operate at base load with natural gas-fired plants meeting most of the remainder of electricity demand [6].

For this study, post-combustion CO_2 capture was assumed to be installed on enough of ERCOT's coal plants for the average coal fleet emissions rate to decrease by roughly 50% if CO_2 capture is operated continuously at 100% load. This goal requires CO_2 capture on 8 of the 15 ERCOT coal-fired facilities and would allow the coal fleet emissions rate to approach that of typical natural gas-fired facilities. Plants were chosen based on the lowest sum of electricity production costs with CO_2 capture at 100% load plus the capital charges of any required CO_2 and sulfur dioxide (SO_2) removal equipment. In scenarios that allow flexibility, CO_2 capture may operate at 100% and 20% load, and performance at these operating points is defined using results from the dynamic process model described in Sections 4 and 5 of this paper. CO_2 that is not captured was assumed to be vented to the atmosphere. System response time was not included explicitly, but it was assumed that the results from one hour calculation intervals will approximate those found when considering the system response time calculated using the dynamic process model described later in this report. A more flexible CO_2 capture system may allow several possible operating points, but this study chooses 100% and 20% load to investigate operation between two extremes.

The model used a specified CO_2 price along with fuel costs and other operation and maintenance (O&M) costs to determine electricity production costs for each plant in dollars per Megawatt-hour. These costs were then used to create a dispatch order from which the model chooses to use plants from the least to most expensive until demand in a particular hour is met. To represent ERCOT's competitive market for electricity, the production cost of the final (and most expensive) plant dispatched in a given hour was assumed to set the electricity price in that hour, from which operating profits of all plants can then be calculated. Because capital charges do not factor directly into dispatch decisions, they were not included in electricity production costs. Calculated plant generation is used to determine CO_2 emissions.

Though the model does not consider transmission constraints or any other technical limitations of plant dispatch, the basic representation of dispatch and the electricity market still provides an effective framework to analyze the effects of flexible CO_2 capture on an electric grid.

The following scenarios are considered.

(1) *BAU*: The business as usual scenario considers the actual ERCOT grid in 2006 without any CO_2 capture.
(2) *CCS Base*: For the base case CO_2 capture scenario, CO_2 capture systems are operated at 100% load continuously throughout the year.
(3) *FLEX Op Costs*: In this flexible scenario, plants with CO_2 capture choose the operating condition (20% or 100% load) that has the lowest electricity production costs. When there is no cost of emitting CO_2, it will always be least expensive to operate at 20% load, and increasing the CO_2 price will eventually allow lower production costs at 100% load.
(4) *FLEX Profit*: This flexible scenario operates under the assumption of perfect knowledge of electricity demand and dispatch ordering prior to deciding whether to operate CO_2 capture at 20% or 100% load. In every hour, each plant with CO_2 capture calculates its hourly profits for two scenarios: if all plants with CO_2 capture operate at (A) 100% load or (B) 20% load. If profits are greater for a particular plant for Option A, that plant will operate capture at 100% load; otherwise, it will operate at 20% load. Because the output capacity of plants with CO_2 capture is lower at 100% load, Option A is likely to have a higher electricity price.

3. Results and discussion of the implications of flexible CO_2 capture in ERCOT

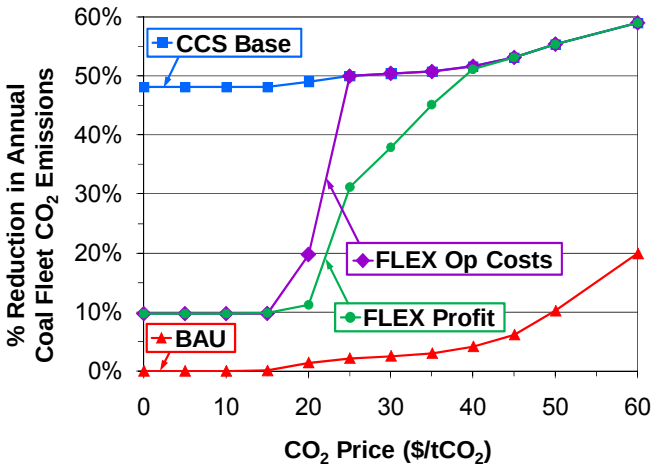

Figure 1: Reductions in annual CO_2 emissions in the ERCOT coal fleet in each scenario vs. CO_2 price

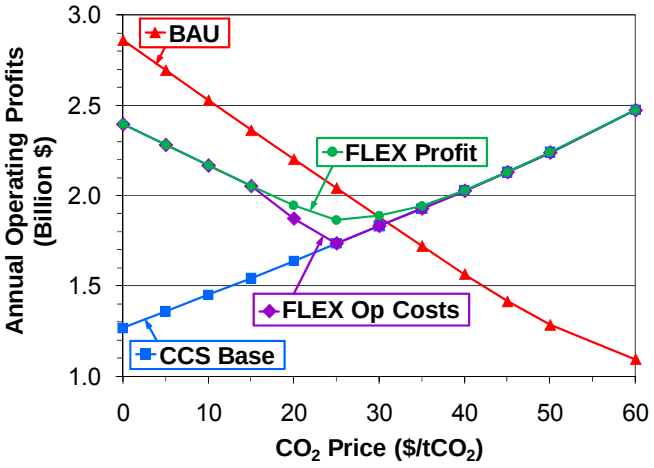

Figure 2: Cumulative annual operating profits in each scenario vs. CO_2 price at the eight coal-fired plants that use CO_2 capture (except in the *BAU* scenario)

Figure 1 displays the reduction in annual coal fleet CO_2 emissions for each scenario with CO_2 prices ranging from \$0-\$60/tCO_2 (2006 US\$ per metric ton of CO_2 emitted), with percent reduction calculated from emissions levels in the *BAU* case with no CO_2 price. Because electricity demand is assumed to be constant across all cases, changes in generation by plant type can be inferred from this figure. Emissions in the *BAU* scenario fall negligibly below \$15/tCO_2, less than 5% below \$40/tCO_2, and begin to decrease significantly at higher CO_2 prices. Coal-fired plants constitute a relatively small proportion of the ERCOT fleet, so CO_2 price must be relatively high before the added emissions costs at coal-based plants move them late enough in the dispatch order to be replaced by natural gas-fired facilities for base load generation. In all scenarios, any reduction in coal-based generation must be met by an equal increase in natural gas-fired generation, partially offsetting coal fleet emissions reductions. However, because natural gas emissions rates are roughly half that of coal without CO_2 capture, net electric grid emissions reductions on a percent basis are at least half of those calculated in the coal fleet.

CCS Base nearly achieves the desired 50% reduction in coal fleet CO_2 emissions at low CO_2 prices, and higher CO_2 prices allow further reductions as fuel switching begins to limit the output of coal-fired plants that do not use CO_2 capture. *FLEX Op Costs* begins with emissions reductions of about 10% at low CO_2 prices (when all CO_2 capture systems operate at 20% load), jumps to 20% when the two most efficient plants with CO_2 capture are less expensive to operate at 100% load, and then follows the *CCS Base* curve (when all CO_2 capture is at 100% load) above \$25/tCO_2. In contrast to plant economic studies that find the CO_2 price for economic viability of CO_2 capture to be around \$40/tCO_2, these data indicate that once a CO_2 capture system is built, the CO_2 price to justify 100% load operation may be closer to \$20-\$25/tCO_2 [7]. *FLEX Profit* requires CO_2 prices of about \$40/tCO_2 before CO_2 systems remain at 100% load throughout the year, indicating that flexible operation could improve operating profits in the \$20-\$35/tCO_2 price range. If CO_2 is vented when CO_2 capture is at part-load, flexibility may prevent the emissions reductions that could be achieved with continuous full-load operation, but reductions are still significant as long as the CO_2 price is high enough for production costs to be lower at 100% load.

Figure 2 displays cumulative annual operating profits at the eight coal-fired facilities using CO_2 capture. When no CO_2 capture is available (*BAU*), operating profits fall dramatically as CO_2 price increases, though it takes a CO_2 price of about \$30/tCO_2 before it is more profitable to operate with CO_2 capture installed. Because lower emitting natural gas-fired plants continue to set electricity prices, electricity production costs at coal-fired plants without CO_2 capture increase faster than electricity prices for a given CO_2 price increase, resulting in rapid profit decline. Though *CCS Base* has lower profits than *BAU* below \$30/tCO_2, it exhibits the opposite trend because emissions rates at coal-based plants with CO_2 capture are less than those of natural gas-fired facilities. *FLEX Op Costs* demonstrates that choosing between 100% and 20% CO_2 capture load allows much greater operating profitability than continuous 100% operation when CO_2 prices are too low to justify the operating expense. In the \$20-\$35/tCO_2 range, *FLEX Profit* improves profitability over *FLEX Op Costs* by allowing generators to consider the balance between production costs, power output, and electricity price at a given electricity demand and choose to operate in the most profitable manner. At \$25/tCO_2, such behavior improves annual operating profits by \$130 million over those earned with continuous 100% load operation. Flexibility has no impact on operating profits above \$35/tCO_2 in this static CO_2 price analysis; however, the value of flexibility is expected to be greater in a cap and trade regime where CO_2 prices could fluctuate between values that justify CO_2 capture operation and those that do not.

4. Dynamic modeling of CO_2 capture

The absorption/stripping system typically consists of two columns. In the absorber, which is operated at atmospheric pressure and 40-60°C, the flue gas from a coal-fired plant containing 10-12% CO_2 contacts with MEA, and CO_2 is absorbed into the solution by physical and chemical mechanisms. The rich solution coming out of the absorber, which typically has a loading of 0.4-0.5 moles of CO_2/mole MEA, is directed to the stripper, operating at 1.5-2 atm and 100-120°C. Water vapor accompanying CO_2 from the top of the stripper is then condensed and returned to the water wash section of the absorber. The hot lean solution exiting the stripper is cooled by the cold rich solution in a cross heat exchanger (5-10°C temperature approach) and is furthered cooled to 40°C before entering the absorber (see Figure 3).

Several existing steady state models for absorption/stripping process with alkanolamines aim to minimize the energy use for CO_2 capture. However, these models do not have the capability of predicting the effects of dynamic operation on the system. No previous work was found on dynamic modeling of the entire absorption/stripping system or the stripper alone. Kvamsdal *et al.* [8] have prepared a dynamic model of CO_2 absorption by MEA using gPROMS® and studied the dynamics of the absorber in response to the start-up and power plant load change scenarios. In order to predict the dynamic behavior of CO_2 capture in response to variations in electricity demand, an accurate dynamic model is required. For this study, a rigorous rate-based dynamic model of the stripper, using 30 wt % MEA, was created in Aspen Custom Modeler®.

4.1 Model Development

In the stripper, mass transfer and chemical reactions occurring in the liquid phase result in desorption of CO_2 from the rich solution. In the present study, the stripper is modeled by the rate-based approach based on film theory, and kinetics is simplified by considering two dominant equilibrium reactions.

$$MEACOO^{--} + MEA^{+} \leftrightarrow 2MEA + CO_2 \quad (1)$$

$$MEA^{+} + HCO_3^{-} \leftrightarrow H_2O + MEA + CO_2 \quad (2)$$

Table 1 provides an overview of the important parameters in the model, along with their sources and literature.

Table 1: important parameters used in the stripper model

Property	Source	Comments
Partial pressure of CO_2 Equilibrium constants Heat of desorption	electrolyte-NRTL model developed by Hilliard	Regressed the points from flash calculation in the Aspen Plus® model by Hilliard
Density and viscosity of loaded MEA	Weiland *et al.* [9]	
Heat capacity of loaded MEA	Hilliard [10]	
Diffusivity of CO_2 in loaded MEA	Versteeg *et al.* [11]	Based on the N_2O analogy and a Stoke-Einstein relation
Liquid hold up	Suess and Spiegel [12]	
Pressure drop across the packing	generalized pressure drop correlation of Kister *et al.* [13]	
Liquid and vapor mass transfer coefficients	Onda *et al.* [14]	

4.2 Ratio-Control Dynamic Strategy

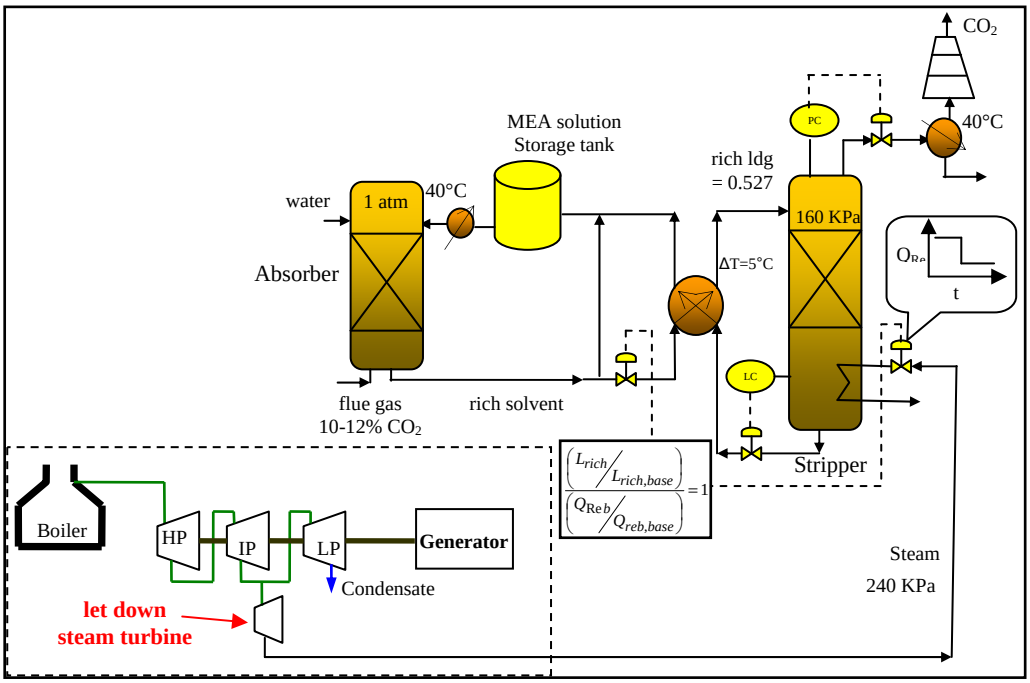

Figure 3: Steam turbines and CO_2 capture with ratio-control strategy

In this dynamic strategy, the absorber operates continuously, but the reboiler steam rate is reduced at the start of the peak period. Consequently, the absorber provides variable CO_2 removal. The non-regenerated rich solvent stream is mixed with the lean solution coming from the stripper and then returned to the absorber. In this option, no additional inventory is needed for rich and lean solvents, and the only input variable that significantly changes in the absorber is the lean loading. (Figure 3)

The following conditions are carried out for steady state design and dynamic simulation:

- CO_2 removal at 100% load: 90%
- Packing height: 2 m; column diameter: 4.6 m
- Overhead pressure is controlled at constant value (160 KPa).
- Liquid level in the reboiler is controlled at a constant level.
- The absorber is controlled such that it gives a constant rich loading in the presence of variable lean loading.

5. Dynamic simulation results and discussion

In order to demonstrate how the stripper responds to the flexible operation, two ratio-control scenarios are simulated:

1. Turn-off scenario: ramp the reboiler heat duty and rich solvent from 100% to 20% load in 15 minutes
2. Turn-on scenario: ramp the reboiler heat duty and rich solvent from 20% to 100% load in 15 minutes

In both cases, the simulation starts with 12 min at the initial load, and then the reboiler heat duty and rich solvent flow rate are ramped linearly to the desired final operating condition in 15 minutes. Figures 4 and 5 show the time response of reboiler temperature and lean loading in both dynamic scenarios. 100% load operation gives a larger pressure drop due to greater liquid and vapor rate and liquid hold up in the packing; consequently, with fixed pressure at top of the column, the reboiler would operate at higher pressure and temperature (see Figure 4).

The time response of the hydraulics of the column is related to the small liquid and vapor hold-up time in the packing. As can be seen in Figure 4, in the turn-off scenario, the liquid is initially cooled beyond the equilibrium point for 20% load because of the instantaneous flash in the simply modeled reboiler, and then the liquid temperature in the reboiler is further heated toward the steady state at the 20% load. This heating process is slow and most likely determined by the liquid hold-up in the reboiler. In the turn-on scenario, similar behavior is seen in the opposite direction.

Figure 5 reflects a very small change in the lean loading due to a change in load. The higher performance at 20% operation can be primarily attributed to the larger mass transfer unit, which is a factor of 1.7 greater than 100% load.

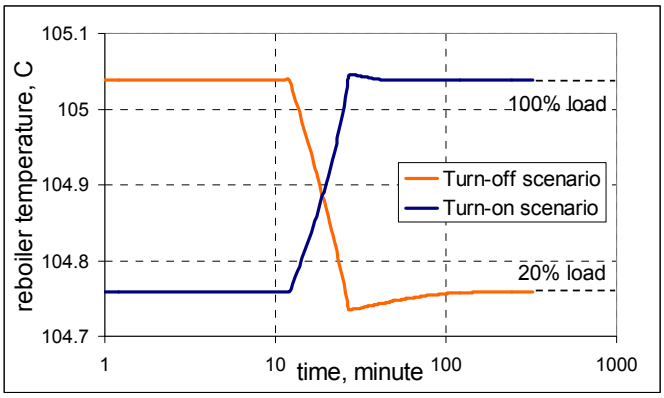

Figure 4: Dynamic responses of reboiler temperature to turn-on and turn-off operations

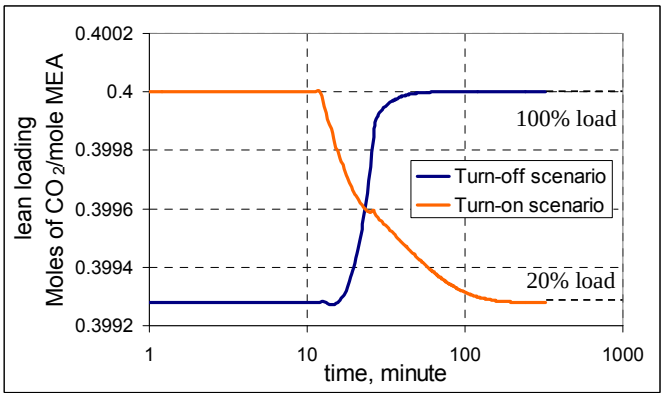

Figure 5: Dynamic responses of the lean loading to turn-on and turn-off operations

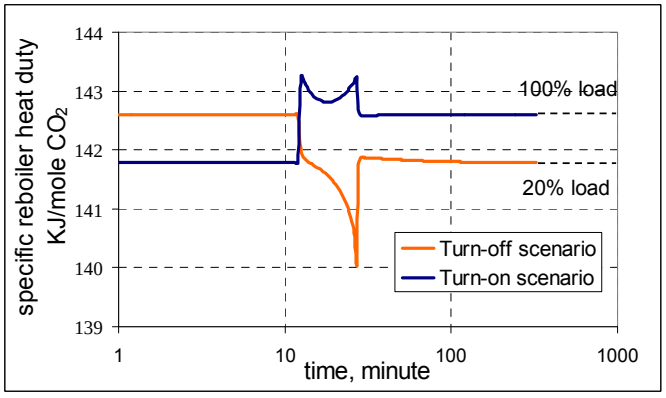

Figure 6: Specific reboiler heat duty calculated for the system operated in turn on and turn off operations

Figure 6 demonstrates how the calculated specific heat duty (KJ/mole CO_2) changes between 20% and 100% load operation. The specific heat duty, representing the performance of the stripper, does not vary significantly with the load. Although the transition curves show some discontinuities and irregular behavior, the temperature and lean loading response reflects smooth stripper behavior in response to the on/off operation. The initial and final step changes in the specific reboiler heat duty might be associated with the delay time in sensing change in the liquid rate in the reboiler. This kind of behavior might not be very realistic and could be eliminated or changed if the dynamics of the regulators of rich solvent and reboiler steam are coupled with the system.

The residence time of the liquid in the reboiler is the predominant factor influencing the response time of the stripper. The simulation shows that the liquid hold up in the reboiler achieves its final steady state value in just a few seconds after the final change is made to the solvent rate. Consequently, the average liquid residence time is very close to that of the final steady state. For this system, the liquid hold up time in the reboiler for 100% and 20% load operation is 5 and 25 minutes respectively. This effect is why turn-on operation reaches steady state approximately 5 times faster than turn-off operation.

In the current study, the overhead pressure is kept constant and simplifying assumptions are made to the rich solvent. In the future, the stripper model will be combined with an absorber model to evaluate the operational challenges in an integrated absorption/stripping system, and the current stripper model will be coupled with a CO_2 compressor model to study and compare the variable-pressure stripper in dynamic operation of CO_2 capture.

6. Conclusions

A basic model of the ERCOT electric grid is used to investigate the implications of flexible CO_2 capture in response to hourly electricity demand variations for a range of CO_2 prices. If CO_2 price is below that justified to operate CO_2 capture, flexibility may improve annual operating profits by hundreds of millions of dollars over those earned with continuous full-load operation, though CO_2 emissions will be greater if additional CO_2 is vented at part-load operation. Significant emissions reductions can be achieved with flexible operation when the CO_2 price is high enough for electricity production costs to be lower with full-load CO_2 capture. Above this CO_2 price, there is an additional range of CO_2 prices where flexibility can improve operating profits by tens or hundreds of millions of dollars above those received with constant 100% load operation by allowing plant operators to examine the balance among production costs, power output, and expected electricity price at different electricity market conditions and choose to operate CO_2 at the load that generates greatest operating profits in a particular hour.

Given these electric grid implications, the process feasibility of flexible CO_2 capture is examined using a rate-based dynamic model that is created in ACM® for the stripper using 30 wt % MEA. The model is capable of representing the dynamic behavior of the stripper column during the flexible operations. When ramping between 20% and 100% load over 15 minutes, the energy in KJ/mole CO_2 removed does not vary more than 2% during the transition. The 18-90 minutes response of flexible operations is determined by the solvent residence time in the reboiler at the end of the ramp.

7. Acknowledgments

This paper was prepared with the support of the Luminant Carbon Management Program, along with the Departments of Chemical and Mechanical Engineering at the University of Texas at Austin.

8. References

1. R.M. Davidson, Post-combustion carbon capture from coal fired plants – solvent scrubbing. IEA Clean Coal Centre. 2007.
2. J.A. Bergerson and L.B. Lave, Baseload Coal Investment Decisions under Uncertain Carbon Legislation. *Environ. Sci. Technol*., 41 10 (2007) 3431-3436.
3. J.R. Gibbins, and R.I. Crane, Scope for reductions in the cost of CO_2 capture using flue gas scrubbing with amine solvents. *Proceedings of the Institution of Mechanical Engineers -- Part A -- Power & Energy* 218 4 (2004) 231-239.
4. H. Chalmers, J. Gibbins, and M. Leach, Initial Assessment of Flexibility of Pulverized Coal-Fired Power Plants with CO_2 Capture, in 3rd International Conference on Clean Coal Technologies for our Future, Sardinia, Italy, 2007.
5. S.M. Cohen, G.T. Rochelle, and M.E. Webber, Turning CO_2 Capture On & Off in Response to Electric Grid Demand: A Baseline Analysis of Emissions and Economics, in ASME 2nd International Conference on Energy Sustainability, Jacksonville, 2008.
6. ERCOT, 2006 Annual Report. 2006.
7. E.S. Rubin, C. Chen, and A.B. Rao, Cost and performance of fossil fuel power plants with CO_2 capture and storage. *Energy Policy*, 35 (2007) 4444-4454.
8. H.M. Kvamsdal, J.P. Jakobsen, K.A. Hoff, Dynamic Modeling and Simulation of a CO_2 Absorber Column for Post-Combustion CO_2 Capture, *Chem. Eng. Process*. (2008) doi:10.1016/j.cep.2008.03.002.
9. R.H. Weiland, J.C. Dingman, D.B. Cronin, G.J. Browning, Density and Viscosity of Some Partially Carbonated Aqueous Alkanolamine Solutions and Their Blends. *J. Chem. Eng. Data*, 43 (1998) 378-382.
10. M.D. Hilliard, Predictive Thermodynamic Model for an Aqueous Blend of Potassium Carbonate, Piperazine, and Monoethanolamine for carbon dioxide capture from flue gas. Ph.D. Dissertation, The University of Texas at Austin, Austin, TX., 1996.
11. G.F. Versteeg, L.A.J. van Dijck, W.P.M. van Swaaij, On the Kinetics Between CO_2 and Alkanolamines both in Aqueous and Non-aqueous Solutions. An Overview, *Chem. Eng. Commun*. 144 (1996) 113.
12. P. Suess and L. Spiegel, Hold-up of Mellapak Structured Packings. *Chem. Eng. Process.* 31 (1992) 119-124.
13. H.Z. Kister, J. Scherffius, K. Afshar, E. Abkar, Realistically Predict Capacity and Pressure Drop for Packed Column. AIChE meeting. Houston, TX, Spring, 2007.
14. K. Onda, H. Takeuchi, Y. Okumoto, Mass Transfer Coefficients between Gas and Liquid Phases in Packed Columns. *J. Chem. Eng. Jpn.* 1 (1968) 56-62.

Available online at www.sciencedirect.com

ScienceDirect

Energy Procedia 00 (2008) 000–000

Energy Procedia

www.elsevier.com/locate/XXX

GHGT-9

MDEA/Piperazine as a solvent for CO_2 capture

Fred Closmann, Thu Nguyen, Gary T. Rochelle*

Dept. of Chemical Engineering, University of Texas at Austin, Austin, TX 78712, USA

Elsevier use only: Received date here; revised date here; accepted date here

Abstract

The solvent blend methyldiethanolamine/piperazine (MDEA/PZ) has been investigated as an alternative for CO_2 capture from coal-fired power plants. MDEA/PZ offers advantages over monoethanolamine (MEA) and MDEA alone because of its resistance to thermal and oxidative degradation at typical absorption/stripping conditions. We measured thermal degradation rates of MDEA and PZ of -7 ± 20 mmolal/day and -9 ± 5 mmolal/day, respectively, in a loaded 7 m MDEA/2 m PZ solvent blend at 120°C. At 135°C, the PZ degradation rate in the loaded solvent blend is -39 ± 11 mmolal/day, which closely matches the appearance of unidentified diamine compounds. When sparged with 98% O_2 at 55°C, 7 m MDEA/2 m PZ with 1 mM Fe^{2+} produced 0.011 ± 0.001 mmoles formate/L-hr. At the same conditions, 7 m MDEA produced 0.024 ± 0.007 mmoles formate/L-hr. We determined that the resistance to oxidative degradation follows the order: MDEA/PZ>MDEA>PZ. The formation of amides in oxidatively degraded samples can be as much as twice the amount of formate produced. In the absence of PZ, MDEA forms amides at an order of magnitude greater rate. The volatility of MDEA in 7 m MDEA/2 m PZ at 40 and 60°C with low CO_2 loading is 6 to 11 ppm and 19 to 30 ppm, respectively. PZ activity decreases by nearly an order of magnitude in the solvent blend as loading of CO_2 is increased to a one-to-one ratio with PZ, giving a PZ volatility at 40°C of 2 to 16 ppm. We calculated a CO_2 capacity of approximately 0.75 moles CO_2/kg amine+water, as compared to a capacity of 0.5 moles CO_2/kg amine+water for MEA under comparable conditions in an absorber/stripper configuration.

Keywords: methyldiethanolamine; piperazine; formate; CO_2 capacity.

1. Introduction

The aqueous solvent methyldiethanolamine (MDEA)/piperazine(PZ) has been investigate as an alternative to aqueous monoethanolamine (MEA) and aqueous K^+/PZ for CO_2 capture from coal-fired flue gases. This is an attractive solvent because it has greater capacity and lower equivalent work for CO_2 removal than MEA. MDEA/PZ has been successfully used for years in the natural gas industry for removal of CO_2 and hydrogen sulfide (H_2S). A full understanding of its resistance to degradation and vapor-liquid equilibrium (VLE) behavior is needed to design effective CO_2 capture systems. As a tertiary amine, MDEA does not form a carbamate and is not susceptible to carbamate polymerization processes that the primary and secondary amines undergo.

We have investigated the thermal and oxidative degradation of the MDEA/PZ solvent blend and compared our results to those for MEA and PZ under similar experimental conditions. We have also investigated the solubility of CO_2 in the MDEA/PZ solvent, and measured the equilibrium partial pressure of MDEA, PZ, and CO_2 in the solvent in a reactor configured with a closed loop measuring system. These measurements allowed us to determine volatility and activity of the amines, and the capacity of this solvent blend for CO_2 capture in flue gas.

2. Degradation Studies

2.1 Thermal Degradation Background

Degradation studies were performed to determine the resistance of the MDEA/PZ blend to thermal and oxidative degradation. Thermal degradation of monoethanolamine (MEA) has been studied at length. It probably degrades through the formation of an oxazolidone from MEA-carbamate. Less is known about the thermal degradation mechanisms which occur with MDEA.

Dawodu and Meisen [1] studied the thermal degradation of CO_2 loaded aqueous blends including MDEA, MDEA + diethanolamine (DEA), and MDEA + MEA using GC and GC/MS techniques. They identified up to fifteen degradation products, and the rate of amine degradation followed the order MDEA<MEA<DEA. Reza and Trejo [2] conducted short-term (90 hours), high temperature (200°C) thermal degradation studies of blended solutions of MDEA, DEA and 2-amino-2-methyl-1-propanol (AMP) loaded with CO_2 and, in some cases, H_2S. In summary, the authors found that MDEA is more resistant to degradation than DEA and AMP in the presence of acid gases. Using similar equipment and methods described for our studies, Freeman [3] found that PZ does not thermally degrade up to 150°C.

2.2 Thermal Degradation Data

In our studies, the thermal degradation of the MDEA/PZ solvent blend was investigated at 100°C to 135°C, which spans the range of practical stripper temperature for CO_2 capture using aqueous alkanolamines. Experiments were performed with the blended system (7 m MDEA/2 m PZ) and with 7 m MDEA at a CO_2 loading of 0.1 to 0.2 moles CO_2/mole alkalinity. Solvents were prepared using gravimetric loading to achieve 0.1 to 0.3 moles CO_2/mole alkalinity in each tested solvent. A single experiment was conducted on the 7 m MDEA/2 m PZ system with the addition of 1 mM Fe^{2+} to investigate catalytic effects of this metal on the thermal degradation process.

The thermal degradation studies were performed using reuseable 10 cm^3 (nominal size) bombs constructed with stainless steel Swagelok® materials. The basic setup for each experiment entailed placing approximately 10 grams of CO_2-loaded solvent in a bomb, placing the bomb in a temperature-controlled oven for periods of up to nine weeks, and removing the bombs from the oven(s) over time, recovering the degraded amine solutions for analysis. Solution was loaded using a gravimetric method with ≥ 99.99% CO_2, and confirmed using a total inorganic carbon (TIC) analyzer (Horiba Model PIR-2000 infrared analyzer) with nitrogen purge. CO_2 concentrations were confirmed in a subset of degraded samples and generally did not vary more than five percent after eight weeks of degradation. The MDEA used in these studies was supplied by Huntsman Chemical (95 to 99.99%) and the PZ supplied by Acros Organics (anhydrous at 99%).

Cation analyses were performed to determine the amount of MDEA and PZ remaining in each solvent sample using a Dionex Ion Chromatograph with a polystyrene-based cation exchange resin column (Dionex IonPac CS17, 4 mm X 250 mm), a Dionex CD25 conductivity detector, CRSR 300 anion suppressor, and ultrapure deinoized water with 55 mM methanesulfonic acid (MSA) as the liquid eluent. The separation method developed for cation analysis utilized a linear gradient of MSA eluent and ultrapure water.

Table 1 summarizes the key conditions for the thermal degradation experiments reported in this paper, and the degradation rates and uncertainties of MDEA and PZ (mmolal/day) based on linear regressions of the data for each compound (MDEA and PZ) using peak areas from the cation chromatograph. The chromatograms for each analysis exhibited unknown compound peaks eluting immediately after PZ, indicating the probable appearance of diamine compounds resulting from PZ degradation.

Estimates of the total concentration (based on the calibration curve for PZ) and rate of appearance of those diamine unknowns were made and presented in Table 1. Figure 1 presents the results of the thermal studies for 7 m MDEA/2 m PZ with 1 mM Fe^{2+} conducted at 100°C, 120°C, and 135°C.

Table 1 – Thermal Degradation Rates – Average MDEA/PZ Loss and Diamine Appearance Rates

Solvent	Temp (°C)	Duration (Days)	MDEA Deg Rate (mmolal/day)		PZ Deg Rate (mmolal/day)		Diamine Appearance Rate (mmolal/day)	
CO_2 Loading (mol/mol alk)			**α = 0.1**	**α = 0.2**	**α = 0.1**	**α = 0.2**	**α = 0.1**	**α = 0.2**
7m MDEA	100	63	-6 ± 6	-18 ± 52	NA	NA	NA	NA
	120	63	-0.3 ± 11	-31 ± 16	NA	NA	NA	NA
7m MDEA/2m PZ	100	54	-3 ± 13	-19 ± 4	-2 ± 4	-6 ± 1	1 ± 2	2 ± 2
	120	54	-11 ± 11	-7 ± 20	-7 ± 3	-9 ± 5	2 ± 2	5 ± 2
7m MDEA/2m PZ 1mM Fe^{2+}	100	42	NA	3 ± 13	NA	-2 ± 5	NA	2 ± 3
	120	49	NA	-18 ± 20	NA	-11 ± 10	NA	12 ± 3
7m MDEA/2m PZ	135	28	-8 ± 37	0 ± 20	-30 ± 15	-39 ± 11	44 ± 12	51 ± 8

In the 7 m MDEA/2 m PZ solvent, MDEA degradation rates generally ranged from immeasurable to -19 ± 4 mmolal/day, while PZ degradation rates ranged from -2 ± 4 mmolal/day to -39 ± 11 mmolal/day. The magnitude of the errors in comparison to the absolute values of the degradation rates suggest that the degradation rates of MDEA and PZ are nearly zero or immeasurable within the time periods studied using cation chromatography. In general, amine degradation rates were greater at higher temperatures (120°C than 135°C) and higher loadings. The greatest extent of MDEA and PZ thermal degradation in the blended solvent experiments occurred at a temperature of 120°C and a loading of 0.2 moles CO_2/mole alkalinity. However, given the error in the regressed degradation rates, we conclude that the catalytic effect of Fe^{2+} on MDEA degradation is undetectable over the time frames studied (63 days maximum). When 7 m MDEA was studied alone, its degradation rates were comparable to the rates of MDEA loss in the blended system at 120°C, but lower when compared to the rates at 100°C. The unknown diamine appearance rates were generally of the same magnitude as the PZ degradation rates for all three temperatures. Diamine appearance rates measured at 135°C were approximately four times as great as the rates measured at 120°C, and twenty-five to fifty times as great as the rates measured at 100°C. The energy of activation of the appearance of unknown diamine compounds is approximately 114 kJ/mol for all loading conditions. We conclude that there is a one-to-one relationship between moles of PZ degraded and moles diamine unknowns appearing with time in the blended solvent system.

3. Oxidative Degradation

3.1 Oxidative Degradation Background

Typical temperatures in an absorber configuration will be in the range of 45°C to 55°C, and it is of interest to understand how much oxidative degradation of alkanolamine solvents occurs at these conditions. Some of the first oxidative degradation studies on alkanolamines were performed by the Girdler Corporation (Kindrick *et al.*) [4] in 1950. The authors screened several alkanolamines for use in CO_2 scrubbing and reported that 50 wt % MDEA exhibited higher resistance to oxidation than other amines screened in the study. Blends of 50 wt % MDEA and MEA and DGA lost less than 4% by weight of free amine. Rooney [5] performed oxidative degradation screening studies on loaded and unloaded alkanolamines. In particular, Rooney looked at the formation of heat stable salts including acetate, formate, glycolate, and oxalate, and concluded that measuring the formation of heat stable salts would be a helpful predictive factor in determining the role of oxygen in the formation of these compounds in an amine plant. Experiments were conducted at 180°F (82°C) for a period of 28 days in stirred reactors, and samples withdrawn weekly for ion chromatography analysis. In these studies, acetate, formate, and glycolate were detected in 30 wt % and 50 wt % solvents after seven days. Greater than 100 ppm of formate was formed in the 30 wt % amine solution at 82°C after only seven days.

3.2 Oxidative Degradation Data

We conducted oxidative degradation studies using an enclosed jacketed glass reactor. Approximately 375 ml of solvent was placed in the reactor and degraded for ten to fourteen days. The jacket-side of the reactor was filled and circulated with a Lauda E100 water bath maintained at 55°C. Solvent samples were retrieved from the reactor at two-day intervals and analyzed using a Dionex Ion Chromatograph for cations (same as above), and a separate Dionex ICS 3000 Ion Chromatograph and conductivity detector with KOH eluent for anions. We used a polystyrene-based anion exchange resin column for separations (Dionex IonPac AS15) to measure the formation of heat stable salts including formate and glycolate. We also performed NaOH treatment of an aliquot of each sample for a period of 24 hours to reverse the formation of amides through hydrolysis back to the heat stable salt and amine.

Table 2 presents formate production rates measured in four experiments conducted in 7 m MDEA and the 7 m MDEA/2 m PZ. Loading was in the range of 0.10 to 0.30 moles CO_2/moles alkalinity. Figure 2 is a plot of formate concentration with time for the four experiments listed in Table 2. Linear regressions of the formate concentrations were performed to generate formate production rates in each experiment. The rate of production of formate in 7 m MDEA (0.024 ± 0.007 mmole/L-hr) was approximately twice the rate observed in three experiments conducted with 7 m MDEA/2 m PZ and various metals, suggesting that PZ inhibits the oxidation of MDEA in the solvent blend. The presence of the corrosion inhibitor, 5 mM Cu^{2+}, did not appreciably increase the production of formate in 7 m MDEA/2 m PZ with other metals. We also observed that the addition of chromium and nickel did not appreciably increase the production of formate. Glycolate eluted from the anion column at approximately 19 minutes with 7 m MDEA/2 m PZ. We estimate the glycolate concentration to be less than 1 ppm in the 7 m MDEA/2 m PZ solvent blend after 14 days, resulting in a formation rate of less than 0.0001 mmol/L-hr. In contrast to these results, Sexton [6] reported formate production rates of 0.39 mmole/L-hr in 7 m MEA, which is approximately twenty-five times the rate of formate production in the 7 m MDEA/2 m PZ solvent blends.

Table 2 - Oxidative Degradation Studies - Formate Production, 55°C, 98% CO_2/2% O_2
375 ml Solvent, Agitated 1400 rpm

Expt No.	Solvent	CO_2 Loading (mol/mol alk)	Duration (Days)	Production Rate (mmol/L-hr)	
				Formate	**Amide
1	7 m MDEA, 1 mM Fe^{2+}	0.10	14	0.024 ± 0.007	0.165 ± 0.095
2	7 m MDEA/2 m PZ, 1 mM Fe^{2+}	0.30	14	0.011 ± 0.001	0.010 ± 0.001
3	7 m MDEA/2 m PZ 0.1 mM Fe^{2+}, 0.6 mM Cr^{3+}, 0.1 mM Ni^{2+}	0.24	10	0.012 ± 0.003	0.027 ± 0.009
4	*7 m MDEA/2 m PZ 0.1 mM Fe^{2+}, 5 mM Cu^{2+}	0.23	10	0.0159 ± 0.006	0.018 ± 0.004

* Glycolate production rate is <0.0001 mmol/L-hr.
** Calculated as difference between formate production with and without hydrolysis of amide by NaOH.

When we reversed the formation of amide in the degraded solvent through treatment of samples with NaOH, we found that the amount of measurable formate (Table 2) increased by a factor of 2 to 3 with 7 m MDEA/2 m PZ , and by an order of magnitude with 7 m MDEA. Sexton [6] reported that in MEA studies, degradation products other than formate can be present in greater quantities than the formate, but are undetectable through standard anion chromatography methods.

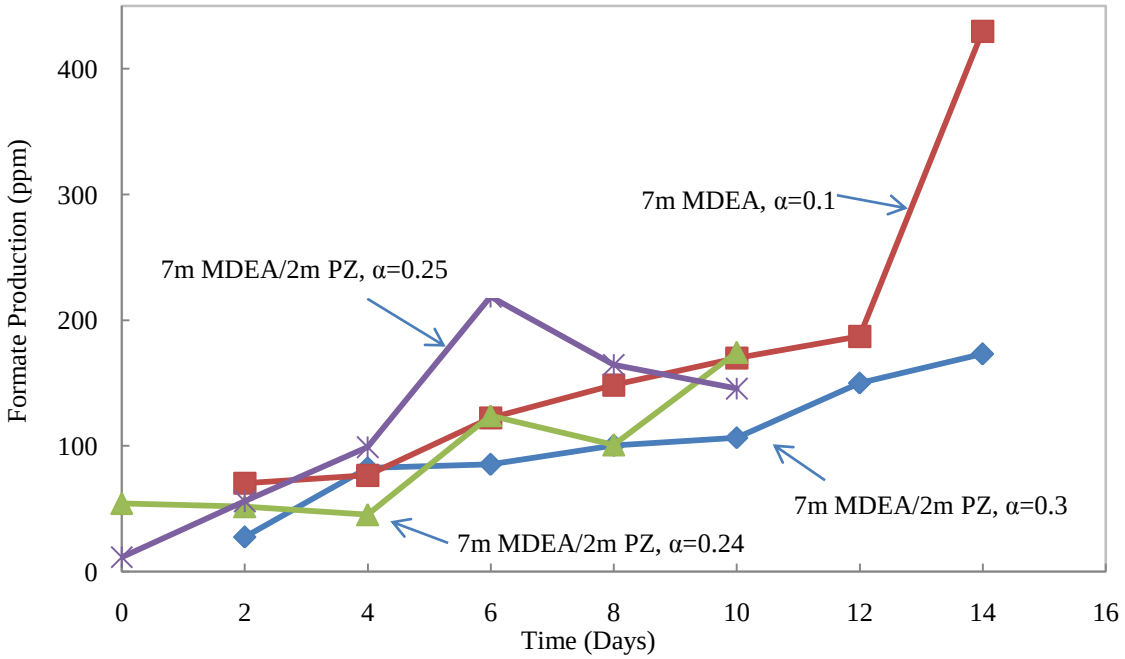

Figure 2: Formate Production, 55°C, 350 mL reactor, 100 mL/min

This work confirms the work of previous groups investigating the oxidative degradation of alternatives to MEA. We conclude that the resistance to oxidative degradation follows the order: MDEA/PZ>MDEA>MEA. In an oxidative degradation study with 50 wt % MDEA and no metals, Rooney reported a formate production rate of 0.008 ± 0.001 mmole/L-hr, which is within our reported range for the 7 m MDEA/2 m PZ blend, but an order of magnitude below the range we are reporting for the 7 m MDEA system with 1 mM Fe^{2+}; the presence of 1 mM Fe^{2+} in the solvent in our experiment may have catalyzed the oxidative degradation of MDEA. We also conclude that the greater formation of amides in the 7 m MDEA solvent experiment when compared to all experiments conducted with MDEA/PZ is indicative of greater formation of amides through the carboxylic acid pathway in the oxidative degradation of MDEA when PZ is not present. Rooney [5] reported the formation of other carboxylic acids including acetate and glycolate at concentrations comparable to those for formate. We did not see appreciable amounts of glycolate in our studies.

4. Volatility

Amine losses in CO_2 scrubbing systems occur through volatilization in the stripper and absorber units. The degree to which these losses occur directly affects amine management system requirements. Using a semi-batch reactor apparatus and Fourier Transform Infrared (FTIR) maintained at 180°C, we performed volatility measurements on loaded MDEA/PZ in an agitated environment by the method of Hilliard [7]. The reactor was sparged with a pre-saturated gas consisting of 98% O_2 and 2% CO_2. Measurements of gas-phase amine concentrations were made with the FTIR at temperatures of 40°C and 60°C with 0.0, 0.5, and 1 moles CO_2/mole PZ. From the amine concentrations and the assumption that solution behavior adheres to a modified Raoult's Law, we also calculated amine activities.

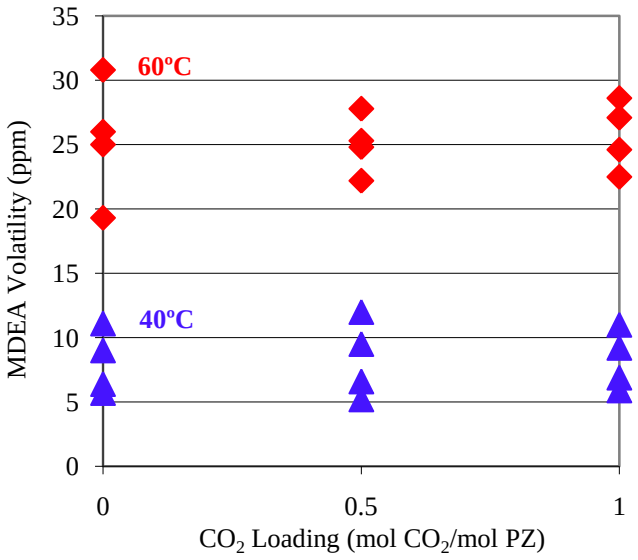

Figure 3: MDEA Volatility for MDEA-PZ Blends (2.7m-8.7mMDEA / 0.4m-2.6m PZ)

Figure 3 presents the volatility (ppm at 1 atm) for MDEA in various MDEA/PZ solvent blends at 40°C and 60°C over the range of tested loading. At 40°C, the gas-phase MDEA was 6 to 11 ppm, with little or no increase when the loading was increased from 0.0 to 1.0 moles CO_2/mole PZ. The gas-phase MDEA concentration increased to 19 to 30 ppm for all the MDEA/PZ blends at 60°C, but was generally unchanged over the range of loading. The MDEA volatility results follow an anticipated relationship with loading and PZ concentration. The formation of the PZ-carbamate (Reaction 1) is more favorable than the formation of bicarbonate from MDEA (Reaction 2). Thus, only after the amount of CO_2 in the solvent exceeds the amount of PZ, will the MDEA actively react with CO_2, resulting in a reduction in the amount of free MDEA in solution and a lower partial pressure of MDEA in the gas phase. Given the maximum loading conducted in our experiments (1 mole CO_2/mole PZ), we did not anticipate a significant decrease in MDEA volatility.

Reaction 1 $H_2O + PZ + CO_2 \leftrightarrow PZCOO^- + PZH^+$

Reaction 2 $MDEA + CO_2 + H_2O \leftrightarrow MDEAH^+ + HCO_3^-$

At 1 atm and 60°C, the PZ volatility was 8 to 66 ppm in the gas phase at 0 to 1 mole CO_2/mole PZ. At the low end of the loading range, the volatility PZ was greater than MDEA, but slightly lower at the high end of the loading. Figure 4 presents the activity of PZ as measured from solubility data generated in the experiments described above. The activity of PZ decreases linearly with loading at both 40°C and 60°C in each of the solvent blends. We attribute this behavior to the reduction in free PZ in the solvent blend as loading increased. In most cases, the activity of the PZ is greater at 60°C for the corresponding MDEA/PZ blend and loading condition. With 8 m MDEA/1.2 m PZ at a loading of 0.5 moles CO_2/ mole PZ, the estimated PZ volatility is 6 ppm at 1 atm.

5. CO_2 Solubility and Capacity

Figure 5 presents measurements of CO_2 solubility in MDEA/PZ solvents. Bishnoi [8] used our wetted wall to generate data for 4 M MDEA/0.6 M PZ (7.7 m/1.1 m) at 40 and 70°C. Recently we have measured CO_2 solubility with the hot gas FTIR at the same time as amine volatility. We have also collected CO_2 equilibrium partial pressure data at 40°C and 60°C over a 7 m MDEA/2 m PZ solvent blend with the wetted wall column (Figure 5). The equilibrium partial pressure of CO_2 increases two orders of magnitude over a low loading range (0.01 to 0.07 moles CO_2/mole alkalinity) at 70°C. Over a higher loading range

(0.025 to 0.25 moles CO_2/mole alkalinity), the partial pressure of CO_2 increases by two and one-half orders of magnitude to approximately 9 kPa at 40°C. Using 7.7 m MDEA/1.2 m PZ in an absorption/stripping system, a lean loading of 0.1 moles CO_2/mole alkalinity would give a CO_2 partial pressure of 0.7 kPa at 40°C, which is well below anticipated conditions at the lean end of an absorber (~1.2 kPa for 90% CO_2 removal). With a rich loading of 0.25 moles CO_2/mole alkalinity at 40°C, the corresponding equilibrium CO_2 partial pressure is 7 kPa, which provides a sufficient driving force for CO_2 absorption (CO_2 @ 12 kPa). At these conditions, the working capacity is 0.75 moles CO_2/(kg amine + water) compared to 0.5 moles CO_2/(kg amine + water) for 7 m MEA (rich and lean loading of 0.55 and 0.45 moles CO_2/mole alkalinity) the heat of CO_2 absorption of the blended solvent is about 75 kJ/mol, compared to about 84 kJ/mol for 7 m MEA. The closeness in values is a result of the fact that the PZ and MEA form carbamates in the primary reaction with CO_2.

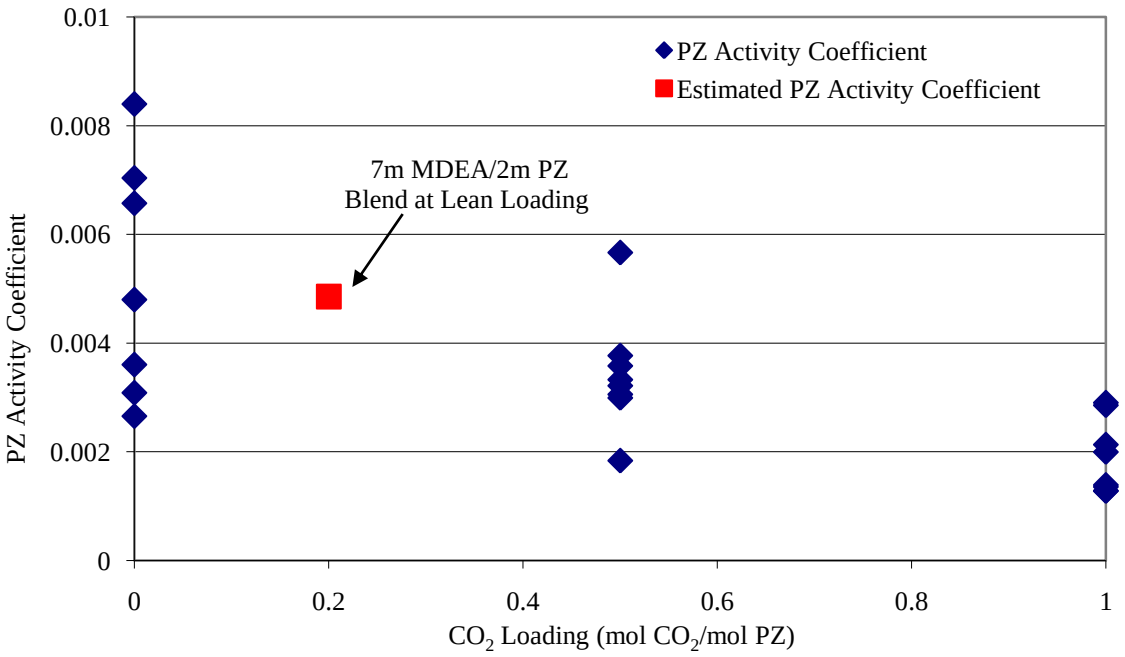

Figure 4: PZ Volatility in MDEA-PZ Blends at 40-70°C (2.7m-8.7m MDEA / 0.4m-2.6m PZ)

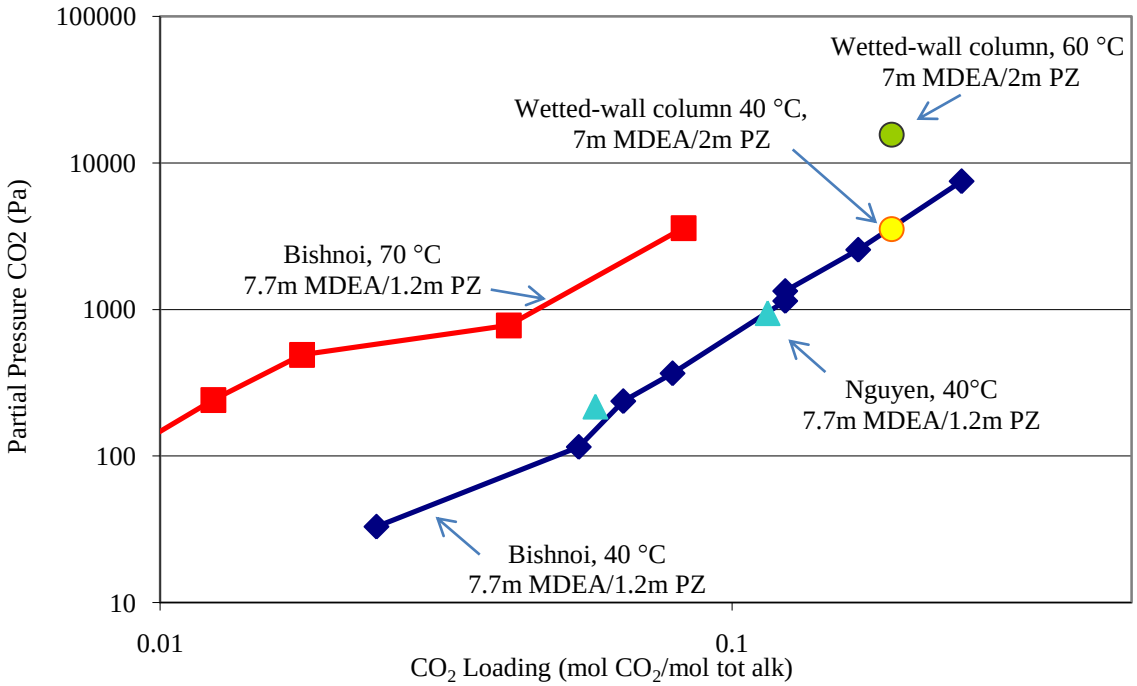

Figure 5: CO_2 Solubility for MDEA-PZ Blend

6. Conclusions

The MDEA/PZ solvent blend provides greater stability than MEA (30 to 50 wt %) when tested at conditions pertinent to CO_2 scrubbing in flue gas. We found that a 7 m MDEA/2 m PZ blend was resistant to thermal degradation up to 120°C at a loading of 0.2 moles CO_2/mole alkalinity, with the highest measured total degradation rates -18 ± 20 mmolal/day for MDEA and -39 ± 11 mmolal/day for PZ at 120°C. The presence of PZ in the MDEA/PZ solvent blend may inhibit the thermal degradation of MDEA. At comparable conditions, MEA degrades at a rate of -20 mmolal/day. Formate production rates in oxidative degradation experiments conducted at 55°C were in the range of 0.010 to 0.016 mmoles formate/L-hr, as compared to formate production rates in MEA under comparable conditions (0.39 mmole/L-hr). Formate production in solvents adhered to the following order: MEA>MDEA>MDEA/PZ. Amide production rates are roughly twice the formate production rates in the MDEA/PZ solvent blend.

The volatility of MDEA in the MDEA/PZ solvent does not change over a range of loading at typical absorber conditions (40°C to 60°C) as long as the predominant reactions involve PZ. The PZ activity in this solvent decreased with loading and temperature over the loading range 0.0 to 1.0 moles CO_2/mole PZ, which we anticipated due to the fast reaction which results in the formation of a PZ-carbamate species. The volatility of PZ for the 8 m MDEA/1.2 m PZ solvent blend was measured as 8 to 66 ppm at 1 atm. We calculated a capacity of 0.75 moles CO_2/kg amine + water, which compares favorably to a value of 0.5 moles CO_2/kg amine + water for a 7 m MEA solvent.

7. Acknowledgements

The authors acknowledge the support of the Luminant Carbon Management Program and the Process Science and Technology Center at the University of Texas.

8. References

1. F.O. Dawodu and A. Meisen, “Identification of products resulting from carbonyl sulphide-induced degradation of diethanolamine,” *J. Chrom*., 587, p. 237–246, 1991.
2. J. Reza and A. Trejo, “Degradation of Aqueous Solutions of Alkanolamine Blends at High Temperature, under the Presence of CO_2 and H_2S”, *Chem. Eng. Comm*. 193: 129–138, 2006.
3. S. Freeman and G.T. Rochelle, “Carbon Dioxide Capture with Concentrated Aqueous Piperazine”, Proceedings of GHGT-9, October 2008.
4. R.C. Kindrick, K. Atwood and M.R. Arnold, “The Relative Resistance to Oxidation of Commercially Available Amines”, Report No. T2.15-1-30, May 19, 1950.
5. P.C. Rooney, M.S. Dupart and T.R. Bacon, “Oxygen’s Role in Alkanolamine Degradation”, Hydrocarbon Processing, 77(7), 109, July 1998.
6. A. Sexton and G.T. Rochelle, “Oxidative Degradation of Amines in CO_2 Capture”, Semi-annual Research Review Meeting, Luminant Carbon Management Program”, July 15, 2008.
7. M.D. Hilliard, “A Predictive Model for an Aqueous Blend of Potassium Carbonate, Piperazine, and Monoethanolamine for CO_2 Capture from Flue Gas”, Ph.D. Dissertation (2008).
8. S. Bishnoi, “Carbon Dioxide Absorption and Solution Equilibrium in Piperazine Activated Methyldiethanolamine”, Ph.D. Dissertation (2000).